Deciphering the regulation of perforin-2-mediated endocytic escape in dendritic cells

Marco Laub

University of Cambridge

Wolfson College

MRC Laboratory of Molecular Biology

This thesis is submitted for the degree of Doctor of Philosophy

April 2024

Preface

This thesis is the result of my own work and includes nothing which is the outcome of work done in collaboration except as declared in the preface and specified in the text. It is not substantially the same as any work that has already been submitted, or, is being concurrently submitted, for any degree, diploma or other qualification at the University of Cambridge or any other University or similar institution except as declared in the preface and specified in the text. It does not exceed the prescribed word limit for the relevant Degree Committee.

The NT, Mpeg1^{KO} and AEP^{KO} MutuDC lines used in this thesis were generated by Patrycja Krawczyk. Isolation of splenic DCs and generation of Flt3L BMDCs was done with the help of Pablo Rodríguez Silvestre. Mass spectrometry experiments (Fig. 5.2 and 6.6) were performed in collaboration with the Borner lab at the Max Planck Institute of Biochemistry in Martinsried, Germany. Analysis of microscopy data was done in collaboration with Jerome Boulanger from the LMB Light Microscopy facility (Fig. 5.10 – 5.13).

Summary

Dendritic cells (DCs) are important players in the initiation of cytotoxic CD8+ T cell-mediated immune responses against pathogens and tumours. DCs continuously sample their environment for antigens and load them on their MHC class I molecules to prime naïve CD8+ T cells in a process known as cross-presentation. Unlike most cell types, cross-presenting DCs have leaky endocytic compartments from where internalised proteins can escape into the cytosol for proteasome-mediated generation of MHC-I-binding peptides. Prior to my project, the Kozik lab had identified the pore-forming protein perforin-2 as a dedicated effector of endocytic escape that allows cytosolic entry of exogenous antigen during cross-presentation. Perforin-2 is a member of the membrane attack complex and perforin superfamily (MACPF) and, similar to perforin and complement, can form oligomeric pores on liposomes *in vitro*. However, the regulation of perforin-2 pore formation in the context of endocytic escape *in vivo* is still poorly understood.

The aim of my PhD project was to decipher the mechanisms that enable DCs to assemble perforin-2 pores on their own membranes for endocytic escape without causing uncontrolled lysis of intracellular compartments. Analysis of its steady-state distribution showed that perforin-2 was proteolytically processed with full-length and cleaved forms present in early and late endocytic compartments, respectively. Since perforin-2 was recruited to antigen-containing phagosomes, I studied its stepwise proteolytic processing during phagosome maturation. Flow cytometry analysis of isolated phagosomes revealed that, in line with previous *in vitro* studies, perforin-2 processing was dependent on acidification. However, by developing an assay to monitor perforin-2 activity at the phagosome, I discovered that inhibiting acidification had no impact on the efficiency of perforin-2-mediated escape. In addition, perforin-2 activity had no detectable effect on the luminal pH or degradative potential of phagosomes. To better understand the role of pH-dependent processing of perforin-2 during phagosome maturation, I studied the proteases involved. The analysis showed that the pore-forming ectodomain was cleaved off the transmembrane domain by cysteine proteases and further processed by asparagine endopeptidase while the remaining membrane stub was removed by γ-secretase. Specific inhibition of these proteases had no impact on perforin-2-mediated endocytic escape suggesting that they are not directly required for pore formation. However, analysis of a perforin-2 trafficking mutant suggested that a currently unknown processing step may be necessary for efficient perforin-2 activity at the phagosome. In summary, this thesis offers novel insights into the regulation of perforin-2 which potentially releases antigens for cross-presentation early during phagosome maturation.

Acknowledgements

I am deeply grateful to many outstanding individuals for making my time at the MRC LMB such an enjoyable experience. First and foremost, Patrycja, thank you for teaching me how to do science and how to do it well. I really appreciate all the support, guidance and understanding you have given me over the past 4 years. It was a real pleasure for me to have been a part of your research group. I also like to thank all the past and present members of the lab for making it such a fun and supportive place to work. My project really was a team effort, and I would like to thank all the fantastic scientists at the LMB for their help. In particular, I want to extend a heartfelt thanks to the talented people at the flow cytometry and light microscopy facilities. Your advice and input helped me get the most out of my data. I am also thankful to Manu Hedge and Gillian Griffiths for insightful discussions and interest in my project. Outside the lab, I'm grateful to all my friends here in the UK – thank you for giving me so many cheerful memories. Also, a big thank you goes to all my friends in Germany who have made the continuous effort to visit me regularly since I left for the UK in 2013. I would like to thank my mother for always believing in me and supporting me in so many ways. Finally, I would like to thank my amazing partner Giulia for always being there for me. Thanks for putting up with my constant moaning and encouraging me to keep going. I could not have done it without you all - thank you.

Table of contents

Abbreviations

ADAM	a disintegrin and metalloprotease domain
AEP	asparagine endopeptidase
ALG2	alpha-1,3/1,6-mannosyltransferase
ALIX	ALG-2-interacting protein X
AP1-4	adaptor protein complex 1-4
APC	antigen-presenting cell
APP	amyloid-beta precursor protein
AQP3	aquaporin 3
ARF1	ADP-ribosylation factor 1
ATP	adenosine triphosphate
AXL	AXL receptor tyrosine kinase
BACE1	beta-site amyloid precursor protein cleaving enzyme
BCA	bicinchoninic acid
BCL-XL	B-cell lymphoma-extra large
BFA	brefeldin a
BFP	blue fluorescent protein
BLAST	basic local alignment search tool
BM	bone marrow
BMDC	bone marrow-derived dendritic cell
BMMO	bone marrow-derived macrophage
BSA	bovine serum albumin
CCR7	C-C chemokine receptor type 7
CCV	clathrin-coated vesicle
CD	cluster of differentiation
cDC	conventional dendritic cell
CDC	Cholesterol-dependent cytolysins
CFSE	carboxyfluorescein succinimidyl ester
CIP	calf intestinal alkaline phosphatase
CLIC1	chloride intracellular channel 1
CLP	common lymphoid progenitor
CMP	common myeloid progenitor
COX2	cyclooxygenase 2
CRL	cullin-RING E3 ubiquitin ligase
CTLA4	T-lymphocyte antigen 4
CTT	C-terminal tail
CXCL2	chemokine ligand 2
DAMP	Damage-associate molecular patter
DC	dendritic cell
DMEM	dulbecco's modified eagle medium
DNGR1	DC, NK lectin group receptor 1
DTT	dithiothreitol

ECL	enhanced chemiluminescence
EGF	epidermal growth factor
ER	endoplasmic reticulum
ERAAP	Endoplasmic reticulum aminopeptidase 1
ERAD	ER-associated protein degradation
ERC	endosomal recycling compartment
ERGIC	ER-Golgi intermediate compartment
ESCRT	endosomal sorting complex required transport
FACS	fluorescence-activated cell sorting
FBS	fetal bovine serum
GEF	guanine nucleotide exchange factor
GFP	green fluorescent protein
GGA	golgi-localized, γ-ear-containing, Arf-binding proteins
GILT	gamma-interferon-inducible lysosomal thiol reductase
GPI	glycosylphosphatidylinositol
GSDMD	gasdermin D
GTP	guanosine triphosphate
HEK	human embryonic kidney
HLA	human leukocyte antigen
HMGB1	high mobility group box 1 protein
HRP	horseradish peroxidase
HS-AFM	high-speed atomic force microscopy
HSP90	heat-shock protein 9-
IFN	interferon
ILV	intraluminal vesicle
IMDM	iscove's modified dulbecco's medium
IP	immunoprecipitation
IRAP	insulin-regulated aminopeptidase
IRES	internal ribosome entry site
ITAM	immunoreceptor tyrosine-based activation motif
LFQ	label-free quantification
LIMP2	lysosomal integral membrane protein 2
LKKR2	leucine-rich repeat kinase 2
LPS	lipopolysaccharide
LRP1	low density lipoprotein receptor-related protein 1
MABP	MVB12-associated β-prism
MAC	membrane attack complex
MACPF	MAC/perforin family
MEF	mouse embryonic fibroblast
MFI	mean fluorescence intensity
MHC	major histocompatibility complex
MMP	matrix metalloproteinase
MPEG1	macrophage-expressed gene 1

MVB	multivesicular bodies
NADPH	nicotinamide adenine dinucleotide phosphate
NK	natural killer cell
NOD	nucleotide oligomerisation domain
NOX2	NADPH oxidase 2
NT	non-targeting
OVA	ovalbumin
PAMP	pathogen-associated molecular pattern
PBS	phosphate-buffered saline
PCR	polymerase chain reaction
PDB	protein data bank
PFA	paraformaldehyde
PI	phosphatidylinositol
PI4K2	phosphatidylinositol 4-kinase type 2 alpha
PLC	peptide loading complex
PM	plasma membrane
PRR	pattern recognition receptor
PS	phosphatidylserine
PTM	post-translational modification
RAB	ras-associated binding proteins
RANBP9	ran-binding protein 9
RFP	red fluorescent protein
RIG	retinoic acid inducible
RIP	ribosome-inactivating protein
ROS	reactive oxygen species
SEM	standard error of the mean
SNARE	SNAP receptor
SPDP	succinimidyl 3-(2-pyridyldithio)propionate
STIM1	stromal interaction molecule 1
SV40LgT	simian virus 40 large T antigen
SYK	spleen-associated tyrosine kinase
TAP	transporter associated with antigen processing
TCR	T cell receptor
TFEB	transcription factor EB
TGN	trans-golgi network
TIDE	tracking of indels by decomposition
TLR	toll-like receptor
TM	transmembrane
TMD	transmembrane domain
TMH	transmembrane hairpin
TNF	tumor necrosis factor
TRAIL	TNF-related apoptosis-inducing ligand
VEGF	vascular endothelial growth factor

WDFY4	WD repeat- and FYVE domain-containing protein 4
WT	wild-type
XCR1	x-c motif chemokine receptor 1

Chapter 1 – Introduction

1.1 Cross-priming by dendritic cells

The ability to accurately discriminate between “self” and “non-self” is central to the proper functioning of the immune system. In adaptive immunity, self/non-self discrimination is achieved by antigen processing and presentation on major histocompatibility complex (MHC) class I and class II proteins for recognition by T cells (*1, 2*). Both classes of MHC present antigenic peptides in the form of peptide-MHC complexes which can interact with cognate antigen-specific T cell receptors (TCRs) (*3*). Engagement of a TCR by a peptide-MHC complex initiates signalling events that lead to the proliferation and differentiation of T cells (often referred to as “T cell priming”). MHC-II is only expressed by professional antigen-presenting cells (APCs; e.g. dendritic cells (DCs), macrophages and B cells) and is recognised by CD4+ T cells (*4*). MHC-II antigen processing and loading occurs almost exclusively in endocytic compartments and therefore involves primarily exogenous antigens, i.e. proteins internalised via endocytosis or phagocytosis. In contrast, MHC-I is expressed by all nucleated cells and can be recognised by CD8+ T cells. Canonical MHC-I presentation mostly involves endogenous antigen, i.e. proteins that were synthesised within the cell. Cell-derived cytosolic proteins are degraded by the proteasome and the resulting peptides imported into endoplasmic reticulum (ER) where MHC-I loading occurs (*2*). However, endogenous antigen can also be processed in endocytic compartments and be presented by MHC-II in some circumstances (*5, 6*). Likewise, MHC-I can present exogenous antigen in a process called cross-presentation.

The first observation of cross-presentation dates back to 1976 when Michael Bevan showed that immunisation of mice with allogeneic (“non-self”) cells results in the priming of recipient cytotoxic CD8+ T cells specific for transplant-derived antigenic peptides restricted for host MHC-I (*7*). These results seemingly contradicted the prevailing notion that MHC-I strictly presents endogenous antigen and suggested that allogeneic peptides had “crossed” into the MHC-I pathway of host APCs (*8*). The phenomenon of “cross-priming” remained contentious for decades because it was discovered before there was a comprehensive understanding of how T cells recognise antigens and how different types of APCs are involved in antigen processing (*9*). However, evidence for the *in vivo* relevance of cross-priming continued to accumulate and DCs eventually emerged as the main APC responsible for this form of CD8+ T cell priming (*10-12*). Today, it is firmly established that cross-priming is essential for the initiation of immune responses against viruses and many tumours (*13*). Notably, it provides an explanation for how APCs can prime CD8+ T cell responses against pathogens and

tumours even when APCs are not infected or malignant themselves. In addition, cross-presentation of self-antigens has been shown to be important to remove autoreactive T cells and helps to maintain central and peripheral tolerance (*14-16*).

The following sections discuss the functions of the DC lineage, its subsets and their role in cross-priming as well as the molecular models proposed for cross-presentation.

1.1.1 DCs link innate to adaptive immunity

As originally postulated by Janeway (*17*), the immune system not only needs to be able to discriminate “self” from “non-self”, but it must also mount a response that aligns with the threat posed by the “non-self” entity. To achieve this, the innate immune system analyses the threat and subsequently guides the generation of appropriate T cell- and B cell-responses. Central to this process are DCs, a heterogeneous group of leukocytes that shapes adaptive immune responses by integrating diverse environmental inputs (*18, 19*). DCs populate most lymphoid and peripheral tissues where they continuously survey their environment for signs of infection or tissue injury. Innate stimulation of DCs can trigger their activation, a process which encompasses a range of phenotypic changes that render the previously resting DC competent to convey information to other cells of the adaptive and innate immune systems (*20*).

Innate DC activation is mostly based on their ability to recognise pathogen-associated molecular pattern (PAMPs) through the expression of pattern recognition receptors (PRRs) (*21*). The best studied PRRs are membrane-bound Toll-like receptors (TLRs) which allow sensing of a range of PAMPs including lipopolysaccharides (LPS; TLR4), double-stranded DNA (TLR9), double-stranded RNA (TLR3), flagellin (TLR5) and peptidoglycan (TLR2) (*22*). DCs may also sense PAMPs via other PRRs including membrane-bound C-type lectin receptors as well as cytosolic NOD-like and RIG-I-like receptors (*23-25*). In addition to microbial-derived molecules, innate DCs activation can also be triggered by damage-associated molecular patterns (DAMPs), although this may be less efficient than PAMP-mediated activation (*26*). DAMPs are cell-derived molecules that are released in response to tissue-damage either in the presence or absence of pathogens (*27, 28*). For example, the chromatin-associated protein HMGB1 is a prototypical DAMP that can be sensed by several PRRs including TLR2 and TLR4 (*29, 30*). Other examples include ATP, calreticulin and heat-shock proteins. Finally, DC activation may be mediated by other cells (e.g. neutrophils) via secretion of inflammatory cytokines (e.g. TNF-α or type I interferons) (*31*).

Activated DCs can directly support the innate immune response by secreting immunomodulatory cytokines and chemokines that stimulate other innate cells. For example,

DCs may recruit neutrophils by secreting VEGF or CXCL2 or activate natural killer cells through NKGD2 signalling and secretion of IL-12 and IL-15 (*32-36*).

However, activated DCs not only convey messages to innate immune cells but also to cells of the adaptive immune system including T cells. The communication with T cells is antigen specific and involves the display of short antigen-derived peptides on MHC molecules for recognition by the T cells. DC activation is central to this process as it initiates several pathways that transform DCs into antigen-presenting cells with an enhanced capacity to prime naïve T cell responses. Activated DCs increase the surface expression of MHC molecules and upregulate proteins involved in antigen processing (*37-41*). In addition, activation of DCs in the periphery allows them to encounter T cells by enabling their migration to lymphoid tissue through increased expression of the chemokine receptor CCR7 (*42*). Lymph-node resident DCs can also present antigen to T cells which they acquire from lymphatic fluid or capture from migratory DCs (*43*). Finally, activated DCs upregulate co-stimulatory molecules and secrete cytokines that shape the outcome of the DC-T cell interaction (*41*). Depending on the stimuli that led to their activation, DCs may instruct T cell differentiation into cytotoxic CD8+ T cells, CD4+ helper T cells (Th1, Th2 or Th17) or tolerogenic T regulatory cells (*20, 41, 44*).

In summary, DCs express a wide range of innate immune receptors which allow them to sense pathogens and tissue damage. The ensuing activation endows DCs with the ability to migrate to lymphoid tissue and stimulate an appropriate T cells response. Therefore, DCs have the unique ability to bridge the gap between innate and adaptive immunity.

1.1.2 DCs subsets and cross-priming

Since their initial discovery in the 1970s (*45-47*), it became clear that DCs comprise a heterogeneous group of cells which can be classified into distinct subtypes. Accurate classification of DCs, however, is a major challenge in the field and continues to evolve until today (*48*). Their relatively low abundance makes them difficult to study and preparations of DCs can frequently be contaminated with other cell types such as macrophages. In addition, different groups have used distinct strategies to identify DC subtypes (based on e.g. morphology, function or phenotype) which blurred the definition of bona fide DCs. Finally, it is not always trivial to determine whether a differential marker identifies distinct subtypes or simply represents different activation states of cells of the same subtype.

Currently, the most widely accepted classification of the DC lineage is based on a combination of surface markers, functional characteristics, transcriptional signatures, lineage-tracing and tissue distribution (*20*). DCs are generally divided into conventional DCs

(cDCs), which include cDC1s and cDC2s, and plasmacytoid DCs (pDCs). cDCs and pDCs both express the surface markers CD11c and MHC-II. However, they differ in their ontology and functions.

In mice, hematopoietic bone marrow stem cells give rise to multipotent progenitors that then differentiate into common myeloid progenitors (CMPs) and common lymphoid progenitors (CLPs). pDCs fully differentiate in the bone marrow and early studies indicated that they derive from CMPs and CLPs (*49*). However, more recent studies suggest a predominant CLP origin (*50, 51*). In contrast, cDCs leave the bone marrow as pre-cDCs and continue their differentiation after tissue homing (*52*). Pre-cDCs derive from common DC progenitor (CDP), which in turn derive from CMPs (*53*). The differentiation of cDC1s and cDC2s occurs at the CDP to pre-cDC transition, which results in committed pre-cDC1s or pre-cDC2s (*54*).

pDC are identified by surface markers Siglec-H and B220 and their differentiation depends on the transcription factors Irf8, Runx1, and Tcf4 (*55*). In contrast to cDCs, pDCs are generally regarded as poor antigen-presenting cells (*56*). Instead, pDCs rapidly produce large amounts of type I interferon in response to viral PAMPs (*57, 58*). Given their distinct ontogeny and function, pDCs have recently been proposed to be classified as innate lymphoid cells rather than DCs (*59*).

The development of cDC1 depends on the transcription factors Irf8, Batf3, Nfil3, and Id2 and they selectively express the chemokine receptor Xcr1 and the C-type lectin receptor Clec9a (*55*). Expression of the CD8αα homodimer and the E-cadherin-binding integrin CD103 are commonly used as additional markers to define lymphoid-resident and peripheral cDC1s, respectively. In contrast, cDC2s are more heterogenous than cDC1s. They depend on transcription factors Irf4, Zeb2 and Relb but can be further divided into Notch2- and Klf4-dependent cDC2s or T-BET+ cDC2As and RORγt+ cDC2Bs (*55, 60, 61*). In general, most cDC2s express high levels of CD11b and Sirpα and lymphoid-resident cDC2s additionally express CD4. However, these markers do not uniquely identify cDC2s because they can also be expressed by other CD11c+MHC-II+ myeloid cells such as macrophages.

cDC subsets have unique adaptations such as the expression of different PRRs and secretion of different cytokines following activation endowing them with specialised functions (*62, 63*). cDC2s are generally considered to be the main subset required for effective CD4+ T helper cell differentiation via MHC-II antigen presentation (*58*). In contrast, cDC1s have emerged as the main cross-presenting subset responsible for cross-priming cytotoxic CD8+ T cells (*58*). The requirement for cDC1s to mount effective cytotoxic CD8+ T cell responses comes is supported by several studies reporting a failure of cDC1-deficient mice (Baft3-/- or Irf8-/-) and other cDC1 *in vivo* models to efficiently control viral infections and reject tumours

(64-70). While cDC1s appear to be the predominant cross-priming cells *in vivo*, other DC subsets as well as macrophages and monocytes may also be able to cross-prime under certain conditions (*71-73*).

1.1.3 DC activation and licensing for cross-priming

The widely accepted model of CD8+ T cell priming by cDC1 postulates that DCs deliver three signals, aptly named Signal 1,2 and 3, which regulate the differentiation of naïve T cells (*74, 75*). Signal 1 refers to the recognition of peptide-MHC-I complexes on the cDC1 by a cognate T cell receptors (TCRs) on the naïve CD8+ T cell. This signal encodes the specificity in the T cell response. However, when received in the absence of additional cues, Signal 1 alone leads to T cell inactivation and therefore peripheral tolerance (*76, 77*). Signal 2 is delivered through co-stimulatory receptor-ligand interactions. The most prominent example of co-stimulation involves signalling through CD28 on the CD8+ T cell when it engages CD80 and/or CD86 on the DC which is important for T cell clonal expansion and differentiation into effector cells (*78*). CD28 stimulation functions in concert with signalling through CD27 following its interaction with CD70 on the DC which also supports clonal expansion of activated CD8+ T cells (*79*). However, CD80/CD86 can also engage cytotoxic T-lymphocyte antigen 4 (CTLA4) which is a negative regulator of T cell activation (*80*). Similarly, other co-stimulatory interactions, including receptor/ligand pairs from the TNF superfamily, may stimulate but also inhibit T cell activation (*81*). Thus, Signal 2 can be immunogenic or tolerogenic depending on the balance of positive and negative co-stimulatory interactions. Finally, Signal 3 refers to cytokines secreted by the DC that regulate the differentiation of CD8+ T cells. Production of IL-12 and IL-15 by cDC1s have been shown to be important for the priming of cytotoxic CD8+ T cells and the induction of tissue-resident memory T cells (*82, 83*). Signal 3 also encompasses additional cytokines such as type I interferon which can be secreted by DCs as well as other innate cells (*84*).

As mentioned in Section 1.1.1, DCs can be activated by PAMPs and DAMPs which enhance their cross-presentation capacity as well as upregulate their co-stimulatory molecules and cytokine production thus contributing to Signals 1,2 and 3. However, to what extent innate signalling facilitates cross-priming at the level of cross-presentation (Signal 1), or co-stimulation (Signals 2 and 3) has not been fully resolved (*39*).

Besides activation by innate signals, induction of CD8+ T cells proliferation and differentiation by cDC1s also requires help by CD4+ T cells (**Fig. 1.1**). The concept of a three-cell-type model for CD8+ T cell activation emerged from studies conducted in the 1980s demonstrating that CD4+ T cells play a crucial role in promoting CD8+ priming against minor histocompatibility antigens (*85*). It was shown that this process requires direct

interaction between antigen-specific CD4+ and CD8+ T cells with the same APC (*86*). Studies in the 1990s identified that the basis of CD4+ T cell help for CD8+ T cell responses could largely be attributed to CD40-stimulaton of DCs (*87, 88*). It was also discovered that

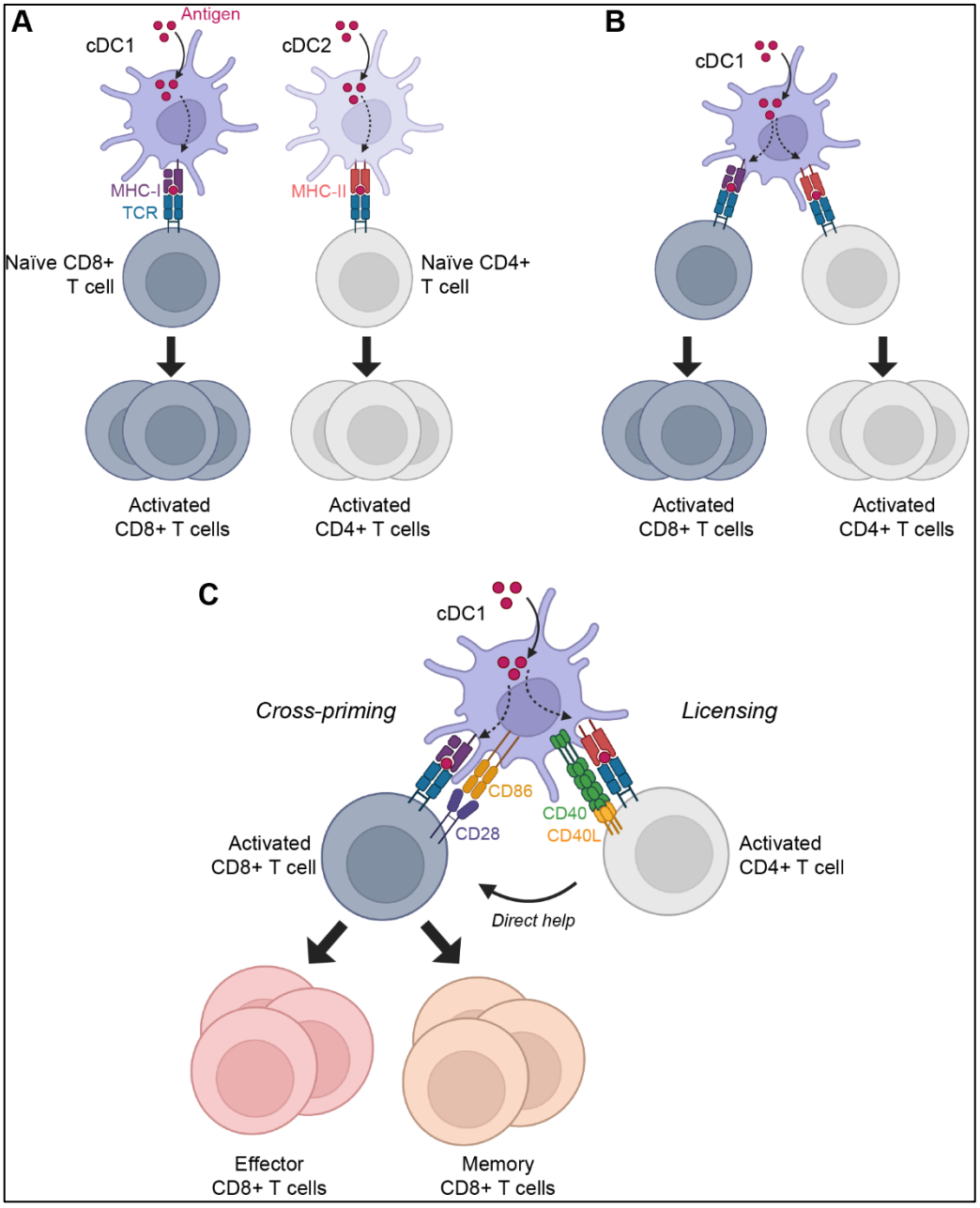

Fig. 1. 1. Cellular and molecular interactions in the licensing of cDC1s and cross-priming of naïve CD8+ T cells. (**A, B**) The current model of cDC1 licensing and CD4+ help postulates that naïve CD8+ and CD4+ T cells are first activated in the absence of "help" signals. The encounter of antigen during this first priming step may occur on different types of cDCs (A) or on cDC1s alone (B). (**C**) In a second priming step, activated CD8+ T cells and CD4+ T cells engage the same cDC1 in an interaction that boosts the differentiation of CD8+ T cells into effector and memory cells. Activated CD4+ T cells license the cDC1 for cross-priming through the interaction of CD40L and CD40. Licensed cDC1s express high levels of CD86 and/or CD80 (not shown) which interacts with CD28 on CD8+ T cells. CD4+ T cell-derived cytokines can also support the CD8+ T cell response directly. The figure was created with Biorender and adapted from (*89*).

the interaction between T cells and DCs does not need to occur simultaneously but a sequential two-cell encounter is sufficient for the induction of cytotoxic CD8+ T cell responses (*90*). Collectively, these observations led to the concept of 'DC licensing' by CD4+ helper T cells (*91*). The outcome of CD40-mediated licensing contributes to Signal 3 through the production of cytokines such as IL-12 (*83, 92*). Recently, it has been shown that CD40 ligation on DCs also increases expression of CD70, COX-2 and BCL-XL leading to enhanced co-stimulation, metabolic adaptations and enhanced survival of cDC1s to support anti-tumour immunity (*93*).

Initially, the contributions of innate signals and CD4+ T cell help to the priming of CD8+ T cells were considered redundant (*94*). However, innate signals alone are not sufficient for the differentiation of memory CD8+ T cells (*95, 96*). In addition, CD4+ T cell help has been found to shape key aspects of CD8+ T cell effector functions, including the expression of cytotoxic effector molecules, improved migration, and the downregulation of co-inhibitory receptors (*97*). Given these discoveries, innate signals and CD4+ T cell help are now seen as complementary each providing distinct cues for DC activation (*89*).

To be able to license DCs, CD4+ T cells need to be primed themselves. The prevailing model suggests that, in a first step, CD4+ T cells are primed by cDC2s through MHC-II presentation (*98*). Then, in a second step, the primed CD4+ T cells can re-engage different APCs, including cDC1, to license them to prime CD8+ T cell responses (*99, 100*). Notably, in the context of a tumour model, it has been shown that cDC1s may prime CD4+ T cells themselves which in turn license the cDC1s to optimally cross-prime CD8+ T cells (*101*).

In summary, the cross-priming of CD8+ T cells requires the integration of innate signals and CD4+ T cell activity by cDC1s which is achieved through the regulated expression of co-stimulatory molecules and cytokines.

1.2 Mechanisms of cross-presentation

In 1976, Michael Bevan reported observations that were seemingly inconsistent with concept of MHC restriction, i.e. T cell recognition of antigen only in the context of a specific MHC-encoded allelic product (*7*). In these experiments, F1 mice that are heterozygous at the MHC-I locus, expressing H-2^d and H-2^b alleles, were immunised with live splenocytes from B10.D2 mice which are homozygous for H-2^d but differing in minor histocompatibility antigens (alloantigens) to the recipients. This means that, the immunising cells could direct an immune response by engaging host T cells (since both have H-2^d) which would recognise the presented alloantigens as "non-self". Accordingly, the immunised mice developed cytotoxic CD8+ T cells that could lyse targets derived from B10.D2 ($H2^d$) mice. However,

unexpectedly, the CD8+ T cells primed in this way could also lyse targets derived from B10 (H-2^b) mice. The priming of a H-2^b-restricted response by immunisation with H-2^d cells appeared to refute the concept of MHC restriction. Bevan correctly reasoned that MHC restriction was in fact not violated but instead alloantigens of the immunising cells were internalised by host H-2^b-expressing APCs for cross-priming of CD8+ T cell.

These observations were soon substantiated by further reports of *in vivo* cross-priming (*102-104*). However, the molecular details of cross-presentation were not of immediate concern because, at the time, the nature of antigen recognition by T cells was still poorly understood (*9*). Although it was already known that recognition of viral and allo-antigens is MHC-I restricted, the molecular correlate of the MHC-I locus was elusive (*105-107*). The first evidence for the requirement of antigen processing for a CD8+ T cell response was only reported in 1980 (*108*). Subsequent studies, using the chicken egg-derived model antigens ovalbumin and lysozyme, revealed that MHC-II gene products bind protein derived peptides (*109-111*) and the same was shown for MHC-I gene products (*112, 113*). The peptide binding groove and residues involved in peptide binding were later revealed by crystal structures of peptide-bound human MHC-I (*114, 115*). Around the same time, the identity of the cognate entity on the T cell became increasingly well understood culminating in the cloning of the T cell receptor (*116, 117*). Collectively, these discoveries paved the way for the molecular dissection of cross-presentation, an endeavour that continues until today.

1.2.1 Classical MHC-I antigen presentation

MHC-I antigen presentation provides a means to survey the proteome of a cell by presenting peptides derived from endogenous protein synthesis and degradation (**Fig. 1.2**) (*2, 118*). MHC-I molecules are heterodimers comprising a membrane-bound glycoprotein heavy chain, which forms the antigen-binding groove, and a non-covalently associated small subunit called β2-microglobulin. The heavy chain of classical MHC-I molecules is highly polymorphic and encoded by alleles of the H2-D, H2-K and H2-L loci in mice and the equivalent HLA-A, HLA-B, and HLA-C loci in humans (*119*). In an outbred population, each individual typically expresses up to six different types of MHC-I proteins each binding a different range of peptides due to variations in the peptide binding groove (*120, 121*). This large diversity of possible peptide-MHC-I complexes ensures that antigen-specific CD8+ T cell responses can be mounted against a broad range of targets.

Under homeostatic conditions, peptide-MHC-I complexes are generated from “self” protein-derived peptides which do not active CD8+ T cells because self-reactive T cells are removed by negative selection in the thymus (*122*). However, if a cell is infected or becomes cancerous, the peptides presented by MHC class I may derive from “non-self” entities such

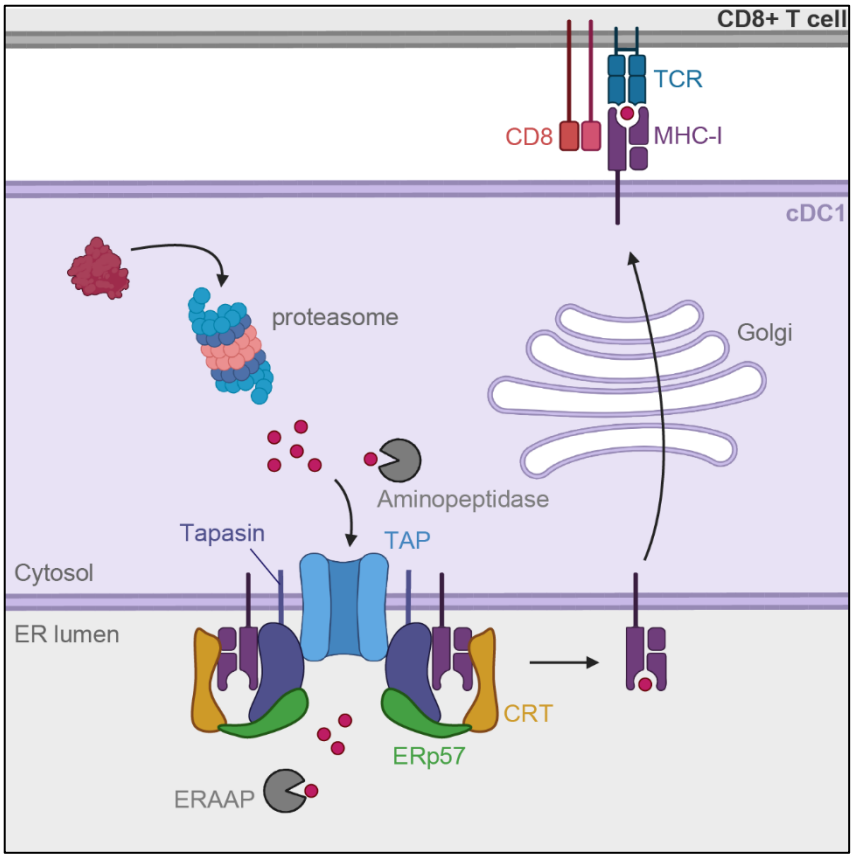

Fig. 1. 2. Classical MHC-I antigen presentation. Endogenous, cytosolic proteins are degraded by the proteasome. The resulting peptides are destroyed by cytosolic aminopeptidases but a fraction of them is spared by transport into the ER lumen mediated by TAP. The imported peptides may be trimmed N-terminally by ER-resident ERAAP. Newly synthesised MHC-I molecules are stabilised by calreticulin (CRT) and recruited into the peptide loading complex (PLC) comprising MHC-I, TAP, CRT, tapasin and ERp57. After loading of peptides onto MHC-I, the PLC dissociates and the peptide-MHC-I complex traffics, via the Golgi, to the cell surface for antigen presentation to CD8+ T cells. The figure was created with Biorender and adapted from (*2*).

as viral or mutated proteins allowing cytotoxic CD8+ T cells to detect and destroy these cells by releasing cytotoxic granules whose contents induce apoptosis (*123*).

The generation of peptides for MHC-I presentation does not only depend on the natural half-life of proteins. A large fraction of peptides (30 – 70%) is instead derived from proteins that are degraded almost immediately after synthesis due to defects in translation or folding. These products are knowns as defective ribosomal products (DRiPs) (*124, 125*). DRiPs are important to mount rapid CD8+ T cell responses that are independent of the half-life of viral proteins (*126*). Misfolded membrane and soluble endolysosomal proteins also contribute to the pool of MHC-I presented peptide following their transport into the cytosol and proteasomal degradation via the ER-associated degradation (ERAD) system (*127*).

Proteins are tagged for proteasomal degradation by ubiquitination which is governed by a cascade of E1, E2 and a large family of E3-type ubiquitin ligases (*128*). The proteasome, a 26S protein megacomplex, recognises these ubiquitin-tagged proteins and degrades them into 2 to 24 residue long peptides (*129*). Substrate recognition is mediated by two 19S caps

while the proteolytic activity resides in the 20S core barrel (*130*). The catalytic subunits in the 20S barrel, β1, β2 and β5, are constitutively expressed in all cells. DCs and lymphocytes, as well as non-immune cells upon exposure to pro-inflammatory cytokines, additionally express the alternate active site subunits β1i, β2i and β5i leading to the assembly of the immunoproteasome (*131, 132*). The constitutive and immuno-proteasomes have different substrate specificity and as a result produce altered peptide repertoires (*133*). Peptides generated by the immunoproteasome may be presented preferentially on MHC-I thus supporting the initiation of CD8+ T cell responses (*132, 134*). The immunoproteasome is also important to preserve cell viability under conditions of immune stress by pathological protein aggregation (*135*).

Many peptides generated by the proteasome are lost for MHC-I presentation due degradation of peptides by cytosolic aminopeptidases (*136*). However, a fraction of them escapes degradation by translocation into the ER lumen via the transporter associated with antigen processing (TAP), a MHC-encoded heterodimeric member of the ATP-binding cassette-containing family of transporters (*137*). TAP is a key component of the peptide loading complex (PLC) that additionally comprises MHC-I, tapasin Erp57 and calreticulin (*138*). The PLC acts as a quality control system that ensure proper folding and loading of MHC-I molecules. Each subunit of TAP, TAP1 and TAP2, binds MHC-encoded tapasin which in turn recruits MHC-I molecules awaiting peptides (*139, 140*). Empty MHC-I are only partially folded and the interaction with tapasin is important for their stability (*140, 141*). Besides bridging TAP and MHC-I, tapasin is also involved in peptide proofreading which promotes the binding of high affinity peptides (*142, 143*). Peptide proofreading is mediated by the ability of tapasin to alter the conformation of the peptide binding groove on MHC-I (*144*). The thiol oxidoreductase ERp57 forms a disulfide-linked heterodimer with tapasin and aids in MHC-I recruitment and peptide proofreading (*144, 145*). Finally, the role of calreticulin is to stabilise newly synthesised MHC-I molecules to ensure their recruitment into the PLC (*146*). The PLC can efficiently load peptides with 8 to 10 residues and in many cases, imported peptides require additional trimming by the ER aminopeptidase ERAAP (*147*). The binding of high-affinity peptides to MHC-I eventually induces its dissociation from the PLC (*148, 149*). Low-affinity peptides that fail to bind are retrotranslocated into the cytosol via the ERAD pathway (*150*).

Fully assembled peptide-MHC-I complexes exit the ER, aided by cargo receptors such as Bap31 (*148, 151*). MHC-I molecules that are not optimally loaded at this stage are subject to an additional quality control step mediated by PLC components. Both, tapasin and calreticulin associate with peptide-MHC-I in the ER-to-Golgi intermediate compartment (ERGIC) where they can catalyse peptide loading or mediate recycling of sub-optimal

complexes back to the ER by means of their ER retention/retrieval signal (KDEL) (*152-154*). MHC-I molecules that pass the ERGIC quality control can traffic to the plasma membrane for presentation to CD8+ T cells. Interestingly, surface MHC-I molecules can undergo peptide exchange with exogenous peptides (*155*).

The residence time at the cell surface is dependent the stability of the peptide-MHC-I complex and complexes with low affinity peptides are internalised faster (*156*). Surface MHC-I undergoes clathrin-independent endocytosis mediated by the small GTPase Arf6 (*157*). After endocytosis, MHC-I complexes are delivered to sorting endosomes, from where they can be routed, depending on their stability (*158*), to endolysosomal compartments for degradation or recycled back the plasma membrane via a fast or a slow route. Fast recycling is mediated by Rab4 or Rab35 while slow recycling entails transit through a morphologically distinct organelle known as the endosomal recycling compartment (ERC) mediated by Rab11a (*159, 160*). From the ERC, MHC-I molecules are sorted back to the plasma membrane in tubular recycling endosomes formed by EHD1 and Rab22a (*161*). Notably, in DCs, the ERC acts as an intracellular storage site from where MHC-I molecules can be recruited to phagosomes which is an important pathway in cross-presentation as discussed in the following sections (*162*).

1.2.2 Antigen internalisation for cross-presentation

The first step in cross-presentation involves the internalisation of exogenous antigens by DCs which may occur via multiple routes including macropinocytosis, receptor-mediated endocytosis and phagocytosis. The mechanism of uptake is largely dictated by the form of antigen and has been shown to influence the efficiency of cross-presentation.

After the initial description of cross-presentation for cell-associated alloantigens (*7*), studies in the 1990s used the model antigen ovalbumin to show that soluble antigens can also be cross-presented *in vitro* by splenic APCs to prime CD8+ T cell responses (*163, 164*). However, priming of CD8+ T cell responses *in vivo* was found to be much more efficient when ovalbumin was conjugated to beads compared to soluble ovalbumin leading to the model that soluble antigens are cross-presented with substantially lower efficiency (*165, 166*). Particulate bead-associated ovalbumin is cross-presented with higher efficiency in many DC models although some report a requirement for TLR signalling potentially reflecting differences in bead preparation methods (e.g. covalent coupling or passive absorption) (*162, 167, 168*). Interestingly, cross-presentation efficiency for soluble ovalbumin can be potentiated following uptake by mannose receptor-mediated endocytosis or by antibody-directed receptor-mediated endocytosis compared to uptake by micropinocytosis (*169, 170*) . Similarly, ovalbumin/α-ovalbumin immune complexes, which are internalised by engaging

Fcγ receptors, are cross-presented more efficiently than soluble antigen (*171*). The improved efficiency in these settings can partly be explained by an enhancement in antigen uptake but is also attributable to routing of antigen into specific endocytic compartments (*169-171*). Notably, comparative studies in different DC subsets have shown that the dominant role of cDC1s in cross-presentation of soluble and bead-conjugated ovalbumin is largely independent of uptake suggesting that cDC1s have subcellular compartments that are uniquely conducive to cross-presentation (*172, 173*).

In a physiological setting, important sources of exogenous antigen for cross-presentation include microbes and dying cells. cDC1s have been reported to be superior to cDC2s in cross-presenting phagocytosed heat-killed Listeria monocytogenes *in vitro* while paraformaldehyde-fixed E. coli were cross-presented with comparable efficiency in both subsets (*67, 174*). These discrepancies suggest that innate signalling may influence the processing and cross-presentation of microbial-associated antigens in different APCs. Internalisation of necrotic cells can be mediated by the C-type lectin receptor Clec9A which is selectively expressed by CD8αα+ DCs (*175*). Clec9A-deficient mice display a defect in cross-presentation of cell-associated antigen and fail to efficiently prime CD8+ T cell responses against cytopathic viruses (*82, 176*). In line with previous studies showing that the selective capability of CD8α+ DCs to cross-present cell-associated antigens is independent of uptake, Clec9A was found to promote cross-presentation in cDC1s by signalling-induced changes in antigen handling (*10, 177*). Other receptors that induce uptake of necrotic and/or apoptotic cells include C-type lectin DEC-205 and a complex comprising AXL/LRP-1/RANBP9 (*178, 179*).

In summary, antigen capture greatly influences the efficiency of cross-presentation and cDC1s are particularly well equipped for the internalisation of cell-associated antigen. However, their dominant role in cross-presentation cannot be fully explained by superior antigen uptake suggesting that cDC1s have a specialised intracellular machinery for cross-presentation.

1.2.3 Pathways for peptide generation and loading for cross-presentation

Two main pathways have emerged to explain how exogenous antigens are processed for cross-presentation. In the vacuolar pathway, antigen processing and loading occur exclusively in endocytic compartments, independent of cytosolic proteasomal degradation (*180*). In contrast, the cytosolic pathway involves the processing of exogenous antigen by the proteasome suggesting transfer of internalised material into the cytosol (*181*). The loading of cytosolic peptides on MHC-I molecules may occur in the ER involving TAP-mediated peptide import, as for classical MHC-I antigen presentation, or in endocytic

compartments following re-import of peptides by TAP-dependent and TAP-independent mechanisms (*182, 183*). The vacuolar and cytosolic pathways are not mutually exclusive (*184*) but their relative contributions to cross-presentation are still subject of debate. This is in large part due to the wide range of experimental setups that have been used to study this phenomenon over the past 25 years (*66*). Of relevance here are the different forms of antigens, discussed in Section 1.2.3, which can strongly influence its route of internalisation and subsequent processing. In addition, different cellular models have been used to study cross-presentation *in vitro* including macrophages and bone-marrow-derived dendritic cells (BMDCs). Many studies employed GM-CSF-derived BMDCs which are a heterogenous mixture of macrophage-like and DC-like cells, neither of which resembles cDC1s (*185*). Lastly, the readouts for cross-presentation often measure the activation, proliferation or cytokine production of CD8+ T cells upon exposure to DCs and are therefore in fact readouts of cross-priming. As mentioned in Section 1.1.3, in these settings it is usually not possible to clearly distinguish effects on cross-presentation (signal 1) from effects on co-stimulation (signals 2 and 3).

1.2.4 The vacuolar pathway

The hallmark of the vacuolar pathway (**Fig. 1.3**) is its independence of cytosolic proteasome- and TAP-mediated processing of exogenous antigen (*168, 180, 186, 187*). The first description of this pathway reported that inhibition of protein synthesis (by cycloheximide) or protein traffic from ER to Golgi (by brefeldin A) in macrophages had no effect on the efficiency of cross-presentation of phagocytosed bacterial antigen (a H-2K^b-restricted 257-264 epitope of ovalbumin expressed in E. *coli* by fusion to Crl protein) (*180*). This suggested the involvement of pre-existing post-Golgi MHC-I molecules onto which exogenous peptides are loaded. These MHC-I molecules were either previously occupied with endogenous peptide (which are displaced through peptide exchange (*188*)) or unoccupied. Accordingly, TAP1-deficient macrophages, which are impaired in classical MHC-I presentations due to defects in cytosolic peptide import into the ER (*189*), could nonetheless cross-present soluble viral proteins and particular bacterial antigens (*168, 186, 187*). In addition, chimeric mice with a TAP-deficient hematopoietic cell compartment were shown to mount a protective CD8+ T cell response to viral infection suggesting cross-priming by TAP-deficient DCs *in vivo (190).*

In the vacuolar pathway, proteasome activity is replaced by endosomal proteases as evidenced by the inhibition of vacuolar cross-presentation following treatment with leupeptin or chloroquine (*168*). The lysosomal protease cathepsin S plays a dominant role in

generating peptides for the TAP-independent pathway since mice deficient in cathepsin S have defects in cross-priming CD8+ T cell against virally infected cells *in vivo* (*184*).

A potential source of post-Golgi MHC-I molecules for cross-presentation of exogenous peptides was suggested by a study showing delivery of MHC-I to the phagosome from the ERC following TLR engagement (*162*). A separate study showed that the SNARE Sec22b potentiates cross-presentation by recruiting PLC components (Tap2, tapasin and calreticulin) from the ERGIC to phagosomes in a TLR-independent manner (*182*). Although neither study specified whether the peptides were generated in the cytosol or endocytic compartments, TLR-dependent delivery of MHC-I and Sec22b-mediated delivery of the PLC could in principle support the generation of peptide-MHC-I complexes in the vacuolar pathway (*191*). Recently, it was shown that in TAP-deficient GM-BMDCs, MHC-I accumulates in the ERGIC and efficient cross-presentation relied on its recruitment to phagosomes in a Sec22b-dependent manner suggesting that Sec22b can participate in the vacuolar pathway under these conditions (*190*).

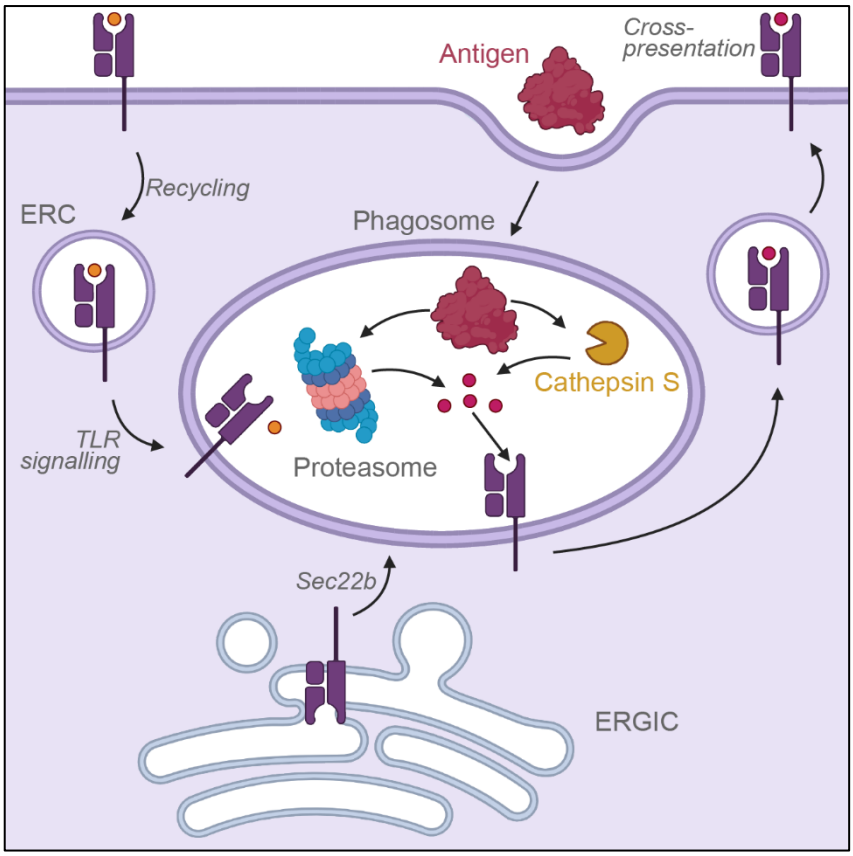

Fig. 1. 3. The vacuolar pathway of cross-presentation. Exogenous antigens are internalised and degraded within the phagosome by luminal proteases such as cathepsin S. It has also been reported that proteasomes can be imported into the lumen of endocytic compartments which may contribute to the degradation of internalised antigen. The resulting peptides are loaded onto MHC-I within endocytic compartments and trafficked to the cell surface for cross-presentation. The recruited MHC-I molecules may derive from the endocytic recycling compartment (ERC) or the ER-Golgi intermediated compartment (ERGIC). The figure was created with Biorender and adapted from (*192*).

However, it remains unclear how MHC-I molecules, which dissociate a pH < 5.0 (*188*), can be stabilised in the acidic environment required for lysosomal protease activity. Another question concerns how much overlap there is between peptides generated by lysosomal proteases and the proteasome (*193*). This is important since infected or malignant target cells present proteasome-derived peptides via classical MHC I presentation. Nonetheless, it appears to be largely a matter of chance that CD8+ T cells are cross-primed by protease-derived peptides which are identical to proteasomal peptides displayed on target cells. However, recent studies have shown that proteasomes can be delivered into endocytic compartments, possibly by fusion with proteasome-containing autophagosomes (*194*), to generate proteasomal peptides in a TAP-independent, but proteasome-dependent, vacuolar pathway (*195, 196*). Thus, the vacuolar pathway may involve proteasome-independent as well as proteasome-dependent routes although the contribution of the latter to cross-priming *in vivo* remains to be investigated.

1.2.5 The cytosolic pathway

The cytosolic pathway (**Fig. 1.4**), also referred to as the phagosome-to-cytosol pathway, was first postulated in a study showing that cross-presentation of bead-associated ovalbumin by peritoneal macrophages was sensitive to proteasome inhibitors, brefeldin A and TAP mutations (*181*). Furthermore, the same study showed that phagocytosis of beads conjugated to the ribosome-inactivating enzyme gelonin led to an inhibition of protein synthesis suggesting transfer of intact gelonin from phagosomes into the cytosol. Analogous results were obtained in a different study showing evidence for endocytic escape of soluble, rather than bead-conjugated, ovalbumin and gelonin (*197*). Subsequent reports documented endocytic escape in DCs *in vitro* using various model antigens including horseradish peroxidase and β-lactamase (*182, 198, 199*). Notably, subcellular fractionation experiments revealed that endocytic escape of ovalbumin was more efficient in a splenic-derived DC cell line than in BM-derived macrophages (*198*). In addition, *in vivo* administration of soluble cytochrome c, an initiator of apoptosis, was found to selectively deplete CD8α+ DCs indicating that endocytic escape of exogenous antigens preferentially occurs in cDC1s *in vivo (200).*

TAP-dependence has been proposed as a hallmark for the cytosolic pathway and is often interpreted as evidence that cross-presentation relies on TAP-mediated transport of cytosolic peptides (*181, 199, 201, 202*). Macrophages and BMDCs from TAP-deficient mice were less efficient in cross-presentation of soluble and bead-conjugated ovalbumin *in vitro (181, 199)*. Further, chimeric mice reconstituted with TAP-deficient BM cells failed to cross-prime against tumor antigens *in vivo (202)*. However, since MHC-I molecules in TAP-deficient cells are

retained in the ERGIC (*190*), more unstable in endocytic compartments (*203*) and depleted from the cell surface (*189*), TAP-dependence does not conclusively exclude a role of the vacuolar pathway.

The site of action for TAP-mediated transport of proteasome-derived peptides for MHC-I loading has also not been fully resolved. Initially, it was assumed that after endocytic escape of antigens, their peptides were simply fed into the classical MHC-I loading pathway following their transport into the ER by TAP. Consistent with this model, cross-presentation of cell-associated antigen was impaired in BMDCs from mice deficient in ER-associated aminopeptidase 1 (ERAP1) (*204*). However, a later study showed that TAP-dependent cross-presentation also relies on peptide trimming by insulin-regulated aminopeptidase (IRAP) (*205*). IRAP localises to Rab14+ endosomal vesicles in human DCs and its involvement therefore suggested peptide import into endocytic compartments for MHC-I loading (*205*). Accordingly, several studies reported the recruitment of TAP, along with other ER-resident proteins such as MHC-I and PLC, to phagosomes (*206-208*).

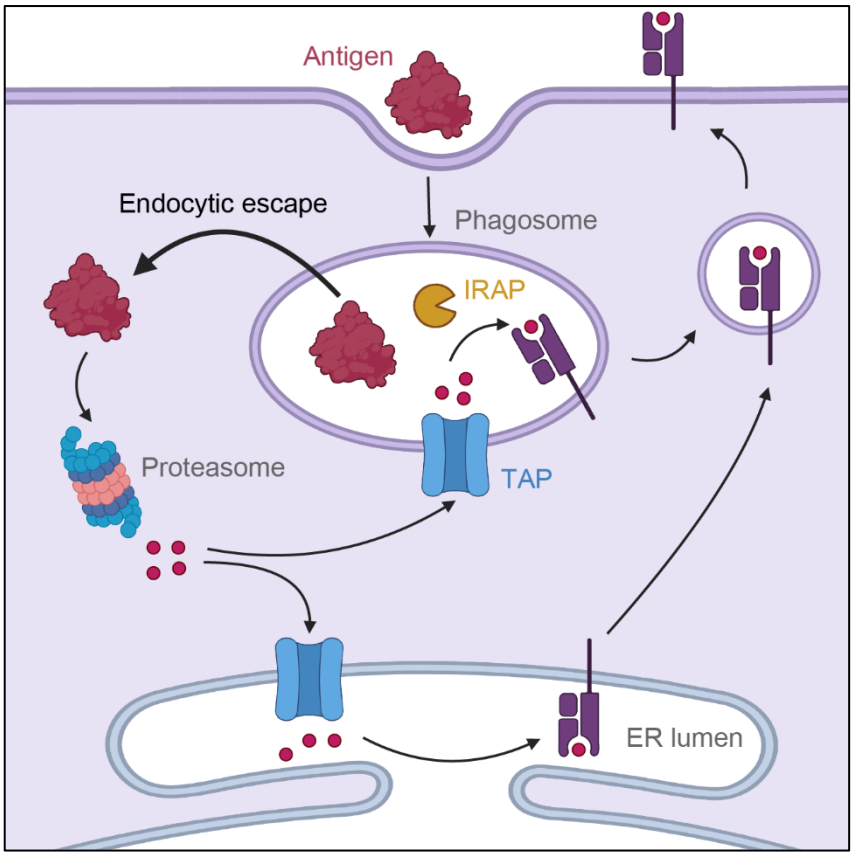

Fig. 1. 4. The cytosolic pathway of cross-presentation. Exogenous antigens are internalised and escape from endocytic compartments into the cytosol where they are degraded by the proteasome. The resulting peptides are then loaded on MHC-I molecules in the lumen of the ER or endocytic compartments. Peptides in the ER lumen may be trimmed by ERAAP (Fig 1.2) while peptides in endocytic compartments are trimmed by insulin-regulated aminopeptidase (IRAP). The assembled peptide-MHC-I complexes then traffic to the cell surface for cross-presentation. The figure was created with Biorender and adapted from (*192*).

Analysis of isolated phagosomes *in vitro* confirmed that TAP can mediate peptide transport into the phagosome lumen (*201, 208*). Collectively, these findings raised the possibility that MHC-I loading of cross-presented peptides occurs in endocytic compartments rather than the ER.

The involvement of phagosomal TAP, rather than TAP in the ER, in cross-presentation of particulate antigen has so far not been demonstrated conclusively. However, using soluble antigen, one study documented that targeting an inhibitor of TAP (a viral protein called US6) to early endosomes by fusion with transferrin led to an inhibition of cross-presentation but not classical MHC-I presentation (*209*). In addition, using a specific monoclonal antibody (25D1.1), another study detected MHC I:SIINFEKL complexes on phagosomes which was taken as indirect evidence for peptide loading onto MHC-I molecules inside the phagosome (*201*). The authors suggested that the MHC-loading machinery may be delivered through the formation of a specialised ER-phagosome fusion compartments. However, this model was challenged by a later study which could not find any evidence for a contribution of ER membranes to phagosomes (*210*). Notably, this does not exclude other mechanisms of ER-phagosome communication such as the delivery of ER-resident proteins by Sec22b-mediated vesicle fusion (*69*). Another unresolved question concerns the source of recruited MHC-I molecules. While not mutually exclusive, some studies propose direct delivery of MHC-I from the ER (*206*) while others provide evidence for the participation of recycling MHC-I molecules in the TAP-dependent cross-presentation of exogenous antigen (*209*). Recently, a study showed that MHC-I molecules in the DC line DC3.2R were delivered to phagosomes in a Rab39-dependent manner and this could be inhibited by BFA arguing for a ER-Golgi origin (*211*).

In contrast to the vacuolar pathway, cross-presentation via the cytosolic pathway is enhanced by inhibiting degradation of antigen in endocytic compartments (*212, 213*). It has been suggested that increased antigen stability favours endocytic escape of intact proteins, or large protein fragments, and therefore enables the generation of proteasome-derived peptides for MHC-I loading (*170, 214, 215*). Accordingly, endocytic compartments of CD11c+ DCs have been shown to be less proteolytic than those of macrophages (*215*). Antigen stability in DCs is favoured by lower levels of lysosomal proteases and increased luminal pH which in turn dampens protease activity (*215, 216*). The increased pH results from an incomplete assembly of functional V-ATPase complexes as well as increased NADPH oxidase 2 (NOX2) activity (*37, 216*). Phagosomal recruitment of NOX2 is regulated by Rab27a and phagosomes of GM-CSF BMDCs from Rab27a-deficient mice displayed

increased acidification and enhanced proteolysis which was accompanied by inhibited cross-presentation (*217*). Finally, the routing of antigen into less degradative compartments is coupled to the mechanism of internalisation. For example, mannose-receptor-mediated endocytosis targets antigen to early endosomes which enhances cross-presentation (*218, 219*).

1.2.6 Pathways of endocytic escape in cross-presentation

A number of studies suggest that the endocytic escape of antigen is a rate-limiting step in cross-presentation (*220, 221*). Treatment of DCs with the lysosomotropic agent prazosin was shown to induce endolysosomal membrane damage which was accompanied by increased escape efficiency of soluble and cell-associated antigen and enhanced *in vitro* cross-priming. Similarly, fusion of a membrane disrupting moiety (Accum (*222*)) to ovalbumin led to an enhancement of cross-presentation *in vitro* and improved anti-cancer vaccination *in vivo (221)*. Antigen escape is believed to occur from early endocytic compartments due to the detection of full-length and enzymatically active proteins in the cytosol (*181, 182, 198, 199, 201, 207*). This is supported by kinetic experiments showing that antigens appear in the cytosol within 15 minutes (for soluble antigens) to 60 minutes (for particulate antigens) after internalisation (*198, 199, 201, 207*). Several studies suggested that the slower escape kinetics observed for particulate antigens indicates that these antigens require a certain level proteolysis due to the size-dependent nature of escape (*198, 207*). Accordingly, pulse-chase microscopy experiments showed that soluble dextrans with a molecular weight ranging from 3K to 40K are detectable in the cytosol, while those with a molecular weight between 500 and 2000K are not (*198*).

Several mechanisms have been put forward to explain the endocytic escape of antigen. Some studies invoke the existence of specific transporters (“transporter model”) while others propose that antigen escape following induction of endocytic membrane rupture (“rupture model”) (*223*). The transporter model emerged from studies in the early 2000s reporting the recruitment of Sec61 to phagosomes of cross-presenting DCs (*201, 207*). In earlier studies it had been shown that, in addition to its role in co-translational import of secretory proteins into the ER, Sec61 can act in the reverse direction to mediate protein transfer into the cytosol for ERAD (*224*). The first evidence for the involvement of Sec61 in cross-presentation came from a study showing that inhibition of retrotranslocation via Sec61, with the bacterial toxin Exotoxin A, prevented the transfer of exogenously delivered antigen into the cytosol and inhibited cross-presentation *in vitro* (*225*). Similarly, siRNA-mediated inhibition of Sec61 in GM-CSF BMDCs inhibited soluble ovalbumin entry into the cytosol and impaired cross-presentation (*226, 227*). The same results were obtained following intrabody-

mediated retention of Sec61 in the ER consistent with a role of Sec61 in retrotranslocation from endocytic compartments (*226*).

However, the involvement of Sec61 in ERAD itself remains controversial due to several technical issues in studies describing its role as a retrotranslocon (*228*). Additionally, its involvement in endocytic escape has been challenged by a study reporting that acute inhibition of Sec61 with mycolactone had no effect on antigen escape and cross-presentation (*229*). The same study further showed that prolonged inhibition of Sec61 inhibits cross-presentation indirectly due to the downregulation of MHC-I on the cell surface consistent with the role of Sec61 in co-translational protein biogenesis (*229*). Other proteins which function as potential protein channels in ERAD, instead of or in concert with Sec61, include the E3 ligase Hrd1 (*230*) and the protease Der1 (*231*) but there is no strong evidence implicating either of them in cross-presentation (*232*).

Another ERAD component that has been linked to endocytic escape is the cytosolic AAA ATPase p97. p97 associates with ERAD substrates as they exit the translocon and provides the energy for their release into the cytosol (*233*). RNAi-mediated inhibition of p97 or expression of a dominant-negative mutant of p97 led to a defect in cross-presentation in human DCs (*225, 234*). Further, addition of wild-type, but not mutant, p97 resulted in the ATP-dependent release of luciferase from isolated phagosomes *in vitro* (*225*). Notably, at least some ERAD substrates need to be unfolded prior to retrotranslocation suggesting that luciferase, and other enzymatically active model antigens used to study endocytic escape, would need to be refolded in the cytosol to be functional (*235*). In human DCs, refolding of exogenous luciferase was shown to be mediated by the heat-shock protein Hsp90 (*236*). Additionally, GM-CSF BMDCs from Hsp90-deficient mice were shown to be defective in endocytic escape of soluble ovalbumin and cross-presentation *in vitro* suggesting that Hsp90 plays a role in retrotranslocation of antigen (*237*).

The rupture model of endocytic escape emerged from a study in 1995 suggesting that large particles are cross-presented more efficiently than smaller ones because they cause phagosomal overload which ruptures endocytic compartments leading to more efficient escape (*167*). Over 10 years later, the first evidence emerged that endocytic rupture in DCs may be a regulated process. LPS stimulation of GM-BMDCs was shown to induce VAMP8-mediated recruitment of NOX2 to endosome and phagosomes which in turn resulted in increased ROS production and lipid peroxidation (*238, 239*). ROS-mediated lipid peroxidation increases the polarity of lipids and reduces the length of their lipid tails resulting in membrane destabilisation (*240*). Accordingly, inhibition of lipid peroxidation by α-tocopherol treatment or VAMP8 knockdown reduced the efficiency of endocytic escape and

led to a defect in cross-presentation *in vitro* (*238, 239*). In addition to NOX2, the aquaporin AQP3 has recently been shown to mediate lipid peroxidation and endocytic escape in cDC1s by importing hydrogen peroxide into the lumen of endocytic compartments (*241*). AQP3-deficient mice also showed a moderate decrease in cross-priming efficiency *in vivo* (*241*).

Finally, the endocytic receptor Clec9A, which is selectively expressed in cDC1s, has been implicated in mediating endocytic rupture following the internalisation of dead cell-associated antigens (*177*). The current model suggests that the engagement of F-actin-myosin (FM) complexes on dead cells by Clec9A triggers the activation of spleen tyrosine kinase (SYK) which then activates NOX2 by an unknown mechanism leading to lipid peroxidation and endocytic escape. SYK activation is mediated by a hemITAM motif in the cytosolic tail of Clec9A which engages SYK and induces its phosphorylation (*175*). Knockout of Clec9A in MutuDCs, a cDC1-like cell line (*242*), resulted in lower levels of phagosomal damage following uptake of FM-ovalbumin-coated beads, as measured by galectin-3 recruitment, and this phenotype could be rescued by overexpressing wild-type but not hemITAM signalling-incompetent Clec9A. In addition, it was shown that genetic ablation of NOX2 in Flt3-ligand BMDCs resulted in lower levels of phagosomal damage and a reduced efficiency of *in vitro* cross-priming of ovalbumin-specific CD8+ T cells. Finally, experiments in mixed bone marrow chimeras provided evidence that robust cross-priming of CD8+ T cells in response to FM-ovalbumin-conjugated beads required Clec9A and NOX2 expression specifically in cDC1s. Consistent with the rupture model, another study reported that RNAi-mediated inhibition of endosomal sorting complex required for transport (ESCRT)-III, a mediator for the repair of endocytic membrane damage, resulted in increased endocytic escape and cross-presentation *in vitro (243).*

In summary, several potential mediators of endocytic escape have been identified which either act as specific channels (Sec61) or as inducers of lipid peroxidation (NOX2, AQP3 and Clec9A). Even though the expression or activity of some of these mediators is enriched in cDC1s over cDC2s (NOX2 and Clec9a) (*244, 245*), their ablation does not completely abolish cross-presentation neither *in vitro* nor *in vivo* suggesting the existence of (partially) redundant pathways. More work is needed to untangle the proposed pathways of endocytic escape and establish which mediators are essential for cross-priming CD8+ T cell responses *in vivo* and under which conditions.

1.3 The pore-forming protein perforin-2 (Mpeg1)

At the start of my project, the Kozik lab had recently identified the pore-forming protein perforin-2 (Mpeg1) (*246, 247*) as a dedicated effector of endocytic escape in cDC1s and other cross-presenting APCs such as splenic macrophages. The discovery followed the

development of a flow cytometry-based endocytic escape assay that monitored the escape of saporin, a ribosome-inactivating enzyme similar to gelonin (*181, 248*) (see Chapter 3 for assay details). The assay was used in splenic cDC1-like MutuDCs (*242*) to screen a pooled CRISPR-Cas9 sgRNA library targeting 281 genes highly expressed in cDC1s relative to cDC2s. The screen yielded perforin-2 as the single strongest hit. Validation experiments confirmed that perforin-2 was required for endocytic escape in cDC1s, and ectopic expression of perforin-2 was sufficient to induce endocytic escape in nonimmune cells such as HEK293Ts. During the course of my project, Pablo Rodríguez Silvestre further showed that perforin-2-deficient mice failed to efficiently cross-prime CD8+ T cells in response to cell-associated, but not soluble, antigen *in vivo* (see (*249*) for experiment details).

1.3.1 The role of perforin-2 in anti-bacterial immunity

Perforin-2 was first identified in 1995 in a cDNA library screen as an intron-less gene that is highly expressed in mature macrophage cell lines (*250*). The study noted extensive sequence homology with perforin-1, a pore-forming protein expressed by cytotoxic CD8+ T cells and NK cells (*250*). Based on its sequence, perforin-2 was predicted to be a type I transmembrane protein with a luminal ectodomain and a short cytosolic C-terminal tail (*251*). Part of the ectodomain comprises a conserved fold known as the membrane attack complex/perforin (MACPF) domain. The domain name derives from earlier studies showing that components of the complement membrane attack complex (MAC; C6, C7, C8α, C8β and C9) and perforin-1 share extensive structural and functional similarities (*252-254*). When perforin-2 was discovered, both MAC and perforin-1 were already known to form pores and perform lytic functions in innate and adaptive immunity (*255, 256*). Based on the shared MACPF domain, as well as unpublished observations that perforin-2 overexpression was toxic to cells, a conference paper in 2007 proposed perforin-2 as the third pore-forming protein of the mammalian immune system (*251*).

With the advent of the BLAST search tool in 1997 (*257*), it became clear that members of the MACPF protein family were not only present in vertebrates but also in plants, protozoa, fungi and many bacteria (*258*). Equally, orthologues of perforin-2 were identified and cloned in several phyla of the kingdom *Animalia* including molluscs (*259-262*) and sea sponges (*263*). In the sponge S. *domunucla*, perforin-2 was shown to be upregulated upon LPS treatment and the recombinant ectodomain of its perforin-2 orthologue inhibited the growth of bacteria *in vitro (263).* Analogous results were reported for perforin-2 from molluscs implicating perforin-2 as an ancient effector of innate immunity against gram-positive and gram-negative bacteria in invertebrates (*260-262*). In line with these observations, bioinformatics analysis

suggested that a gene duplication of perforin-2 gave rise to the mammalian MAC and perforin-1 (*264*).

Experimental evidence for a role of perforin-2 in the mammalian immune system was first reported in 2013 by the Podack lab. One study showed that perforin-2 expression could be induced in murine embryonic fibroblasts (MEFs) by interferon (IFN) stimulation and knockdown of IFN-induced perforin-2 enhanced intracellular replication of gram-positive methicillin-resistant Staphylococcus *aureus*, gram-negative Salmonella *typhimurium* and acid-fast Mycobacterium *smegmatis (265).* A second study showed that knockdown of perforin-2 in macrophage cell lines resulted in increased intracellular replication of Chlamydia *trachomatis* while ectopic expression of perforin-2 in HeLa cells suppressed chlamydial growth (*266*). Later studies from the same group extended these findings showing that perforin-2 expression was required to control bacterial growth in neutrophils, BM-derived macrophages and parenchymal cells (*267-269*). Additionally, perforin-2-deficient mice were shown to be unable to control bacterial infections *in vivo (267-269).* Finally, germline mutations in perforin-2 have been associated with recurrent pulmonary non-tuberculous mycobacterial infections in humans (*270*).

The proposed model to explain the bactericidal activity of perforin-2 invoked that perforin-2 forms pores on the bacterial surface leading to direct lysis or the delivery of anti-microbial agents (*265-272*). In support of this model, transmission electron microscopy revealed putative perforin-2 pores on the surface of bacteria that were isolated from infected MEFs (*267*). In addition, perforin-2 rendered phagocytosed bacteria susceptible to the effects of lysozyme, ROS, nitric oxide and phagosomal proteases (*265, 267, 273*).

However, the role of perforin-2 in antibacterial immunity was recently challenged by a study which could not detect any defects in bacterial killing in an independently generated line of perforin-2-deficient mice (*274*). Similarly, in unpublished experiments, members of the Kozik lab could not reproduce the reported requirement for perforin-2 in controlling bacterial growth *in vitro*. The reason(s) for these discrepancies are currently unknown.

1.3.2 The regulation of pore formation by MAC and perforin-1

The three mammalian MACPF proteins MAC, perforin-1 and perforin-2 depend on cellular mechanisms to safely guide their activity. While perforin-2 has come into focus only recently, the mechanisms that regulate pore formation by MAC and perforin-1 have been under investigation for decades (*275*). Our understanding of these related mammalian MACPF proteins therefore often serves as a foundation for developing models of perforin-2 regulation.

The ability of mammalian MACPF proteins to form lytic oligomeric complexes has been known since the 1980s (*276, 277*). However, in the absence of structural data, an appreciation for the mechanism of pore formation remained elusive for many years. This changed when two studies in 2007 reported the crystal structures of the bacterial MACPF protein Plu-MACPF and mammalian complement C8α (*278, 279*). The structures revealed extensive structural homology with bacterial pore-forming cholesterol-dependent cytolysins (CDCs) suggesting that MACPF and CDC proteins represent two major branches of a MACPF/CDC superfamily (*258*). The conserved MACPF domain comprises a central, L-shaped β-sheet that harbours, at one end, two regions of α-helices known as transmembrane hairpins (TMHs) 1 and 2 (*278, 279*). Bioinformatics analysis further revealed a conserved Y/F-G-X_2-F/Y-X_6-G-G motif within the MACPF domain while the surrounding auxiliary domains were found to be highly divergent across the MACPF family (*280*).

The identified structural homology suggested that MACPF proteins may use a pore formation mechanism that is similar to that of CDC proteins (*281-286*). At the time, the CDC mechanism of pore formation was already well characterised thanks to extensive structural, biophysical and biochemical studies (*258, 278, 279*). In the archetypal MACPF/CDC mechanism, pore formation proceeds by sequential membrane binding and oligomerisation of monomers followed by membrane insertion. The signals that trigger the transition between soluble and pore conformations are, however, not fully understood. Membrane insertion is accompanied by dramatic structural rearrangements that include refolding of TMH1 and TMH2 into transmembrane β-hairpins. In the resulting β-barrel pores, each monomer typically contributes one four-stranded lipid-embedded β-sheet.

Both MAC and perforin-1 broadly conform to this archetypal mechanism although minor variations have been identified (*287-289*). Most notably, whereas perforin-1 and many CDC proteins are thought to assemble into pre-pores prior to the concerted release of their transmembrane β-hairpins, C9 subunits of the MAC may be recruited to the growing pore directly from solution undergoing the conformational transition one-by-one (*287, 288*). In addition, pore formation by perforin-1 may not always involve complete rings as both pre-pore and pore arcs have been observed *in vitro* (*289*).

MAC is the terminal effector of the complement pathway which primarily functions to form cytotoxic pores on the surface of microbes including gram-negative bacteria, enveloped viruses and parasites (*290-292*). The MAC components C5, C6, C7, C8 (comprising C8α, C8β, and C8γ), and C9 are secreted by hepatocytes and rely on an extracellular enzymatic chain reaction to assemble into a pore. The main pore-forming component, C9, is recruited to the target membrane by a complex that comprises C5b-C8 (C5b is a cleavage product of

C5). Assembly of the C5b-C8 complex is initiated by the recognition of a target through either the classical, lectin or alternative complement pathway (*293*). All pathways eventually converge on the cleavage of C3 yielding the active C3b fragment. C3b assembles into a complex that acts as a protease to cleave C5 into C5b which then binds C6 followed by C7(*287, 294-298*). Recruitment of C7 triggers a cascade of conformational changes within C6 and C7 which cause the TMHs in both C6 and C7 to unfurl and anchor the C5bC6C7 complex to the membrane (*287, 294, 298*). Subsequent binding of the C8 trimer then initiates polymerisation and membrane insertion of up to 18 copies of C9 (*287, 299*). Notably, the outlined MAC assembly cascade can be controlled at multiple stages. The GPI-anchored glycoprotein CD59 inhibits binding of C8 and C9 to the growing pore and helps to protect host cells from accidental MAC assembly (*300-302*). In addition, the soluble glycoproteins clusterin and vitronectin can inhibit C5b-8 formation or polymerisation of C9 subunits (*303, 304*).

Unlike MAC components, perforin-1 is stored intracellularly as a soluble protein in secretory granules of cytotoxic CD8+ T cells and natural killer cells (*305*). Upon granule secretion, perforin-1 pores deliver lethal granzyme proteases into target cells (*305*). Perforin-1 is synthesised as an immature pro-protein comprising the MACPF domain as well as an epidermal growth factor (EGF) domain and a C-terminal, Ca^{2+}-binding domain (C2) required for association with the membrane (*306, 307*). Immature perforin-1 is inactive partly because a bulky glycan in the C-terminal domain (Asn549) interferes with oligomerisation by steric hinderance (**Fig. 1.5A**) (*308*). This glycan is also important for efficient sorting of perforin-1 into post-Golgi cytotoxic granules (*309*). The granules are lysosome-related organelles containing proteases which cleave perforin-1 to remove a ~2 kDa C-terminal fragment, including the inhibitory Asn549-glycan (**Fig. 1.5A**) (*308, 310*). The processing can be carried out by multiple proteases and does not involve a specific cleavage motif (*308*). Removal of the C-terminal glycan primes perforin-1 for activation but the protein is nonetheless kept inactive by the low pH environment within the granule lumen (*306, 311*). Acidic pH leads to the protonation of key residues involved in ionic interactions between monomers thus preventing oligomerisation (*311*). In addition, protonation of Asp residues in the C2 domain is expected to reduce Ca^{2+} binding, which is critical for the association of perforin-1 with the target membrane (*306*).

In summary, MAC components and perforin-1 are synthesised as proproteins and their assembly into pores is primarily regulated at the stage of membrane binding and oligomerisation. Their activation requires proteolysis and/or an ionic environment that is conducive to pore formation.

1.3.3 The regulation of pore formation by perforin-2

Unlike MAC and perforin-1, perforin-2 is synthesised as an integral type I transmembrane protein comprising a large ectodomain and a short cytosolic tail (**Fig. 1.5A**) (*251*). The ectodomain is composed of a N-terminal MACPF domain, an EGF-like domain, a membrane-binding P2 domain (also known as a MABP (MVB12-associated β-prism)-like domain) as well as an unknown fold named CTT domain (*246, 247*).

As initially postulated by studies of perforin-2 in antibacterial immunity, recent cryo-EM structures showed that the soluble ectodomain (lacking the TM domain and cytosolic tail) can assemble into ring-like pre-pores and pores in solution (*246, 247*). The pre-pore comprises 16 subunits which form a central MACPF core with the P2 domain of each subunit

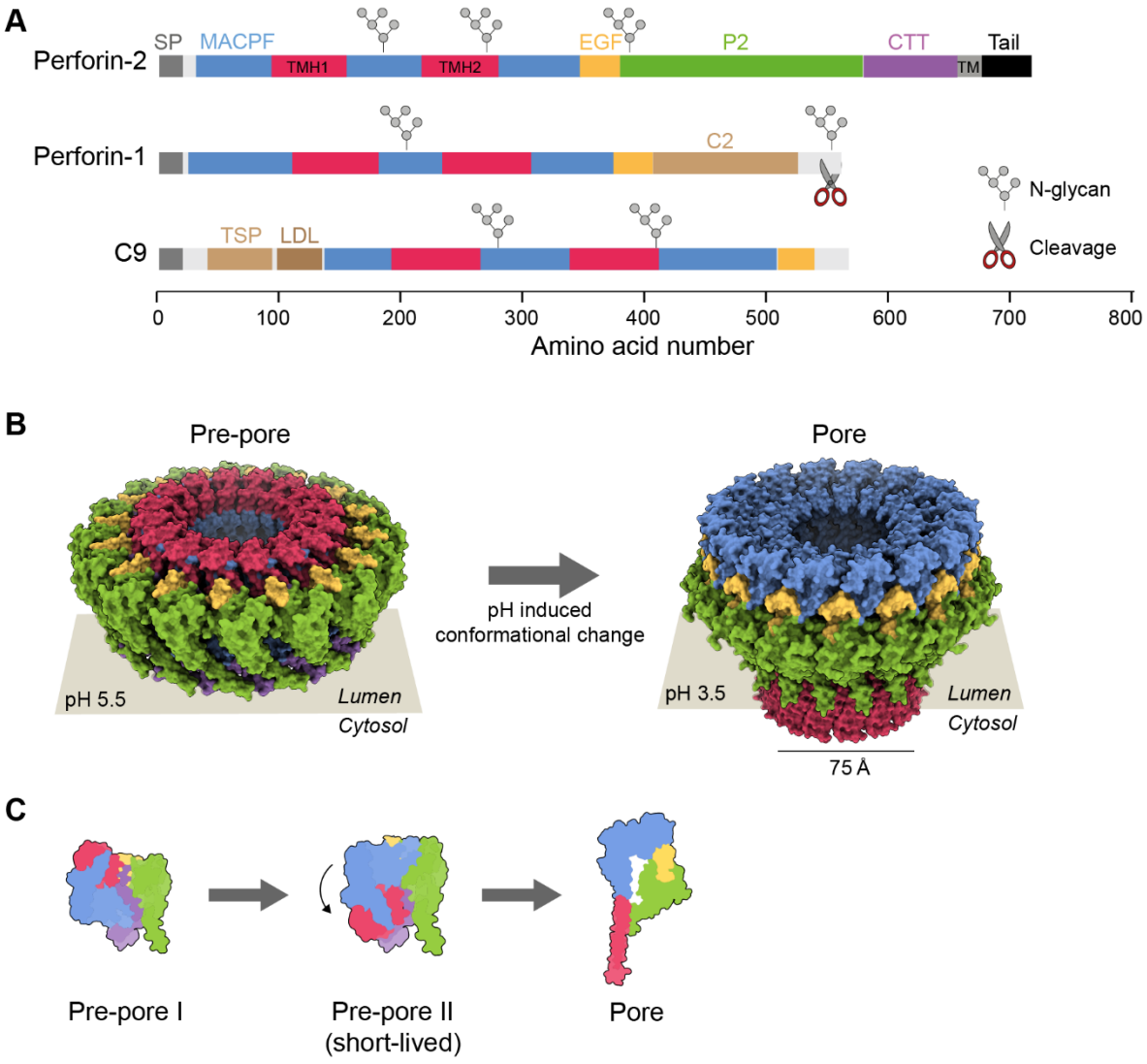

Fig. 1. 5. The regulation of pore formation by perforin-2. (**A**) Domain structure of perforin-2 and comparison to perforin-1 and complement C9. N-glycosylation sites as well as the regulatory cleavage of perforin-1 are also indicated. (**B**) Pre-pore (PDB 6SB3) and pore (PDB 6SB5) structures of the perforin-2 ectodomain (lacking the TMD and cytosolic tail). Acidification induces a 180° reorientation of the MACPF with respect to the membrane-binding P2 domain. (**C**) Current model of conformational transitions based on HS-AFM data (*312*). Note that the pre-pore II state has not been resolved structurally but is only inferred.

positioned around the periphery. In the absence of the TM domain, membrane-association is mediated by a β-hairpin in the P2 domain. The β-hairpin contains positively charged and hydrophobic residues which interact with the lipid bilayer in a similar way to the MABP domain of the ESCRT protein MVB12 (*313*). Interestingly, membrane-association via the P2 domain orients the MACPF domain in such a way that the TMH helices would unfurl into the vesicle lumen. Initially, it was proposed that this orientation may help to target phagocytosed bacteria while preventing accidental damage to host membranes (*246, 314*). However, further structural and biophysical characterisation suggested that the pre-pore-to-pore transition involves a ~180° reorientation of the MACPF with respect to the P2 domain (**Fig. 1.5B**) (*247, 312, 315*). This dramatic conformational change could be induced by prolonged incubation in acidified buffer (pH 4.0 – 3.6) suggesting a potential regulatory mechanism to control perforin-2 activity inside cells (*247, 315*).

High-speed atomic force microscopy (HS-AFM) imaging and molecular dynamics simulations indicated that acidification leads to the protonation of titratable residues at interface of neighbouring subunits within the pre-pore ring (*312*). As result, inter-subunit contacts are destabilised leading to ring-opening which enables the ~180° reorientation of the MACPF domain and subsequent unfurling of the TMH helices (*312*). Thus, unlike any other MACPF/CDC protein, perforin-2 appears to adopt two pre-pore conformations, both an early-stage pre-pore with MACPF and P2 domains positioned in functionally opposite directions and a late-stage pre-pore with the two domains oriented towards the target membrane (**Fig. 1.5C**).

In contrast to the extensive structural and biophysical characterisation, little is known about the regulation of perforin-2 in an intracellular context. Under steady-state conditions, overexpressed GFP- or RFP-tagged perforin-2 displays diffuse, perinuclear staining which potentially indicates localisation to post-Golgi vesicles (*266, 267*). Upon phagocytosis of bacteria or latex beads, perforin-2 was shown to be recruited to phagosomes (*267, 316*). A potential role for proteolysis in the regulation of perforin-2 was suggested after perforin-2 fragments were observed following bacterial infection of MEFs expressing GFP-tagged perforin-2 (*267*). However, neither the cleavage site(s) nor the relevant protease(s) have been identified and the functional relevance of proteolysis is still unclear.

1.4 Objective

In mouse DCs, perforin-2 is ranked as the top 55th protein by abundance with an estimated $3x10^6$ copies present within each cell (*220, 317*). Yet, how such large amounts of perforin-2 are safely stored and deployed remains largely unexplored. Hence, during

my PhD project I attempted to shed light on how DCs can assemble perforin-2 pores on their own membranes for endocytic escape without causing uncontrolled lysis of intracellular compartments. Specifically, the aims of my project were to investigate how perforin-2-mediated endocytic escape is regulated by 1) phagosomal pH, 2) proteolysis and 3) regulated trafficking of perforin-2.

Chapter 2 – Materials and Methods

2.1 Materials

2.1.1 Antibodies

Table 2.1 Antibodies used in this thesis

Target	Clone	Species	Fluorophore	Working dilution	Supplier	Catalogue number
Biotin	n.a.	Streptavidin	eF450	1:1000	Thermo	48-4317-82
Biotin	n.a.	Streptavidin	AF488	1:1000	Thermo	S11223
BiP	C50B12	Rabbit	n.a.	1:1000	Cell Signaling	3177T
Cathepsin B	D1C7Y	Rabbit	n.a.	1:1000	Cell Signaling	31718T
CD11b	M1/70	Rat	eF450	1:300	Thermo	48-0112-82
CD11c	N418	Hamster	BV605	1:300	BioLegend	117333
CD11c	N418	Hamster	FITC	1:300	BioLegend	117306
CD172a	P84	Rat	BV421	1:300	BD	740071
Cytochrome C	D18C7	Rabbit	n.a.	1:1000	Cell Signaling	11940T
F4/80	T45-2342	Rat	BUV395	1:300	BD	565614
Fixable Viability Dye	n.a.	n.a.	ViaKrome808	1:1000	Beckman	C36628
Goat IgG	Polyclonal	Donkey	AF488	1:1000	Thermo	A11055
Lamp1	1D4B	Rat	Biotin	1:200	Thermo	13-1071-92
Lamp1	1D4B	Rat	n.a.	1:200	BioLegend	121601
MHC-II	M5/114.152	Rat	BV785	1:300	BioLegend	107645
Mouse IgG	Polyclonal	Donkey	AF647	1:1000	Thermo	A31571
Mouse IgG	Polyclonal	Donkey	AF555	1:500	Thermo	A31570
Ovalbumin	Polyclonal	Goat	n.a.	1:200	OriGene	AP33373SU-N
Ovalbumin	Tosgaa1	Mouse	n.a.	1:200	BioLegend	520402
Ovalbumin	Polyclonal	Rabbit	n.a.	1500	Merck	C6534
Perforin-2 C-term	Polyclonal	Rabbit	n.a.	1:500	Biosynth	Custom-made
Perforin-2 MACPF	Polyclonal	Rabbit	n.a.	1:500	Cloud-clone	PAB352Mu01
Perforin-2 N-term	Polyclonal	Rabbit	n.a.	1:500	Biosynth	Custom-made
Perforin-2 P2	Polyclonal	Rabbit	n.a.	1:500	Biosynth	Custom-made
Puromycin	12D10	Mouse	AF647	1:200	Merck	MABE343-AF647
Puromycin	12D10	Mouse	n.a.	1:200	Merck	MABE343
Rabbit IgG	Polyclonal	Donkey	AF555	1:1000	Abcam	Ab150062
Rabbit IgG	Polyclonal	Donkey	AF647	1:1000	Abcam	Ab150075
Rabbit IgG	Polyclonal	Donkey	AF680	1:500	Thermo	A10043
Rabbit IgG	Polyclonal	Donkey	AF488	1:1000	Abcam	Ab150073
Saporin	Polyclonal	Rabbit	n.a.	1:300	Thermo	PA1-18425
Siglec-H	eBio440c	Rat	APC	1:300	Thermo	17-0333-82
Vps35	A21109	Mouse	n.a.	1:1000	SantaCruz	Sc-374372
XCR1	ZET	Mouse	BV785	1:300	BioLegend	148225

2.1.2 Plasmids

Table 2.2 Plasmids used in this thesis

Plasmid	Description	Markers	Origin
pHR-mScarlet	Lentiviral vector expressing mScarlet	Ampicillin	Kozik lab; Derived from Addgene #60906
pHR-MPEG1-IRES-mScarlet	Lentiviral vector expressing wild-type murine Mpeg1	Ampicillin, IRES-mScarlet	Kozik lab; Derived from Addgene #60906
pHR-MPEG1-SbfI-IRES-mScarlet	Lentiviral vector expressing murine Mpeg1 with a silent point mutation at codon 495 to introduce a SbfI site	Ampicillin, IRES-mScarlet	This thesis
pHR-MPEG1-SbfI-IRES-mScarlet G212V/A213V	Lentiviral vector expressing murine Mpeg1 carrying the G212V and A213V mutations	Ampicillin, IRES-mScarlet	This thesis
pHR-MPEG1-SbfI-IRES-mScarlet K251C/G286C	Lentiviral vector expressing murine Mpeg1 carrying the K251C and G286C mutations	Ampicillin, IRES-mScarlet	This thesis
Lenti-sgRNA-hygro	Lentiviral vector for sgRNA expression	Ampicillin, Hygromycin	Addgene #104991
Lenti-sgRNA-hygo-Ncstn	Lentiviral vector expressing sgRNA against Ncstn	Ampicillin, Hygromycin	This thesis
Lenti-sgRNA-hygo-Psen2	Lentiviral vector expressing sgRNA against Psen2	Ampicillin, Hygromycin	This thesis
Lenti-sgRNA-hygro-Aph1c	Lentiviral vector expressing sgRNA against Aph1c	Ampicillin, Hygromycin	This thesis
pHR-MPEG1-SbfI-IRES-mScarlet YxxPhi	Lentiviral vector expressing murine Mpeg1 carrying the YxxPhi mutation	Ampicillin, IRES-mScarlet	This thesis
pHR-MPEG1-SbfI-IRES-mScarlet Tailless	Lentiviral vector expressing murine Mpeg1 carrying the Tailless mutation	Ampicillin, IRES-mScarlet	This thesis
psPAX2	Lentiviral packaging vector	Ampicillin	Addgene #12260
pMD2.g	VSV-G envelop expressing vector	Ampicillin	Addgene #12250

2.1.3 Reagents

Table 2.3 Reagents used in this thesis

Item	Supplier	Catalogue number
20X TBS buffer	Thermo	28358
Amicon Ultra-15 centrifugal filters	Amicon	UFC9003
Bafilomycin A1	Cayman	11038
BCA protein assay kit	Thermo	23227
BD Cytofix/Cytoperm kit	BD Biosciences	554714
BlpI	NEB	R0585S
Bolt Reducing agent	Thermo	NP0009
Brefeldin A	Santa Cruz	Sc-200861c
BSA	Merck	A7979
BsmBI	NEB	R0739
BstXI	NEB	R0113L
Bsu36I	NEB	R0524S
CO_2-independent medium	Thermo	18045088
DAPI	Cell Signaling	4083
Dialyzed FBS	Thermo	A3382001
DMEM	Gibco	31966021
DNAse I	Merck	11284932001
DNeasy blood and tissue kit	Qiagen	69504
DTT	Merck	D9779
EasyTag™ EXPRESS35S Protein Labeling Mix, [35S]-, 2mCi	Perkin Elmer	NEG772002MC
ECL prime reagent	Cytiva	RPN2236
ECL reagent	Cytiva	RPN2209
EDTA	Thermo	15575020
EDTA-free protease inhibitor cocktail	Roche	11873580001
Endo H	NEB	P0702L
EZ-Link Sulfo-NHS-LC-Biotinylation Kit	Thermo	21435
FBS	HyClone	SH30084.03
Flat3 Ligand	Miltenyi	130-097-372
Gel extraction kit	Qiagen	28706X4
Glutamax	Gibco	12440053
Glutaraldehyde	Merck	G5882
Glycine	Merck	G5417
GM-CSF	Miltenyi	130-095-746
HEPES	Gibco	15630106
Hygromycin B	Thermo	10687010
IMDM	Gibco	31980030
Imidazole	Merck	56748
Liberase-TL	Merck	5401020001
Lysotracker Red DND-99	Thermo	L7528
MluI-HF	NEB	R0198S
Mouse pan-dendritic cell isolation kit	Miltenyi	130-1000-875
NaCl	Fisher Scientific	S/3120/63

Non-essential amino acids	Gibco	11140050
NuPage LDS sample buffer	Thermo	NP0007
Ovalbumin	Worthington	LS0030540
Opti-MEM	Thermo	31985062
PBS	Thermo	14190144
PCR purification kit	Qiagen	28104
Penicillin/streptomycin	Gibco	11548876
pHrodo iFL Red STP ester, amine reactive dye	Thermo	P36011
Plasmid maxi kit	Qiagen	12162
Plasmid mini kit	Qiagen	12123
PMSF	Merck	P7626
PNGase F	NEB	P0704L
Polybead Amino Microspheres 3.00 µm	Polysciences	17145-5
Poly-L-lysine	R&D systems	3438-100-01
Prolong Gold with DAPI	Thermo	P36931
Puromycin	Thermo	A1113803
Q5 DNA polymerase	NEB	M0491S
Quick CIP	NEB	M0525S
Red Blood Cell Lysis Buffer Hybri-Max	Merck	R7757-100ML
RIPA buffer	Thermo	R0278
RPMI-1640	Gibco	6180036
RPMI-1640 lacking methionine and cystine	Merck	R7513
Saporin	Merck	S9896
SbfI-HF	NEB	R3642L
SDPD	Thermo	21857
SnaBI	NEB	R0130S
Sodium pyruvate	Gibco	11360070
Sucrose	Fisher Scientific	1046150
T4 DNA ligase	NEB	M0202
T4 Polynucleotide Kinase	NEB	M0201S
Top10 chemically competent E. *coli*	Thermo	C404003
TransIT-LT1	Mirus	MIR2304
Traut's reagent	Thermo	26101
Triton X-100	Fisher Bioreagents	BP151-500
Trypsin	Merck	T6567
Tween-20	G-Bioscience	786-517
Zeba Spin 7K MWCO desalting columns	Thermo	10415545
β-mercaptoethanol	Gibco	31350010
µ-slide 8-well chamber	Ibidi	80826
InstantBlue Coomassie stain	Abcam	Ab119211

2.1.4 Protease inhibitors

Table 2.4 Protease inhibitors used in this thesis

Inhibitor	Target	Supplier	Catalogue Number
DAPT	γ-secretase	Cambridge Bioscience	SM15-10
E64D	Cysteine proteases	Merck	E3132
GI254023	ADAM10 and ADAM17	Bio-Techne	3995
GM6001	Matrix metalloproteinases	Bio-Techne	2983
GW280264x	ADAM10 and ADAM17	Bio-Techne	7030
Leupeptin A	Serine/Cysteine proteases	Merck	L2884
LY-411,575	γ-secretase	Miltenyi	130-103-924
LY-685,458	γ-secretase	Bio-Techne	2627
Pepstatin A	Aspartic proteases	Merck	P5318
TAPI-2	ADAM17 and matrix metalloproteinases	Bio-Techne	6013
Verubecestat	β-secretase	Cambridge Bioscience	21115
Z-FA-FMK	Cysteine proteases	Santa Cruz	Sc-201303
Z-VAD-FMK	Cysteine proteases	Stratech Scientific	A1902-APE

2.1.5 Equipment

Table 2.5 Equipment used in this thesis

Equipment	Manufacturer	Catalogue Number
iBlot 1 Gel Transfer Device	Thermo	IB1001 (discontinued)
Bioruptor Plus sonication device	Hologic Diagenode	B01020001
CytoFLEX Flow cytometer	Beckman Coulter	NA
Optima MAX-XP Ultracentrifuge	Beckman Coulter	NA

2.2. Cloning

2.2.1 Generation of Mpeg1 expression plasmids

Vectors and gene fragments were digested for 2 hours at 37°C with the restriction enzymes indicated below. Digested vectors were gel purified from a 1% agarose gel using the QIAquick Gel extraction kit and digested gene fragments were purified using the QIAquick PCR purification kit. Ligations were performed using T4 DNA ligase according to the manufacturer's instructions. Transformations were performed using Top10 chemically-competent E. coli according to the manufacturer's instructions.

All Mpeg1 variants were generated by cloning gene fragments (**Table 2.5**) into pHR-MPEG1-IRES-mScarlet which was already available in the lab. The wild-type murine Mpeg1 was replaced with the WT-Mpeg1^{SbfI} encoding wild-type murine Mpeg1 with a silent point mutation to introduce a SbfI restriction site. The gene fragment was cloned using BstXI and BlpI restriction enzymes. pHR-MPEG1-SbfI-IRES-mScarlet-G212V/A213V and pHR-

MPEG1-SbfI-IRES-mScarlet-K215C/G286C were cloned by inserting the respective gene fragments using BstXI and SbfI restriction enzymes. pHR-MPEG1-SbfI-IRES-mScarlet-YxxPhi was cloned by inserting the gene fragment using BstXI and BlpI restriction enzymes. pHR-MPEG1-SbfI-IRES-mScarlet-Tailess were cloned by inserting the gene fragments using SnaBI and Bsu36I restriction enzymes.

Table 2.5

Gene fragment	Sequence (5' – 3')
WT-Mpeg1^{SbfI}	ACGAAGATGGCCACCTACCTGGCAGAGCTCTTGATCCTCAACTATGGCACACACGTAATCACCAGTGTGGAT GCTGGGGCTGCACTGGTTCAGGAGGATCACGTAAGATCCTCCTTCCTTCTGGACAACCAGAATAGCCAGAAC ACCGTGACCGCTTCTGCAGGGATTGCCTTCTTAAACATTGTGAACTTCAAAGTTGAAACAGACTACATTTCTC AGACCAGTTTGACGAAGGACTACCTGTCGAACAGGACCAACTCCAGGGTGCAGAGTTTTGGAGGGGTTCCC TTCTATCCAGGCATCACCTTAGAAACCTGGCAGAAGGGCATCACTAACCACCTAGTGGCAATAGACCGTGCT GGCTTGCCTCTGCATTTCTTCATTAAACCTGACAAGCTACCTGGCTTGCCAGGTCCCTTGGTGAAGAAGCTG TCAAAGACAGTGGAAACTGCTGTGAGACACTATTACACTTTTAACACTCACCCAGGATGCACAAATGTTGATT CCCCCAACTTTAATTTTCAAGCCAATATGGATGATGATTCCTGTGATGCGAAAGTCACCAACTTCACATTTGGT GGAGTTTATCAGGAATGCACTGAACTGTCAGGTGATGTTCTTTGCCAAAACCTCGAGCAGAAGAACCTGCTC ACAGGTGATTTCTCTTGTCCCCCTGGCTACACCCCTGTCCATCTGCTCTCCCAGACCCATGAAGAGGGTTAC AGTCGTCTGGAATGTAAAAAGAAATGCACCCTCAAGATTTTCTGCAAGACAGTGTGTGAAGATGTGTTCAGAG TGGCCAAGGCTGAATTTAGGGCTTATTGGTGTGTGGCTGCTGGCCAAGTACCTGACAACTCAGGACTTCTCT TTGGAGGAGTCTTCACTGACAAGACCATCAACCCTATGACAAATGCACAGTCATGCCCTGCAGGCTACATCC CACTGAACCTGTTTGAAAGCCTCAAGGTATGTGTGTCCCTGGATTATGAGTTGGGGTTCAAGTTTTCAGTCCC CTTTGGTGGGTTCTTCAGTTGTATAATGGGGAACCCCTTGGTTAATTCTGATACAGCTAAAGACGTCAGAGCA CCATCTCTGAAAAAGTGTCCCGGGGGCTTCAGCCAACACCTAGCTGTTATCAGTGATGGATGCCAAGTGTCC TACTGTGTCAAGGCTGGAATCTTCACAGGAGGGTCCCTGCTCCCTGTCAGGCTCCCACCTTATACCAAACCA CCTCTTATGAGCCAGGTTGCCACCAACACTGTCATAGTGACCAATAGTGAGACTGCCAGATCCTGGATTAAGG ACCCTCAGACCAACCAGTGGAAGCTGGGAGAACCTCTGGAGCTACGTAGGGCCATGACAGTCATCCATGGG GACAGTAATGGAATGTCAGGAGGGGAAGCTGCTGGAATCACTTTGGGAGTCACCATAGCACTAGGAGTTGTC ATTACCTTGGCCATCTATGGTACTCGGAAGTACAAGAAGAAGGAATACCAGGAAATTGAGGAGCAGGAGAGT TTGGTTGGAAGCTTAGCAACAGATGCA
Mpeg1$^{G212A/V213A}$	TGTGACCAACTAGAGAAAAACCAGACGAAGATGGCCACCTACCTGGCAGAGCTCTTGATCCTCAACTATGGC ACACACGTAATCACCAGTGTGGATGCTGTGGTCGCACTGGTTCAGGAGGATCACGTAAGATCCTCCTTCCTT CTGGACAACCAGAATAGCCAGAACACCGTGACCGCTTCTGCAGGGATTGCCTTCTTAAACATTGTGAACTTC AAAGTTGAAACAGACTACATTTCTCAGACCAGTTTGACGAAGGACTACCTGTCGAACAGGACCAACTCCAGG GTGCAGAGTTTTGGAGGGGTTCCCTTCTATCCAGGCATCACCTTAGAAACCTGGCAGAAGGGCATCACTAAC CACCTAGTGGCAATAGACCGTGCTGGCTTGCCTCTGCATTTCTTCATTAAACCTGACAAGCTACCTGGCTTGC CAGGTCCCTTGGTGAAGAAGCTGTCAAAGACAGTGGAAACTGCTGTGAGACACTATTACACTTTTAACACTC ACCCAGGATGCACAAATGTTGATTCCCCCAACTTTAATTTTCAAGCCAATATGGATGATGATTCCTGTGATGCG AAAGTCACCAACTTCACATTTGGTGGAGTTTATCAGGAATGCACTGAACTGTCAGGTGATGTTCTTTGCCAAA ACCTCGAGCAGAAGAACCTGCTCACAGGTGATTTCTCTTGTCCCCCTGGCTACACCCCTGTCCATCTGCTCT CCCAGACCCATGAAGAGGGTTACAGTCGTCTGGAATGTAAAAAGAAATGCACCCTCAAGATTTTCTGCAAGA CAGTGTGTGAAGATGTGTTCAGAGTGGCCAAGGCTGAATTTAGGGCTTATTGGTGTGTGGCTGCTGGCCAAG TACCTGACAACTCAGGACTTCTCTTTGGAGGAGTCTTCACTGACAAGACCATCAACCCTATGACAAATGCACA GTCATGCCCTGCAGGCTACATCCCACTGAACCTGTTTGAAAGCCTCAAGGTATGT
Mpeg1$^{K251C/G286C}$	TGTGACCAACTAGAGAAAAACCAGACGAAGATGGCCACCTACCTGGCAGAGCTCTTGATCCTCAACTATGGC ACACACGTAATCACCAGTGTGGATGCTGGGGCTGCACTGGTTCAGGAGGATCACGTAAGATCCTCCTTCCTT CTGGACAACCAGAATAGCCAGAACACCGTGACCGCTTCTGCAGGGATTGCCTTCTTAAACATTGTGAACTTC TGCGTTGAAACAGACTACATTTCTCAGACCAGTTTGACGAAGGACTACCTGTCGAACAGGACCAACTCCAGG GTGCAGAGTTTTGGAGGGGTTCCCTTCTATCCATGCATCACCTTAGAAACCTGGCAGAAGGGCATCACTAAC CACCTAGTGGCAATAGACCGTGCTGGCTTGCCTCTGCATTTCTTCATTAAACCTGACAAGCTACCTGGCTTGC CAGGTCCCTTGGTGAAGAAGCTGTCAAAGACAGTGGAAACTGCTGTGAGACACTATTACACTTTTAACACTC ACCCAGGATGCACAAATGTTGATTCCCCCAACTTTAATTTTCAAGCCAATATGGATGATGATTCCTGTGATGCG AAAGTCACCAACTTCACATTTGGTGGAGTTTATCAGGAATGCACTGAACTGTCAGGTGATGTTCTTTGCCAAA ACCTCGAGCAGAAGAACCTGCTCACAGGTGATTTCTCTTGTCCCCCTGGCTACACCCCTGTCCATCTGCTCT CCCAGACCCATGAAGAGGGTTACAGTCGTCTGGAATGTAAAAAGAAATGCACCCTCAAGATTTTCTGCAAGA CAGTGTGTGAAGATGTGTTCAGAGTGGCCAAGGCTGAATTTAGGGCTTATTGGTGTGTGGCTGCTGGCCAAG TACCTGACAACTCAGGACTTCTCTTTGGAGGAGTCTTCACTGACAAGACCATCAACCCTATGACAAATGCACA GTCATGCCCTGCAGGCTACATCCCACTGAACCTGTTTGAAAGCCTCAAGGTATGT
Mpeg1^{YxxPhi}	ACGAAGATGGCCACCTACCTGGCAGAGCTCTTGATCCTCAACTATGGCACACACGTAATCACCAGTGTGGAT GCTGGGGCTGCACTGGTTCAGGAGGATCACGTAAGATCCTCCTTCCTTCTGGACAACCAGAATAGCCAGAAC ACCGTGACCGCTTCTGCAGGGATTGCCTTCTTAAACATTGTGAACTTCAAAGTTGAAACAGACTACATTTCTC AGACCAGTTTGACGAAGGACTACCTGTCGAACAGGACCAACTCCAGGGTGCAGAGTTTTGGAGGGGTTCCC TTCTATCCAGGCATCACCTTAGAAACCTGGCAGAAGGGCATCACTAACCACCTAGTGGCAATAGACCGTGCT GGCTTGCCTCTGCATTTCTTCATTAAACCTGACAAGCTACCTGGCTTGCCAGGTCCCTTGGTGAAGAAGCTG TCAAAGACAGTGGAAACTGCTGTGAGACACTATTACACTTTTAACACTCACCCAGGATGCACAAATGTTGATT CCCCCAACTTTAATTTTCAAGCCAATATGGATGATGATTCCTGTGATGCGAAAGTCACCAACTTCACATTTGGT GGAGTTTATCAGGAATGCACTGAACTGTCAGGTGATGTTCTTTGCCAAAACCTCGAGCAGAAGAACCTGCTC ACAGGTGATTTCTCTTGTCCCCCTGGCTACACCCCTGTCCATCTGCTCTCCCAGACCCATGAAGAGGGTTAC

	AGTCGTCTGGAATGTAAAAAGAAATGCACCCTCAAGATTTTCTGCAAGACAGTGTGTGAAGATGTGTTCAGAG TGGCCAAGGCTGAATTTAGGGCTTATTGGTGTGTGGCTGCTGGCCAAGTACCTGACAACTCAGGACTTCTCT TTGGAGGAGTCTTCACTGACAAGACCATCAACCCTATGACAAATGCACAGTCATGCCCTGCAGGCTACATCC CACTGAACCTGTTTGAAAGCCTCAAGGTATGTGTGTCCCTGGATTATGAGTTGGGGTTCAAGTTTTCAGTCCC CTTTGGTGGGTTCTTCAGTTGTATAATGGGGAACCCCTTGGTTAATTCTGATACAGCTAAAGACGTCAGAGCA CCATCTCTGAAAAAGTGTCCCGGGGGCTTCAGCCAACACCTAGCTGTTATCAGTGATGGATGCCAAGTGTCC TACTGTGTCAAGGCTGGAATCTTCACAGGAGGGTCCCTGCTCCCTGTCAGGCTCCCACCTTATACCAAACCA CCTCTTATGAGCCAGGTTGCCACCAACACTGTCATAGTGACCAATAGTGAGACTGCCAGATCCTGGATTAAGG ACCCTCAGACCAACCAGTGGAAGCTGGGAGAACCTCTGGAGCTACGTAGGGCCATGACAGTCATCCATGGG GACAGTAATGGAATGTCAGGAGGGGAAGCTGCTGGAATCACTTTGGGAGTCACCATAGCACTAGGAGTTGTC ATTACCTTGGCCATCTATGGTACTCGGAAGTACAAGAAGAAGGAAGCTCAGGAAGCTGAGGAGCAGGAGAGT TTGGTTGGAAGCTTAGCAACAGATGCA
Mpeg1^{Tailless}	ACGAAGATGGCCACCTACCTGGCAGAGCTCTTGATCCTCAACTATGGCACACACGTAATCACCAGTGTGGAT GCTGGGGCTGCACTGGTTCAGGAGGATCACGTAAGATCCTCCTTCCTTCTGGACAACCAGAATAGCCAGAAC ACCGTGACCGCTTCTGCAGGGATTGCCTTCTTAAACATTGTGAACTTCAAAGTTGAAACAGACTACATTTCTC AGACCAGTTTGACGAAGGACTACCTGTCGAACAGGACCAACTCCAGGGTGCAGAGTTTTGGAGGGGTTCCC TTCTATCCAGGCATCACCTTAGAAACCTGGCAGAAGGGCATCACTAACCACCTAGTGGCAATAGACCGTGCT GGCTTGCCTCTGCATTTCTTCATTAAACCTGACAAGCTACCTGGCTTGCCAGGTCCCTTGGTGAAGAAGCTG TCAAAGACAGTGGAAACTGCTGTGAGACACTATTACACTTTTAACACTCACCCAGGATGCACAAATGTTGATT CCCCCAACTTTAATTTTCAAGCCAATATGGATGATGATTCCTGTGATGCGAAAGTCACCAACTTCACATTTGGT GGAGTTTATCAGGAATGCACTGAACTGTCAGGTGATGTTCTTTGCCAAAACCTCGAGCAGAAGAACCTGCTC ACAGGTGATTTCTCTTGTCCCCCTGGCTACACCCCTGTCCATCTGCTCTCCCAGACCCATGAAGAGGGTTAC AGTCGTCTGGAATGTAAAAAGAAATGCACCCTCAAGATTTTCTGCAAGACAGTGTGTGAAGATGTGTTCAGAG TGGCCAAGGCTGAATTTAGGGCTTATTGGTGTGTGGCTGCTGGCCAAGTACCTGACAACTCAGGACTTCTCT TTGGAGGAGTCTTCACTGACAAGACCATCAACCCTATGACAAATGCACAGTCATGCCCTGCAGGCTACATCC CACTGAACCTGTTTGAAAGCCTCAAGGTATGTGTGTCCCTGGATTATGAGTTGGGGTTCAAGTTTTCAGTCCC CTTTGGTGGGTTCTTCAGTTGTATAATGGGGAACCCCTTGGTTAATTCTGATACAGCTAAAGACGTCAGAGCA CCATCTCTGAAAAAGTGTCCCGGGGGCTTCAGCCAACACCTAGCTGTTATCAGTGATGGATGCCAAGTGTCC TACTGTGTCAAGGCTGGAATCTTCACAGGAGGGTCCCTGCTCCCTGTCAGGCTCCCACCTTATACCAAACCA CCTCTTATGAGCCAGGTTGCCACCAACACTGTCATAGTGACCAATAGTGAGACTGCCAGATCCTGGATTAAGG ACCCTCAGACCAACCAGTGGAAGCTGGGAGAACCTCTGGAGCTACGTAGGGCCATGACAGTCATCCATGGG GACAGTAATGGAATGTCAGGAGGGGAAGCTGCTGGAATCACTTTGGGAGTCACCATAGCACTAGGAGTTGTC ATTACCTTGGCCATCTATGGTACTCGGAAGTACAAGAAGAAGGAAGCTCAGGAAGCTGAGGAGCAGGAGAGT TTGGTTGGAAGCTTAGCAACAGATGCA

2.2.2 Generation of sgRNA expression plasmids

To generate sgRNA expression plasmids, Lenti-sgRNA-hygro was digested with BsmBI, dephosphorylated using Quick CIP according to the manufacturer's instructions and purified using the QIAquick PCR purification kit. The sgRNA oligos were purchased as IDT RxnReady Primer Pools (**Table 2.6**). The oligos were phosphorylated using T4 Polynucleotide Kinase according to the manufacturer's instructions and then heated to 95°C for 5 minutes to ensure hybridisation. The cut vector and hybridised oligos were then ligated and transformed as described in Section 2.2.1.

Table 2.6 Sequences of sgRNA oligos

Target	Forward oligo (5'-3')	Reverse oligo (5'-3')
Aph1c	CACCGGCGCAACCGAAGAACAC	AAACGTGTTCTTCGGTTGCGCC
Ncstn	CACCGCCAGCTGAGTGACAAAGG	AAACCCTTTGTCACTCAGCTGGC
Psen2	CACCGATGGCACCCAAGATGACCC	AAACGGGTCATCTTGGGTGCCATC
Non-targeting (NT)	CACCACCGGTCGAAGTCTGGGATT	AAACAATCCCAGACTTCGACCGGT

2.3 Cell culture

The MutuDC1940 cell line (Supplier: abm, catalogue number: T0528) used in this study was derived from CD11c:SV40LgT-transgenic C57/BL/6 mice (*318*). The cell line was generated

by long-term *in vitro* culture of isolated splenocytes which selected for immortalised splenic CD8α+ cDCs (*319*). MutuDCs stably express cytosolic GFP due to the GFP reporter in the CD11c:SV40LgT transgene.

Non-targeting (NT) control, Mpeg1^{KO} and AEP^{KO} MutuDCs were already available in the lab. Briefly, a stable line of Cas9-expressing MutuDCs was generated by lentiviral transduction of wild-type MutuDCs with a lentiCas9-Blast vector (Addgene #52962). Following blasticidin selection of the bulk population, Cas9-expressing MutuDCs were transduced with a lentivirus carrying the respective sgRNAs (non-targeting, anti-Mpeg1 or anti-AEP) and blue fluorescent protein (BFP) as a selection marker. Each cell line was established by sorting for the bulk BFP positive population. Knockout efficiency in each sorted population was analysed by Sanger sequencing and TIDE analysis (disruption efficiency of at least 80%) as well as by Western blot analysis (protein depletion of at least 75%). NT and Mpeg1^{KO} MutuDCs have been described in (*249*).

MutuDCs were maintained in IMDM supplemented with 8% heat-inactivated FBS, 10 mM HEPES, 500 µM 2-mercaptoethanol, 1X GlutaMAX, penicillin (100 units/mL) and streptomycin (100 µg/mL) at 37°C and 5% CO_2. For passaging, cells were harvested by incubating with PBS supplemented with 5 mM EDTA for 5 minutes, resuspended in fresh medium and plated at a confluency of 4-6M cell per 10 cm dish.

HEK-293Ts were maintained in DMEM supplemented with 10% heat-inactivated FBS and 1X GlutaMAX at 37°C and 5% CO_2.

2.3.1 Lentiviral transduction of MutuDCs

For lentiviral production, 3×10^6 HEK-293T were seeded in a 10 cm dish. The next day, the cells were transfected with a mixture of 45 µL TransIT-LTI, 7 µg of the expression vector with the gene of interest along with 7 µg psPAX2 and 0.7 µg pMD2.g in 1 mL of OptiMEM. The medium was replaced 18 hours post transfection with fresh medium supplemented with 1% BSA. After 48 hours post transfection, viral supernatant was collected, passed through a 0.45 µm-syringe filter and 10X concentrated using Amicon Ultra-15 centrifugal filters with a 100,000 MW cut-off. Aliquots were stored at -80°C.

For transduction, $2.5x10^6$ MutuDCs were seeded in a 6 cm dish in 3 mL of media. After letting the cells adhere for at least 2 hours, 1 mL of 10X concentrated virus was added in the presence of 6 µg/mL polybrene. The next day, the virus was removed and replaced with fresh culture medium. Two days post transduction, cells were either sorted or selected with 200 µg/mL hygromycin for one week. Mpeg1 variants were transduced into Mpeg1^{KO} MutuDCs and sgRNA guides for creating γ-secretase deficient cells were transduced into

Cas9-expressing MutuDCs, both of which were already available in the lab (see Section 2.3). To test the knockout efficiency, genomic DNA was isolated and regions around the cut sites were amplified by PCR (**Table 2.7**). The amplicons were sequenced and analysed using TIDE (http://shinyapps.datacurators.nl/tide/).

Table 2.7 Sequences of primers for knockout validation

Target	Forward primer (5'-3')	Reverse primer (5'-3')
Aph1c	gccagaaaccgcccctaa	acggaaagactaaggctcca
Ncstn	tgtgggactagaacctgacg	aagcgaaacagagagaccca
Psen2	aacctagactgggacgtgtg	ggtaaacgctctgcttcctg

2.3.2 Generation of BMDCs

Bone marrow was recovered from femurs and tibiae of from 8–13-week-old male or female C57BL/6J mice and resuspended in in RPMI-1640 supplemented 10% heat inactivated FBS, 10 mM HEPES, 500 µM 2-mercaptoethanol, 1X sodium pyruvate, 1X non-essential amino acids, penicillin (100 units/mL) and streptomycin (100 µg/mL).

For GM-CSF cultures, 4x10^6 cells were seeded in a non-treated 10 cm dish and supplemented with 20 ng/mL GM-CSF (Day 0). Cells were differentitated for 7 days with the addition of 10 mL of fresh media with 20 ng/mL GM-CSF on Day 3.

For Flt3-L cultures, $15x10^6$ cells were seeded in a non-treated 10 cm dish and supplemented with 5 ng/mL GM-CSF and 200 ng/mL Flt3-L (Day 0). Cells were differentiated for 10 days with the addition of 10 mL of fresh media with 5 ng/mL GM-CSF and 200 ng/mL Flt3-L on Day 5 and 5 mL of fresh media containing 20 ng/mL GM-CSF on Day 7.

2.3.3 Isolation of splenic DCs

Splenic DCs were isolated with the help of Pablo Rodríguez Silvestre. Spleens were perfused with a solution of RPMI-1640, 0.1 mg/mL Liberase-TL and 0.1 mg/mL DNAse I, minced and digested for 25 min at 37˚C. Heat-inactivated FBS was added at 10% (v/v) to stop the digestion, before mashing tissues through a 70 µM filter. Red blood cells were lysed with Hybri-Max for 3 min at room temperature. Dendritic cells were isolated using a Miltenyi Pan-DC Isolation Kit (negative selection) according to the manufacturer's instructions.

2.4 Microbead preparations

2.4.1 Preparation of ovalbumin-coated beads (Ova beads)

Microbead preparations were prepared using polystyrene microspheres with a mean diameter of 3 µm and a coefficient of variance of 8% (defined as: [standard deviation] /

[actual diameter] x 100). The beads contain surface primary amine groups for covalent coupling of proteins. Amino-modified polystyrene microspheres were washed twice in PBS and preactivated with 8% (vol/vol) glutaraldehyde for 4 h at room temperature. Preactivated beads were washed once in PBS and then incubated overnight at 4°C with ovalbumin at a concentration of 0.5 mg/mL in PBS. The next day, beads were quenched in 0.4 M glycine in PBS for 30 minutes, washed twice in PBS and used immediately for phagocytosis.

Biotin-Ova beads were produced the same way except that biotinylated ovalbumin was used at a concentration of 1.2 mg/mL in PBS. Ovalbumin was biotinylated using the EZ-Link Sulfo-NHS-LC-Biotinylation Kit according to the manufacturer's instructions.

2.4.2 Preparation of BSA- or saporin-coated beads (Saporin beads)

Saporin or BSA were conjugated to Ova beads (or biotin Ova beads) through disulfide bonds. For efficient conjugation, free sulfhydryl groups were introduced by reacting 0.6 mL of 2.5 mg/mL saporin or BSA with 12 µL of 2 mg/mL Traut's reagent in PBS containing 2 mM EDTA for 60 minutes at room temperature. Excess reagent was removed using a Zeba spin desalting column equilibrated with PBS containing 2 mM EDTA. Ova beads (prepared as detailed in Section 2.4.1) were resuspended in PBS containing 2 mM EDTA and reacted with 1 mM SPDP for 30 minutes at room temperature. The beads were then washed twice in PBS containing 2 mM EDTA and incubated with different mixtures of cysteine-modified saporin and BSA overnight at room temperature. Saporin was titrated across the mixtures (1 mg/mL to 0 mg/mL) and substituted with BSA so that the total protein concentration in each mixture remained constant at 1 mg/mL. The next day, beads were washed three times in PBS and immediately used for phagocytosis.

2.4.3 Preparation of pHrodo-coated beads (pHrodo beads)

Amino-modified polystyrene microspheres described in Section 2.4.1 were washed twice in PBS, resuspended in 100 mM sodium bicarbonate (pH 8.5) and reacted with 0.2 mM pHrodo iFL Red Ester dye for 1 hour at room temperature. The beads were then washed once in PBS and any reactive ester moieties were quenched by incubating the beads in 1X TBS for 10 minutes. After an additional two washes in PBS, the beads were coated with 1 mg/mL ovalbumin by passive absorption for 1 hour at room temperature. The beads were then washed three times in PBS and immediately used for phagocytosis.

2.5 Cell-based assays

2.5.1 phagoFACS assay

MutuDCs were collected, washed once in PBS and resuspended in ice-cold internalisation medium (CO_2-independent medium containing 1X GlutaMAX) to a density of $20x10^6$ cells/mL. Ova beads were added at a 10:1 ratio of beads:cells and incubated for 25 minutes at 16°C followed by a 5-minute incubation at 37°C to allow phagocytic binding and internalisation of beads. To remove non-internalised beads, cells were first washed twice with 10 mL ice-cold PBS at 100 x g for 4 minutes at 4°C and then resuspended in 1 mL PBS, applied to a 5 mL FBS cushion and centrifuged at 150 x g for 4 minutes at 4 °C. The cell pellet was then resuspended to $20x10^6$ cells/mL in cell culture medium and divided into different time points comprising $5x10^6$ cells each. For drug treatments the culture medium was supplemented with 0.5 µM bafilomycin A1, 0.1 µM brefeldin A, 10 µM DAPT or 10 µM z-FA-FMK. The chase was performed at 37°C for different periods of time and stopped by adding ice-cold PBS. Non-internalised beads were stained on ice with a goat αOvalbumin antibody (1:100) for 30 minutes followed by an αGoat-AF488 antibody (1:200) for 30 minutes. Cells from each time point were resuspended in 0.5 mL homogenization buffer (250 mM sucrose, 3 mM imidazole, 2 mM DTT, 2 mM PMSF and 1X protease inhibitor cocktail, pH 7.4) and passed 25 times through a 22-G needle. Intact cells and debris were pelleted by centrifugation at 150 x g for 4 minutes and the phagosome-containing post-nuclear supernatants transferred to a V-bottom 96-well plate. The enriched phagosomes were washed with PBS containing 1% (vol/vol) BSA and stained with different primary antibodies overnight at 4°C. The next day, the samples were incubated with appropriate secondary antibodies for 45 minutes on ice. Phagosomes were analysed by flow cytometry using a CytoFlex flow cytometer. The data were analysed using FlowJo software.

2.5.2 Bead saporin-puromycin assay by flow cytometry

The bead saporin-puromycin was performed in cell culture medium lacking β-mercaptoethanol (βM-free) to avoid reduction of the conjugating disulfide bond on saporin beads.

MutuDCs were collected, washed once in PBS and seeded in a 96-well U-bottom plate with $5x10^5$ cells per well in 100 µL βM-free cell culture medium. Saporin beads were added at a beads:cells ratio of 10:1 in 50 µL βM-free medium. For drug treated cells, the βM-free medium was supplemented with a final concentration of 0.5 µM bafilomycin A1 0.1 µM brefeldin A, 10 µM DAPT or 10 µM z-FA-FMK. Cells were incubated with beads at 37 °C for the indicated times. Then, puromycin was added at 10 µg/mL for 30 minutes and cells were subsequently washed in ice-cold PBS. Non-internalised beads were stained on ice with a

rabbit αOvalbumin antibody (1:200) for 30 minutes followed by an αRabbit-AF455 antibody (1:1000) for 30 minutes. After labelling dead cells with ViaKrome 808 (1:1000) for 10 minutes on ice, cells were fixed and permeabilised using the BD Fix/Perm and Perm/Wash buffers. Puromycin incorporation was determined by staining with an αPuromycin-AF647 antibody (1:200) in Perm/Wash buffer for 45 minutes on ice. Cells were analysed by flow cytometry using a CytoFlex flow cytometer. The data were analysed using FlowJo software.

2.5.3 pHrodo assay

For pHrodo assays with MutuDCs and BMDCs, the pulse with pHrodo beads was performed as described in Section 2.5.1. For pHrodo assays with splenic DCs, the pulse was adjusted to 15 minutes for 37°C to allow comparison to a previous study (*245*). The chase was performed at 37°C for different periods of time and stopped by adding ice-cold PBS. For drug treated cells, the medium was supplemented with a final concentration of 0.5 µM bafilomycin A1 or 5 µM DPI. Non-internalised beads and dead cells were labelled in PBS containing 1% (vol/vol) BSA with a rabbit anti-OVA antibody for 30 min on ice followed by a staining with donkey anti-rabbit-AF647 and ViaKrome 808 for 30 min on ice. For pHrodo assays with BMDCs and splenic DCs, non-specific antibody binding was blocked using αCD16/CD32 prior to staining. The staining also included antibodies against surface markers. Stained cells were immediately analysed on a CytoFlex flow cytometer using a chilled sample stage. The data were analysed using FlowJo software.

2.5.4 Intracellular staining

Intracellular staining was performed on ice using the Cytofix/Cytoperm Kit according to the manufacturer's instructions.

2.5.5 Immunofluorescence microscopy

MutuDCs were seeded in poly-L-lysine coated µ-slide 8 well dishes with 150,000 cells per well in 300 µL cell culture medium and allowed to adhere overnight. To label lysosomes and other acidic compartments, the cell culture medium was replaced with fresh medium containing 1 µM LysoTracker Red and cells were incubated for 30 minutes at 37°C. Cells were then washed twice with PBS and fixed in 4% formaldehyde (diluted in PBS) for 10 minutes at room temperature. After two washes with PBS, the samples were permeabilised with 0.15% Triton X-100 in PBS for 10 minutes at room temperature followed by three washes with PBS. To block non-specific binding and quench excess formaldehyde, the cells were incubated in blocking buffer (1% BSA, 0.3 M glycine, 0.1% Tween 20 in PBS) for 30 minutes. Primary and secondary antibody incubations were performed in PBS containing 1% BSA for 1 hr at room temperature with three washes in PBS after each incubation. Nuclei

were labelled by incubating the cells for 10 minutes with DAPI (1:1000, BD Biosciences) followed by two washes in PBS. Images were acquired on a VisiTech iSIM swept field confocal super resolution system coupled to a Nikon Ti2 inverted microscope stand equipped with a 100x/1.49 NA SR Apo TIRF objective lens. The images were processed and analysed in Fiji.

2.5.6 Bead-saporin puromycin assay by microscopy

MutuDCs were seeded in poly-L-lysine coated µ-slide 8 well dishes with 250,000 cells per well in 300 µL cell βM-free medium and allowed to adhere overnight. Biotin-saporin beads were added at a beads:cells ratio of 20:1 in 30 µL βM-free medium and incubate for 5 hours at 37°C. Then, puromycin was added at 10 µg/mL for 30 minutes and cells were subsequently washed twice in ice-cold PBS. Cells were fixed in 1% formaldehyde (diluted in PBS) for 20 minutes at room temperature. Excess formaldehyde was blocked by incubating the cells in blocking buffer (2% BSA, 0.3 M glycine in PBS) for 20 minutes at room temperature. After washing once with PBS containing 2% BSA, the samples were permeabilised for 30 minutes in permeabilization buffer (RPMI-1640 media containing 0.2% saponin and 10% FBS). Primary antibodies and fluorescently-labelled streptavidin were diluted in permeabilization buffer and incubated at 4°C overnight. Samples were washed three times with permeabilization buffer and then incubated with secondary antibodies diluted in permeabilization buffer for 1.5 hours at room temperature. Samples were then washed three times in PBS and covered in Prolong Gold antifade with DAPI. Images were acquired on a Nikon W1 spinning disk inverted microscope equipped with a 100x/1.4 NA oil objective lens. The images were processed and analysed in python (code is available here: https://github.com/jboulanger/three-microns-beads-in-cells).

2.6 Biochemical assays

2.6.1 Western blotting

For Western blotting of drug treated cells, MutuDCs were seeded into a 6-well dish at $2x10^6$ cells/well in 2 mL of cell culture media. The next day, cells were incubated with inhibitors as indicated in the relevant figure legends. Drug-treated, or untreated cells, were pelleted and washed once in ice-cold PBS. Pellets were lysed in RIPA buffer supplemented with 1X protease inhibitor cocktail for 20 minutes at 4°C while shaking at 800 rpm. Insoluble material was pelleted by centrifugation at 20,000g for 10 minutes. Supernatants were mixed with NuPAGE LDS Sample Buffer and heated at 70 °C for 10 minutes in the presence or absence of 1X Bolt reducing agent. Samples were run in MOPS buffer (0.2 mM MOPS free acid, 0.05 mM sodium acetate, 0.01 mM disodium EDTA) on NuPAGE 4–12% Bis-Tris gels at 150V for 60 minutes and transferred onto nitrocellulose membrane using an iBlot1 system. Loading

was controlled by Ponceau staining. Membranes were then blocked by incubation with blocking buffer (PBS containing 5% milk 0.1% Tween-20) for 1 hour at room temperature. Primary antibodies were diluted in blocking buffer and incubated at 4°C overnight. After washing three times with PBS containing 0.1% Tween-20, membranes were incubated with HRP-conjugated secondary antibodies diluted in blocking buffer for 1 hour at room temperature. Membranes were again washed three times with PBS containing 0.1% Tween-20 and then incubated with ECL reagent for 10 minutes. The resulting signal was detected using X-ray films with varying exposure times.

2.6.2 Cell fractionation

For fractionation experiments, $60x10^6$ MutuDCs were washed once in ice-cold PBS and once in hypotonic buffer (50 mM sucrose, 0.5 mM $MgCl_2$, 0.2 mM EDTA and 25 mM Tris-HCl). Cells were then resuspended in 3mL of hypotonic buffer supplemented with 1X protease inhibitors and lysed by passing the suspension through a 22-G needle for 25 times on ice. The osmolarity was adjusted to 250 mM sucrose before spinning at 1000 x g for 10 minutes to pellet nuclei and debris. Supernatant was transferred to a fresh tube and centrifuged at 4,000 x g for 10 minutes. The resulting pellet (4K fraction) was stored on ice and the supernatant transferred to an ultracentrifuge tube. Samples were then centrifuged at 10,000 x g for 10 minutes in a Beckman ultracentrifuge using a TLA-110 rotor and the resulting pellet stored on ice (10K fraction). This procedure was repeated with centrifugations at 20,000 x g (20K fraction) and 40,000 x g (40K fraction) for 20 minutes each and a final centrifugation at 80,000 x g for 30 minutes (80K fraction). All centrifugations were performed at 4°C. The resulting pellets were lysed in RIPA buffer or in PBS with 1% (v/v) Triton-X100. Samples were heated at 70°C for 10 minutes and then sonicated with fifteen 30 second on/off cycles at maximum intensity on a Bioruptor. Samples were then processed by Western blot analysis as described in Section 2.6.1

2.6.3 Radioactive pulse-chase analysis

For radioactive pulse-chase analysis, $24x10^6$ MutuDCs were washed once in PBS and resuspended in pre-warmed starvation medium (RPMI-1640 lacking cysteine/methionine and supplemented with 10% heat inactivated, dialyzed FBS, 10 mM HEPES, 500 µM 2-mercaptoethanol, 1X sodium pyruvate, 1X non-essential amino acids, penicillin (100 units/mL) and streptomycin (100 µg/mL)). After incubation at 37°C for 1 hour, cells were pelleted and resuspended in 1 mL of starvation medium supplemented with 18 µCi of EasyTag EXPRESS ^{35}S Protein Labelling Mix (^{35}S-L-methionine and ^{35}S-L-cysteine). Cells were intubated in labelling media for 15 to 30 minutes at 37°C. Next, cells were washed once with PBS, resuspended in pre-warmed, regular RPMI-1640 medium (as described in

Section 2.3.2) and chased for different periods of time at 37°C. The chase was stopped by adding ice-cold PBS and cells were washed twice in ice-cold PBS.

Cells were lysed by incubation in 200 µL lysis buffer (PBS supplemented with 1% Triton X-100 and 1X protease inhibitor cocktail) for 20 minutes on ice. Insoluble material was pelleted by centrifugation at 20,000g for 10 minutes. The supernatant was incubated with 25 µL of Protein A/G magnetic beads (pre-washed twice in lysis buffer) and incubated on a shaker at 900 rpm for 30 minutes at 4°C. The beads were removed with the help of a magnetic stand and the pre-clear lysate was incubate with 5 µL αC-term antibody on a shaker at 900 rpm overnight at 4°C. The next day, 25 µL of washed Protein A/G magnetic beads were added and incubated for one additional hour. The magnetic beads were recovered using a magnetic stand and washed 4 times in lysis buffer.

Proteins were eluted from the beads by incubation in 60 µL elution buffer (1X NEB glycoprotein denaturing buffer containing 0.5% SDS and 40mM DTT) on a shaker at 900 rpm for 10 minutes at 95°C. Next, the beads were pelleted by centrifugation and the eluate was recovered into a fresh Eppendorf tube. For deglycosylation, 3x 20µL of eluate were either treated with Endo H or PNGase F in 1X NEB glycobuffer according to the manufacturer's instructions or, as a control, only incubated with 1X NEB glycobuffer alone and incubated for 2 hours at 37°C.

Samples were incubated with NuPAGE LDS Sample Buffer at 70°C for 10 minutes and run in MOPS buffer on NuPAGE 4–12% Bis-Tris gels at 150V for 60 minutes. The gel was stained with InstantBlue Coomassie for 20 minutes and destained in water. Next, the gel was dried on a piece of filter paper using a gel dryer for 60 minutes at 80°C under vacuum. The dried gel was placed on a phosphor screen for 14 hours which was then imaged using a Typhoon biomolecular imager.

2.7 Mass spectrometry

Mass spectrometry analysis was carried out in collaboration with the Borner lab and is described in detail in (*249*). The Borner lab took over following cell lysis.

Briefly, for analysis of perforin-2 processing in bafilomycin A1 treated cells, $10x10^6$ MutuDCs were cultured overnight 37°C in the presence or absence of 1 µM bafilomycin A1. Cells were then harvested, washed three times in PBS and lysed in lysis buffer (2.5% (w/v) SDS in 50 mM Tris, pH 8.0) at 72°C for 5 minutes. Protein concentrations were determined by BCA assay and 100 µg of protein were precipitated using acetone. Precipitated protein pellets were denatured in buffer containing 8 M urea and alkylated using iodoacetamide. Samples were digested using LysC and trypsin and the resulting peptides were purified and

fractionated. For proteomic analysis, 500 ng of peptides were separated by reverse phase chromatography on an EASY-nLC 1000 system which was coupled to a Q Exactive HF-X Hybrid Quadrupole-Orbitrap mass spectrometer via a nanoelectrospray source.

For analysis of perforin-2 processing in AEP-deficient cells, $10x10^6$ NT or AEP^{KO} MutuDCs were lysed and prepared for proteomic analyse as described for bafilomycin A1 treated cells. For proteomic analysis, 300 ng of peptides were separated by reverse phase chromatography on an EASY-nLC 1200 system which was coupled to a Orbitrap Exploris 480 mass spectrometer via a nanoelectrospray source.

After raw files were processed in MaxQuant, label-free quantification was performed using the MaxLFQ algorithm. To detect semi-tryptic peptides, the enzyme mode was set to semi-specific. To assess abundance of peptides independent of protein abundance changes, peptide intensities were divided by their corresponding protein intensities. Data were filtered subjected to a two-sided student's t-test. Multiple hypothesis correction was done by permutation-based FDR with s0=0.1 using Perseus.

Chapter 3 – Perforin-2 processing in endocytic compartments

3.1 Introduction

At the beginning of my project, we knew that perforin-2 mediates the escape of internalised antigen into the cytosol. From cryo-EM studies we also knew that it forms detergent-solubilised oligomeric pores in solution (*246, 247*). Together these findings strongly suggested that perforin-2 forms pores in host cell membranes to mediate endocytic escape. I therefore wondered how DCs safely express and store large amounts of this putatively toxic protein. Based on studies of related pore-forming proteins, candidate strategies to manage the inherent toxicity of perforin-2 include regulated trafficking, proteolytic processing and pH-sensitivity but none of these had been explored in detail (*320*). The only insight came from i*n vitro* studies of the recombinant perforin-2 ectodomain which suggested that pore formation is triggered by acidic pH (*246, 247*). While this finding provided a partial explanation for how perforin-2 can be controlled, it is at odds with the general understanding that DCs maintain a high phagosomal pH to preserve antigens for cross-presentation (*216, 217, 245, 321*). One caveat of the *in vitro* studies is that they were performed with soluble perforin-2. *In vivo* perforin-2 is synthesised as a transmembrane-anchored protein which may drastically impact its response to changes in pH or other triggers.

To better understand the steps that control perforin-2 pore-formation *in vivo*, I first analysed its steady-state distribution by confocal microscopy and followed its biosynthesis with a radioactive pulse-chase analysis. I then studied the assembly of perforin-2 on phagosomes using polystyrene beads as the phagocytic cargo. Polystyrene beads are an established model for particulate antigen which is relevant in the context of perforin-2 given perforin-2's role in cross-presentation of particulate cell-associated antigen (rather than soluble antigen). The bead phagosomes can be isolated and analysed by flow cytometry in a method known as phagoFACS which allows for the simultaneous analysis of antigen degradation and changes in phagosomal membrane composition (*322, 323*). By using domain specific antibodies to perforin-2 in this system, I attempted to delineate the steps of pore assembly in a time-resolved manner. To complement these studies of perforin-2 processing, I also developed an assay to monitor perforin-2 activity on bead phagosomes. This assay was then used to study the relationship between perforin-2 processing and activity.

3.2 Results

3.2.1 Perforin-2 exists as two distinct pools within the endosome/lysosome system

Perforin-2 was first described in macrophages (*250*), but it is also highly expressed in DCs, particularly cDC1s (*249*). I therefore used the GFP-expressing, murine cDC1-like cell line MutuDCs to study the regulation of perforin-2 (*242*). Mpeg1^{KO} MutuDCs were generated by Patrycja Krawczyk and were already available at the beginning of my project.

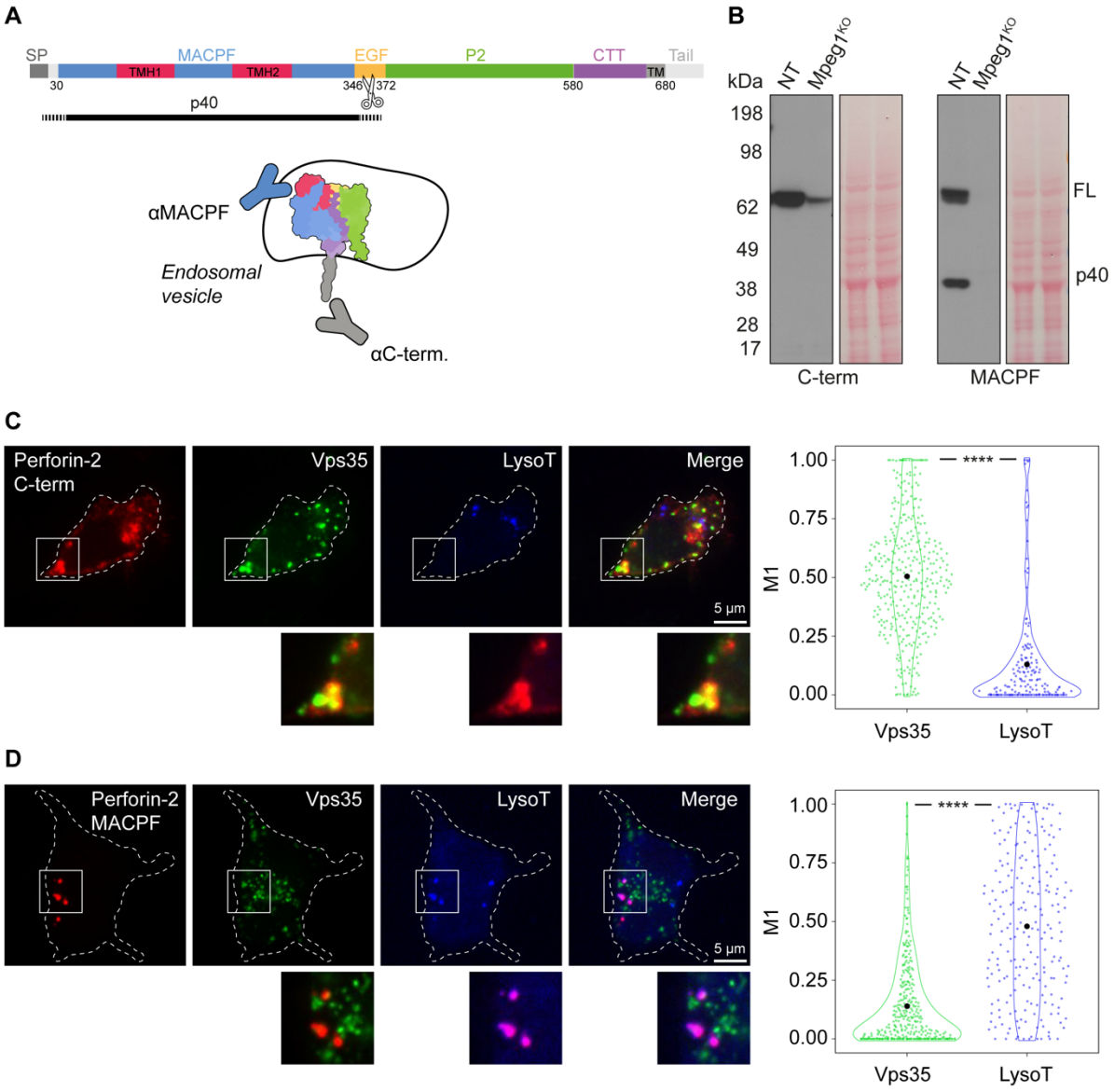

Fig. 3. 1 Perforin-2 exists as two distinct pools within the endosome/lysosome system. (**A**) Schematic representation of monomeric perforin-2 in the pre-pore conformation. The approximate epitopes of the αC-term and αMACPF antibodies are indicated. (**B**) Western blot analysis of whole cell lysate from NT and Mpeg1^{KO} MutuDCs under non-reducing conditions. Data are representative for at least five independent experiments. (**C, D**) Confocal microscopy analysis of perforin-2 in NT MutuDCs showing co-staining with Vps35 (green) and LysoTracker (blue) and either the αC-term (C) or αMACPF (D) antibodies (red). The data represent two independent experiments each with at least 80 cells. The mean of each Manders' colocalization coefficient (M1) is indicated by a dot in the quantification. ***P < 0.0001 using a Kolmogorov-Smirnov test.

For an analysis of the perforin-2 steady-state distribution, I used two antibodies against different domains of the protein (**Fig. 3.1A**). One antibody binds the cytosolic C-terminus (αC-term) and the other binds in the luminal MACPF domain (αMACPF). In a Western blot analysis, both antibodies detected full-length perforin-2 at 70 kDa (**Fig. 3.1B**). The αMACPF also detected a 40-kDa fragment which is consistent with a cleavage in the EGF domain that has been reported previously (*274*). As discussed in more detail in Chapter 5, perforin-2 undergoes additional cleavage events including rapid turnover of the C-terminal tail which explains why the αC-term antibody did not detect any corresponding cleavage fragments but only recognised the full-length protein.

Confocal microscopy with the αC-term antibody showed that full-length perforin-2 was present in retromer subunit Vps35+ compartments but absent in acidic lysotracker+ compartments (**Fig. 3.1C**). In contrast, the αMACPF antibody colocalised with lysotracker, but not with Vps35. These results indicate the presence of full-length and cleaved pools of perforin-2 within the endosome/lysosome system. The αC-term detects full-length perforin-2 residing in (or transiting through) endosomes but the signal is lost as the C-terminus is cleaved off upon reaching more proteolytic low pH compartments. The αMACPF antibody, on the other hand, binds a conformation-sensitive epitope on perforin-2 that is only revealed in acidic compartments by cleavage or a conformational change.

As a complementary approach to confocal microscopy, the perforin-2 steady-state distribution was analysed by subcellular fractionation. MutuDCs were mechanically lysed, and the post-nuclear supernatant was crudely fractionated by a series of five differential centrifugation steps. The 4K and 10K fractions were enriched in lysosomes as indicated by a higher abundance of Lamp1 and cathepsin B (**Fig. 3.2A**). Consistent with the microscopy analysis, the cleaved p40 fragment detected by the αMACPF antibody was enriched in these two fractions and the full-length protein detected by the αC-term antibody was depleted (**Fig. 3.2, B and C**). Conversely, the 20K – 80K fractions were enriched with full-length perforin-2 and the cleaved p40 fragment was completely undetectable. Paradoxically, full-length perforin-2 displayed a different distribution when detected with the αC-term or the αMACPF antibody. Closer inspection reveals that the αMACPF in fact detects a doublet at 70 kDa. The bottom band corresponds to full-length perforin-2 which is also detected by the αC-term antibody. The top band (which is the one present in the 4K and 10K fractions in Fig 3.2, B and C), on the other hand, likely comprises a species that lacks the αC-term epitope. Its apparent molecular weight would be consistent with a dimeric p40 fragment. The αMACPF blot in Fig 3.2C also reveals a band at 60 kDa which corresponds to the ectodomain produced by cleavage in the P2 or CTT domain (see Chapter 5). The oligomeric species detected in Fig. 3.2, B and C, don't show a consistent pattern and are therefore difficult to

interpret. This may partly be due to the dry-transfer method used for generating the blots which can yield inconsistent results for high molecular weight species.

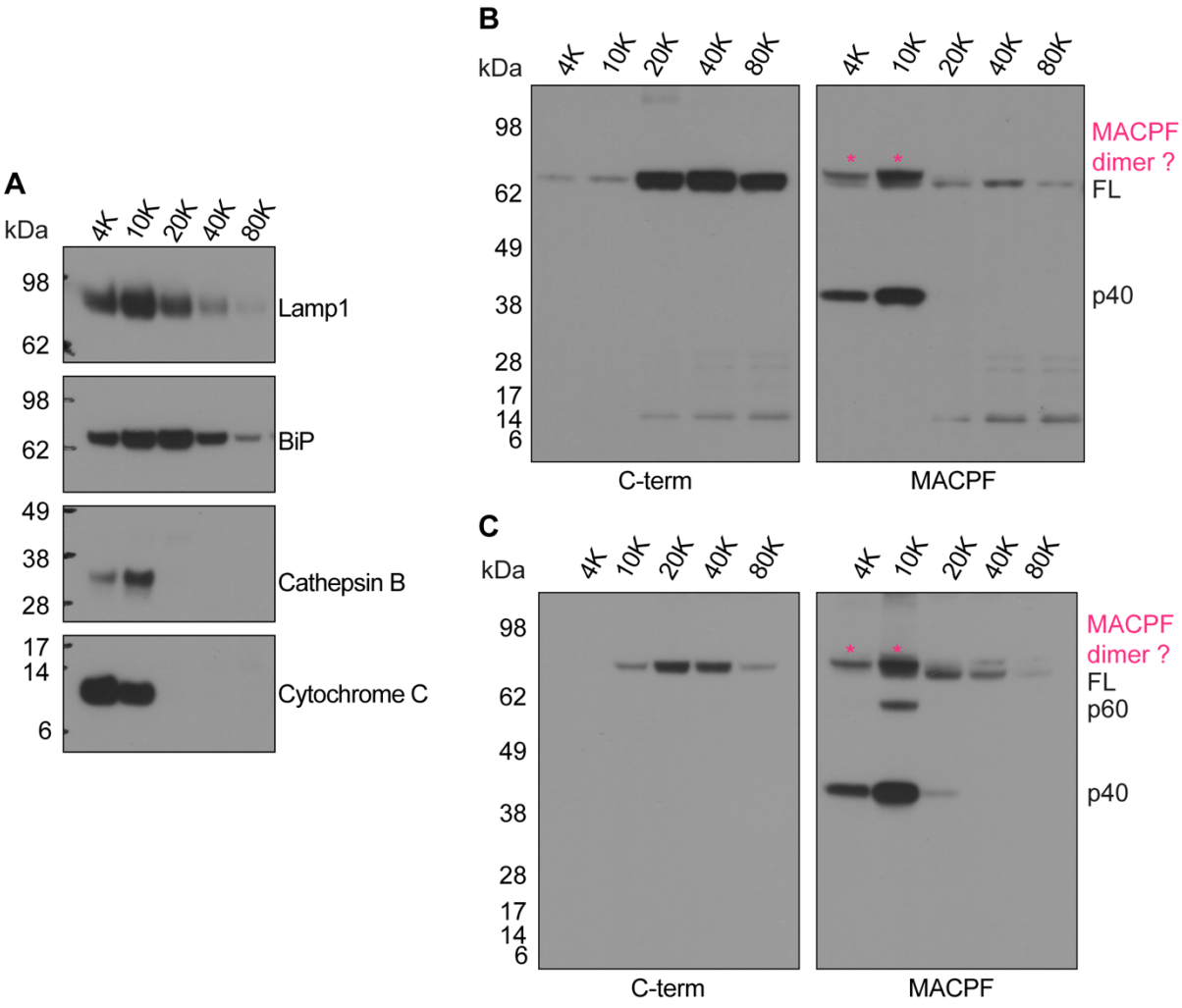

Fig. 3. 2. The majority of perforin-2 in late endocytic compartments is cleaved. (**A**) Homogenised NT MutuDCs were fractionated by differential ultracentrifugation and analysed by Western blot under non-reducing conditions with antibodies against Lamp1 (lysosomes), BiP (ER), cathepsin B (lysosomes) and cytochrome C (mitochondria). (**B, C**) Western blot analysis of fractionated NT MutuDCs homogenate under non-reducing conditions. The fractions in (B) were solubilised in RIPA buffer and those in (C) were solubilised in 1% Triton X-100.

Together, the microscopy and fractionation analyses show that full-length and cleaved species of perforin-2 are present in early and late endocytic compartments, respectively. As a next step, I wanted to investigate the kinetics of the proteolytic processing that takes place as perforin-2 traffics towards lysosomes.

To analyse the perforin-2 processing, I performed a radioactive pulse-chase analysis. Cells were starved for 60 min in medium lacking methionine/cysteine and then pulsed for 30 min (**Fig. 3.3A**) or 15 min (**Fig. 3.3B**) with ^{35}S-labelled methionine/cysteine. After the different chase periods, the cells were lysed, perforin-2 was precipitated with the αC-term antibody and analysed by autoradiography. The C-terminus was turned over quickly, and the majority

of the labelled protein was lost after the 5 h chase period. The pulse-chase analysis further showed that perforin-2 enters the Golgi within 15 – 30 min post synthesis as indicated by the acquisition of Endo H resistance within this timeframe. Perforin-2 can potentially be glycosylated at three sites (N185, N269 and N375) and at least one of these glycans remains partially sensitive to Endo H even after passing through the Golgi. The IP with the αC-term antibody also produced a contaminating band which, given its size of ~40 kDa and its high abundance, most likely corresponds to actin. Overall, the pulse-chase experiments are consistent with proteolytic cleavage of the C-terminus.

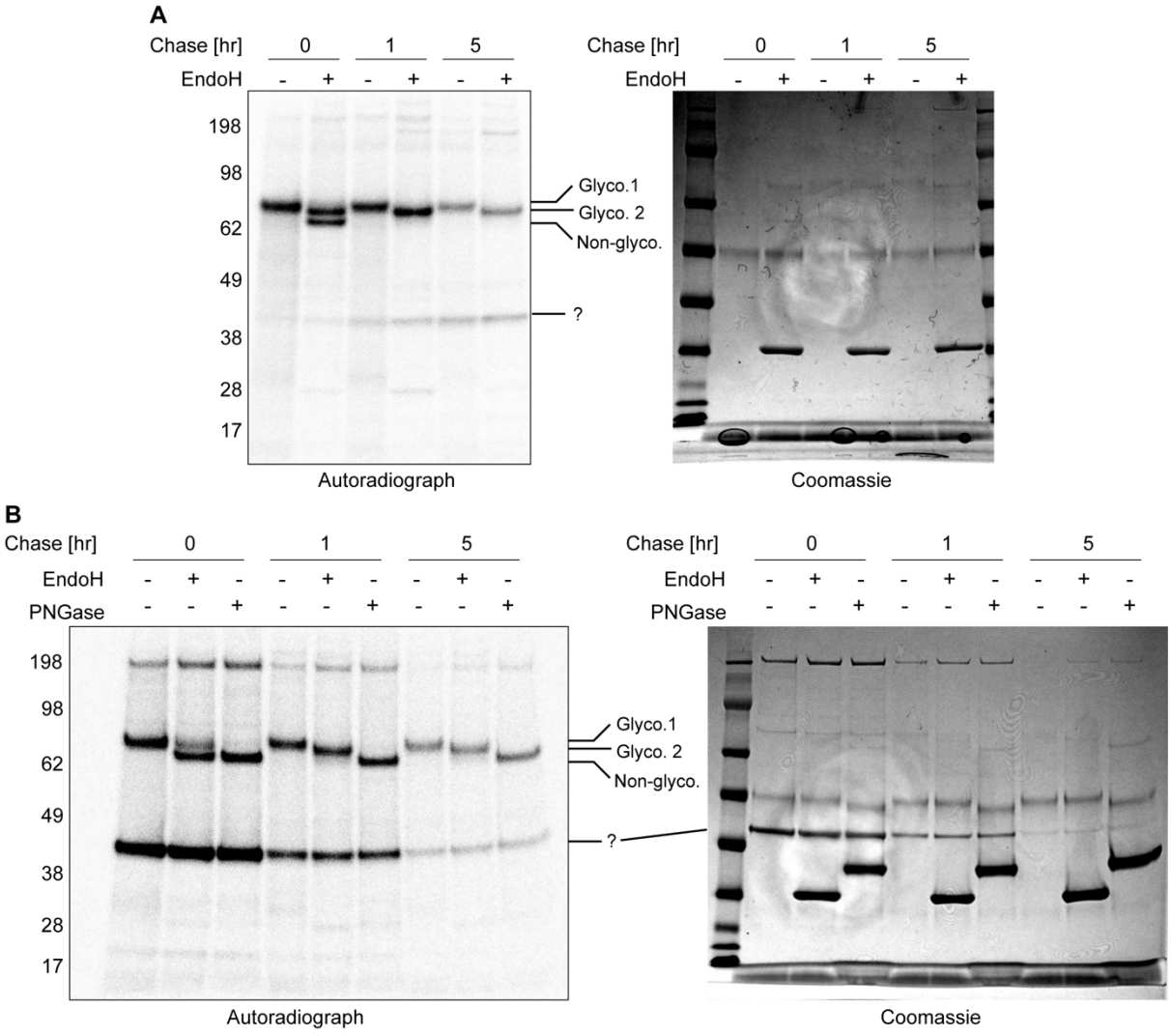

Fig. 3. 3. Analysis of perforin-2 processing by radioactive pulse-chase. (**A, B**) Autoradiograph analysis of full-length perforin-2 after immunoprecipitation with the αC-term antibody from NT MutuDCs which were pulse-labelled with ^{35}S-methionine/cysteine. Cells were starved in media lacking methionine/cysteine for 60 min, followed by a pulse with ^{35}S-methionine/cysteine for 30 min (A) or 15 min (B) at 37°C. Following immunoprecipitation, samples were left untreated or digested with EndoH and PNGase (B).

However, the insights from this analysis are limited because perforin-2 is cleaved at multiple sites (see Chapter 5), and the αC-term antibody can only precipitate the full-length protein. Thus, it cannot be formally excluded that labelled full-length protein is not simply lost

because it is degraded during the chase. Precipitation of the other fragments, such as p40, was not possible with the available antibodies. I therefore explored alternative approaches to study the processing of perforin-2 in a time-resolved manner which led me to investigate its assembly on phagosomes.

3.2.2 Perforin-2 undergoes continuous processing in endocytic compartments

To test whether perforin-2 is recruited to phagosomes, I followed phagosome maturation in MutuDCs using phagoFACS (**Fig. 3.4A**). Cells were pulsed with ovalbumin-coated polystyrene beads (OVA beads) for 25 min at 16°C followed by 5 min at 37°C to allow for synchronised internalisation of the beads. Then, cells were washed in PBS to remove any non-internalised beads and either put on ice (chase point 0 h) or incubated at 37°C for different periods. The phagosomes were then crudely isolated by mechanic disruption of the cells and subsequent recovery of OVA beads on a sucrose cushion. At this point, the phagosomes were stained with antibodies. Notably, no additional permeabilisation was required to stain luminal epitopes suggesting that the isolation procedure partly disrupts the phagosomal membrane.

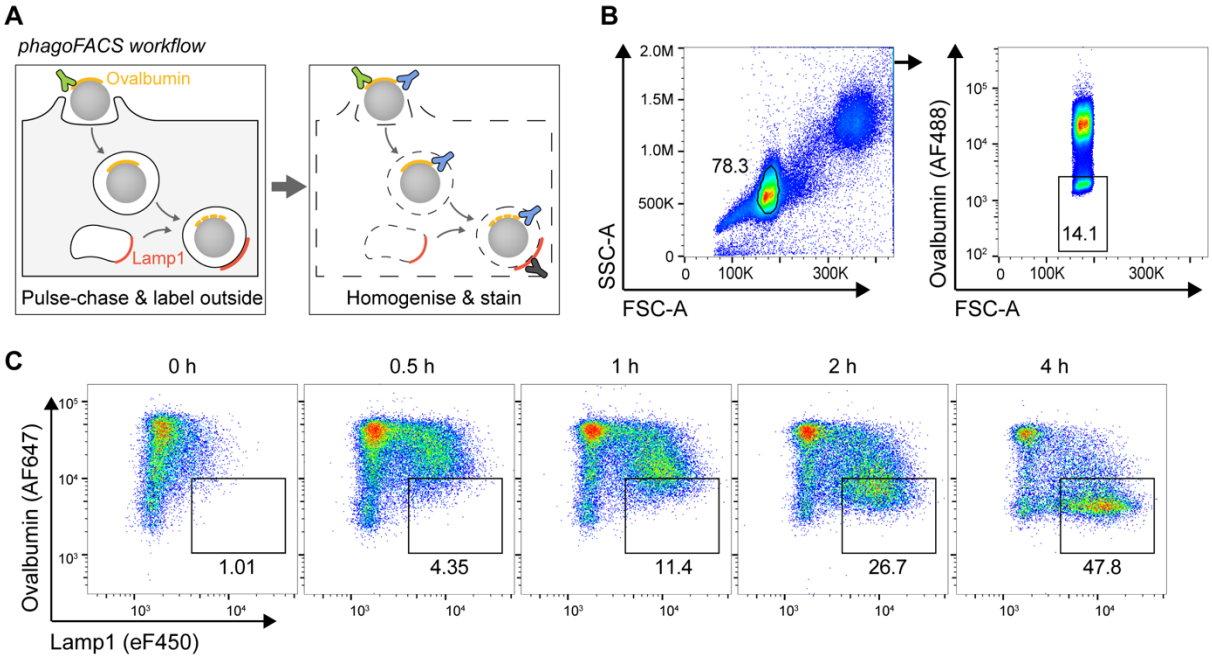

Fig. 3. 4. Phagosome maturation in MutuDCs. (**A**) Schematic representation of the phagoFACS assay. (**B**) Gating strategy for the phagoFACS assay. (**C**) NT MutuDCs were pulsed with OVA beads for 25 min at 16°C followed by 5 min at 37°C and either immediately placed on ice (0 h) or chased for the indicated time. Isolated phagosomes were stained with antibodies against ovalbumin and Lamp1. The gate indicates mature phagosomes. Data are representative for at least five intendent experiments.

I first ensured that the assay captures some of the hallmarks of phagosome maturation by staining with antibodies against ovalbumin and Lamp1 (**Fig. 3.4, B and C**). Staining for Lamp1 confirmed that the phagosome gradually fused with lysosomes. Accordingly, staining for ovalbumin showed that it was gradually degraded over time confirming that the phagosomes became increasingly proteolytic. Together, these results confirmed that phagosome maturation proceeded as expected.

Using the αC-term antibody, I found that perforin-2 was rapidly recruited to phagosomes, reaching its highest levels within 30 min (**Fig. 3.5, A and B**). This rapid acquisition of full-length perforin-2 is consistent with its localisation in early endosomal vesicles but could also indicate that a fraction of perforin-2 may be delivered from the plasma membrane as it

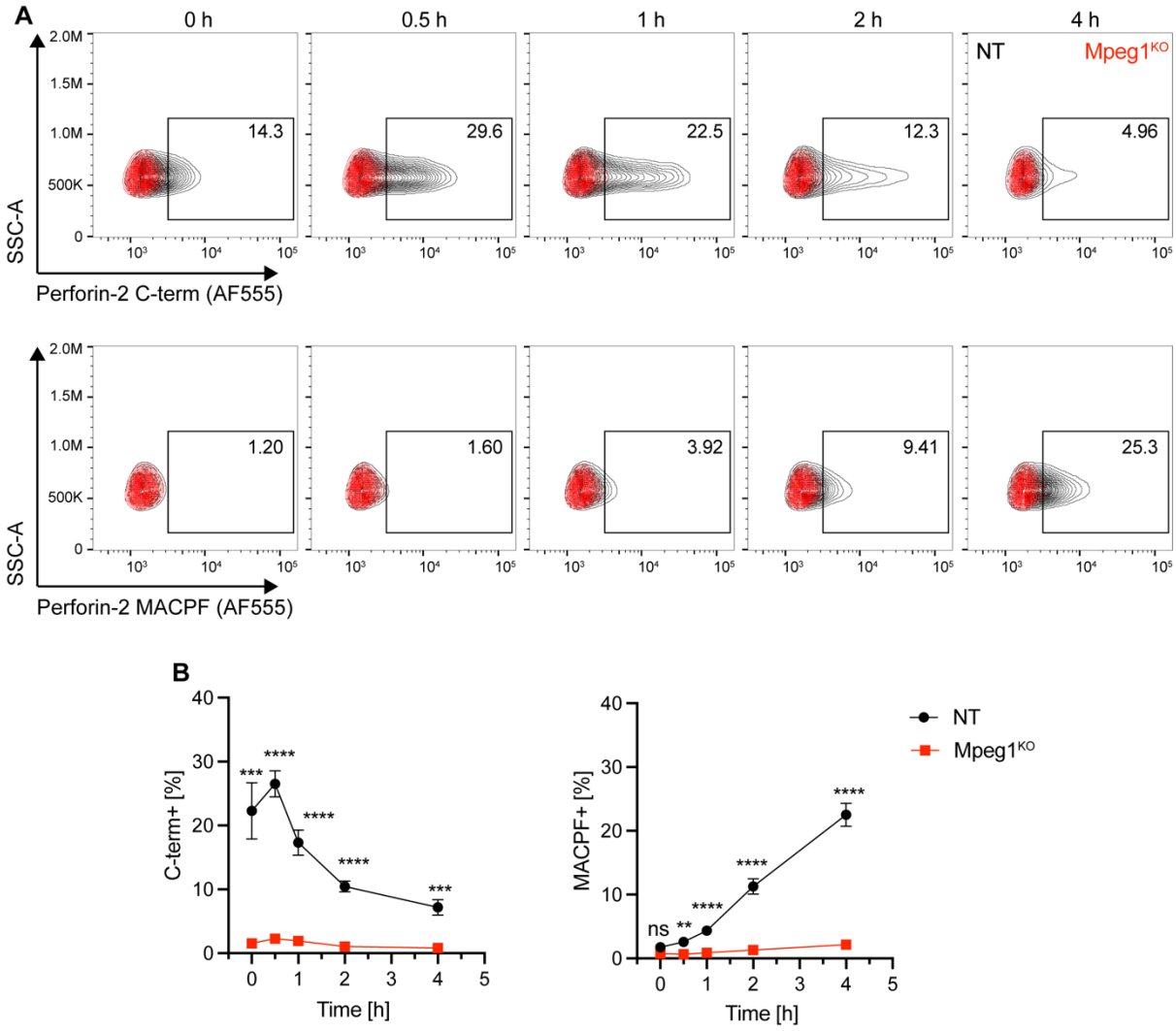

Fig. 3. 5. Perforin-2 is recruited to phagosomes and proteolytically processed. (**A**) NT or Mpeg1^{KO} MutuDCs were pulsed with OVA beads for 25 min at 16°C followed by 5 min at 37°C, washed and either immediately placed on ice (0 h) or chased for the indicated time. Isolated phagosomes were stained with αC-term (top) or αMACPF (bottom) antibodies. (**B**) Quantification of perforin-2^{+} phagosomes based on the gating shown in (A). Data represent mean and SEM of four independent experiments. ns, not significant; **P<0.01; ***P<0.001; ****P<0.0001 using a multiple paired t-test (two-stage step-up, Benjamini, Krieger and Yekutieli).

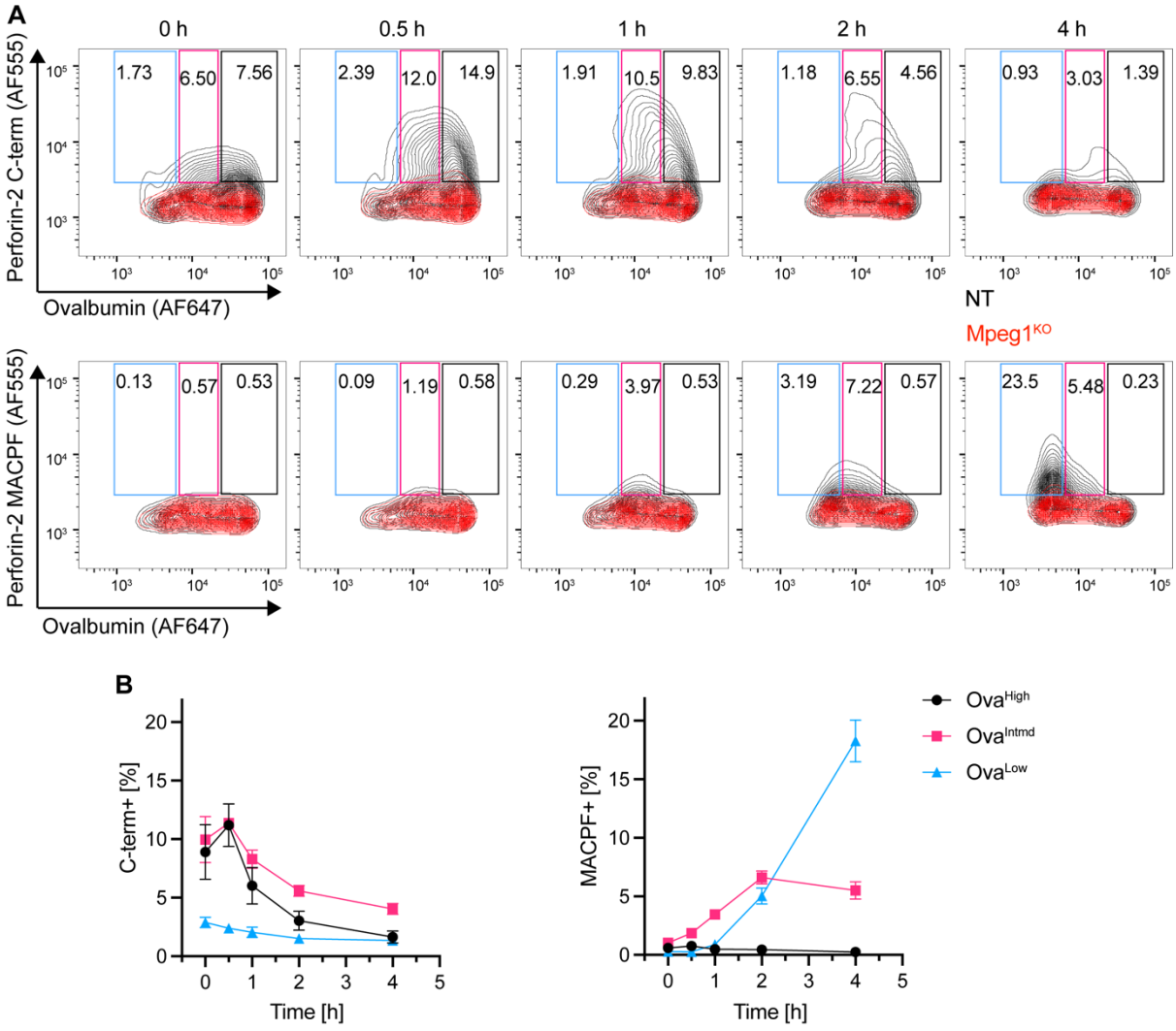

Fig. 3. 6. Comparison of perforin-2 processing and ovalbumin degradation. (**A**) NT or Mpeg1^{KO} MutuDCs were pulsed with OVA beads for 25 min at 16°C followed by 5 min at 37°C, washed and either immediately placed on ice (0 h) or chased for the indicated time. Isolated phagosomes were stained with αOvalbumin and with αC-term (top) or αMACPF (bottom) antibodies. (**B**) Quantification of perforin-2^{+} phagosomes based on the gating shown in (A). Data represent mean and SEM of four independent experiments.

donates membrane to the forming phagosome (*210*). As phagosome maturation continued, the αC-term signal was gradually lost while the αMACPF signal started to accumulate. Thus, similar to the steady-state distribution of perforin-2 in the endosome/lysosome system, the αC-term and αMACPF antibodies mark to mutually exclusive species of perforin-2 in early and late phagosomes, respectively.

To define perforin-2 processing more accurately during phagosome maturation, I co-stained phagosomes for either ovalbumin (**Fig. 3.6**) or Lamp1 (**Fig. 3.7**). Full-length perforin-2, detected by the αC-term, was mostly present in early Ova$^{High/Intmd}$ and Lamp1^{Intmd} phagosomes. In contrast, the species of perforin-2 detected by the αMACPF antibody was mostly present in late Ova^{Low} and Lamp1$^{High/Intmd}$ phagosomes.

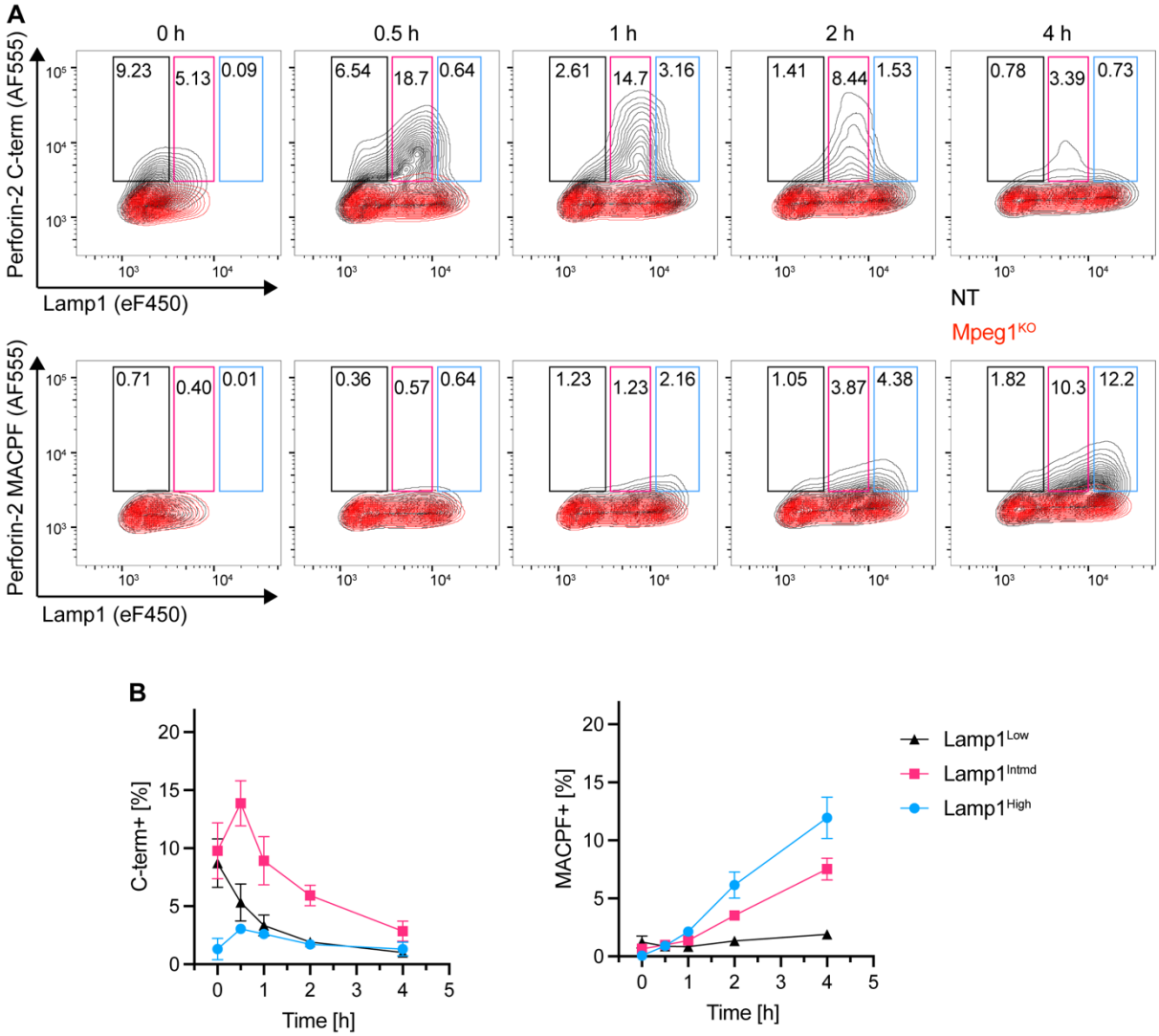

Fig. 3. 7. Comparison of perforin-2 processing and Lamp1 degradation. (**A**) NT or Mpeg1^{KO} MutuDCs were pulsed with OVA beads for 25 min at 16°C followed by 5 min at 37°C, washed and either immediately placed on ice (0 h) or chased for the indicated time. Isolated phagosomes were stained with aLamp1 and with αC-term (top) or αMACPF (bottom) antibodies. (**B**) Quantification of perforin-2^{+} phagosomes based on the gating shown in (A). Data represent mean and SEM of four independent experiments.

The loss of αC-term signal during phagosome maturation suggests that the cytosolic tail is cleaved off and degraded. This interpretation is substantiated by a more detailed analysis of the proteolytic processing of perforin-2 in Chapter 5. The appearance of the αMACPF signal, on the other hand, is more difficult to interpret. While it seems that the antibody is conformation-sensitive, it is difficult to say which conformation the antibody is detecting because it is polyclonal and its precise epitope within the MACPF domain is not known. According to the manufacturer, the antibody was raised against the recombinant MACPF domain (Cys34 – Ala306) which means that the epitope could be masked by the presence of the other domains in the full-length protein. However, it is not clear by which mechanism the epitope becomes exposed. Given that the phagosome acidifies over time and perforin-2

undergoes the pre-pore to pore transition upon acidification *in vitro (246, 247),* one explanation could be that it is this conformational change that reveals the αMACPF epitope. Another explanation could be that the antibody detects the p40 fragment which lacks all the other domains that otherwise mask the epitope. In this latter scenario, a related question is whether the p40 fragment is generated by cleavage of the perforin-2 pool that is delivered during phagosome formation or whether it originates from a pre-existing pool of p40 fragments in lysosomes (**Fig. 3.1D**) and is delivered through a second wave of recruitment at later stages of phagosome maturation.

3.2.3 Perforin-2 processing is sensitive to brefeldin A and bafilomycin A1

To investigate the origin of perforin-2 on phagosomes, I tested the effects of brefeldin A (BFA), an inhibitor of membrane trafficking. The best characterised effect of BFA is the disassembly of the Golgi and its redistribution into the ER (*324, 325*). Mechanistically, BFA inactivates a subset of Sec7-type GTP exchange factors (GEFs) that catalyse the activation of a small GTPase called Arf1. Arf1, in turn, is important for the budding of vesicles from the cis-Golgi by recruiting COPI coat proteins. The BFA-induced loss of COPI-coats leads to a redistribution of the Golgi into the ER and a block a protein secretion. BFA also interferes with various trafficking steps in the endosome/lysosome system by inhibiting clathrin-mediated vesicle formation, but the specific effects appear to be cell-type dependent and are less well characterised (*326-329*).

I found that, if MutuDCs were incubated with beads in the presence of BFA during the chase period, recruitment of full-length perforin-2 was markedly impaired (**Fig. 3.8A** and **3.9A**). These results indicate that perforin-2 is recruited to phagosomes directly from the early secretory pathway during the early phases of the chase. The origin of the phagosomal perforin-2 pool at time 0 h cannot be deduced from this data since BFA was not present during the pulse. The BFA treatment also inhibited the appearance of the αMACPF signal, but, consistent with previous reports in macrophages (*330*), it had no effect on the recruitment of Lamp1 (**Fig. 3.8B** and **3.9, B and D**).

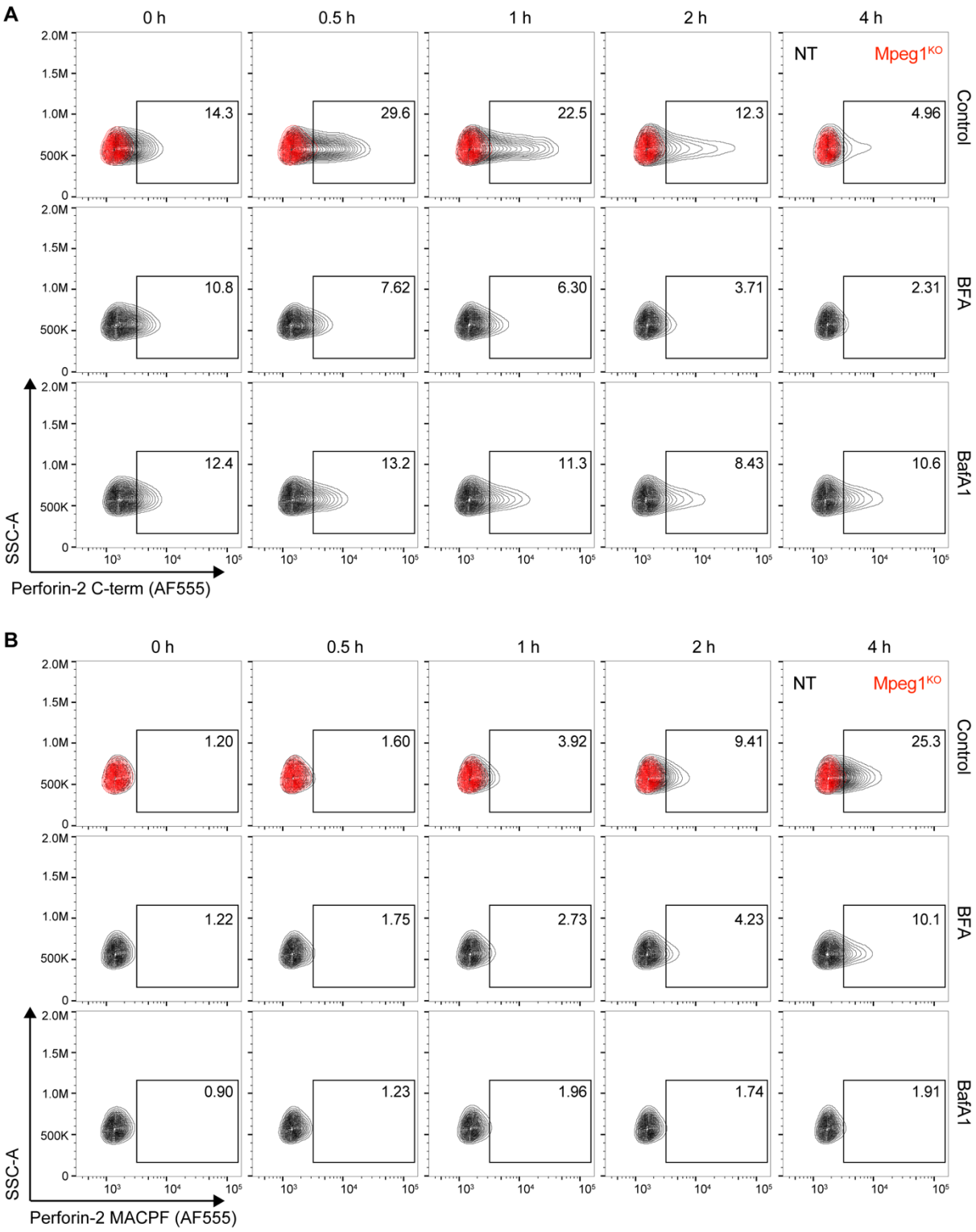

Fig. 3. 8. Effects of brefeldin A and bafilomycin A1 on perforin-2 processing. (**A, B**) NT or Mpeg1^{KO} MutuDCs were pulsed with OVA beads for 25 min at 16°C followed by 5 min at 37°C, washed and resuspended in fresh media with or without 5 μM brefeldin A or 0.5 μM bafilomycin A1. Samples were then either immediately placed on ice (0 h) or chased for the indicated time. Isolated phagosomes were stained with αC-term (A) or αMACPF (B) antibodies.

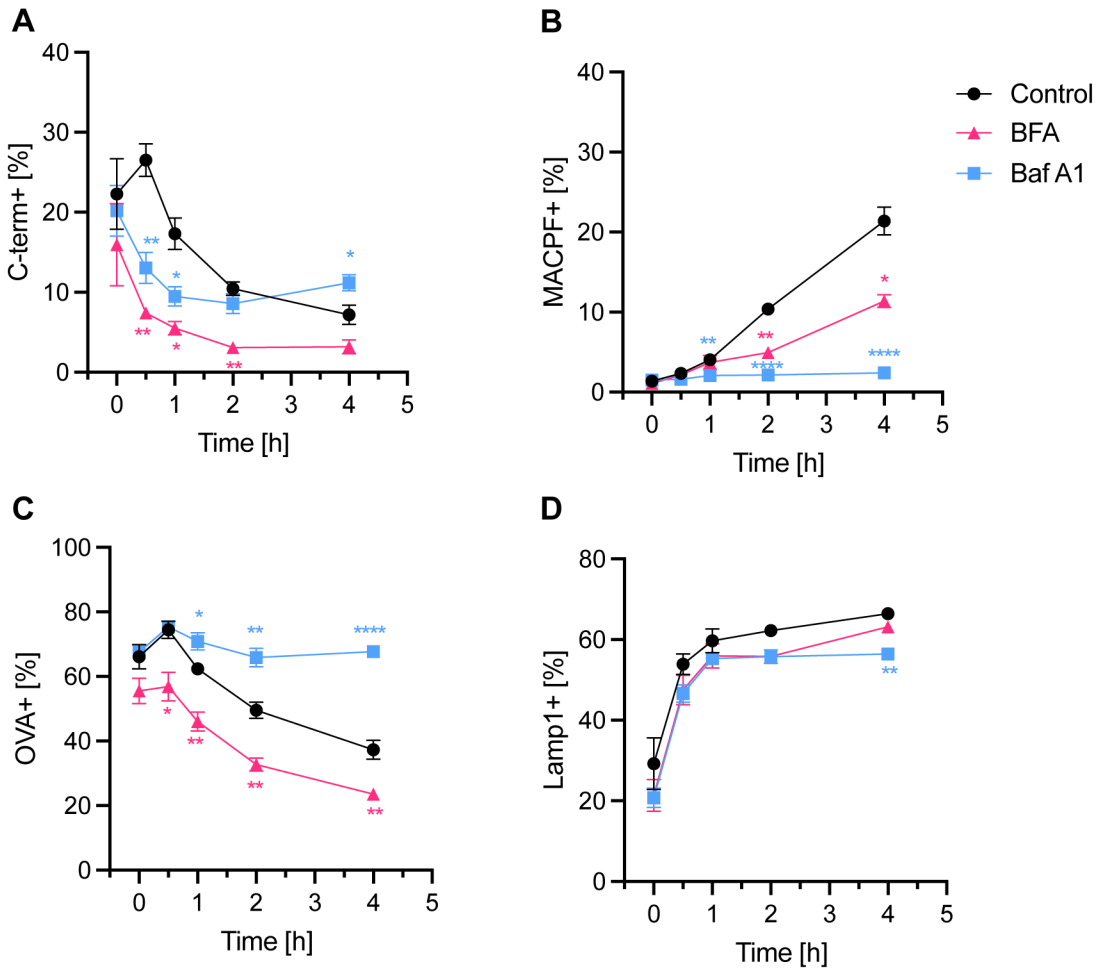

Fig. 3. 9. Effects of brefeldin A and bafilomycin A1 on perforin-2 processing and phagosome maturation. (**A, B**) Quantification of perforin-2^{+} phagosomes based on the gating shown in Fig. 3.9. (**C, D**) Quantification of ovalbumin^{+} (C) and Lamp1^{+} (D) phagosomes. Data represent mean and SEM of four independent experiments for control and BafA1 and two independent experiments for BFA conditions. *P<0.1, **P<0.01, ***P<0.001; ****P<0.0001 using a multiple paired t-test (two-stage step-up, Benjamini, Krieger and Yekutieli) versus Control.

To investigate the effects of phagosomal acidification on perforin-2 processing, I also tested the effects of bafilomycin A1 (BafA1), a V-ATPase inhibitor that blocks acidification. I found that the presence of BafA1 during the chase period led to impaired recruitment of full-length perforin-2 which can be explained by the known role of the V-ATPase in vesicular trafficking (**Fig. 3.8A** and **3.9A**) (*331-333*). BafA1 led to an increased retention of full-length perforin-2 at later timepoints consistent with the inhibitory effect of BafA1 on lysosomal proteases (**Fig. 3.9C**). However, Lamp1 acquisition was unaffected suggesting phagosome-lysosome fusion was not impaired which is consistent with previous studies (**Fig. 3.9D**) (*334*). Strikingly, the BafA1 treatment also completely blocked the appearance of the αMACPF signal (**Fig. 3.8B** and **3.9B**). Given the caveats outlined in Section 3.2.2, it is difficult to interpret which perforin-2 processing step was impaired. It could be the pre-pore to pore transition, the proteolytic generation of the p40 fragment or both.

3.2.4 Perforin-2 mediates endocytic escape from phagosomes

Since perforin-2 appeared to be subject to regulation at the phagosome, I next wanted to develop an assay to measure its activity which would allow me to relate my findings about perforin-2 processing to its function. I therefore adopted the so called “saporin-puromycin assay” that had been developed previously in the lab to measure perforin-2 pore formation at the phagosome (**Fig. 3.10A**).

The assay makes use of the 28-kDa type I ribosome-inactivating protein (RIP) saporin. Type I RIPs have been used as tools to study endocytic escape. Gelonin, a RIP similar to saporin, was used 30 years ago to show that antigen can escape from phagosome into the cytosol (*181*). Unlike type II RIPs such as ricin, type I RIPs are typically unable to cross cellular membranes of their own accord. However, if they are allowed into the cytosol, they potently inhibit translation by irreversibly inactivating ribosomes through their N-glycosidase activity (*335*). The depurination of the conserved sarcin-ricin loop in the 28S rRNA interferes with the binding of elongation factor 2 and therefore leads to translation arrest (*336*). These properties make saporin an excellent tool to study endocytic escape. To measure saporin-induced translation inhibition, the saporin-puromycin assay uses an adaptation of the surface sensing of translation (SUnSET) method (*337*) which employs the antibiotic puromycin, a structural analogue of aminoacyl tRNAs. When used at high concentration, puromycin stops translation elongation after being incorporated into nascent polypeptides. However, at low concentrations the levels of puromycin incorporation are proportional to the rate of translation. The intracellular puromycylated polypeptides can be labelled with the 12D10 antibody and detected by flow cytometry to serve as a measure for saporin-induced translation inhibition.

To measure endocytic escape from the phagosome, I conjugated saporin to the OVA beads. For the assay to work, saporin needs to be able to come off the bead. While this can occur following ovalbumin degradation, I introduced a second potential mechanism by conjugating saporin via a disulfide bond using the heterobifunctional cross-linker SPDP. The disulfide bond can be cleaved (reduced) through the activity of phagosomal Gamma-interferon–inducible lysosomal thiolreductase (GILT) releasing saporin into the lumen (*338*). I confirmed that the saporin conjugation was successful by staining the beads with an αSaporin antibody (**Fig. 3.10B**). I also noted that the amount of conjugated saporin could be reliably titrated.

To measure the activity of perforin-2 at the phagosome, NT or Mpeg1^{KO} MutuDCs were incubated with saporin beads (or BSA beads as control) for 5 h at 37°C followed by a 30 min pulse with puromycin. The cells were then chilled on ice and non-internalised beads labelled with an αOvalbumin antibody. After fixation and permeabilisation, the puromycylated

peptides were labelled with the 12D10 antibody and detected by flow cytometry (**Fig. 3.10C**). Saporin escaped into the cytosol in a perforin-2-dependent manner and only in cells with an internalised bead, but not in cells with no bead, confirming that the assay worked as expected (**Fig. 3.10D**).

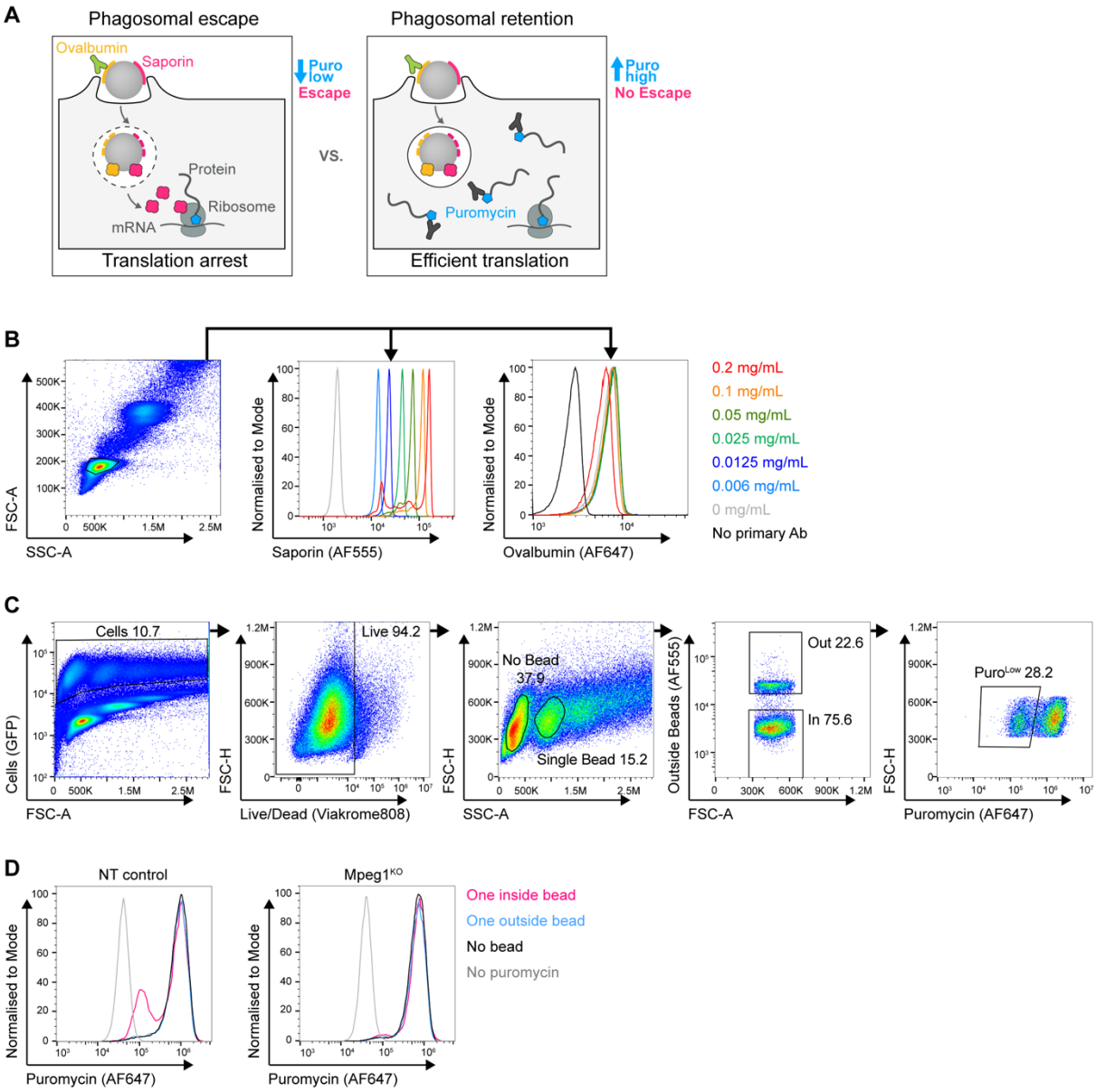

Fig. 3. 10. Perforin-2 mediates saporin escape from phagosomes. (**A**) Schematic representation of the bead saporin-puromycin assay. (**B**) Amino beads were coated in ovalbumin followed by conjugation with different concentrations of saporin as indicated. Beads were then stained with αSaporin and αOvalbumin antibodies. (**C**) Gating strategy for the bead saporin-puromycin assay. (**D**) NT or Mpeg1^{KO} MutuDCs were incubated with saporin beads for 5 h followed by an incubation with puromycin for 30 min. Cells were then placed on ice and outside beads labelled with an αOvalbumin antibody. After fixation and permeabilisation, levels of puromycin incorporation were detected with an αPuromycin antibody. Data are representative for more than five independent experiments.

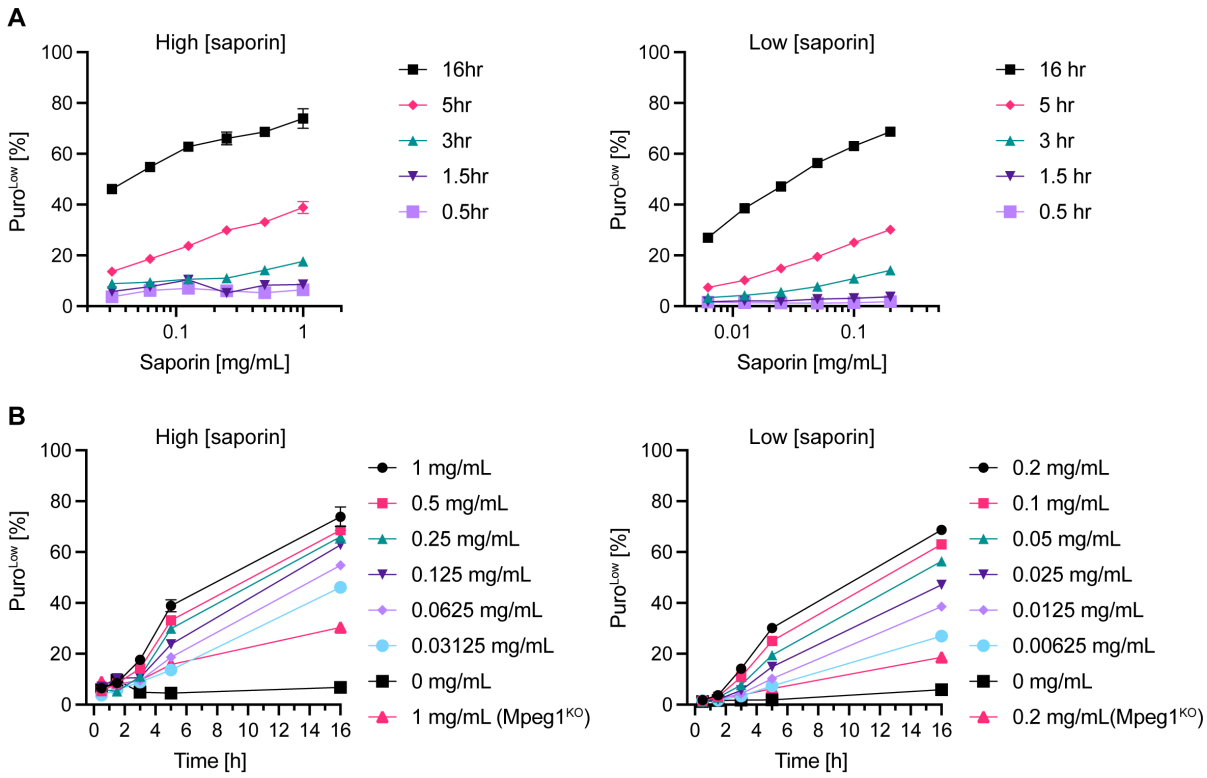

Fig. 3. 11. Quantification of perforin-2 activity across different saporin concentrations and timepoints. (**A, B**) Quantification of cells in translation arrest (Puro^{Low}) based on the gating shown in Fig. 3.10C. NT MutuDCs were incubated with a high (left) and low (right) concentration series of saporin beads for the indicated times. Mpeg1^{KO} MutuDCs were only incubated with beads with the highest saporin concentration of each series. The Puro^{Low} quantification is plotted in relation to saporin concentration (A) and time (B). Data represent mean and SEM of two technical repeats of one experiment.

To further characterise perforin-2-mediated endocytic escape at the phagosome, I varied the concentration of saporin on the beads with a 2-fold serial titration starting at 1 mg/mL or at 0.2 mg/mL (refers to the saporin concentration during the conjugation reaction) (**Fig. 3.11A** and **3.11B**). I incubated the cells with these beads for different periods of time (0.5 h, 1.5 h, 3 h, 5 h and 16 h). The dose-response curve for saporin beads was approximately log-linear and escape was detectable after 3 h with concentrations of 0.05 mg/mL or above. The proportion of cells in which saporin escaped continued to increase with prolonged incubation. Surprisingly, even after 16 h the phagosomes remained intact and the escape of saporin was still largely perforin-2 dependent. The titration revealed that reducing the saporin concentration by 50% only led to a relatively small decrease in the percentage of cells with an escape event. For example, reducing the concentration from 0.2 to 0.1 mg/mL with a 5 h incubation changed the percentage of Puro^{Low} cells from ~28% to ~24% suggesting that at 5h, a ~14% decrease in cells with translation arrest corresponds to a 2-fold decrease in escape efficiency.

3.2.5 Effects of brefeldin A and bafilomycin A1 on saporin escape

Given that BFA led to an impairment in perforin-2 recruitment to the phagosome (**Fig. 3.8A** and **3.9A**), I wanted to test whether this translates to a reduced level of saporin escape in the bead saporin-puromycin assay. I therefore incubate NT and Mpeg1^{KO} with saporin beads in the presence or absence of BFA for 5 h. Surprisingly, BFA treatment increased, rather than decreased, the percentage of Puro^{Low} cells (**Fig. 3.12**). The effect was especially pronounced in Mpeg1^{KO} cells, and it was dependent on the saporin concentration on the bead suggesting that BFA mediates the escape of saporin independently of perforin-2. Nonetheless, BFA-treated NT cells still showed higher levels of escape than BFA-treated Mpeg1^{KO} cells implying that the drug did not block perforin-2-mediate escape completely.

Next, I tested the effects of BafA1 on perforin-2-mediated saporin escape. I incubated NT and Mpeg1^{KO} MutuDCs with a single concentration of saporin beads (1 mg/mL) in the presence or absence of BafA1 for 5 h. Surprisingly, BafA1 treatment had no effect on escape efficiency in this assay. (**Fig. 3.13**) This result was unexpected given the earlier described BafA1-mediated inhibition of perforin-2 recruitment and processing at the phagosome. The concentration of saporin in these experiments was quite high (1 mg/mL) and I reasoned that functional differences may be masked if the concentration is saturating. I therefore repeated the experiment with saporin beads at lower concentrations of conjugated saporin (max. 0.2 mg/mL). In this setup, BafA1 treatment resulted in a decrease in Puro^{Low} NT cells corresponding to an approximate 2-fold reduction in escape efficiency while fraction of Puro^{Low} Mpeg1^{KO} remained unaltered (**Fig. 3.14**). However, this experiment was conducted only once and additional repeats are necessary to confirm the results. Collectively, these findings suggest that, although BafA1 treatment may inhibit perforin-2-mediated escape, it does not completely abolish it, contrary to what might have been expected based on the pH-dependent regulation of pore formation *in vitro*.

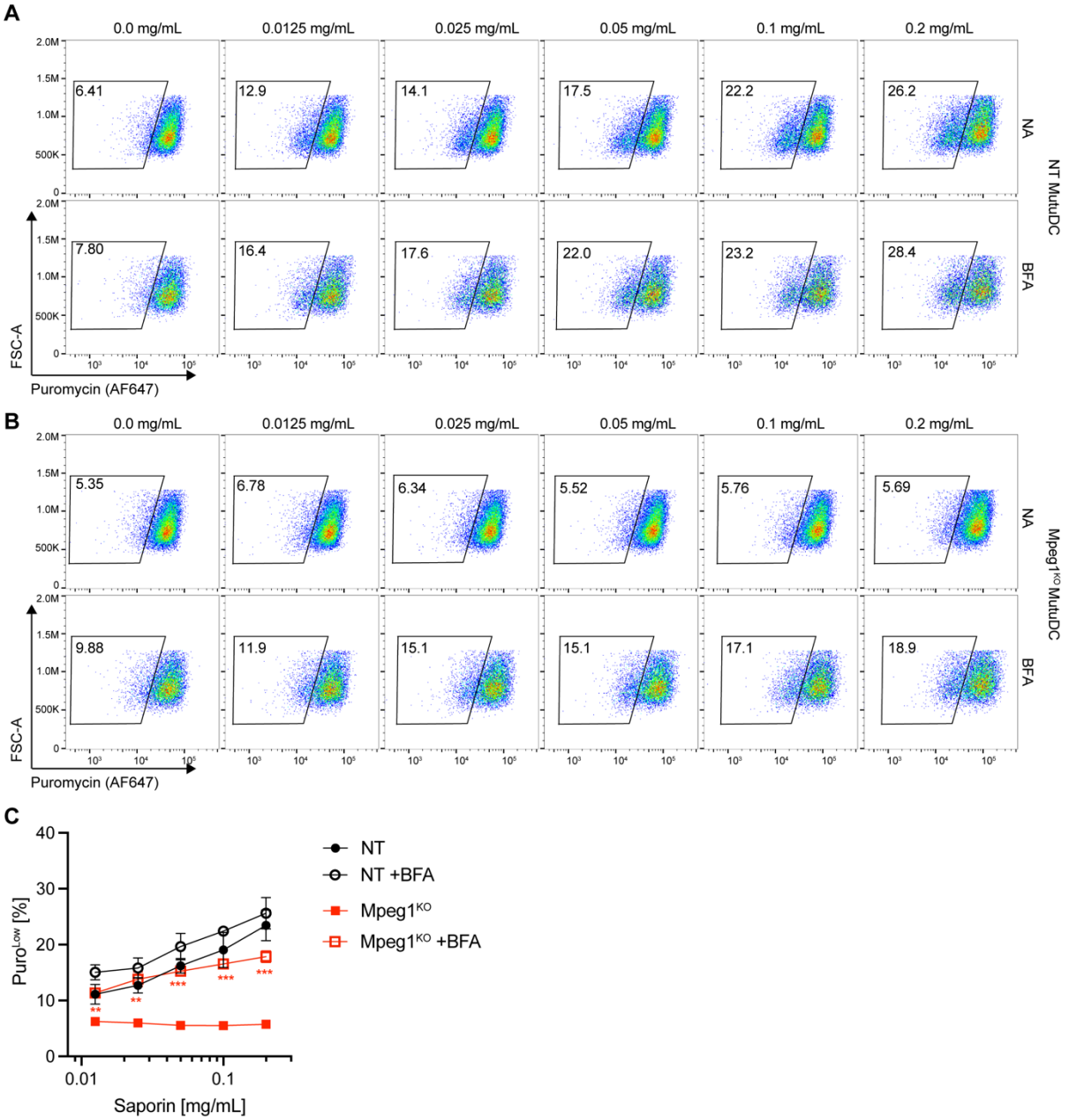

Fig. 3. 12. Effects of brefeldin A on endocytic activity. (**A, B**) NT (A) or Mpeg1^{KO} (B) were assayed in the bead saporin-puromycin assay in the presence or absence of 5 µM brefeldin A. Cells were incubated with saporin beads for 5 h followed by an incubation with puromycin for 30 min. Cells were then placed on ice and outside beads labelled with an αOvalbumin antibody. After fixation and permeabilisation, levels of puromycin incorporation were detected with an αPuromycin antibody. (**C**) Quantification of cells in translation arrest (Puro^{Low}) based on the gating shown in (A) and (B). Data represent mean and SEM of two independent experiments. **P<0.01, ***P<0.001 using a multiple paired t-test (two-stage step-up, Benjamini, Krieger and Yekutieli) versus no addition (NA) control. The difference between NA and BFA-treated NT MutuDCs was not significant.

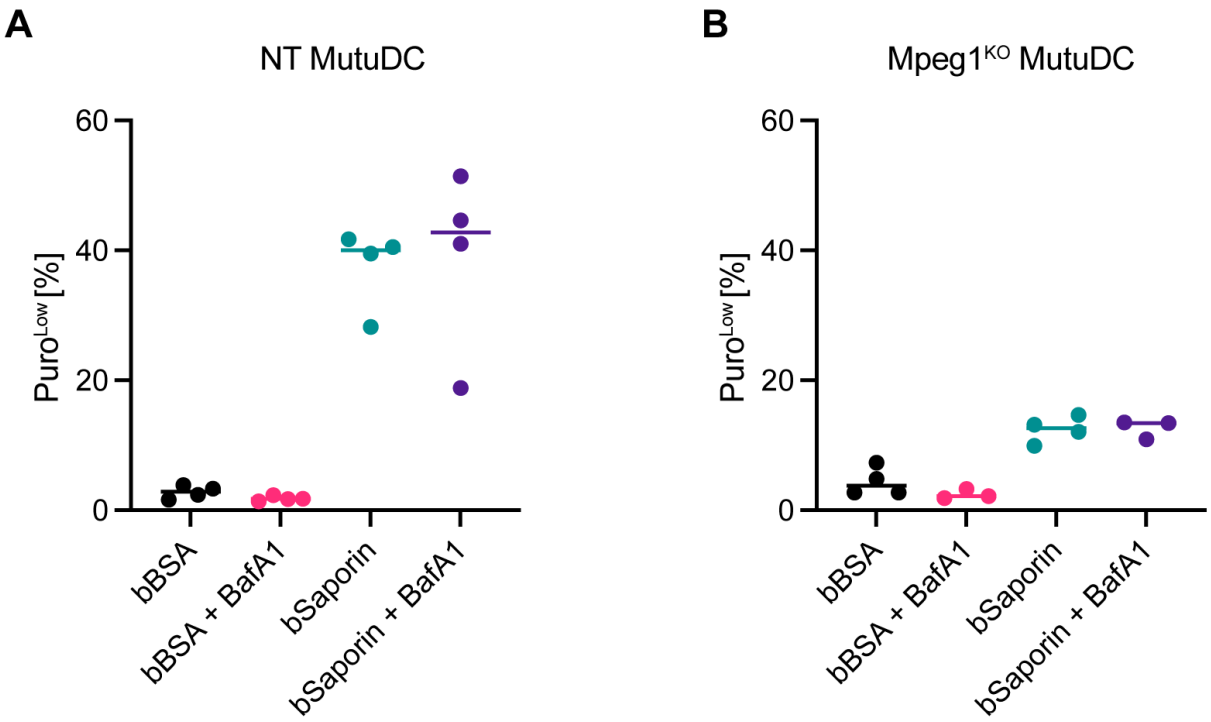

Fig. 3. 13. Effects of bafilomycin A1 on saporin escape. (**A, B**) NT (A) MutuDCs and Mpeg1^{KO} (B) MutuDCs were assayed in the bead saporin-puromycin assay with 1 mg/mL saporin beads for 5 h in the presence or absence of 0.5 μM bafilomycin A1. Data represent mean of four independent experiments.

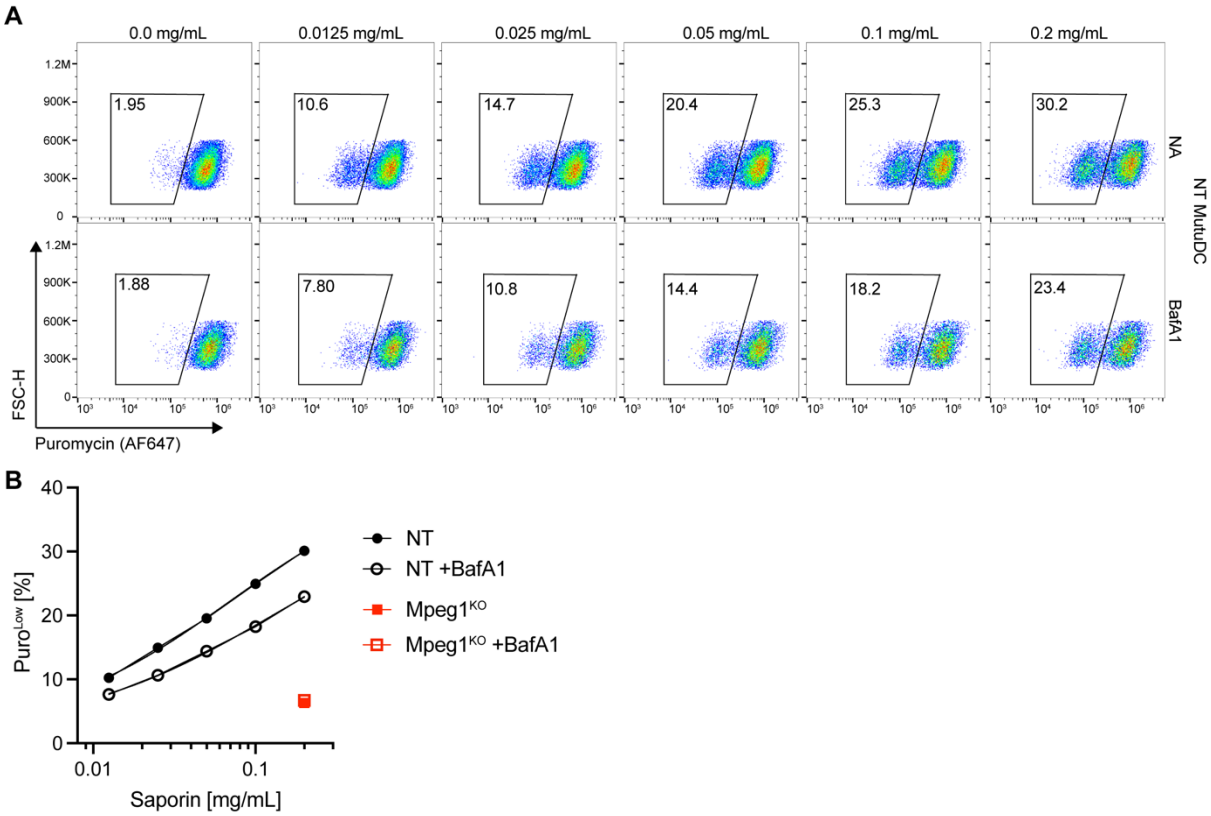

Fig. 3. 14. Effects of bafilomycin A1 on perforin-2 escape. (**A**) NT MutuDCs were assayed in the bead saporin-puromycin assay as in Fig. 3.12 in the presence or absence of 0.5 μM bafilomycin A1. (**B**) Quantification of cells in translation arrest (Puro^{Low}) based on the gating shown in (A). Data represent mean and SEM of three independent experiments with BafA1 treated Mpeg1^{KO} cells and four independent experiments with all other conditions. Data represent mean of two technical repeats of one experiment.

3.2.6 Perforin-2 processing and activity are impaired in a disulfide trapped mutant

To further characterise the relationship between perforin-2 processing and activity, I decided to take a genetic approach and study rationally designed perforin-2 mutants in phagoFACS and bead saporin-puromycin experiments. In one mutant, which I termed “VV-mutant” (G212V/A213V), I mutated the last two residues within the highly conserved MACPF motif (Y-G-T-H-V-X6-**G**-**A**) of perforin 2 which maps to one of the central beta-strands (**Fig. 3.15A**). Previous mutagenesis studies of this region in related MACPF/CDC proteins suggest that the “G-A/G” motif acts as a hinge point for conformational changes during the pre-pore to pore transition (*283, 339*). In the other mutant, which I termed “CC-mutant” (K251C/G286C), I introduced a disulfide bond that prevents the unfurling of TMH2 from the MACPF domain (**Fig. 3.15A**) (*247*).

cDNAs encoding wild-type or mutant perforin-2 were cloned into a plasmid with an IRES-mScarlet reporter cassette. Mpeg1^{KO} MutuDCs were then stably reconstituted with these constructs by lentiviral transduction and sorted for equal levels of mScarlet expression. Western blot analysis and intracellular staining with the αC-term antibody confirmed that all reconstituted lines had similar levels of perforin-2 expression (**Fig. 3.15, B and D**). As expected, both mutants were completely inactive in the saporin-puromycin assay (**Fig. 3.15E**)

Western blot analysis with the αC-term further showed that the full-length VV-mutant was unable to form high-molecular weight oligomers (**Fig. 3.15B**). This could suggest a defect in pre-pore assembly as reported for recombinant perfringolysin O after mutagenesis of the equivalent G-A/G motif (*283*). In addition, Western blot analysis with the αMACPF antibody revealed that the p40 fragment was undetectable suggesting that the responsible cleavage in the EGF domain was abolished (**Fig. 3.15C**). These results are consistent with the interpretation that the VV-mutant is arrested at an early stage of the pore formation pathway. The CC-mutant, on the other hand, was able to form high-molecular weight oligomers as detected by the αC-term antibody (**Fig. 3.15B**). Nonetheless, the levels of the p40 fragment were significantly reduced (**Fig. 3.15C**). These findings suggest that the unfurling of the TMH2 is necessary for the cleavage to occur efficiently.

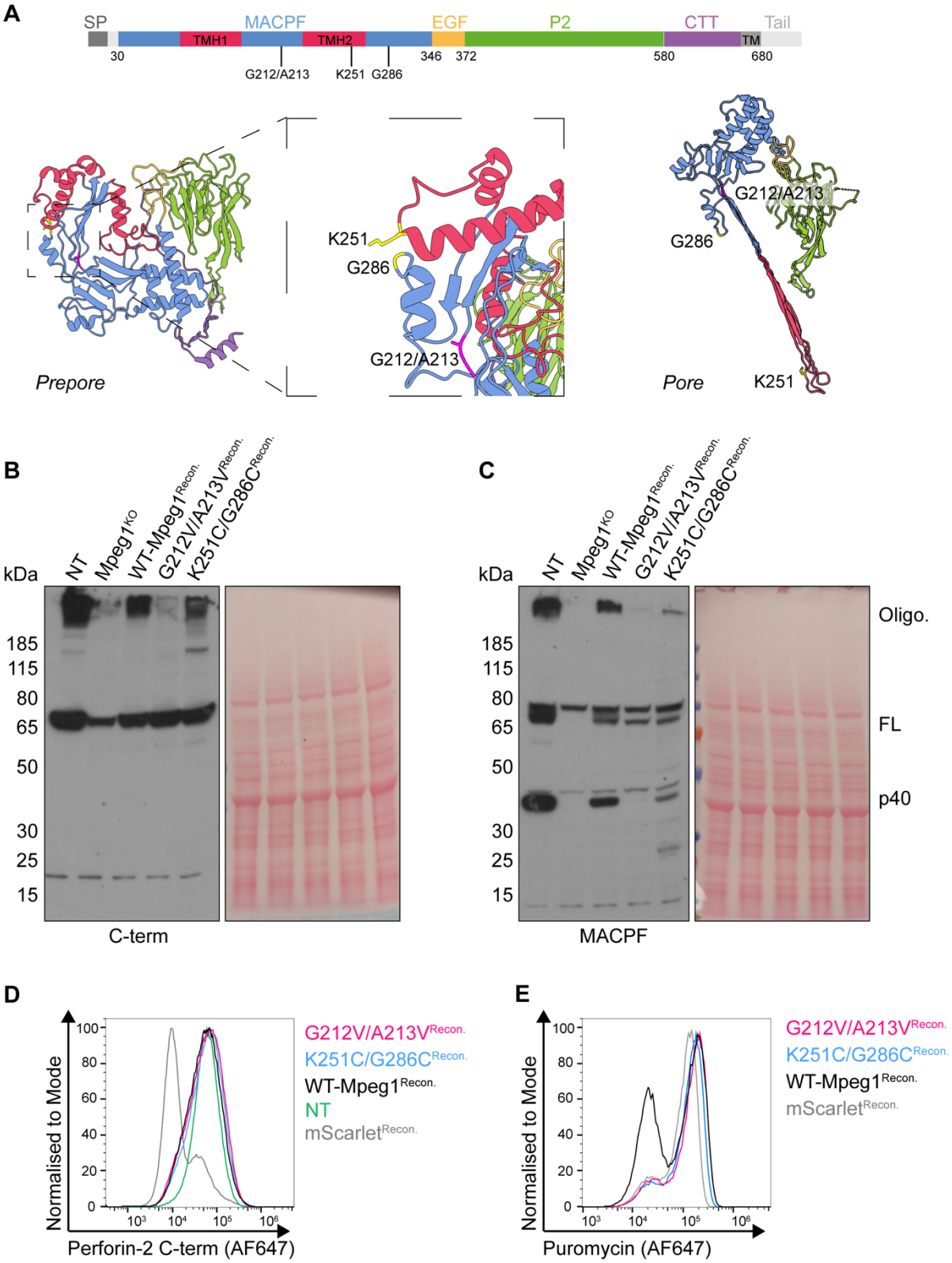

Fig. 3. 15. Generation of perforin-2 mutants which are defective in pore formation. (**A**) Schematic representation of perforin-2 in pre-pore and pore conformation. The mutated residues in the G212V/A213V VV-mutant are shown in magenta and those in the K251C/G286C CC-mutant are shown in yellow. (**B, C**) Western blot analysis of whole cell lysate from the indicated MutuDC lines probed with the αC-term (B) or αMACPF (C) antibody under non-reducing conditions. Data are representative for two independent experiments. (**D**) Intracellular staining of the indicated MutuDC lines using the αC-term antibody. (**E**) The indicated MutuDC lines were assayed in the soluble saporin-puromycin assay using 0.1 mg/mL saporin. Data are representative for two independent experiments.

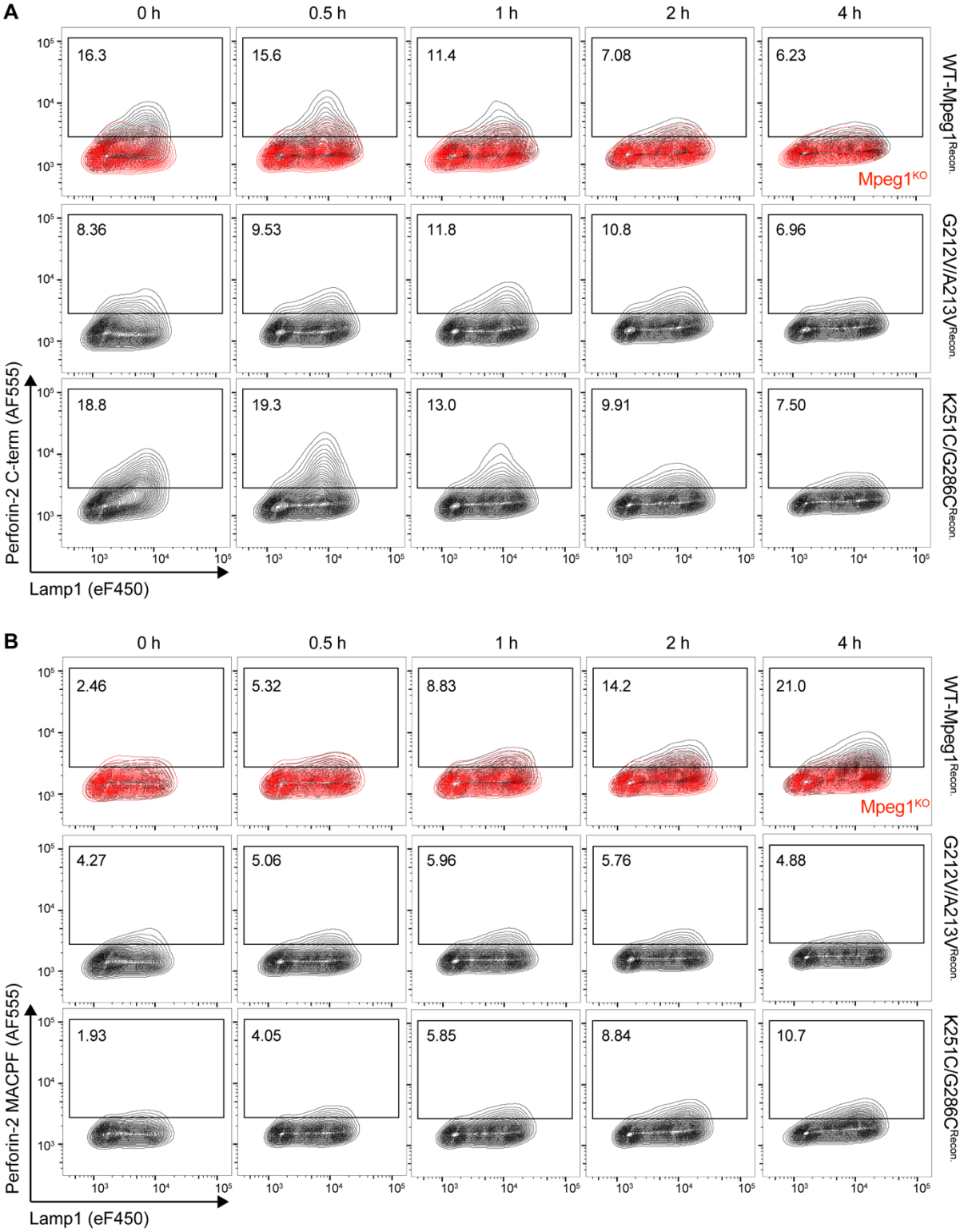

Fig. 3. 16. Effects of the G212V/A213V and K251C/G286C mutations on perforin-2 processing. (**A, B**) The indicated MutuDC lines were pulsed with OVA beads for 25 min at 16°C followed by 5 min at 37°C, washed and either immediately placed on ice (0 h) or chased for the indicated time. Isolated phagosomes were stained with aLamp1 and with αC-term (A) or αMACPF (B) antibodies. Data are representative for three independent experiments.

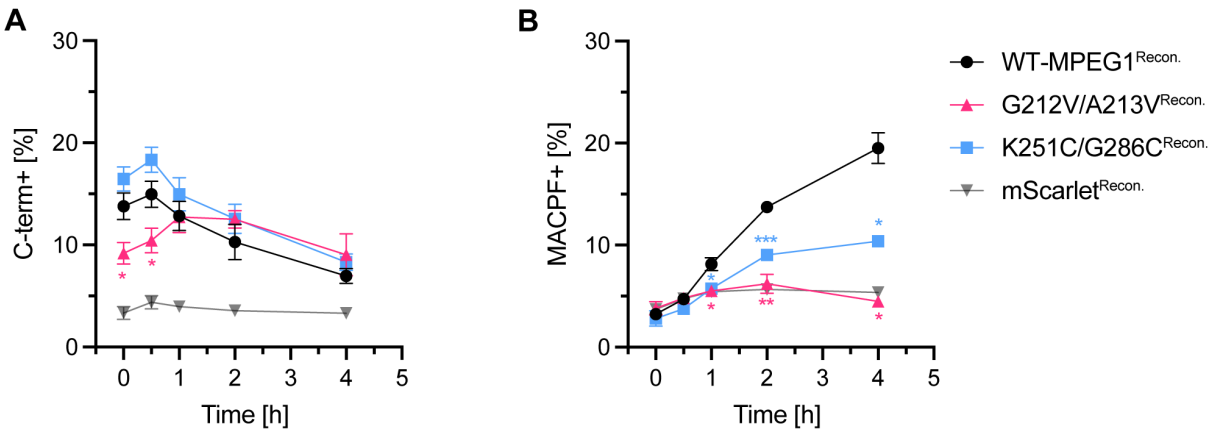

Fig. 3. 17. Quantification of the effects of the G212V/A213V and K251C/G286C mutations on perforin-2 processing. (**A, B**) Quantification of perforin-2^{+} phagosomes based on the gating shown in Fig. 3.17. Data represent mean and SEM of three independent experiments. *P<0.1, **P<0.01, ***P<0.001using a multiple paired t-test (two-stage step-up, Benjamini, Krieger and Yekutieli) versus WT-Mpeg1$^{Recon.}$.

Next, I analysed MutuDCs reconstituted with wild-type or mutant perforin-2 in phagoFACS. Recruitment of the full-length VV-mutant was delayed but reached wild-type levels after 1 h (**Fig. 3.16A** and **3.17A**). The impaired recruitment at earlier timepoints suggests that the VV-mutant is mistrafficked at steady-state. Consistent with the Western blot results, processing of the VV-mutant to the species detected by the αMACPF was completely abolished (**Fig. 3.16B** and **3.17B**). The full-length CC-mutant was recruited normally (**Fig. 3.16A** and **3.17A**), however, acquisition of the αMACPF signal was diminished (**Fig. 3.16B** and **3.17B**). These findings suggest that processing of the CC-mutant at the phagosome was impaired as might be expected from the Western blot analysis. Given that the CC-mutant is likely to be trapped in a pre-pore state, it seems that the αMACPF signal represents a pore or post-pore state. However, it remains impossible to deduce the exact conformation recognised by this antibody. The locking of the TMH2 could diminish the αMACPF signal either because the blocked conformational change normally exposes the epitope directly or because it is required for the p40 cleavage to expose the epitope indirectly.

3.3 Discussion

One of the central goals of this thesis is to identify the processing step that are required for perforin-2 pore formation. The regulation of pore-forming proteins is typically multi-layered and the data in this chapter suggest that perforin-2 is no exception. The results indicate that perforin-2 is subjected to proteolytic processing, potentially at multiple sites, both in the endosome/lysosome system and on phagosomes. Perforin-2 is recruited to the phagosome in its TMD-anchored form mostly from a BFA-sensitive intracellular compartment. Once recruited, it appears to undergo stepwise processing involving potentially pH-dependent proteolysis and conformational changes. How exactly these conversions relate to pore formation remains to be fully resolved. Nonetheless, the results show that perforin-2, at

some point during its residence at the phagosome, is competent to mediate endocytic escape of luminal antigens into the cytosol.

One question arising from the results in this chapter is at which point in the pore assembly pathway the EGF cleavage (which yields the p40 fragment) occurs. The microscopy and fractionation experiments collectively suggest that the p40 fragment accumulates in acidic late endocytic compartments, probably (endo)lysosomes (*340*). Thus, the EGF cleavage may be pH-dependent and later experiments presented in Chapter 5 indeed showed that this cleavage can be inhibited by BafA1. Acidic pH may be necessary for protease activity, but it could be equally important to mediate a conformational change that exposes the cleavage site. Accordingly, the VV-mutant, which is likely to arrest at or before the pre-pore stage, is not cleaved. On the other hand, the CC-mutant, which is unable to unfurl TMH2, is cleaved with reduced efficiency. This could suggest that the EGF cleavage happens after, or concomitant with, pore insertion. However, it is unclear why the disulfide-lock would not abolish the p40 cleavage completely. One explanation could be that the disulfide-lock is reduced *in vivo* so that a fraction of the CC-mutant can proceed to undergo the pore assembly pathway to completion as observed following reduction *in vitro* (*247*). However, this seems unlikely given that the mutant is completely inactive (**Fig. 3.15E**). A more plausible interpretation is that the disulfide-locked CC-mutant, while attempting to transition into a pore, assumes a hybrid conformation which makes the cleavage site accessible to proteases, albeit with reduced efficiency.

The detectable product of the EGF cleavage, the p40 fragment, lacks the C-terminal transmembrane anchor and the membrane-binding P2 domain and is therefore likely to reside in the (endo)lysosome lumen. Indeed, spatial proteomics conducted by our collaborators in the Borner lab classified peptides derived from the p40 fragments as luminal (see Fig. 3 in (*249*)). These data are consistent with the interpretation that the majority of the (endo)lysosomal pool of perforin-2 has been rendered unable to form pores since it lacks a membrane-targeting domain. Whether the p40 fragment performs any function or is simply a byproduct of the perforin-2 lifecycle is currently unknown.

Following its recruitment to the phagosome, the TMD-anchored perforin-2 undergoes stepwise processing leading to the loss of the αC-term signal and gain of the αMACPF. As mentioned in Section 3.2, the phagoFACS data equally support the possibility that the αMACPF antibody could either recognise a conformational change or identify a cleavage event. The exposure of the αMACPF was inhibited by BafA1 suggesting a pH-dependent mechanism. However, the signal does not appear to correlate with the efficiency of perforin-2-mediated escape given that escape was not completely prevented by BafA1. The non-

correlation is further supported by the CC-mutant data, where escape was completely inhibited even though the epitope remained partly exposed. These data suggest that the mechanism revealing the αMACPF may not be directly linked to pore formation. In Chapters 5 and 6, I will investigate the relationship between perforin-2 processing and endocytic escape in more detail.

Treatment with BFA inhibited the recruitment of perforin-2 to the phagosome. This suggests that perforin-2 may be recruited directly from the ER-Golgi. A BFA-sensitive delivery route has also been reported for other phagosomal proteins including sortilin, cathepsin D and Rab39A (*211, 330, 341, 342*). However, the effects of BFA on perforin-2-mediated escape are ambiguous because it increased saporin escape not only in NT but also in Mpeg1^{KO} MutuDCs. Given the pleotropic effects of BFA on the endosome/lysosome system (*326*), the mechanism for this BFA-mediated escape is difficult to pinpoint. It could be based on BFA-induced membrane destabilisation or alterations in membrane composition making it more conducive to saporin translocation. BFA has previously been reported to enhance the cytotoxicity of antibody-conjugated saporin and ricin A-chain but these studies do not provide any additional mechanistic insights (*343, 344*). Curiously, the BFA-mediated escape mechanism had a differential impact on NT and Mpeg1^{KO} cells. In NT cells, the overall escape efficiency increased by ~20% following BFA treatment. However, in Mpeg1^{KO} cells, the increase was much more pronounced, with an enhancement of ~200%. The differential sensitivity to BFA between the two cell lines could be indicative of an additive effect in NT cells where a combination of a partial inhibition of perforin-2-mediated escape and an enhancement of BFA-mediated escape offset each other.

The treatment with BafA1 did not abolish perforin-2-mediated escape even though pore formation is strictly dependent on acidification *in vitro* (*246, 247*). While only preliminary, these data give rise to the exciting possibility that pore formation *in vivo* may be less dependent on acidic pH which would be consistent with the notion that phagosome of cDC1s do not acidify (*216, 217, 245, 321*). However, BafA1 did inhibit perforin-2-mediated escape to some extent at lower saporin concentrations in at least one experiment. To better understand these findings, I set out to investigate the relationship between perforin-2 pore formation and phagosomal pH in more detail as discussed in Chapter 4.

Chapter 4 – Perforin-2 activity does not alter phagosomal pH

4.1 Introduction

The results in Chapter 3 have shown that perforin-2 can shuttle antigen as large as 30 kDa in size into the cytosol (Fig. 3.10). The specificity of the pores is still unknown but, considering their large size, cargo release is likely to be accompanied with significant ion fluxes across the phagosomal membrane. Perforin-2 pores may therefore have a direct impact on phagosomal pH through non-specific leakage of ions, and I set out to investigate this as described in this chapter.

Phagosome acidification is critical for numerous processes during phagosome maturation including vesicle fusion and the activation of degradative enzymes (*345, 346*). The kinetics and degree of acidification, however, differ among professional phagocytes and are adapted to support their respective functions in the immune system (*347*). In the case of cDC1s, phagosomal acidification is finely tuned to support antigen cross-presentation by preventing the excessive proteolysis of antigens and maintaining their MHC-I binding epitopes (*39, 348*). However, some degree of acidification may be necessary to break down phagocytosed cargo into antigen that is small enough to be delivered across the phagosomal membrane (*198*).

In DCs, endosomal and phagosomal pH is primarily determined by the interplay of V-ATPase and NADPH Oxidase 2 (NOX2) which have opposing effects. The V-ATPase contributes to the acidification of phagosomes and uses ATP to pump protons into the phagosome lumen. The active complex is made up of a peripheral V_1 subdomain, that hydrolyses ATP, and a membrane-integral V_0 subdomain, that contains the proton channel. The rate of proton pumping is not only dictated by factors that regulate the intrinsic activity of the V-ATPase (e.g. subunit composition) but also environmental factors. Since the translocation of protons is unaccompanied by a counterion it leads to a build-up of positive charge in the phagosome lumen. The continued operation of the V-ATPase therefore depends on concomitant anion influx and cation efflux which are provided by several ion channels (*345*). Similar to V-ATPase, NOX2 is a multicomponent enzyme comprising transmembrane proteins $gp91^{phox}$ and $gp22^{phox}$, as well as the three cytosolic components $p40^{phox}$, $p47^{phox}$ and $p67^{phox}$. It transfers electrons from cytosolic NADPH to luminal O_2 to produce superoxide anions (O_2^-), a type of reactive oxygen species (ROS) which are converted to H_2O_2 in an acidic environment, consuming luminal protons. Like V-ATPase, continued NOX2 activity requires charge compensation to alleviate the build-up of protons in the cytosol. Continued ROS

production is made possible by the voltage-gated proton channel 1 (Hv1) which translocates protons from the cytosol into the phagosome providing charge compensation (*345, 349*).

The pH regulation in DCs has been studied in BMDCs, CD11c+ splenocytes and human-derived DCs as summarised in **Table 4.1**. The BMDC studies mostly evaluated pH in the context of DC maturation and its effects on cross-presentation. One studied showed that the decreased cross-presentation efficiency observed in fully mature BMDCs is at least partly due to the LPS-induced upregulation of the transcription factor TFEB which increases lysosomal acidification and proteolysis by upregulating V-ATPase expression (*213*). Conversely, the transient enhancement of cross-presentation seen in BMDCs following intermediate duration LPS treatment (7 – 20 h) can be attributed partly to decreased levels of V-ATPase at the phagosome (*350*). In addition, studies in splenic DCs highlighted a correlation between cross-presentation efficiency and NOX2 recruitment in different DC subsets. Splenic CD8α+CD11c+ murine DCs, but not CD8α- DCs, assemble functional NOX2 on phagosomes via Rab27a-, Rab39a- and Rac2-mediated recruitment of the $p47^{phox}$ and $gp91^{phox}$ subunits of NOX2 (*211, 216, 217, 245*). Similar results have reported in human monocyte-derived DCs (*321*). In addition, splenic CD8α+CD11c+ murine DCs express lower levels of the NOX2 inhibitors SiglecG (*351*). The consensus of these investigations is that cross-presenting DC subsets, most notably cDC1s, have high NOX2 activity and therefore relatively alkaline phagosomes with lower proteolytic activity which presumably stimulates cross-presentation by preventing rapid antigen degradation.

To study the effects of perforin-2 pore formation on phagosomal pH, I performed a range flow cytometry-based pulse-chase experiments using OVA beads conjugated with pHrodo red, a pH sensitive dye. As part of these experiments, I compared phagosomal pH between NT and $Mpeg1^{KO}$ MutuDCs, splenic DCs and BMDCs. I confirmed that the assay measures meaningful changes in pH by treating cells with the V-ATPase inhibitor bafilomycin A1 (BafA1). In addition, I investigated whether the NOX2 inhibitor DPI could be used to artificially decrease the pH of MutuDC phagosomes and stimulate perforin-2 hyperactivity.

Author, Year	**Cell type**	**Set up**	**pH after 1 h chase**	**Result**
Trombetta, 2003 (*37*)	GM-CSF BMDCs	FITC conjugated to dextran (40 kDa and 70 kDa); microscopy	Immature BMDCs: pH 5.0 Mature BMDCs: pH 4.5	Immature DCs have more alkaline endosomal pH compared to mature DCs due to less efficient recruitment of the V1 ATPase subunit.

Savina, 2006 (*216*)	GM-CSF BMDCs	FITC conjugated to 3 μm beads; flow cytometry with gating on cells with one bead; no cell surface markers	Wildtype BMDCs: pH 7.5 $gp91^{KO}$ BMDCs: pH 6.5	ConB treatment leads to alkalization suggesting an active process. $gp91^{phox}$-deficient DC failed to alkalise and produce ROS while $gp91^{phox}$-deficient BMMOs showed little difference. Ova degradation is accelerated in absence of active NOX2.
Jancic, 2007 (*217*)	GM-CSF BMDCs	FITC conjugated to 3 μm beads; flow cytometry with gating on cells with one bead; no cell surface markers	Wildtype BMDCs: pH 7.5 $Rab27^{KO}$ BMDCs: pH 6.8	Rab27a-deficient DCs have more acidic phagosomes, increased proteolysis and decreased ROS. Delayed acquisition of gp91 as well as Lamp2 in Rab27a knockouts.
Mantegazza, 2008 (*321*)	Human monocyte-derived DCs (MoDCs)	FITC conjugated to 3 μm beads; flow cytometry with gating on cells with one bead; no cell surface markers	Wildtype MoDCs: pH 7.8 DPI treated MoDCs: pH 6.6	Phagosomal pH increases during the first 2 hours. DCs recruit more NOX2 and less V-ATPase than macrophages. NOX2 inhibition by DPI decreases phagosomal pH.
Savina, 2009 (*245*)	CD11c+ splenocytes	FITC conjugated to 3 μm beads; flow cytometry with gating on cells with one bead; CD8α staining	Wildtype CD8α+: pH 7.5 $Cybb^{KO}$ CD8α+: pH 6.0 Wildtype CD8α-: pH 6.0 $Cybb^{KO}$ CD8α-: pH 5.8	pH in CD8α+ DC phagosomes are less acidic than in CD8α- DC phagosomes. CD8α+ DC-specific NOX2 activity drives alkaline pH. CD8α- DC fail to assemble NOX2 due to absence of cytosolic p47phox which is recruited by Rac2. Rac2 is also required for expression V0 V-ATPase.
Rybicka, 2011 (*349*)	GM-CSF BMDCs	CFSE or OGSE conjugated to IgG	Wildtype BMDCs: pH 5.0	NOX2 activity decreases proteolysis but has no effect on

		or mannose beads; microscopy	$Cybb^{KO}$ BMDCs: pH 5.0	phagosomal pH. NOX2-generated ROS negatively affects the reductive capacity of the phagosome and cysteine cathepsin activities in DCs
Samie, 2015 (*213*)	GM-CSF BMDCs,	pHrodo conjugated to 3 µm beads; flow cytometry; gating not specified; no cell surface markers	Wildtype BMDCs: pH 7.2 $TFEB^{OE}$ BMDCs: pH 5.8	TFEB expression in DCs enhances antigen degradation in the phagosomes by inducing the expression of lysosomal proteases and phagosomal acidification. TFEB expression is reduced in cross-presenting CD8+ DCs.
Ding, 2016 (*351*)	$CD8^{+}CD11c^{+}$ splenocytes	FITC conjugated to 3 µm beads; flow cytometry with gating on cells with one bead; no cell surface markers	Wildtype CD8α+: pH 8.3 $Siglecg^{KO}$ CD8α+: pH 7.8	Phagosomes in Siglecg−/− CD8α+ DCs maintain alkalinity, while the pH in phagosomes from Siglecg+/+ CD8α+ DCs become neutral during the first 4 h of phagocytosis. SiglecG inhibits NOX2 activity via phosphorylation of gp49(phox).
Salao, 2016 (*352*)	Flt3L BMDCs	FITC conjugated to IgG-opsonised zymosan particles; microscopy	Wildtype BMDCs: pH 5.5 $CLIC1^{KO}$ BMDCs: pH 6.0	Phagosomes of Flt3L BMDCs acidify over time. Phagosomes from CLIC1−/− BMDCs have impaired acidification
Nunes-Hasler, 2017 (*353*)	GM-CSF BMDCs	FITC or pHrodo conjugated to Ova-zymosan particles; microscopy	Wildtype BMDCs: pH 4.0 – 9.0 with average of pH 7.5	Phagosomes of GM-CSF BMDCs acidify over time. Phagosomes within the same cell can have widely differing pH values.
Oberkampf, 2018 (*354*)	CD8α+ and pDCs purified from mouse spleen	FITC conjugated to 3 µm beads; flow cytometry with gating on	Wildtype CD8α+: pH 7.5 Wildtype pDCs:	CD8α+ DCs have more alkaline phagosomes than pDCs. The pH of pDC phagosomes increases to that of CD8α+ DCs upon

		cells with one bead; CD8α, CD11c and PDAC1 staining	pH 7.0	treatment with the TLR7-agonist R848.
Olatunde, 2018 (*355*)	GM-CSF BMDCs	pHrodo conjugated to E. coli particles; flow cytometry; gating not specified; subpopulations were presorted	MHC^{Int} BMDCs: pH 4.0 $MHCII^{Hi}$ BMDCs: pH 6.0	$CD11c+CD11b+MHCII^{Int}$ BMDCs have more acidic phagosomes than $CD11c+CD11b+MHCII^{Hi}$ BMDCs.
Foote, 2019 (*356*)	cDC2s sorted from human blood and human MoDCs	SNARF-labeled Candida particles; microscopy	Wildtype MoDCs: pH 6.5 Wildtype cDC2s: pH 6.0	Phagosomal pH was slightly less acidic in MoDCs compared with primary circulating cDC2s. DPI treatment acidified phagosomes in both cell types.
Khouili, 2020 (*357*)	CD11c+ GM-CSF BMDCs and CD11c+ Flt3L BMDCs	FITC or pHrodo conjugated to dextran (10 kDa)	Not reported	Endosomes of CD11c+ BMDCs acidify over time. SHP-1 deficiency increases endosomal pH and enhances antigen cross-presentation.
Cruz, 2020 (*211*)	DC line DC3.2R and splenic CD11b+ CD11c+ DCs	pHrodo conjugated to 6 μm beads	Not reported	Rab39a-deficient DCs have more acidic phagosomes, increased proteolysis and decreased ROS likely due to inhibited NOX2 recruitment.

4.2 Results

4.2.1 Phagosomal pH in $Mpeg1^{KO}$ DCs is unaltered

To investigate the role of perforin-2 in phagosome maturation, I first compared phagosomal ovalbumin degradation and Lamp1 acquisition in NT and $Mpeg1^{KO}$ MutuDCs by phagoFACS, the phagosome flow cytometry assay introduced in Chapter 3 (Fig. 3.4). As shown in **Fig. 4.1**, phagosome maturation appeared to be unaffected by perforin-2 activity.

To directly measure the effects of perforin-2 on phagosomal pH, I performed a pulse-chase analysis with beads conjugated to pHrodo dye and coated with ovalbumin (**Fig. 4.2A**). The pHrodo dye is a pH-sensitive probe whose fluorescent intensity increases with decreasing pH. NT and Mpeg1^{KO} MutuDCs were pulsed for 25 min at 16°C followed by 5 min at 37°C. Then, cells were washed in PBS to remove any non-internalised beads and either put on ice (chase point 0 h) or incubated at 37°C for different periods.

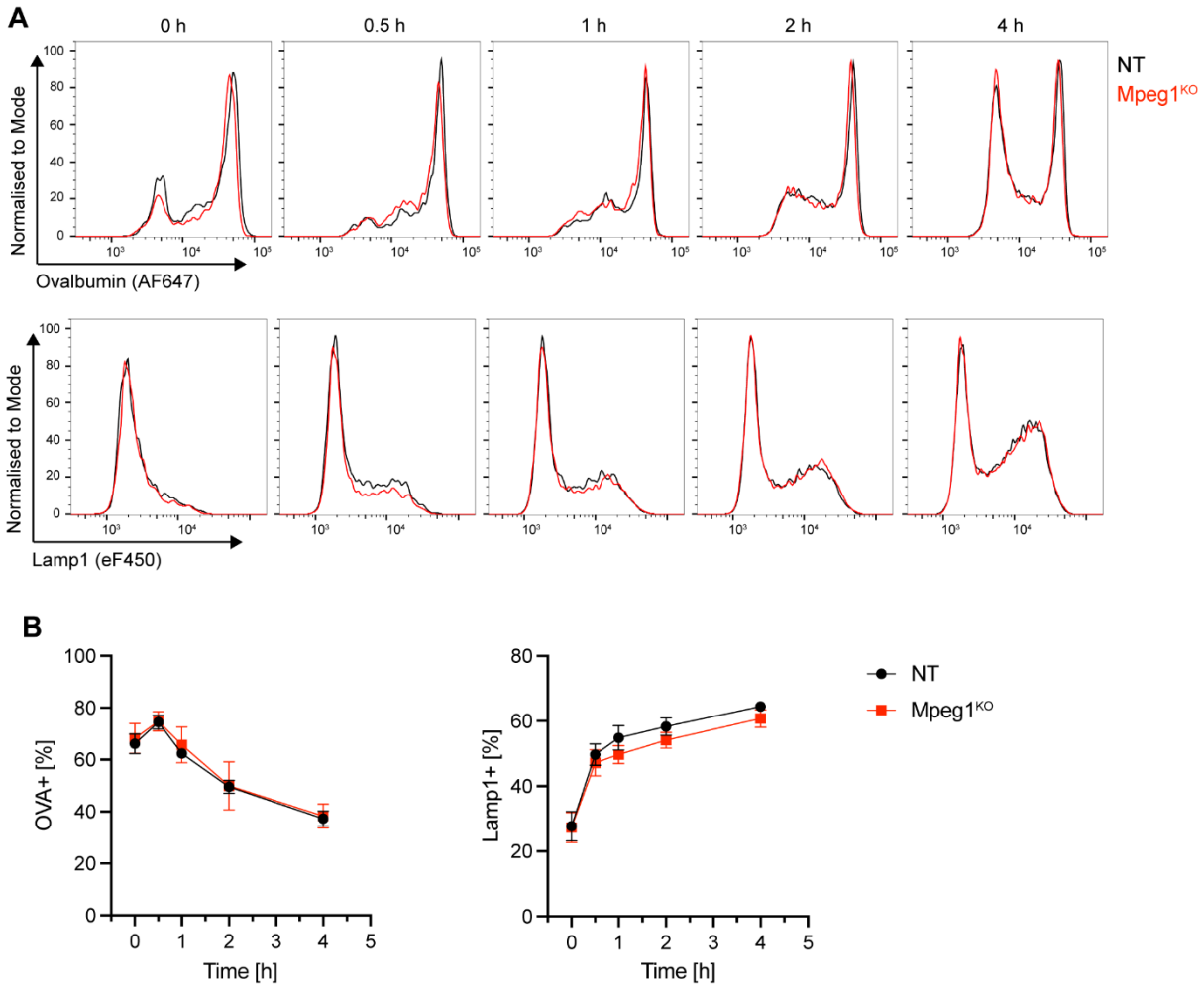

Fig. 4. 1. Phagosome maturation is comparable in NT and Mpeg1^{KO} MutuDCs. (**A**) NT and Mpeg1^{KO} MutuDCs were pulsed with OVA beads for 25 min at 16°C followed by 5 min at 37°C and either immediately placed on ice (0 h) or chased for the indicated time. Isolated phagosomes were stained with antibodies against ovalbumin (top) and Lamp1 (bottom). (**B**) Quantification of ovalbumin+ and Lamp1+ phagosomes. Data represent mean and SEM of four independent experiments. NT vs Mpeg1^{KO} conditions were compared using a multiple paired t-test (two-stage step-up, Benjamini, Krieger and Yekutieli) and found not to be significantly different.

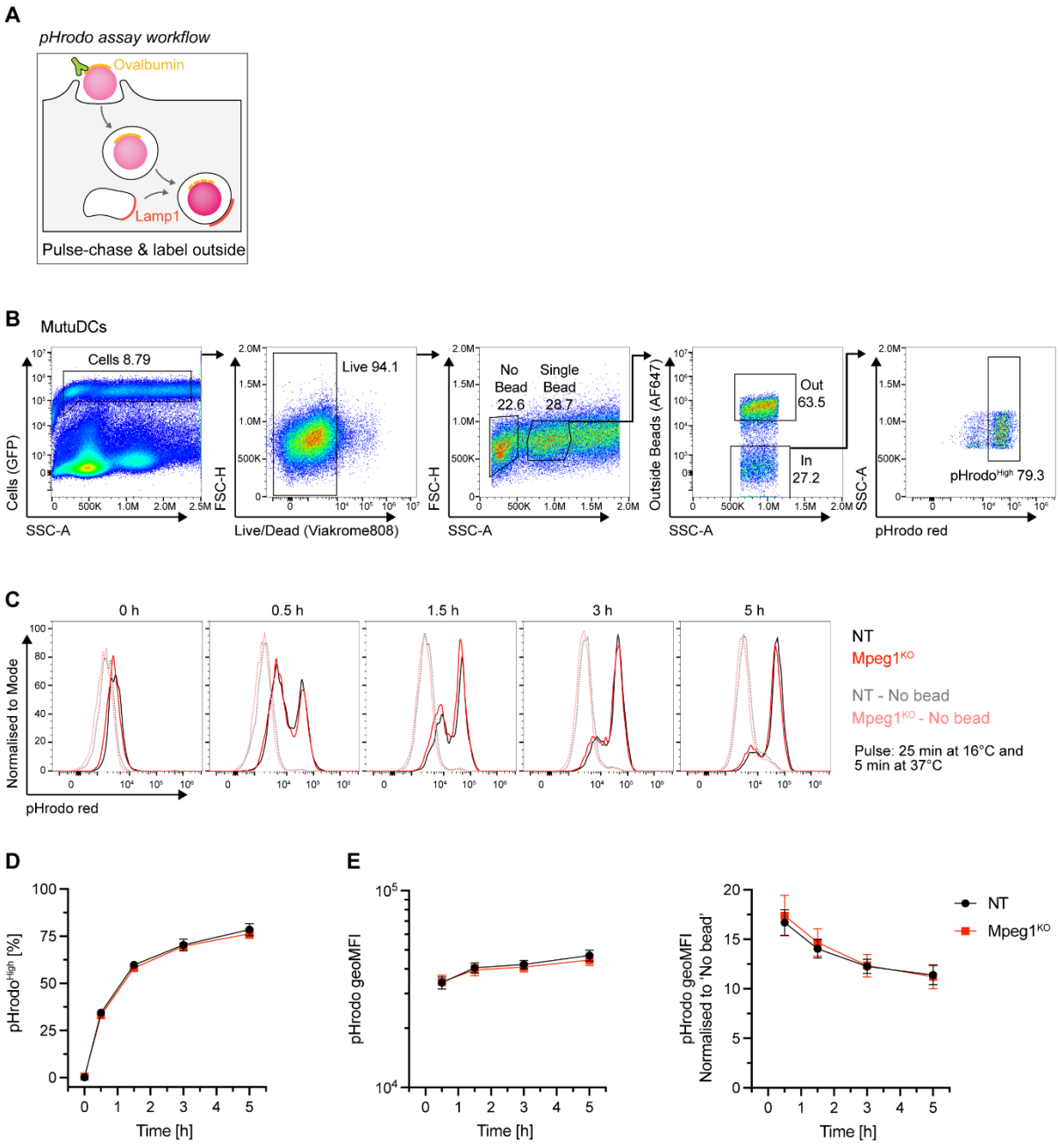

Fig. 4. 2. Phagosome acidification is comparable in NT and Mpeg1^{KO} MutuDCs. (**A**) Schematic representation of the pHrodo bead assay. (**B**) Gating strategy for the pHrodo bead assay. (**C**) NT or Mpeg1^{KO} MutuDCs were pulsed with pHrodo beads for 25 min at 16°C followed by 5 min at 37°C and either immediately placed on ice (0 h) or chased for the indicated time. After labelling of outside beads, samples were analysed by flow cytometry. (**D**) Quantification of pHrodo^{High} based on the gating shown in (B). (**E**) Quantification of the pHrodo geoMFI within the pHrodo^{High} gate. (**F**) Quantification of the phrodo geoMFI within the pHrodo^{High} gate normalised to (divided by) the pHrodo geoMFI of the 'no bead' population. Data represent mean and SEM of five independent experiments. NT vs Mpeg1^{KO} conditions were compared using a multiple paired t-test (two-stage step-up, Benjamini, Krieger and Yekutieli) and found not to be significantly different.

After the chase, non-internalised beads were labelled with an αOvalbumin antibody, and the samples analysed by flow cytometry (**Fig. 4.2B**). When preparing the pHrodo beads, multiple washes were necessary to reduce the concentration of unconjugated dye until it was no longer visible by eye. However, it was possible that cells may take up any residual dye which would result in background fluorescence as the free dye transits through the

endosome/lysosome system. To account for this, the phagosomal pH of a single internalised bead was always compared to the pH of cells without a bead in the same condition. The analysis showed that 30% of phagosomes in NT MutuDCs acidified within 30 min while the remaining phagosomes stayed relatively neutral (**Fig. 4.2, C and D**). The proportion of acidified phagosomes continued to increase and started to plateau at 80% after 5 h. Strikingly, there was no difference in the proportion of acidified phagosomes in NT and Mpeg1^{KO} MutuDCs at any of the timepoints. The geometric mean of pHrodo intensity of acidified (phrodo^{High}) phagosomes was also comparable, suggesting that there was no difference in the degree of acidification (**Fig. 4.2, E and F**). Interestingly, when normalised to the background fluorescence, the relative pHrodo intensity decreased over time suggesting that phagosomes acidify less than the compartments containing the free pHrodo dye (**Fig. 4.2F**).

The observations that MutuDC phagosomes acidify and that knocking out Mpeg1 does not affect this acidification were both unexpected. I therefore set out to test the effects of perforin-2 on phagosomal pH in primary DCs. Spleens of wild-type and Mpeg1^{KO} mice were isolated and tissue-resident DCs enriched using a negative selection pan-DC enrichment kit. The splenic DCs were pulsed with pHrodo beads for 15 min at 37°C, washed and chased for different periods of time. Cells were stained for different DC markers and non-internalised beads were labelled with an αOvalbumin antibody.

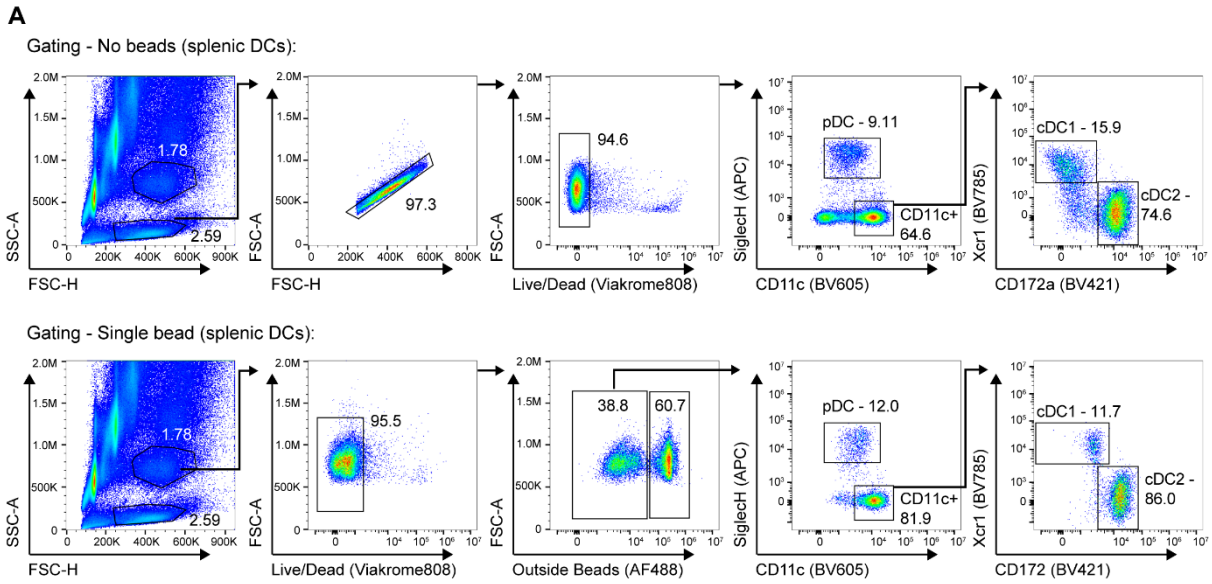

Fig. 4. 3. Gating strategy for the bead pHrodo assay in splenic DCs.

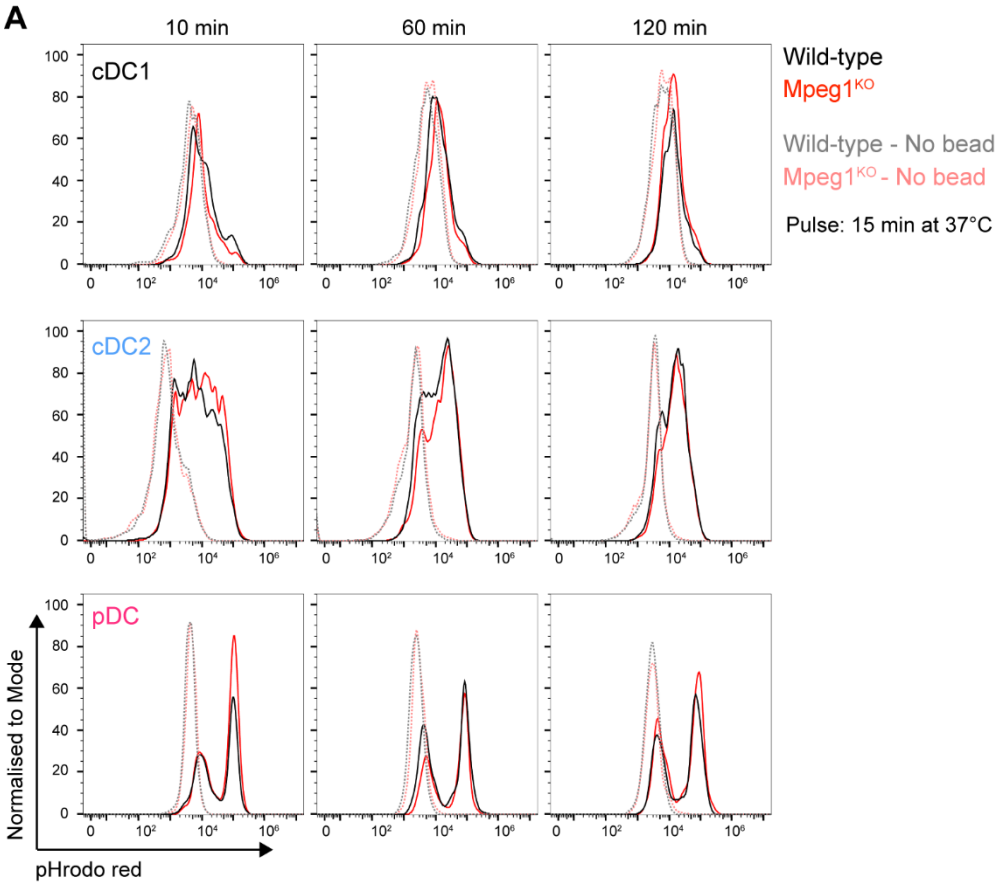

Fig. 4. 4. Phagosome acidification is comparable in wild-type and Mpeg1^{KO} splenic DCs. (**A**) Wild-type or Mpeg1^{KO} splenic DCs were pulsed with pHrodo beads for 15 min at 37°C and chased for the indicated time. After labelling of outside beads, samples were analysed by flow cytometry. Populations are defined according to the gating shown in Fig. 4.3. Data for wild-type and Mpeg1^{KO} splenic DCs are representative for two and one independent experiments, respectively.

before analysis by flow cytometry. Within the enriched splenic DC population, phagosomal pH was compared in cDC1s (CD11c+XCR1+), cDC2s (CD11c+CD172a+) and pDCs (CD11c^{Int}SiglecH+) (**Fig. 4.3**). The acidification profiles of these three DC subpopulations were notably different (**Fig. 4.4**). The cDC1 profile was unimodal, the pDC profile bimodal, and that of cDC2 was intermediate between the cDC1 and pDC profiles. Due to these variations, quantifying pHrodo^{High} proportions or MFI for comparison proved challenging. Consequently, I decided to base comparisons on visual inspection of the histograms. Consistent with previous results (*245, 351*), the pH in cDC1 phagosomes remained at background levels while phagosomes of cDC2s and pDCs gradually acidified during the chase. This acidification was especially pronounced in pDCs with a clear separation of neutral and acidified phagosomes, resembling the pH profile of MutuDC phagosomes. Interestingly, there was again no detectable difference in phagosomes of DCs isolated from wild-type and Mpeg1^{KO} mice, similar to the findings with MutuDCs. The minor differences seen in pDCs are probably due to the low number of events recorded for this subset, although additional repeats are needed for confirmation.

To further substantiate the finding that perforin-2 expression has no effect on phagosomal pH, as observed in MutuDCs and splenic DCs, I tested phagosomal pH in bone-marrow derived DCs (BMDCs). BM cells from wild-type and Mpeg1^{KO} were cultured in the presence of GM-CSF and Flt3L which generates fully differentiated cDC subsets that resemble those found *in vivo* (**Fig. 4.5**) (*53, 358, 359*). Consistent with the results in splenic DCs, phagosomal pH in cDC1s and cDC2s was unaffected by perforin-2 expression (**Fig. 4.6**).

Overall, these data show that phagosomal pH in wild-type and Mpeg1^{KO} DCs is comparable and argue for the presence of compensatory mechanisms that protect phagosomes from the putative ionic imbalances caused by perforin-2.

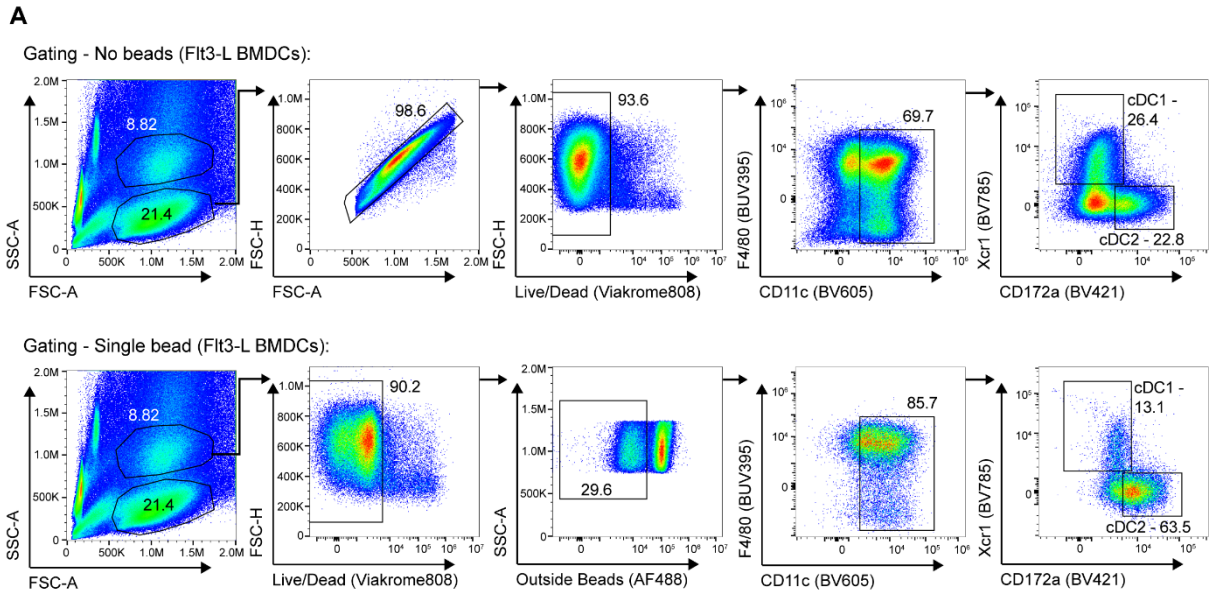

Fig. 4. 5. Gating strategy for the bead pHrodo assay in Flt3L BMDCs.

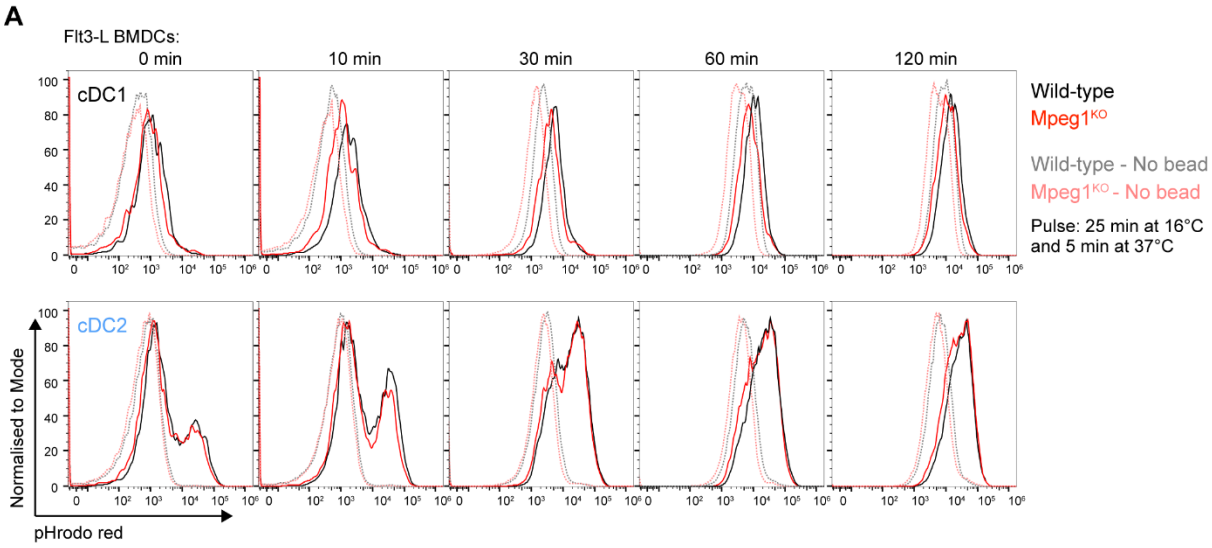

Fig. 4. 6. Phagosome acidification is comparable in wild-type and Mpeg1^{KO} Flt3L BMDCs. (**A**) Wild-type or Mpeg1^{KO} Flt3L BMDCs were pulsed with pHrodo beads for 25 min at 16°C followed by 5 min at 37°C and either

immediately placed on ice (0 h) or chased for the indicated time. After labelling of outside beads, samples were analysed by flow cytometry. Populations are defined according to the gating shown in Fig. 4.5. Data are from one experiment.

4.2.2 Effects of DPI and bafilomycin A1 on phagosomal pH in MutuDCs and Flt3L BMDCs

Inhibition of NOX2 with the inhibitor DPI has been shown to decrease endosomal and phagosomal pH in different murine and human DC populations (*216, 245, 321*). Given the dependence of perforin-2 pore formation on low pH, I wondered whether perforin-2 hyperactivity could be induced by NOX2 inhibition. I therefore tested whether DPI decreases the pH in MutuDC phagosomes. Surprisingly, when I pulse-chased NT MutuDCs in the presence of DPI, I observed no difference in the proportion of cells with pHrodo^{High} phagosomes (**Fig. 4.7, A and B**). The intensity of pHrodo fluorescence in cells with one bead was also comparable. However, the pHrodo^{High} peak in DPI treated cells was closer to the background peak suggesting a slight increase rather than decrease in pH.

To confirm that the bead pHrodo assay can detect meaningful perturbations, I pulse-chased NT MutuDCs with pHrodo beads in the presence of BafA1. As expected, acidification of phagosomes in BafA1 treated cells was severely impaired (**Fig. 4.7A**). The pHrodo intensity in cells with one bead remained essentially static during the chase. On the other hand, in cells without a bead, the pHrodo intensity gradually decreased. This suggests that in the absence of V-ATPase activity, the pH in compartments containing free pHrodo dye may increase. In cells with one bead, the pHrodo signal from the free dye and the bead-conjugated dye are difficult to separate. Assuming that these signals are additive, the residual increase in pHrodo intensity above background levels could suggest V-ATPase-independent acidification of the phagosome.

I also tested the effects of DPI in Flt3L BMDCs. It has been shown that DPI exhibits its effects on phagosomal pH in as little as 15 min (*216*). I therefore added the drug for the final 15 min of a 1 h chase period. Similar to the results in MutuDCs, NOX2 inhibition had no detectable effect on phagosomal pH in cDC1s and cDC2s (**Fig. 4.7C**)

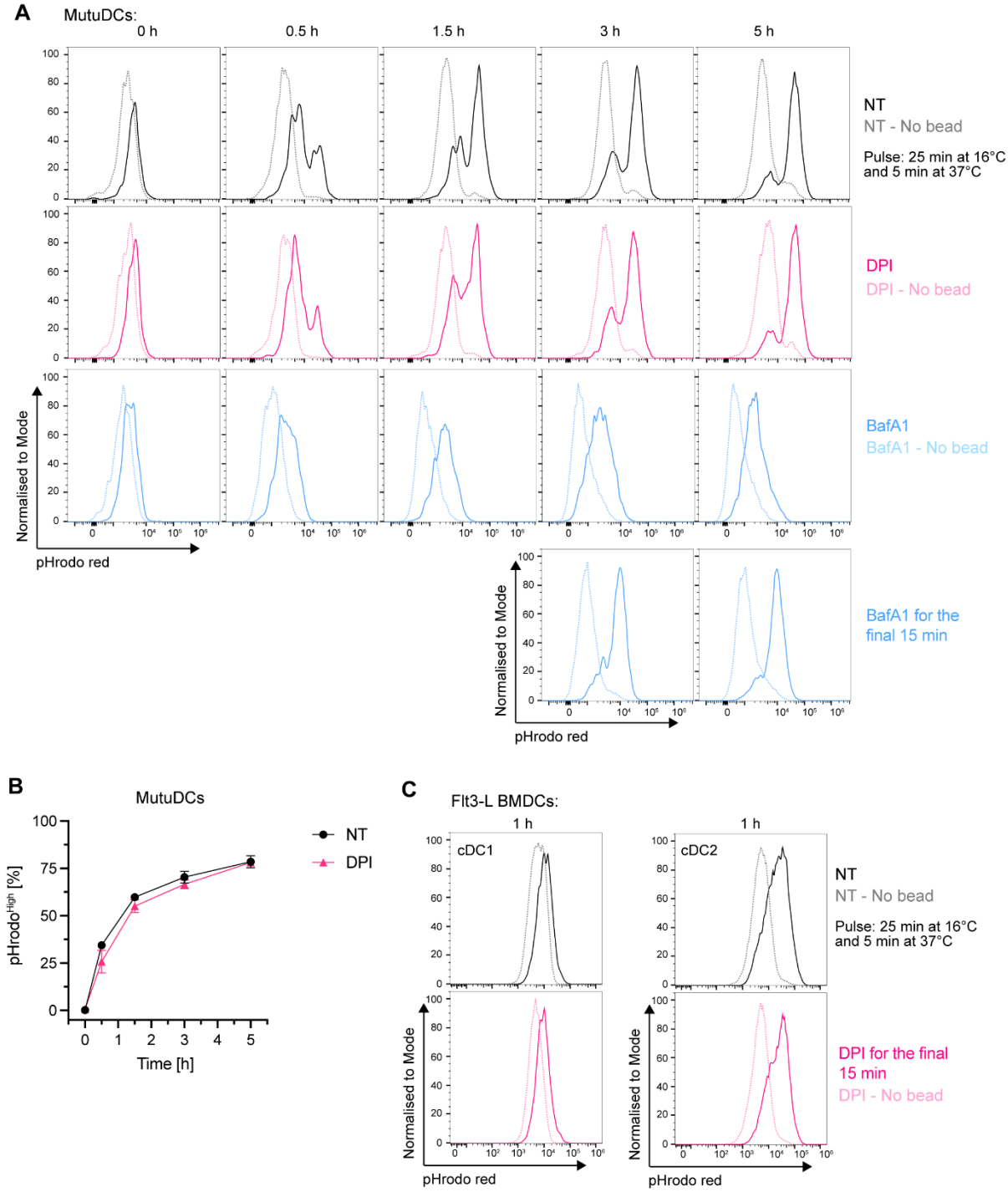

Fig. 4. 7. Effects of DPI and BafA1 on phagosomal pH of MutuDCs and Flt3L BMDCs. (**A**) NT MutuDCs were subjected to the pHrodo bead assay as described in Fig. 4.2 in the presence or absence of either 5 μM DPI or 0.5 μM BafA1 as indicated. (**B**) Quantification of pHrodo^{High} based on the gating shown in Fig. 4.2B. Data represent mean and SEM of five independent experiments. NT vs DPI conditions were compared using a multiple paired t-test (two-stage step-up, Benjamini, Krieger and Yekutieli) and found not to be significantly different. (**C**) Wild-type Flt3L BMDCs were subjected to the pHrodo bead assay as described in Fig. 4.6 in the presence or absence of 5 μM DPI as indicated. Data are representative for one experiment.

Given these unexpected results, I wanted to confirm that the DPI does in fact inhibit NOX2. In addition to decreases in pH, it has been widely observed that NOX2 inhibition leads to an enhancement of phagosomal degradation (*216, 217, 245, 321, 349*). I therefore analysed ovalbumin degradation and perforin-2 processing by phagoFACS in the presence or absence of DPI. Consistent with results reported in BMDCs, NOX2 inhibition led to increased ovalbumin degradation and an accelerated loss of the perforin-2 C-term tail (**Fig. 4.8**). Given the intimate link between protein degradation and pH regulation, it was surprising that NOX2 inhibition in MutuDCs affected the former but not the latter. However, one study reported that NOX2 can modulate phagosomal proteolysis in DCs in a pH-independent manner (*349*).

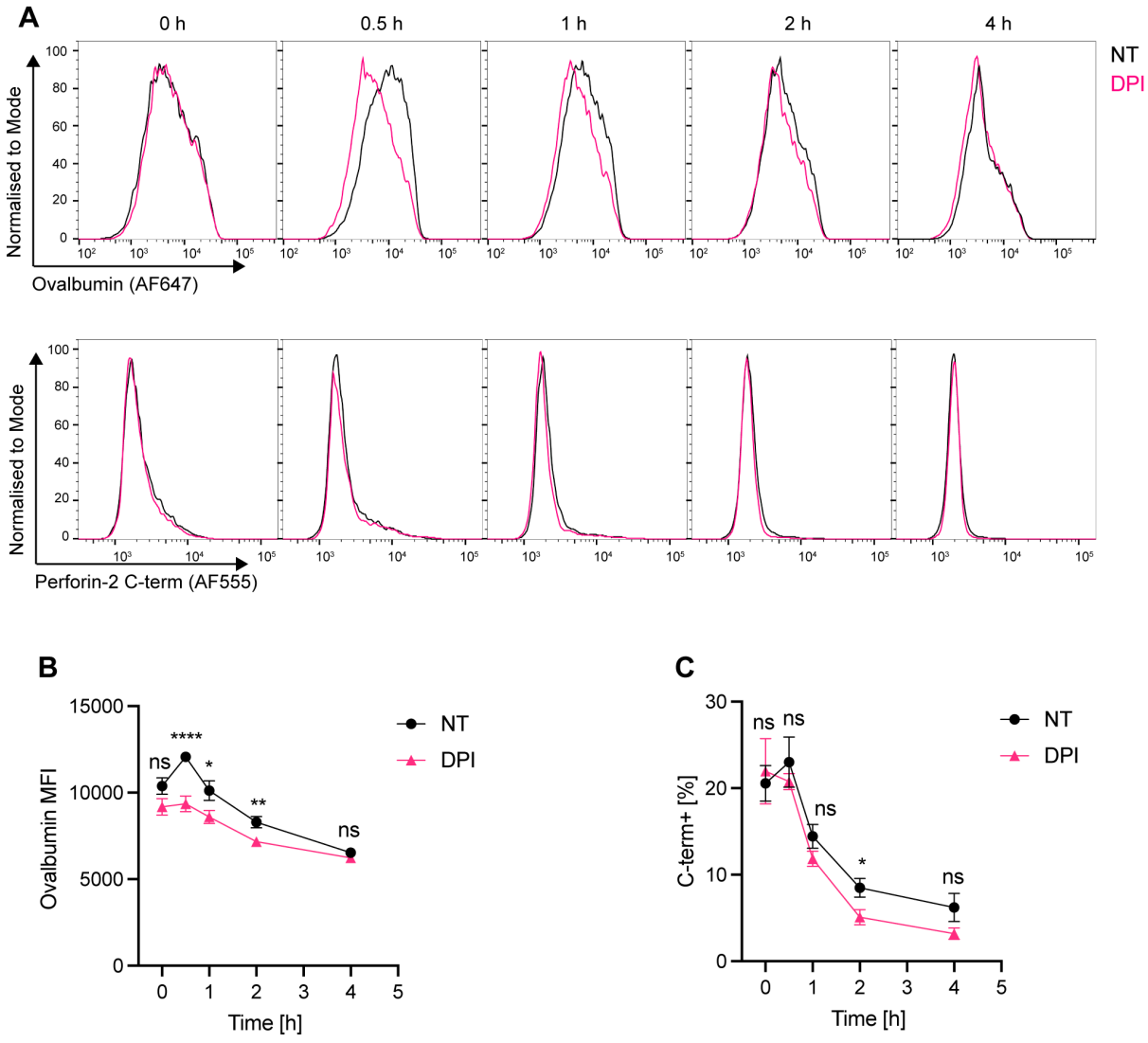

Fig. 4. 8. DPI increases the rate of phagosomal proteolysis in MutuDCs. (**A**) NT MutuDCs were subjected to the phagoFACS assay as described in Fig. 4.1 in the presence or absence of 5 μM DPI. Isolated phagosomes were stained for ovalbumin (top) and perforin-2 C-terminus (bottom). (**B, C**) Quantification of ovalbumin MFI (B) and perforin-2 C-term+ phagosomes (C). Data represent mean and SEM of three independent experiments. *P<0.1, **P<0.01, ****P<0.0001 using a multiple paired t-test (two-stage step-up, Benjamini, Krieger and Yekutieli)

4.2.3 Effects of DPI and bafilomycin A1 on phagosomal pH in GM-CSF BMDCs

Having studied pH regulation in MutuDCs, splenic DCs and Flt3L BMDCs, I also analysed phagosomal pH in GM-CSF BMDCs which, historically, are the most widely used system in the literature. I wanted to establish how GM-CSF BMDCs compare to the other DC populations in the pHrodo assay and how they respond to NOX2 and V-ATPase inhibition.

GM-CSF cultures of bone marrow cells yield a heterogeneous population of cells comprising macrophages and cDC-like cells (*185*). The macrophages are mostly found within the CD11c+CD11b+MHCII^{Int} population while the DC-like cells make up the majority of the CD11c+CD11b+MHCII^{High} population (**Fig. 4.9**). Macrophages have been reported to acidify their phagosomes more rapidly than DCs (*216, 321*). Consistent with these reports, I found that phagosomes of MHCII^{Int} cells acidified much more than those of MHCII^{High} cells (**Fig. 4.10**). In the first repeat of the experiment, cells exhibited a bimodal distribution of pHrodo fluorescence while in the second repeat they had a unimodal distribution. The reason for this is unclear, however, the difference between MHCII^{Int} and MHCII^{High} cells was consistent between the two repeats.

To assess the role of NOX2 and V-ATPase in pH regulation in GM-CSF BMDCs, I pulse-chased wild-type cells with pHrodo beads in the presence of DPI or BafA1. Unlike in MutuDCs and Flt3L BMDCs, DPI increased the proportion and intensity of pHrodo^{High} phagosomes in MHCII^{High} cells and, to a lesser degree, in MHCII^{Int} cells suggesting a decrease in phagosomal pH (**Fig. 4.11 and 4.12**). BafA1 treatment led to a decrease in proportion and intensity of pHrodo^{High} phagosomes in both MHCII^{High} and MHCII^{Int} cells suggesting an increase in phagosomal pH (**Fig. 4.11** and **4.12**). However, as with MutuDCs, there appeared to be some residual V-ATPase independent acidification. A precise quantitative comparison of the different conditions was difficult to obtain due to the divergent profiles of the pHrodo signal between conditions.

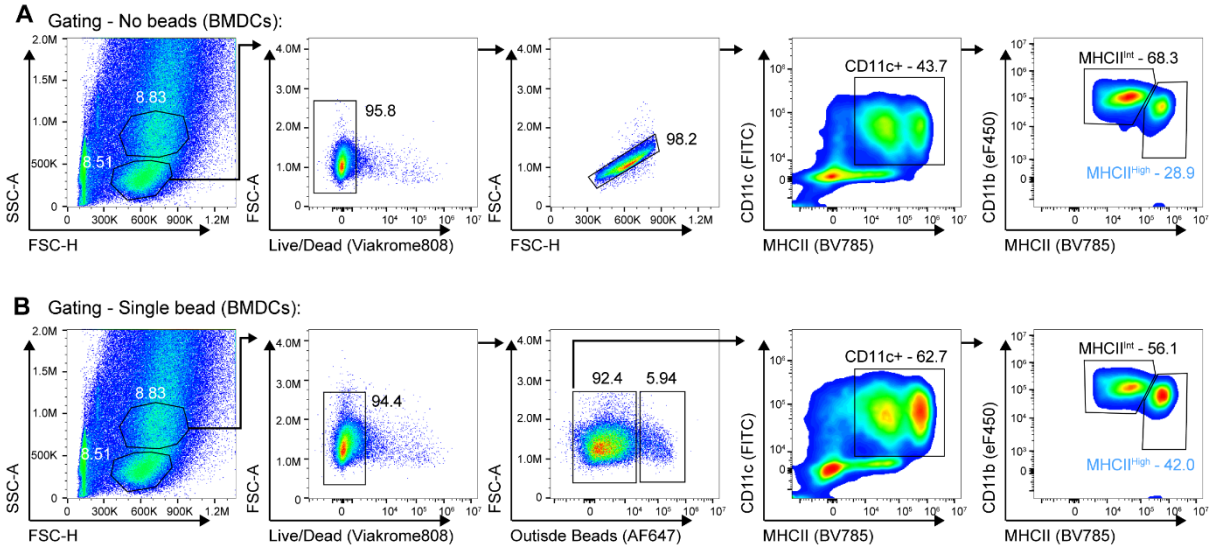

Fig. 4. 9. Gating strategy for the bead pHrodo assay in GM-CSF BMDCs.

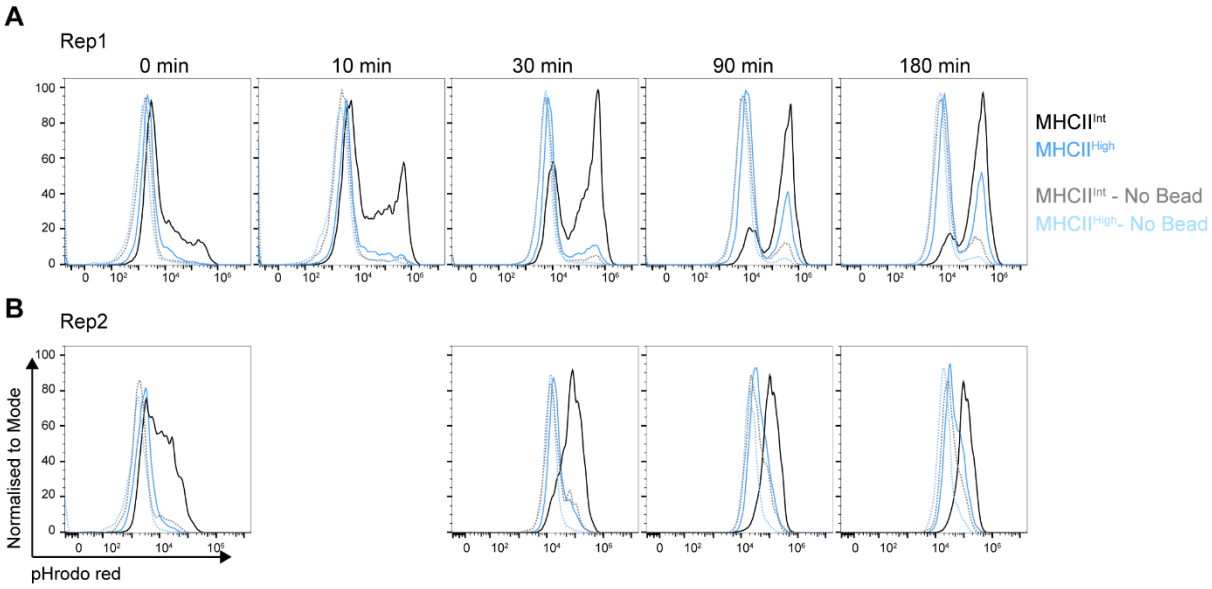

Fig. 4. 10. Phagosome acidification in GM-CSF BMDCs. (**A, B**) Wild-type GM-CSF BMDCs were pulsed with pHrodo beads for 25 min at 16°C followed by 5 min at 37°C and either immediately placed on ice (0 h) or chased for the indicated time. After labelling of outside beads, samples were analysed by flow cytometry. Populations are defined according to the gating shown in Fig. 4.9.

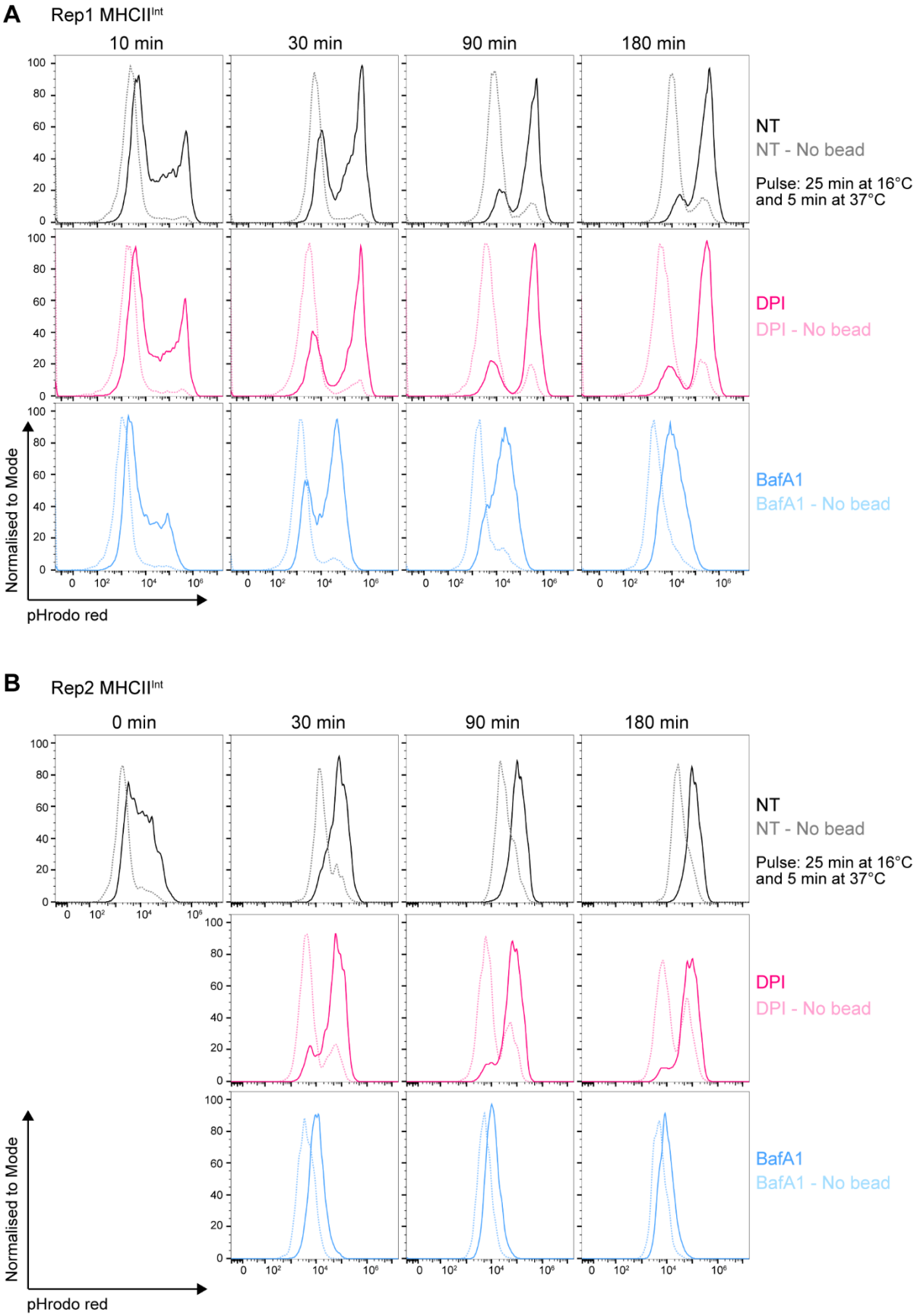

Fig. 4. 11. Effects of DPI and BafA1 on phagosomal pH of MHCII^{High} GM-CSF BMDCs. (**A**,**B**) Wild-type GM-CSF were subjected to the bead pHrodo assay as described in Fig. 4.10 in the presence or absence of 5 μM DPI or 0.5 μM BafA1 as indicated.

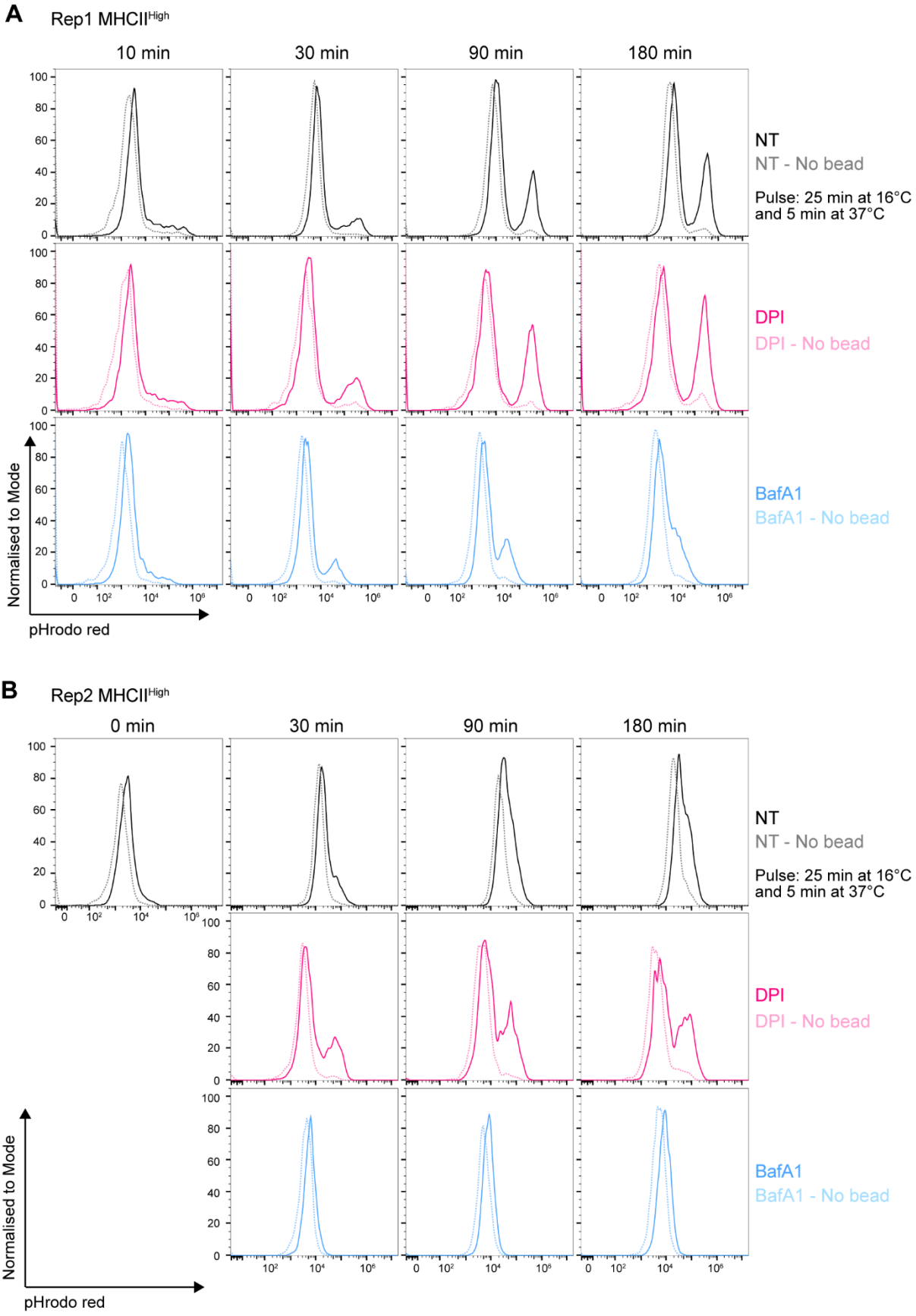

Fig. 4. 12. Effects of DPI and BafA1 on phagosomal pH of MHCII^{Int} GM-CSF BMDCs. (**A,B**) Wild-type GM-CSF were subjected to the bead pHrodo assay as described in Fig. 4.10 in the presence or absence of 5 μM DPI or 0.5 μM BafA1 as indicated.

4.3 Discussion

The way antigen is processed directly influences the efficiency of cross-presentation in DCs and phagosomal pH is a key parameter that determines the rate of antigen proteolysis. Based on the results in Chapter 3, I hypothesized that perforin-2 pore formation may be intimately linked with the regulation of phagosomal pH in cross-presenting DCs. On the one hand, pore formation could influence phagosomal pH by shuttling protons into the cytosol. On the other hand, phagosomal pH could influence pore formation given the dependence on low pH *in vitro (246, 247).* To better understand this relationship *in vivo*, I measured changes in phagosomal pH in a range of wild-type and Mpeg1^{KO} DC models.

In regard to pore formation influencing phagosomal pH, the results show that there is no measurable difference in the acidification of phagosomes of wild-type and Mpeg1^{KO} DCs. The perforin-2-mediated escape pathway is active in all of the DC models used in this thesis (MutuDCs: see Chapter 3; splenic and Flt3L-derived cDC1/2s: see (*249*)). It therefore appears that perforin-2-mediated escape does not damage the membrane integrity of phagosomes in a permanent manner. Accordingly, the rate of Ova degradation was similar in NT and Mpeg1^{KO} MutuDCs (Fig. 4.1) and phagosomes containing Ova beads do not accumulate markers for damaged endocytic compartments, such as galectin-3 (*177*). It remains an open question how DCs control perforin-2 pores in a way that ostensibly allows for endocytic escape without affecting phagosomal pH. In the case of splenic cDC1s, phagosomes barely acidify beyond extracellular pH and perforin-2 pores may simply not have a big impact. However, phagosomes of other DC models, including MutuDCs, do maintain a pH gradient across the phagosomal membrane which could, in principle, be dissipated by perforin-2. One explanation for why this does not happen is that phagosomal pH is quickly restored either by inactivating the perforin-2 pores or by upregulating V-ATPase activity. Such transient changes might have been missed by the flow cytometry-based readout used in this thesis, but they could potentially be detected by real-time confocal microscopy, making it a worthwhile approach to pursue in the future. Another explanation is that perforin-2 pores form at a relatively high pH *in vivo* and therefore do not have a big impact on acidification in mature phagosomes.

To probe the influence of phagosomal pH on pore formation, I tested whether I could acidify phagosomes with DPI which led to the surprising finding that NOX2 inhibition has no effect on phagosomal pH in MutuDCs and Flt3L BMDCs. These results are inconsistent with several studies of splenic CD11c+CD8α+ DCs which showed that genetic or chemical ablation of NOX2 activity has an alkalizing effect (*245, 351, 357*). However, in GM-CSF BMDCs, I did observe alkalization of phagosomal pH upon NOX2 inhibition which had been

reported previously (*216, 217*). But again, at least one study found that NOX2 inhibition had no effect on phagosomal pH in this DC model (*349*). These discrepancies are difficult to reconcile and may be due to both methodological and biological differences between studies.

One methodological difference concerns the use of pH-sensitive dyes. Most studies used FITC which is an indicator for pH 5.0 – 8.0 while some studies, including this thesis, used pHrodo red which is sensitive to change between pH 4.0 – 8.0. It is known that these dyes can be affected by oxidation and chlorination (*349, 360*). The fluorescent stability of pHrodo red was in fact shown to be significantly affected by NOX2 activity which could have hampered the results reported in this thesis (*349*). Another methodological difference concerns the flow cytometry-based readout approach. While the majority of published studies report pH values from cells associated with one bead, they did not determine whether the bead was on the inside or the outside of the cell. In the experiments reported here, the cell-associated bead was internalized in only around 30% of cells (**Fig. 4.2B, 4.3** and **4.5**). Without the labelling of outside beads, it cannot be conclusively ruled out that measurements of phagosomal pH were not hampered by NOX2 inhibition affecting the extracellular pH or the internalization of beads. Similarly, none of the published studies accounted for the possibility that the fluorescence measurement also included signal from free, internalized dye which, as shown here, can also influence the results.

Biological differences may also account for the discrepant NOX2 phenotypes. One confounding factor is the activation state of cells. Several studies have shown that stimulating DCs with PAMPs can alter phagosomal and lysosomal acidification (*37, 354*). Since I did not stain for activation markers, it cannot be ruled out that cells did not get activated by PAMPs present during the isolation procedures or bead preparation. Another confounding factor is the biological variation in the different DC models. *In vitro* derived DCs may not accurately represent all aspects of their *in vivo* counterparts and could therefore have different mechanisms of pH regulation. Such variations could explain why NOX2 inhibition affected the pH of splenic cDC1s but not in the Flt3L-derived cDC1 used in this thesis. In addition, the identity of *in vitro* derived DCs may be affected by differences in the protocols used to derive them (e.g. culture duration or cytokine concentration). Indeed, the reported kinetics and degree of acidification varies significantly for GM-CSF BMDCs with some studies reporting a phagosomal pH of 5.0 and others of 7.5 after 1 h chase (**Table 4.1**).

In line with previous studies, the results presented here show that phagosomes of splenic cDC1s barely acidify *ex vivo*. However, phagosomes of MutuDCs do not recapitulate this

phenotype and the reason for this is unclear. MutuDCs have been derived from a transgenic mouse expressing the SV40LgT oncogene under the CD11c promoter (*318*). The oncogene selectively drove the proliferation of splenic CD8α+ cDC (*319*) and long-term *in vitro* culture of these cells gave rise to the immortalized MutuDC line. Consequently, MutuDCs share many of the surface markers of cDC1s, but not other DC or macrophage cell types. In addition, MutuDCs have similar functional characteristics to cDC1s including the ability to cross-present. It was therefore surprising to see such a strong acidification of MutuDC phagosomes. The pH profile of MutuDCs instead resembled that of splenic pDCs which have poor antigen presentation capacity compared to cDCs (*56*). Even so, pDCs can be induced to cross-present through pre-activation with a TLR7 agonist (*354*). The acquisition of cross-presentation capacity in pDCs in this case was attributed to ROS-mediated pH alkalization and antigen protection. It is therefore possible that MutuDCs also require pre-activation to alkalise their phagosome sufficiently to support cross-presentation. Indeed, when MutuDCs were assayed in the absence of DAMPs and PAMPs, they were unable to cross-present endotoxin-free ovalbumin (*243*).

Regardless of the underlying reason, the difference in pH regulation between MutuDCs and cDC1s raised an interesting question regarding the influence of phagosomal pH on perforin-2 pore formation. Compared to MutuDCs, phagosomes of Flt3L-derived cDC1 are relatively alkaline. Yet, Pablo Rodríguez-Silvestre found that cDC1s display robust perforin-2-mediated escape in the saporin-puromycin assay (see (*249*)). The results in Chapter 3 also show that BafA1 treatment of MutuDCs only leads to a minor impairment of perforin-2-mediated escape. In addition, all of the reported phagosomal pH values for any DC model are well above the required pH for pore formation *in vitro* (pH 3.5 – 4.0) (**Table 4.1**). Together, these data raised the possibility that pore formation *in vivo* is less dependent on acidification. It is thought that low pH enables the structural transition for pore formation by destabilizing a subunit-subunit interface in the pre-pore ring (*312*). However, similar to other pore-forming proteins, perforin-2 pores on artificial lipid membranes are predominantly incomplete arcs, rather than closed rings (*315*). These arcs would form so called “toroidal” pores of varying sizes in which the arc subunits interface with a hemi-toroidal lipid edge to allow cargo transport across the bilayer (*315, 361*). It is possible that the pre-pore to pore transition in these arc structures is less dependent on acidification (*315*). Conceivably, early phagosomes may therefore be permissible to perforin-2 pore formation, at least from a pH perspective. Nonetheless, pore formation may still rely on additional triggers. In particular, it has been hypothesized that the ectodomain of perforin-2 needs to be shed from the transmembrane domain to enable the required conformational changes (*320*). In Chapter 5, I therefore set

out to identify the proteases involved in this process and to test their involvement in the regulation of perforin-2-mediated endocytic escape.

Chapter 5 – Ectodomain shedding may not be a prerequisite for perforin-2-mediated escape

5.1 Introduction

Perforin-2 is the only member of the MACPF family with a transmembrane domain (TMD). The presence of the TMD anchors perforin-2 to the membrane, restricts its conformational freedom and controls its localisation by providing a link to the sorting motifs in the cytosolic tail. The TMD could therefore play a key role in the regulation of perforin-2, and it has been speculated that it serves to prevent premature pore formation (*247, 314, 320, 362*). Accordingly, perforin-2 pores would only assemble after proteolytic shedding of the ectodomain from the TMD. The concept of regulating pore formation by proteolysis is well established for related pore-forming proteins. Perforin-1 requires the proteolytic removal a C-terminal glycan that hinders oligomerisation (*308, 310*) and the assembly of the complement membrane attack complex is regulated by a proteolytic cascade (*363*). Similarly, members of the gasdermin family are dependent on a proteolytic processing step by caspases (*364*).

The first experimental evidence for a role of proteolysis in the control of perforin-2 came from a study by McCormack *et al.* (*267*). Negative stain EM experiments of post-nuclear membranes from perforin-2-overexpressing HEK293 cells identified membrane-bound ring-like oligomers after limited trypsin digestions but not in the absence of proteolytic treatment. These data suggested that proteolysis may be required for oligomerisation of perforin-2, although the relevant cleavage site(s) was not identified. In addition, the same study showed that the MACPF and P2 domains of perforin-2, but not the cytosolic tail, can be detected in bacterial membranes isolated from perforin-2-overexpressing MEF cells. Finally, the phagoFACS experiments presented in Chapter 3 showed that the cytosolic tail of perforin-2 was lost during phagosome maturation while the luminal MACPF domain was retained (Fig. 3.5).

The above data suggest perforin-2 may be regulated by proteolysis but they do not conclusively demonstrate that proteolysis is strictly necessary for pore formation. Indeed, I and others in the Kozik lab have observed TMD-anchored perforin-2 oligomers by Western blot (see Fig. 3.15) suggesting that ectodomain shedding may not be required for oligomerisation. Of potential relevance here are also the effects of BafA1 on perforin-2 processing and activity presented in Chapter 3. BafA1 partially prevented the loss of the cytosolic tail in phagoFACS experiments which may be explained by an inhibition of ectodomain shedding. Nevertheless, BafA1 did not abolish the activity of perforin-2 in the

saporin-puromycin assay. While only circumstantial, these data hinted at the possibility that TMD-anchored perforin-2 can also oligomerise and form pores.

Given this background, I continued an ongoing investigation in the lab studying the role of proteolysis in the regulation of perforin-2. Patrycja Krawczyk had previously shown that asparagine endopeptidase (AEP) could cleave perforin-2 within the EGF domain *in vitro* but did not detect any defects in cleavage in AEP^{KO} MutuDCs *in vivo*. Since then, I designed a custom-made antibody against the perforin-2 P2 domain which had previously remained elusive to detection. Using the αP2 antibody, I continued to characterize the AEP-mediated processing of perforin-2 in NT and AEP^{KO} MutuDCs by Western blot and phagoFACS. To further explore regulation of perforin-2 by proteolysis, I tested the effect of several protease inhibitors on perforin-2 processing by Western blot and phagoFACS and assessed their impact on perforin-2 activity in the bead saporin-puromycin assay.

5.2 Results

5.2.1 Validation of a novel perforin-2 antibody against the P2 domain

The data in Chapter 3 have shown that perforin-2 is cleaved in the EGF domain yielding a N-terminal p40 fragment that is detectable with the αMACPF antibody (Fig. 3.1B). To test whether I could detect any fragments C-terminal to this cleavage, I decided to raise a custom-made antibody against the P2 domain. The antibody was raised against a 16 amino acid peptide epitope with a sequence derived from a loop in the P2 domain (**Fig. 5.1A**). Based on visual inspection of pre-pore and pore structures, the αP2 epitope might be readily accessible in the pore conformation whereas in the pre-pore conformation it might buried in the subunit-subunit interface and therefore only accessible in pre-pore monomers or arcs.

To validate the αP2 antibody, I performed a Western blot with whole cell lysates of NT and $Mpeg1^{KO}$ MutuDCs. A separate membrane of the same lysates was probed with the αC-term antibody for comparison. Under non-reducing conditions, both αP2 and αC-term antibodies detected full-length perforin-2 as expected (**Fig. 5.1B**). Interestingly, the αP2 antibody also detected a p60 fragment whose size is consistent with a cleavage in the membrane-proximal region of the CTT domain (**Fig. 5.1A**). In line with these data, non-reducing Western blots with the αMACPF also frequently detected a p60 fragment (see Fig. 3.2B and 5.2A). However, the abundance of this fragment varied and sometimes it was only visible following overexposure of the x-ray film.

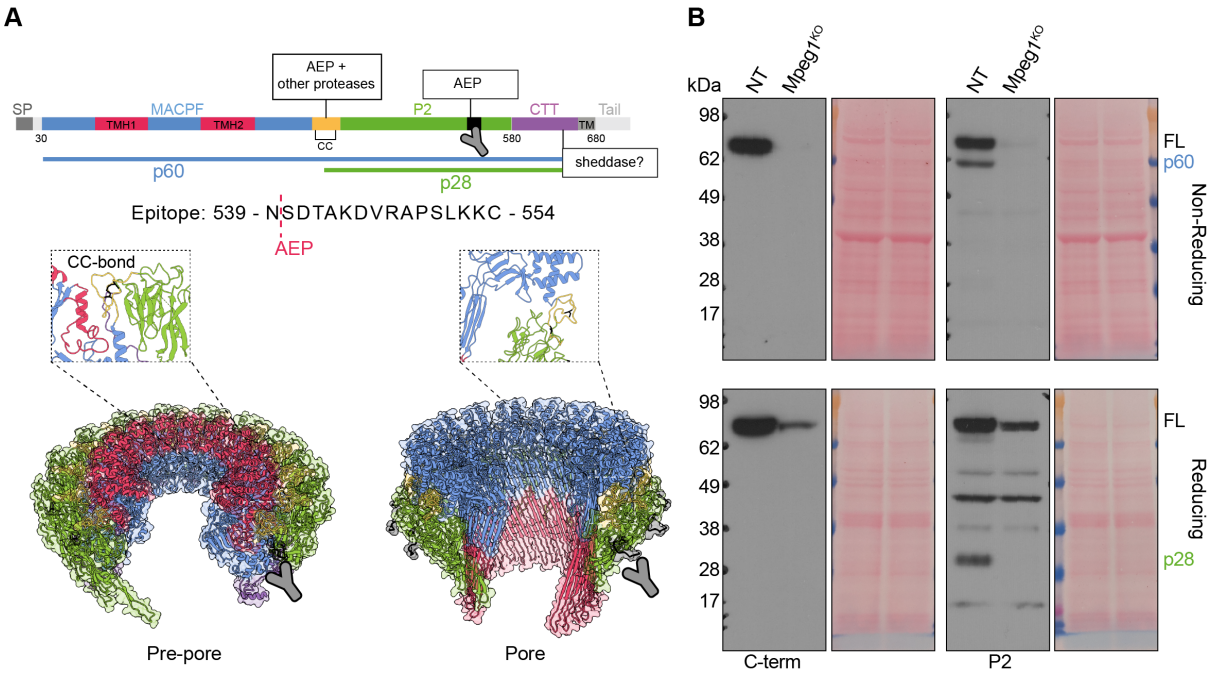

Fig. 5. 1. Validation of a custom-made antibody against the perforin-2 P2 domain. (**A**) Schematic illustrating the sequence and location of the epitope used to generate the αP2 antibody. The epitope (black) is shown in the pre-pore and pore structures. The disulfide bond in the EGF domain is indicated as black sticks. (**B**) Western blot analysis of whole cell lysate from the indicated MutuDC lines probed with the αC-term and αP2 antibodies under non-reducing and reducing conditions. Data are representative for three independent experiments.

Strikingly, under reducing conditions, the p60 fragment was no longer detectable but instead a p28 fragment appeared which was detected by the αP2 but not the αC-term antibody (**Fig. 5.1B**). Based on its apparent molecular weight, the p28 fragment spans the region between the cleavage sites within the EGF and CTT domains (**Fig. 5.1A**). The EGF domain in the pre-pore structure is an unstructured loop with a disulfide bond at its base (**Fig. 5.1A**). Therefore, the loss of the p60 fragment and concomitant appearance of the p28 fragment upon reduction suggests that this disulfide bond holds the MACPF and P2 domains together after cleavage in the EGF loop. Interestingly, this disulfide bond is reduced in the pore structure although the reason for this is unclear.

5.2.2 The role asparagine endopeptidase (AEP) in perforin-2-mediated escape

As mentioned in Section 5.1, Patrycja Krawczyk identified AEP as protease that could cleave perforin-2 in the EGF domain *in vitro* but, at the time, this could not be recapitulated in AEP^{KO} MutuDCs *in vivo*. To confirm these findings, I probed lysates of NT, AEP^{KO} and Mpeg1^{KO} MutuDCs with the αMACPF and the new αP2 antibody. Consistent with the previous results, regular exposure of membranes probed with the αMACPF antibody detected no difference in amounts of full-length perforin-2 or the p40 fragment in NT and AEP^{KO} cells (**Fig. 5.2A**). However, overexposure revealed that AEP^{KO} MutuDCs accumulated more of the p60 fragment compared to NT cells. Notably, the p60 fragment was still present in AEP^{KO} samples under reducing conditions suggesting that the EGF cleavage is less

efficient in the absence of AEP. Staining with the αP2 antibody further revealed that AEP^{KO} MutuDCs accumulated the p28 fragment to levels well beyond those seen in NT cells in both non-reducing and reducing conditions. These results suggest that AEP^{KO} MutuDCs are defective in perforin-2 processing. However, the nature of this defect was puzzling. The reduction in EGF cleavage efficiency was only minor and could not explain the dramatic accumulation of p28 fragments in AEP^{KO} MutuDCs.

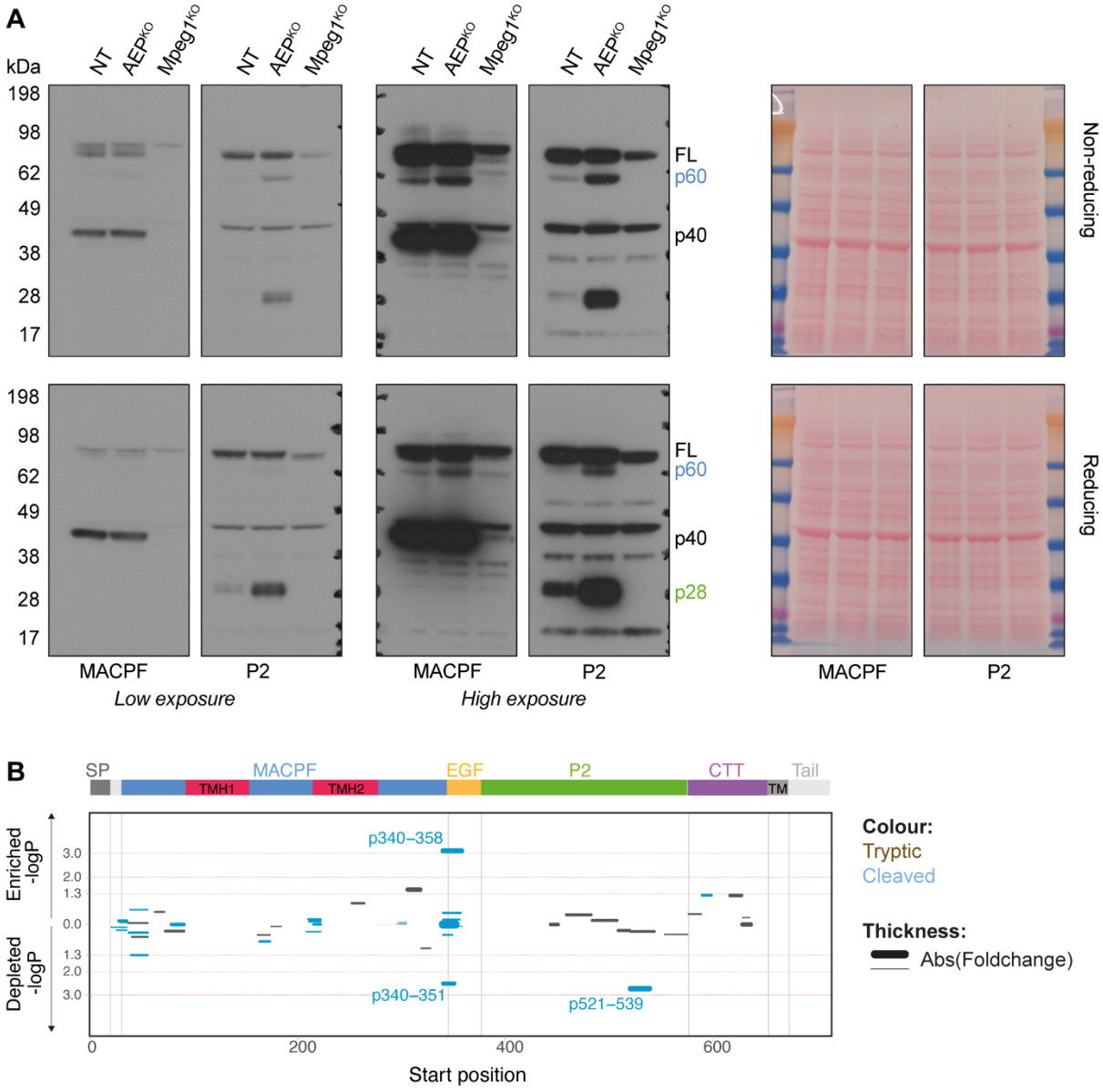

Fig. 5. 2. Analysis of AEP^{KO} MutuDCs with the αP2 antibody. (**A**) Western blot analysis of whole cell lysate from the indicated MutuDC lines probed with the αP2 or αMACPF antibody under non-reducing and reducing conditions. Data are representative for two independent experiments. (**B**) Data generated by the Borner lab showing AEP^{KO}-induced changes in the abundance of tryptic and semi-tryptic perforin-2 peptides. NT and AEP^{KO} MutuDCs were analyzed by mass spectrometry, and peptide intensities were normalized to the corresponding protein intensities. Statistical analysis was performed with a two-sided student's *t* test. *P* values (*y* axis) and fold change in abundance (line thickness) in treated versus control cells are shown. The amino acid position indicates the location of the peptides along the different perforin-2 domains.

Insights into the processing phenotype of AEP^{KO} MutuDCs came from a collaboration with the Borner lab. I prepared whole cell lysates of NT and AEP^{KO} MutuDCs for comparative proteomics analysis conducted by members of the Borner group. The analysis compared perforin-2-derived tryptic and semi-tryptic peptides from NT and AEP^{KO} samples. Tryptic peptides are those that have a tryptic cleavage site at both ends as a result of the trypsin digestion step used to prepare the sample for proteomics. Semi-tryptic peptides have a tryptic cleavage site at only one end. The other end is characterized by a non-tryptic cleavage mediated by a protease other than trypsin. Although, this non-tryptic cleavage could potentially be a consequence of non-specific degradation during sample processing, in most cases, it is derived from endogenous proteolysis occurring prior to sample processing (*365*). The analysis showed that the semi-tryptic peptide p350-351 in the EGF domain was depleted in AEP^{KO} samples suggesting that AEP was responsible for the C-terminal non-tryptic cleavage in this peptide (**Fig. 5.2B**). However, in the same samples, another EGF-derived semi-tryptic peptide, p340-358, was enriched. These results suggest that in the absence of AEP, other proteases can replace its activity with the most likely candidates being cathepsins. This is supported by evidence showing that in the processing of TLR9, cathepsins have the ability to compensate for AEP loss (*366*).

Interestingly, the analysis revealed a third semi-tryptic peptide, p521-539, with a different abundance in NT and AEP^{KO} samples. This peptide had a C-terminal non-tryptic cleavage and was depleted in the absence of AEP suggesting a second AEP cleavage site at N539. Notably, N539 is part of the αP2 epitope (**Fig. 5.1A**). Therefore, it is possible that AEP cleavage at N539 destroys the antibody epitope. This interpretation is consistent with the Western blot analysis of AEP^{KO} MutuDCs and explains the accumulation of the p60 and p28 fragments in these cells (**Fig. 5.2A**). Accordingly, a cleavage in the perforin-2 CTT domain by an unknown protease yields the p60 fragment. Cleavage by AEP and cathepsins in the EGF domain results in the p40 and the p28 fragments. A second cleavage by AEP in the P2 domain of either the p60 or the p28 fragments not only yields additional cleavage products but also destroys the αP2 epitope. As a result, these products become undetectable by the αP2 antibody. The fact that they are also undetectable by the αMACPF antibody suggests that they are rapidly turned over. In the absence of AEP, the αP2 epitope is preserved allowing it to detect the aberrant processing of perforin-2 in AEP^{KO} MutuDCs and the resulting accumulation of p60 and p28.

Next, I set out to test how the defect in perforin-2 processing in the absence of AEP manifests following its recruitment to the phagosome. NT, AEP^{KO} and Mpeg1^{KO} MutuDCs were pulse-chased with Ova beads and the isolated phagosomes stained with antibodies against perforin-2 and Lamp1. The signal for the αC-term antibody was similar in NT and

AEP^{KO} MutuDCs suggesting that turnover of the C-terminal tail was unaffected (**Fig. 5.3, A and B**).

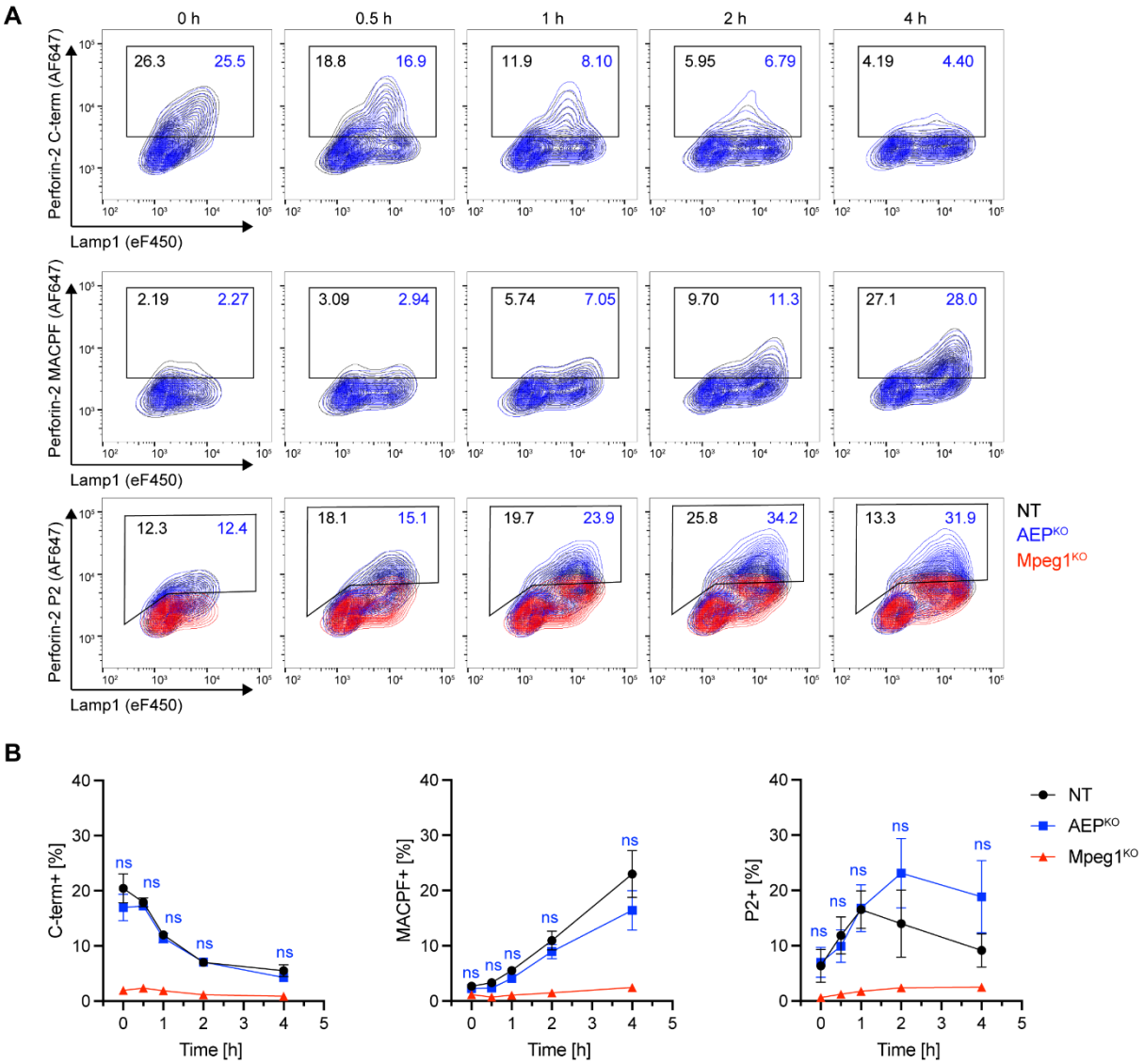

Fig. 5. 3. Processing of perforin-2 at the phagosome in AEP^{KO} MutuDCs. (**A, B**) The indicated MutuDC lines were pulsed with Ova beads for 25 min at 16°C followed by 5 min at 37°C, washed and either immediately placed on ice (0 h) or chased for the indicated time. Isolated phagosomes were stained with αLamp1 and with αC-term, αMACPF or αP2 antibodies. (B) Quantification of perforin-2^{+} phagosomes based on the gating shown in A. Data represent mean and SEM of three independent experiments. ns, not significant using a multiple paired t-test (two-stage step-up, Benjamini, Krieger and Yekutieli) versus NT MutuDCs.

Staining with the αMACPF antibody revealed a minor impairment in the exposure of the MACPF epitope at later stages of phagosome maturation. These results could suggest that the conformational change detected by this antibody is linked to the cleavage in the EGF domain since this cleavage was partially inhibited in the AEP^{KO} MutuDCs (**Fig. 5.2**).

Finally, consistent with the Western blot results (**Fig. 5.2A**), staining with the αP2 antibody revealed a considerable difference in NT and AEP^{KO} MutuDCs. In NT cells, the proportion of αP2+ phagosomes increased during the first hour of chase and then gradually declined. In

AEP^{KO} cells, αP2+ phagosomes accumulated at similar rate but instead of declining, their proportion continued to increase and remained elevated at 2- to 3-fold higher levels than in NT cell. The difference did not reach statistical significance, likely due to the variability between repeats. However, the αP2 signal was consistently higher in AEP^{KO} MutuDCs within each repeat.

The divergence in the proportion of αP2+ phagosomes after 1 hour could suggest that AEP initiates the cleavage of the P2 domain around this time which, in NT cells, leads to the destruction of the antibody epitope. Alternatively, the divergence could be explained by the possibility that phagosomes continue to fuse with late endosomal vesicles harboring perforin-2 with an intact αP2 epitope in AEP^{KO} cells but a cleaved epitope in NT cells. Conversely, the similar levels of αP2+ phagosomes in NT and AEP^{KO} cells during the first hour suggest that AEP does not significantly impact perforin-2 processing prior to its recruitment to early phagosome. Finally, it is interesting to compare the staining pattern of the αP2 antibody to that of the αC-term antibody during this early period. Whereas the αC-term signal is already elevated after the pulse (time 0 h) and reaches its peak within 30 min, the αP2 signal is at its lowest level at 0 h and only peaks after 1 h (**Fig. 5.3B**). These data are consistent with the interpretation that the αP2 the epitope is initially hidden in pre-pore oligomeric rings but becomes exposed upon pore formation (**Fig. 5.1A**). However, as mentioned earlier, the αP2 epitope could also be available in pre-pore monomers or arcs and the oligomeric state of perforin-2 upon delivery to the phagosome is not known. It remains equally possible that the different levels of perforin-2 detected at time 0 are simply due to the varying sensitivities of the antibodies.

Next, I wanted to test whether the defect in perforin-2 processing in the absence of AEP has any effect on perforin-2-mediated escape. Thus, NT, AEP^{KO} and Mpeg1^{KO} MutuDCs were incubated with saporin beads for 5 h at 37°C. Following a 30 min pulse with puromycin, non-internalised beads were labelled with an αOvalbumin antibody and puromycylated peptides stained with the 12D10 antibody in preparation for flow cytometry. Strikingly, the proportion of Puro^{Low} cells across the titration was similar in NT and AEP^{KO} cells (**Fig. 5.4**). These results suggest that proteolysis of the ectodomain by AEP is not required for perforin-2-mediated escape.

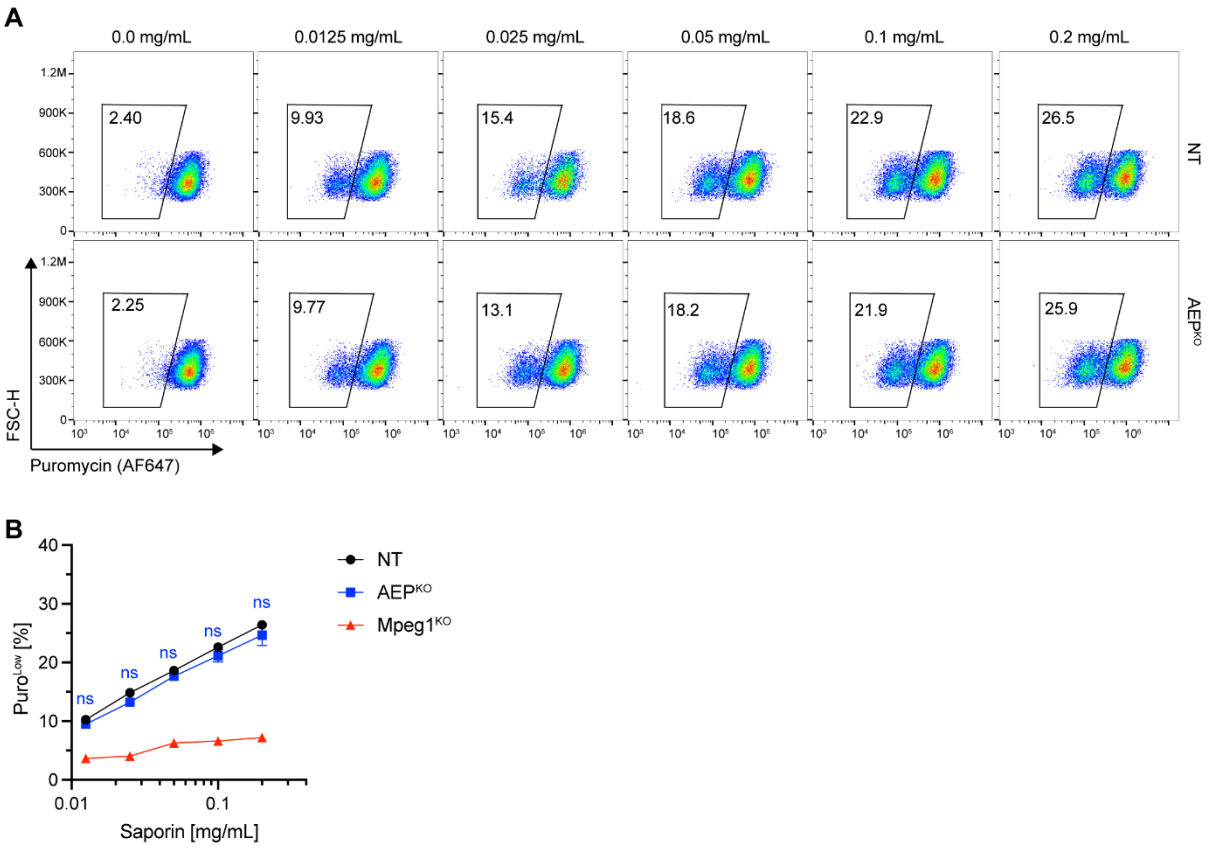

Fig. 5. 4. Efficiency of perforin-2-mediated escape in AEP^{KO} MutuDCs. (**A**) The indicated MutuDC lines were incubated with saporin beads for 5 h followed by an incubation with puromycin for 30 min. Cells were then placed on ice and outside beads labelled with an αOvalbumin antibody. After fixation and permeabilisation, levels of puromycin incorporation were detected with an αPuromycin antibody. Gating strategy is the same as in Fig. 3.10C. (**B**) Quantification of Puro^{Low} cells based on the gating shown in A. Data represent mean and SEM of two independent experiments. ns, not significant using a multiple paired t-test (two-stage step-up, Benjamini, Krieger and Yekutieli) versus NT MutuDCs.

5.2.3 The perforin-2 TMD is cleaved by γ-secretase

To identify additional proteases involved in the regulation of perforin-2, I tested the effects of different inhibitors by Western blot. NT MutuDCs were treated for 6 hours with the aspartic acid protease inhibitor pepstatin A, the cysteine protease inhibitor E64D or BafA1 which inhibits lysosomal proteases indirectly by blocking V-ATPase activity. Cells were lysed and analysed by Western blot using either the αC-term or αMACPF antibodies. Treatment with pepstatin A or E64D had no detectable effect on perforin-2 processing, although it cannot be excluded that the treatment duration or concentrations were insufficient for the inhibitors to inactivate their targets (**Fig 5.5A**). On the other hand, treatment with BafA1 led to an accumulation of full-length perforin-2 and a depletion of the p40 fragment suggesting that it inhibited the proteases responsible for the cleavages in the EGF, P2 and CTT domains.

Since pepstatin A and E64D had no effect, I continued the search for relevant proteases with additional inhibitors. NT MutuDCs were treated for 6 hours with the serine/cysteine protease inhibitor leupeptin or the γ-secretase inhibitor DAPT. Western blot analysis of leupeptin-

treated cells revealed a minor accumulation of full-length perforin-2 compared to untreated cells but the generation of the p40 fragment appeared to be unaffected (**Fig. 5.5B**). Interestingly, DAPT-treated cells accumulated a ~12 kDa C-terminal fragment. The size of this fragment suggests that it comprises the cytosolic tail, the TMD and a small portion of the luminal CTT domain of perforin-2. γ-secretase is an intramembrane protease with over 100

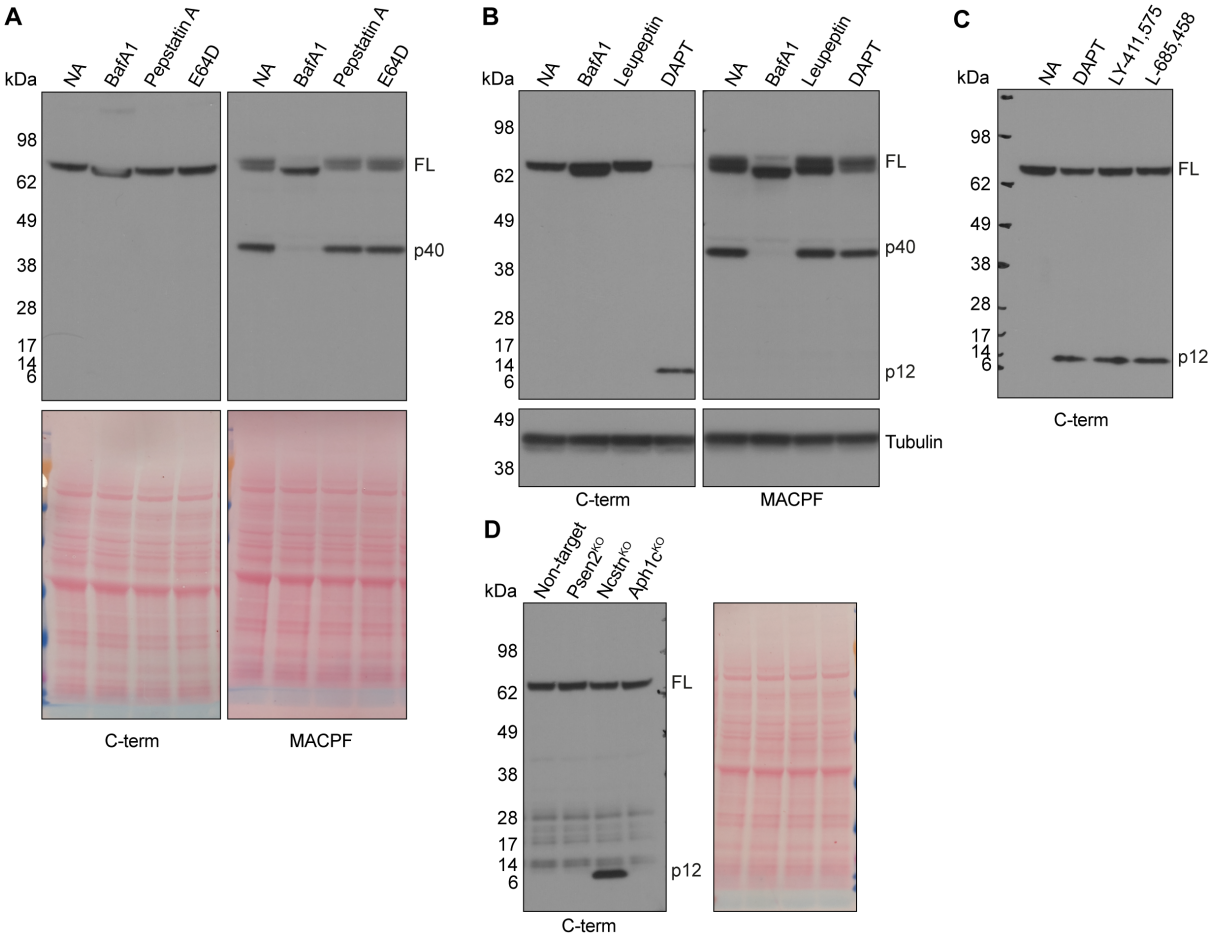

Fig. 5. 5. Perforin-2 is cleaved by γ-secretase. (**A**) Western blot analysis of NT MutuDCs treated for 8 hours with either 0.5 μM bafilomycin A1, 10 μM pepstatin A or 10 μM E64D. (**B**) Western blot analysis NT MutuDCs treated for 8 hours with 0.5 μM bafilomycin A1, 100 μM leupeptin or 50 μM DAPT. (**C**) Western blot analysis of NT MutuDCs treated for 8 hours with 10 μM DAPT, 10 μM LY-411,575 or 50 μM DAPT. (**D**) Western blot analysis of whole cells lysates from the indicated MutuDC lines. All membranes were probed with the indicated antibodies under non-reducing conditions.

known substrates including the amyloid precursor protein and the Notch receptor (*367*). γ-secretase cleaves within the TMD of type I transmembrane proteins. The products of this cleavage on either side of the membrane are then free to diffuse into the cytosol and vesicular lumen (or extracellular space), respectively. One of the main functions of γ-secretase is to clear membrane-bound protein stubs generated by ectodomain shedding (*368*). In fact, γ-secretase can only cleave substrates with an ectodomain of < ~50 amino acids and therefore frequently acts in concert with other proteases that remove the larger ectodomains in a preceding cleavage step (*369, 370*). The accumulation of a perforin-2 C-

terminal p12 fragment upon γ-secretase inhibition is therefore consistent with the shedding of the perforin-2 ectodomain by a membrane-proximal cleavage within the CTT domain.

The DAPT treatment also led to a depletion of full-length perforin-2 (**Fig. 5.5B**). However, the cells started to detach from the culture dish during the course of the treatment and I therefore suspected that the inhibitor may be toxic and cause non-specific effects. To mitigate this, I repeated the treatment with a 5-fold lower concentration of DAPT which had less of an impact on full-length perforin-2 levels but still caused accumulation of the p12 fragment (**Fig. 5.5C**). Furthermore, I treated the cells with alternative γ-secretase inhibitors LY-411,575 and LY-685,458. Both inhibitors caused accumulation of the p12 fragment without depleting full-length perforin-2 (**Fig. 5.5C**).

Finally, I generated MutuDC lines deficient in γ-secretase activity to confirm its role in perforin-2 processing. γ-secretase consists of a proteolytically active subunit, presenilin (Psen), and the three auxiliary subunits nicastrin (Ncstn), anterior pharynx defective 1 (Aph1) and presenilin enhancer 2 (Psenen). In mice, presenilin is encoded by the homologous genes Psen1 and Psen2 while Aph1 is encoded by Aph1a, Aph1b and Aph1c. For practical reasons, I only designed sgRNA guides against Psen2, Ncstn and Aph1c. To generate γ-secretase deficient cells, these guides were transduced into Cas9-expressing MutuDCs using a lentivirus with a hygromycin resistance gene. In parallel, a control population was generated in the same way using a non-targeting sgRNA (NT). Following hygromycin selection, disruption of the target loci was confirmed by sanger sequencing of a PCR amplicon around the predicted cut site. Western blot analysis of the resulting knockout lines showed that disruption of the Psen2 and Aph1c loci had no apparent effect on perforin-2 processing (**Fig. 5.5D**). In contrast, disruption of the Ncstn locus caused accumulation of the perforin-2 C-terminal p12 fragment that was also observed in DAPT-treated cells. Together, these results confirmed that perforin-2 TMD is cleaved by γ-secretase. The finding that the p12 fragment was not detectable in $Psen2^{KO}$ and $Aph1c^{KO}$ MutuDCs suggests that the knockout efficiency in these lines was poor or that the activity of the targeted loci was rescued by their respective homologues.

5.2.4 The perforin-2 ectodomain is shed by a cysteine protease

As discussed in Section 5.2.3, the relevant substrate for γ-secretase is not full-length perforin-2 but instead the p12 fragment. To generate this fragment, the luminal ectodomain of perforin-2 needs to be shed by a so called “sheddase” in a cleavage event that precedes the cleavage by γ-secretase. Thus, if the relevant sheddase is inhibited, the expectation would be that the p12 fragment is no longer generated and therefore does not accumulate upon γ-secretase inhibition. To test this hypothesis, I reasoned I could potentially inhibit the

elusive sheddase with BafA1 since it causes the accumulation of full-length perforin-2 (**Fig. 5.5**). Therefore, NT MutuDCs were pretreated for 2 hours with BafA1 and then incubated with DAPT for 6 hours in the continued presence of BafA1. As a control, cells were not pretreated and only incubated with DAPT for 6 hours. Cells in the control condition accumulated the p12 fragment as expected, but cells pretreated with BafA1 did not, suggesting that BafA1 inhibited the proteases responsible for shedding (**Fig. 5.6A**). These results also indicate that a 2-hour period was sufficient for γ-secretase to turnover any p12 fragments that were generated prior to BafA1 addition.

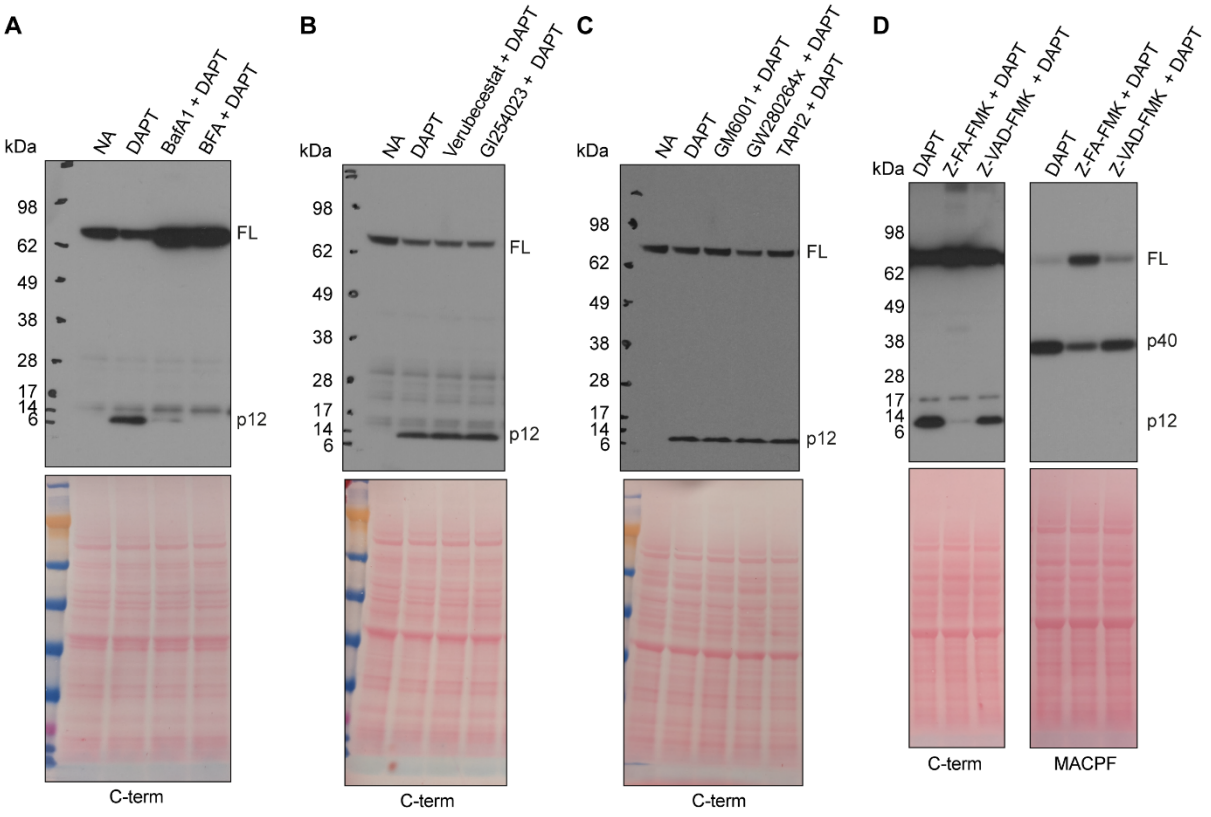

Fig. 5. 6. Identification of the perforin-2 sheddase(s). (**A**) Western blot analysis of NT MutuDCs pretreated for 2 hours with 0.5 μM BafA1 or 5 μM BFA and then incubated with 10 μM DAPT for 6 hours in the continued presence of BafA1 or BFA. (**B**) As in (A) using 1 μM Verubecestat or 10 μM GI254023. (**C**) As in (A) using 10 μM GM6001, 10 μM GW280264x or 20 μM TAPI2. (**D**) As in (A) using 10 μM z-FA-FMK or 50 μM z-VAD-FMK. All membranes were probed with the indicated antibodies under reducing conditions.

The ectodomain shedding of γ-secretase substrates is mediated by a diverse group of proteases (*370*). In many cases, they belong to “a disintegrin and metalloprotease” (ADAM), beta-site APP cleaving enzyme (BACE) or matrix metalloprotease (MMP) families. To identify the sheddase of perforin-2, I tested a range of inhibitors that target proteases of these families for their ability to inhibit the accumulation of the p12 fragment. As with BafA1, I pretreated NT MutuDCs for 2 hours with each inhibitor followed by a 6-hour incubation with DAPT in the continued presence of the inhibitor. At the tested concentrations, none of the sheddase inhibitors blocked the generation of the p12 fragment (**Fig. 5.6, B and C**).

Since BafA1 was so far the only inhibitor that interfered with perforin-2 shedding, I decided to screen inhibitors of cathepsins which are likely BafA1 targets due to their pH-dependency. To this end, I used the inhibitors z-FA-FMK and z-VAD-FMK. z-FA-FMK primarily targets cathepsin B and L whereas z-VAD-FMK targets cathepsin B and H (*371-374*). Both inhibitors also target additional cysteine proteases such as caspases (*374-376*). The p12 fragment accumulated normally in cells pretreated with z-VAD-FMK (**Fig. 5.6D**). Excitingly, however, the fragment was undetectable in cells pretreated with z-FA-FMK. In addition, treatment with z-FA-FMK, but not z-VAD-FMK, caused accumulation of full-length perforin-2 and inhibited the generation of the p40 fragment (**Fig. 5.6D**). These results suggest that z-FA-FMK targeted the protease(s) responsible for perforin-2 ectodomain shedding. In addition, it appears that z-FA-FMK also inhibited the proteases that cleave in the EGF domain to yield the p40 fragment. Alternatively, cleavage in the EGF domain may be blocked if the ectodomain is not first shed from the TMD.

5.2.5 Ectodomain shedding and γ-secretase cleavage of perforin-2 at the phagosome

So far, the data suggested that, during its journey through the endosome/lysosome system, the perforin-2 ectodomain is shed from the TMD by a cysteine protease and the remaining membrane stub removed by γ-secretase. As a next step, I wanted to test whether these events also occur following perforin-2's recruitment to the phagosome.

NT MutuDCs were pulse with Ova beads and then chased in the presence or absence of either DAPT or z-FA-FMK. The isolated phagosomes were stained with antibodies against perforin-2 and Lamp1. Consistent with the results discussed in Chapter 3, the signal for the cytosolic C-terminal tail on phagosomes from control cells peaked within 30 min and was gradually lost during the chase (**Fig. 5.7A** and **5.8A**). However, the presence of DAPT partially inhibited C-terminal tail loss. The proportion of αC-term+ phagosomes in control cells decreased from decreased from ~15% to ~3% whereas in DAPT-treated cells it remained relatively constant at ~14% across the 4 hours of chase. The effects of z-FA-FMK were even more pronounced. Here, the proportion of αC-term+ phagosomes continued to increase during the 1 hour of chase to ~30% before dropping to ~24% during the remaining 3 hours. Notably, in both DAPT- and z-FA-FMK-treated cells, the αC-term+ gradually shifted towards $Lamp1^{High}$ phagosomes whereas in control cells it was predominantly present on $Lamp1^{Int}$ phagosomes. In contrast to the αC-term signal, staining with the αMACPF antibody was not affected by either DAPT or z-FA-FMK and accumulated to similar levels as in control cells (**Fig. 5.7B** and **5.8B**).

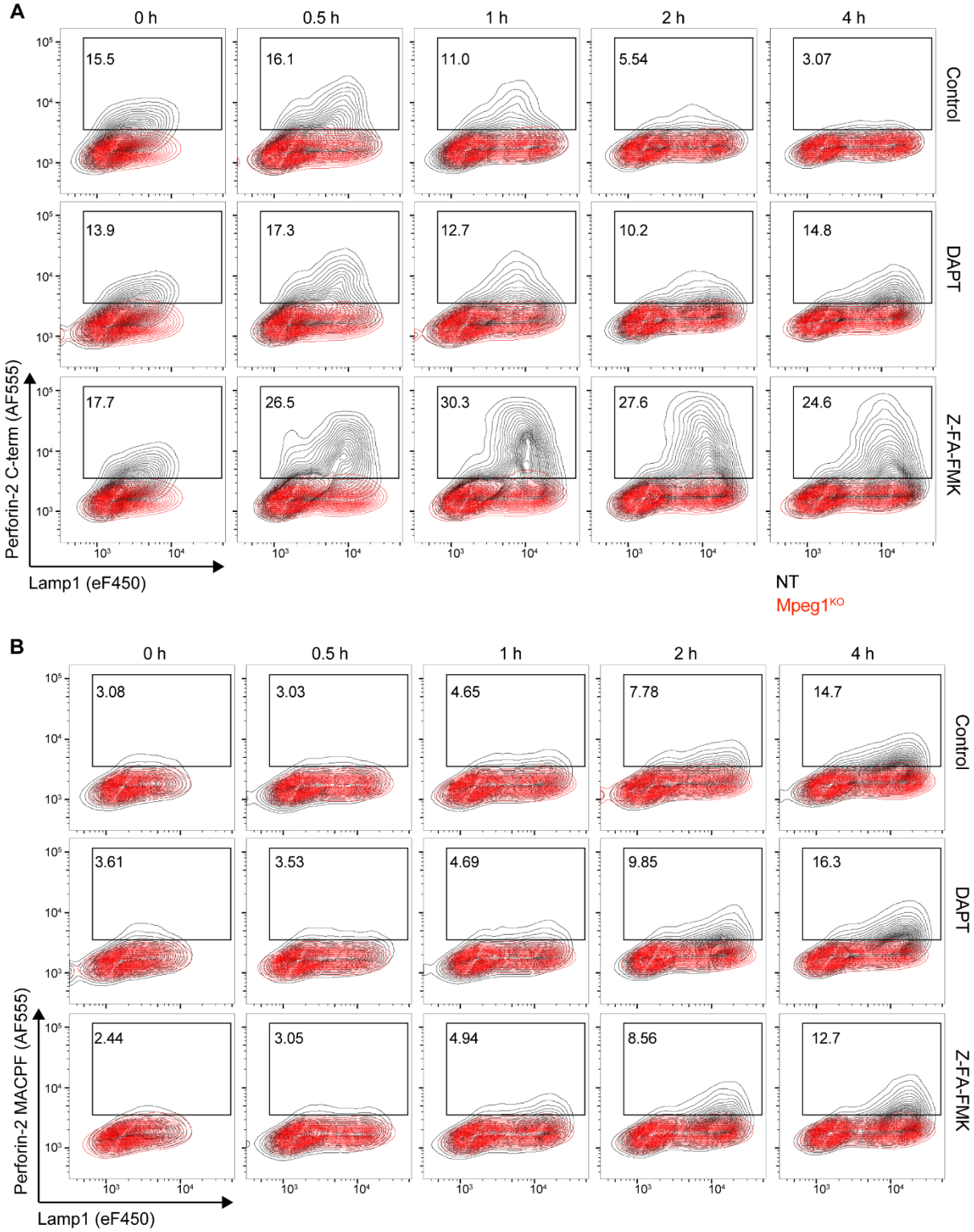

Fig. 5. 7. Effects of DAPT and z-FA-FMK on the processing of perforin-2 on the phagosome. (**A, B**) NT MutuDCs were pulsed with OVA beads for 25 min at 16°C followed by 5 min at 37°C, washed and resuspended in fresh media with or without 10 μM DAPT or 10 μM z-FA-FMK. Samples were then either immediately placed on ice (0 h) or chased for the indicated time. Isolated phagosomes were stained with αC-term and αLamp1 antibodies. Data are representative of two (DAPT) or one (z-FA-FMK) independent experiments.

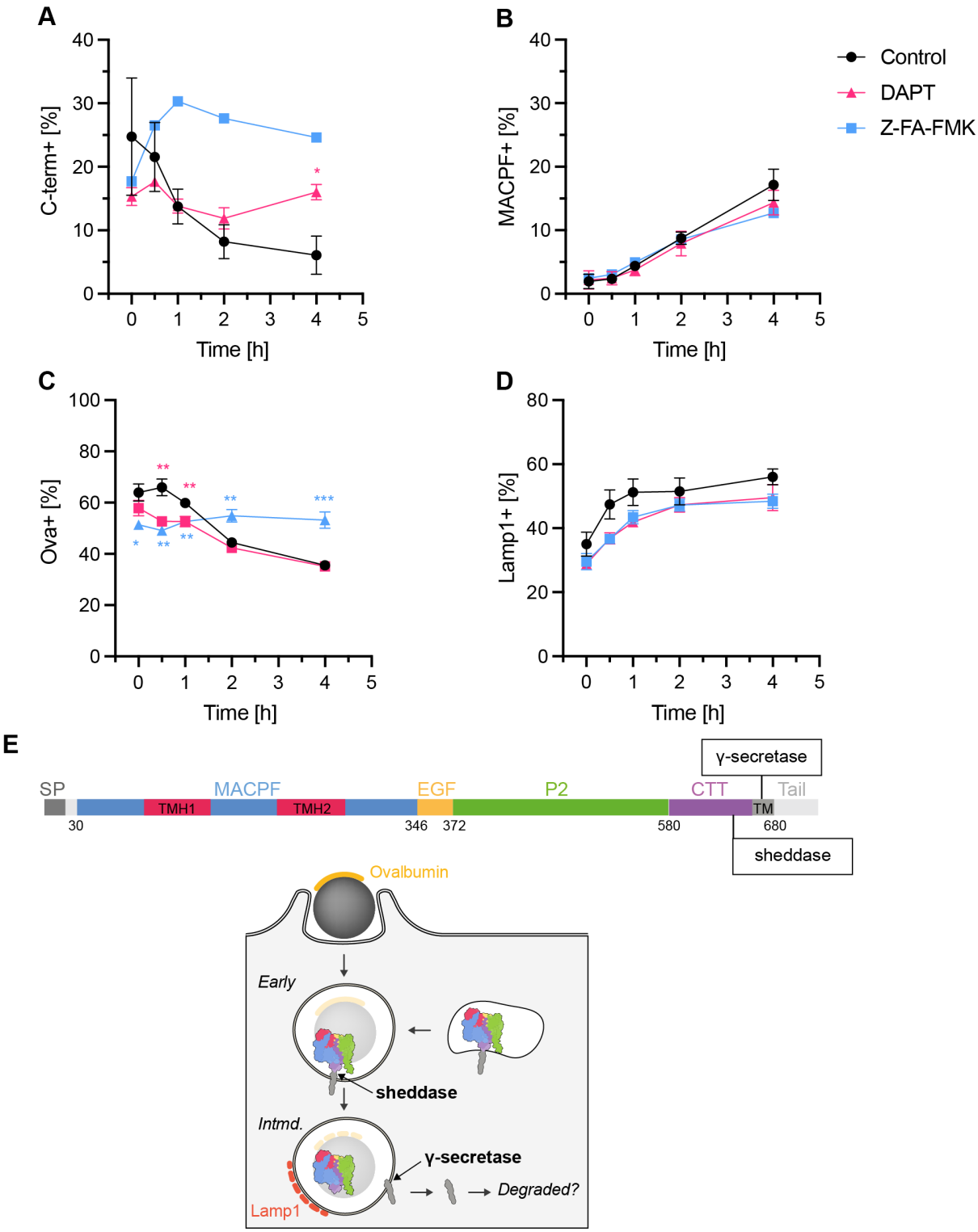

Fig. 5. 8. Effects of DAPT and z-FA-FMK on perforin-2 processing and phagosome maturation. (**A, B**) Quantification of perforin-2$^+$ phagosomes based on the gating shown in Fig. 5.3. (**C, D**) Quantification of ovalbumin$^+$ (C) and Lamp1$^+$ (D) phagosomes. Data represent mean and SEM of two (DAPT) and one (z-FA-FMK) independent experiments. *P<0.1, **P<0.01, ***P<0.001 using a multiple paired t-test (two-stage step-up, Benjamini, Krieger and Yekutieli) (**E**) Schematic representation of perforin-2 processing by a sheddase and γ-secretase.

Both inhibitors also impacted phagosome maturation, albeit to varying degrees. DAPT treatment seemed to accelerate ovalbumin degradation early during the chase but then the degradation rate returned to control levels after 2 hours (**Fig. 5.8C**). In contrast, when treated with z-FA-FMK, ovalbumin degradation was almost completely inhibited suggesting a general impairment of phagosomal proteolysis. However, neither inhibitor affected the recruitment of Lamp1 to the phagosome (**Fig. 5.8D**).

In summary, the data are consistent with the hypothesis that, following recruitment to the phagosome, the ectodomain of perforin-2 is shed by a z-FA-FMK-sensitive protease(s) and the remaining membrane stub is removed by the DAPT-sensitive γ-secretase (**Fig. 5.8E**). Accordingly, inhibition of shedding would lead to an accumulation of full-length perforin-2 on the phagosome and inhibition of stub removal would accumulate the p12 fragment explaining the observed increase in αC-term following z-FA-FMK and DAPT treatment, respectively. Interestingly, the αC-term signal increase was more pronounced in the z-FA-FMK condition and possible explanations for this are discussed in Section 5.3. Strikingly, despite its effects on perforin-2 processing, z-FA-FMK had no impact on the αMACPF signal. While the mechanism leading to the exposure of the αMACPF epitope remains elusive, these data could suggest that it does not require shedding of the ectodomain. However, since the inhibitor was only added during the chase, it remains possible that the antibody detects a pre-existing pool of perforin-2 that was processed in the endosome/lysosome system before z-FA-FMK addition but delivered to phagosomes after the inhibitor was introduced.

5.2.6 Inhibition of ectodomain shedding has no effect on perforin-2-mediated escape

Next, I wanted to address whether ectodomain shedding is a necessary step in perforin-2-mediated escape. To this end, NT or Mpeg1^{KO} MutuDCs were incubated with saporin beads for 5 h at 37°C in the presence or absence of z-FA-FMK. Following a 30 min pulse with puromycin, non-internalised beads were labelled with an αOvalbumin antibody and puromycylated peptides stained with the 12D10 antibody in preparation for flow cytometry. Surprisingly, the presence of z-FA-FMK had no detectable effect on saporin escape (**Fig. 5.9, A and B**). As mentioned in Section 5.2.5, it was possible that phagosomes acquire a functional pool of perforin-2 that was processed prior to z-FA-FMK addition. To test this, I preincubated cells with z-FA-FMK for 5 hours or 16 hours before adding the saporin beads in the continued presence of the inhibitor. Again, inhibition by z-FA-FMK had no impact in saporin escape (**Fig. 5.9, C and D**). These results suggest that shedding of the perforin-2 ectodomain is not required for endocytic escape. It is also notable that z-FA-FMK did not affect saporin escape despite impairing phagosomal proteolysis (**Fig. 5.8C**). This finding

suggests that the rate of saporin escape does not depend on the activity of proteases to cleave saporin off the bead. Instead, it is possible that saporin is released from the bead primarily through GILT-mediated reduction of the disulfide bond which otherwise binds it to the beads (*338, 377, 378*).

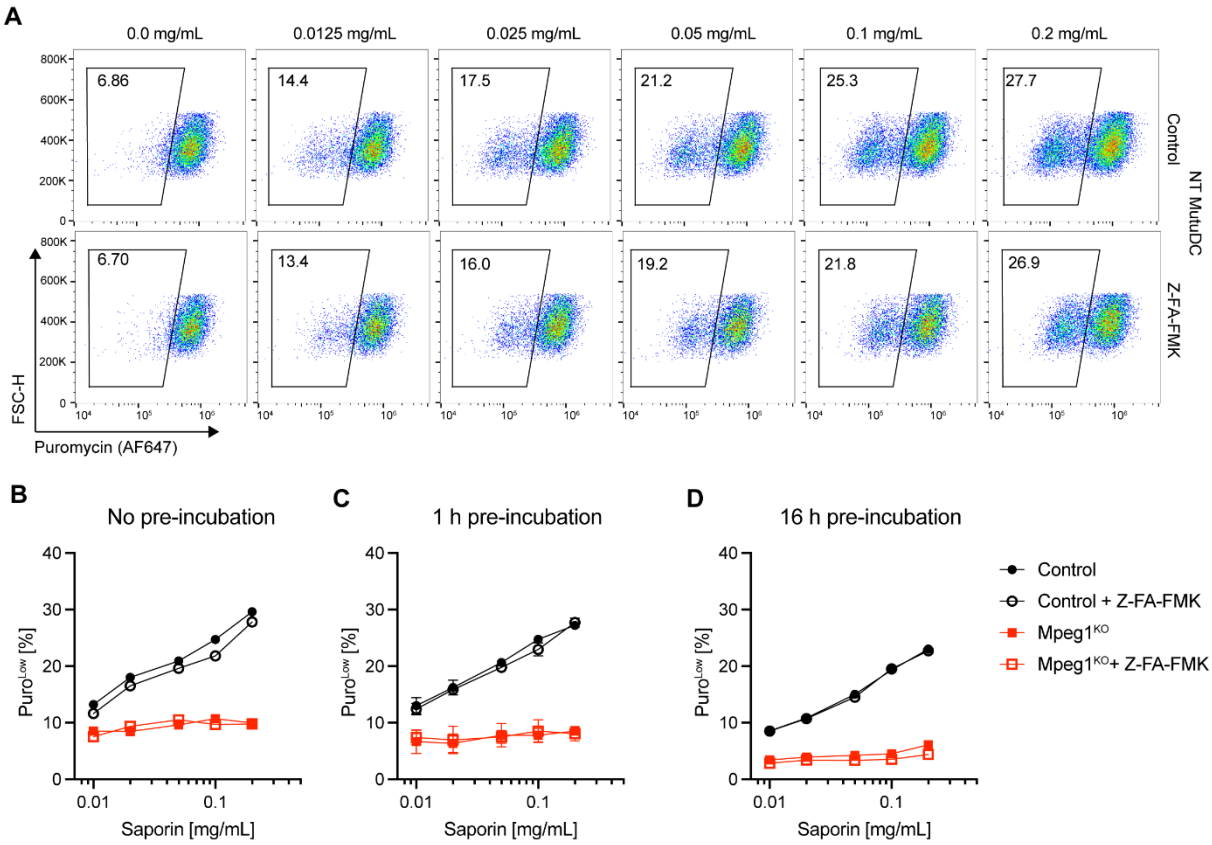

Fig. 5. 9. Effects of z-FA-FMK on perforin-2-mediated escape. (**A**) NT MutuDCs were assayed in the bead saporin-puromycin assay in the presence or absence of 10 μM z-FA-FMK. Cells were incubated with saporin beads for 5 h followed by an incubation with puromycin for 30 min. Cells were then placed on ice and outside beads labelled with an αOvalbumin antibody. After fixation and permeabilistion, levels of puromycin incorporation were detected with an αPuromycin antibody. (**B-D**) Quantification of cells in translation arrest ($Puro^{Low}$) based on the gating shown in (A). Data represent mean and SEM of two (1 h pre-incubation) or one (0 h and 16 h pre-incubation) independent experiments.

5.2.7 Evidence for perforin-2-mediated escape prior to ectodomain shedding

As mentioned in Section 5.1, it has been hypothesised that the TMD may be inhibitory and ectodomain shedding was necessary for perforin-2 activity. Accordingly, pore formation would occur only after phagosomes acquired sufficient proteolytic capacity. However, the findings described here suggest that perforin-2 pore formation could in fact be independent of ectodomain shedding. In addition, although pH may still be an important regulator, the data discussed in Chapter 4 suggest that even the relatively high pH in phagosomes of cDC1 supported the transition from pre-pore to pore. Thus, it is possible that perforin-2 can potentially form pores early during phagosome maturation.

To test this hypothesis, I developed a microscopy-based assay that allowed me to simultaneously follow perfoin-2 processing at the phagosome and perforin-2-mediated saporin escape. NT and Mpeg1^{KO} MutuDCs were seeded in an 8-well chambered coverslip and allowed to adhere overnight. Saporin and BSA beads were prepared as previously except that the beads were coated in ovalbumin that was biotinylated. Cells were incubated with biotinylated saporin beads or BSA beads for 5 hours followed by a 30 min pulse with puromycin. In preparation for microscopy, samples were fixed in 1% PFA and permeabilised

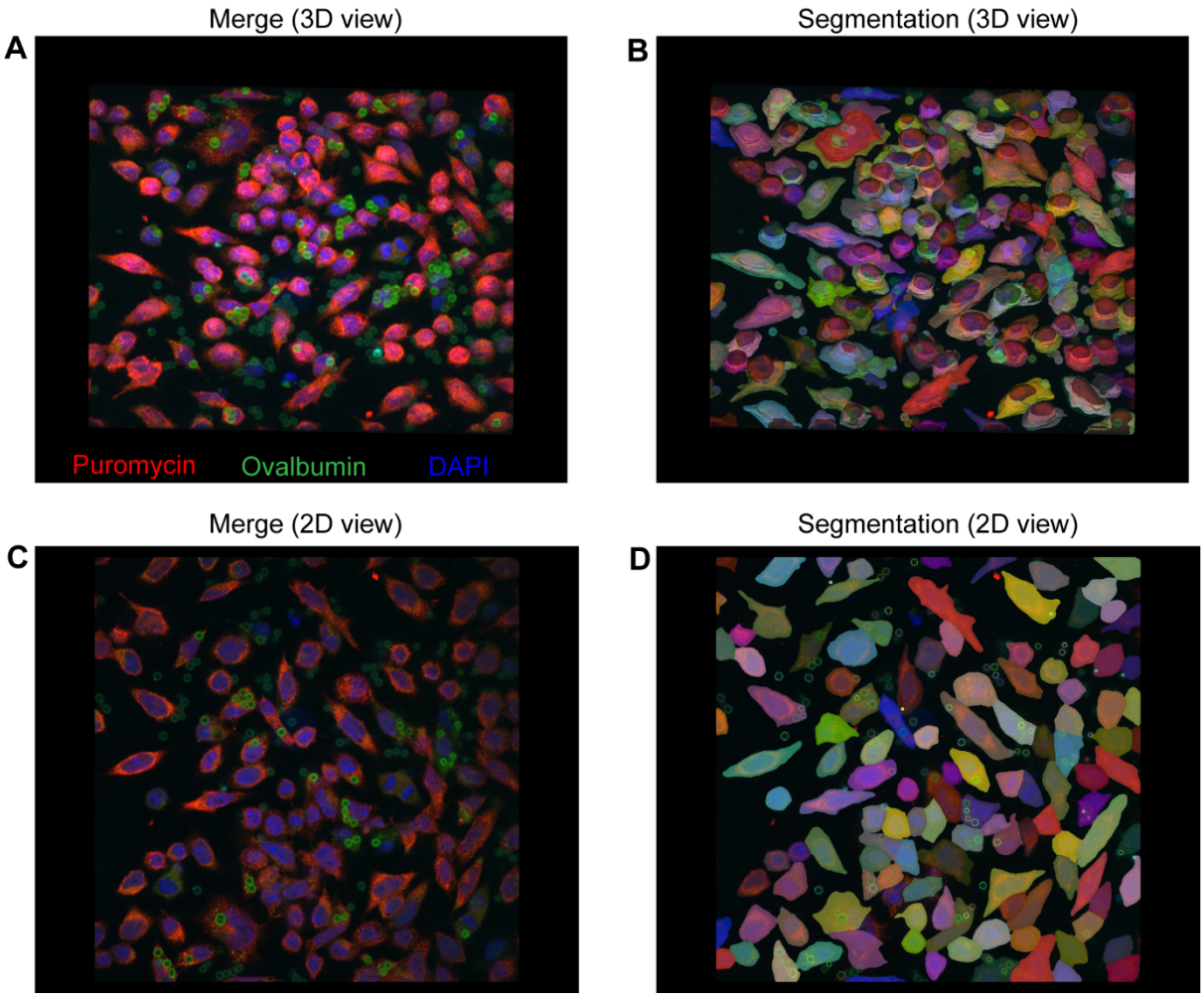

Fig. 5. 10. Segmentation of MutuDCs and beads. (**A, B**) Example field-of-view showing (A) NT MutuDCs in the microscopy-based bead saporin-puromycin assay in 3D view and (B) the corresponding segmentation. (**C, D**) As in (A, B) but in 2D view.

in 0.2% saponin before being stained with primary and secondary antibodies and with fluorescent streptavidin to detect biotin-ovalbumin. The samples were imaged on a confocal microscope by acquiring z-stacks at a minimum of 48 randomly selected fields-of-view per condition. With the help of Jerome Boulanger form the LMB microscopy facility, I developed a python script to automate the image analysis. The script generated 3D masks for each cell and bead in the image (**Fig. 5.10**). For each cell, the fluorescence intensity in the cell mask was used to measure saporin escape and the fluorescence intensity in the bead mask was

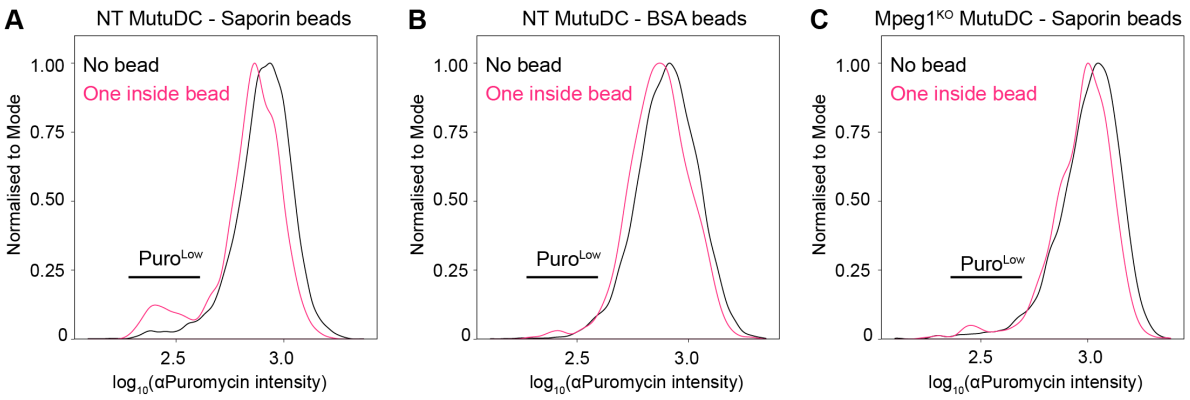

Fig. 5. 11. Measuring perforin-2-mediated escape by microscopy. (**A-C**) NT (A, B) or Mpeg1^{KO} (C) MutuDCs were incubated with either saporin beads (A, C; 1 mg/mL) or BSA beads (B) for 5 h followed by an incubation with puromycin for 30 min. Cells were then fixed, permeabilised and stained with an αPuromycin antibody and imaged by confocal microscopy. 48 FOVs with an average of 80 cells were segmented as shown in Fig. 5.10 and the fluorescence intensity of αPuromycin was determined in cells with either a single internalised bead or no bead. Data are from one experiment.

used to determine protein levels at the phagosome. Only bead masks that overlapped by at least 80% with a cell mask were included in the analysis.

To confirm that the assay could faithfully captured perforin-2-mediated saporin escape, I compared levels of puromycin incorporation in NT and Mpeg1^{KO} MutuDCs incubated with saporin beads. Consistent with the flow cytometry-based saporin-puromycin assay (**Fig. 3.10**), NT MutuDCs that had internalised a single saporin bead had a population of Puro^{Low} cells whereas cells with a BSA bead did not (**Fig. 5.11**). As expected, Mpeg1^{KO} MutuDCs did not acquire a Puro^{Low} population after internalising a saporin bead confirming that the escape of saporin was perforin-2-dependent.

To ensure that the beads were segmented correctly, I compared the ovalbumin and perforin-2 staining from single-internalised beads. Consistent with the phagoFACS assay (**Fig. 3.6**), the αC-term signal was enriched on Ova^{High} beads and depleted on Ova^{Low} beads (**Fig. 5.12**). Similarly, the αMACPF signal was mostly enriched on Ova^{Low} beads as expected. However, by microscopy, the αMACPF antibody detected perforin-2 also on Ova^{High} beads while by flow cytometry it did not. The αMACPF staining has a punctate morphology with punctae sometimes appearing inside the phagosome lumen, on the phagosome membrane, or adjacent to it (see Fig. 5.13D). Thus, a potential explanation for the contradictory observations could be that the microscopy assay captures the αMACPF signal from these adjacent structures, even if they are not fused with the phagosome. In contrast, the flow cytometry method might lose this signal because it involves cell disruption, which could separate these adjacent structures from the phagosome.

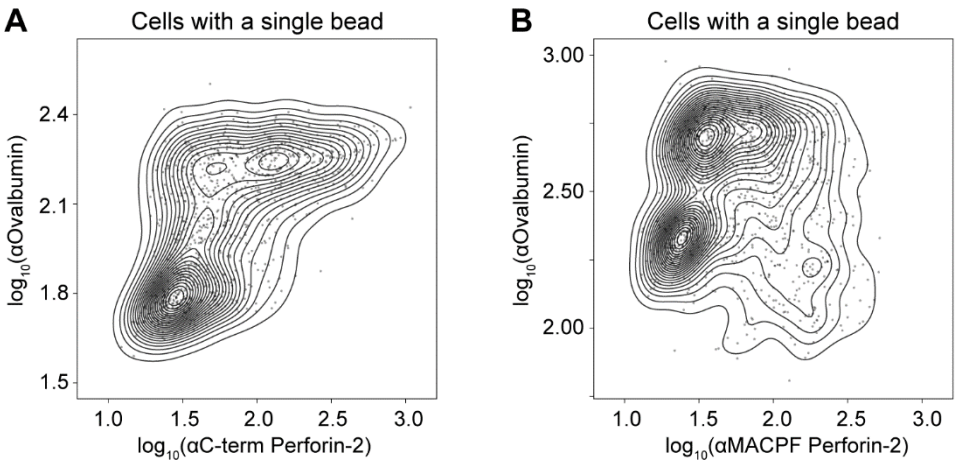

Fig. 5. 12. Measuring phagosomal perforin-2 recruitment by microscopy. (**A, B**) Samples were stained with streptavidin-AF488 (to detect biotin-Ova) and either (A) αC-term or (B) αMACPF antibodies. Plots show signals from single-internalised beads. The data are from the experiment described in Fig. 5.11.

Next, I assessed how saporin escape correlates with the state of perforin-2 processing on the phagosome. Thus, I plotted the αPuromycin signal of cells with a single bead against the associated αC-term signal on that bead. In a large fraction of cells, perforin-2 was recruited to the bead but saporin had not (yet) escaped (**Fig. 5.13, A** and **B,** Q1). In cells where saporin did escape ($Puro^{Low}$), the bead was in many cases αC-term- suggesting that the C-terminus had been cleaved off (Q3). However, there was also a small population in which the bead was still αC-term+ but saporin had already escaped (Q2). Plotting the αPuromycin signal against the associated bead αMACPF signal showed that the majority of $Puro^{Low}$ cells were αMACPF+ (**Fig. 5.13, C** and **D**, Q2). However, there were also many $Puro^{High}$ cells with αMACPF+ phagosomes from which saporin had not escaped (Q1). In addition, there was a small fraction of $Puro^{Low}$ cells in which saporin had escaped but the bead was αMACPF- (Q3). Finally, plotting αPuromycin signal against the associated bead-αOvalbumin signal showed that in many $Puro^{Low}$ cells ovalbumin was degraded (**Fig. 5.13E**, Q3). However, saporin could also escape prior to ovalbumin degradation (Q2).

In summary, the data show that the phagosomes of $Puro^{Low}$ cells are often mature, characterised by staining as αOva-, αC-term-, or αMACPF+. However, instances of $Puro^{Low}$ cells with less mature, αOva+ phagosomes were also observed, where the αMACPF signal was not yet acquired and the αC-term signal persisted, indicating that perforin-2 remained TMD-anchored. While preliminary (repeats of n=1), these results are consistent with the interpretation that saporin can escape from early phagosomes prior to shedding of the perforin-2 ectodomain. The presence of αMACPF signal on phagosomes of $Puro^{High}$ cells could suggest that the mechanism exposing the epitope does not cause saporin release, although this could also be attributed to the segmentation capturing signal from adjacent compartments as mentioned above.

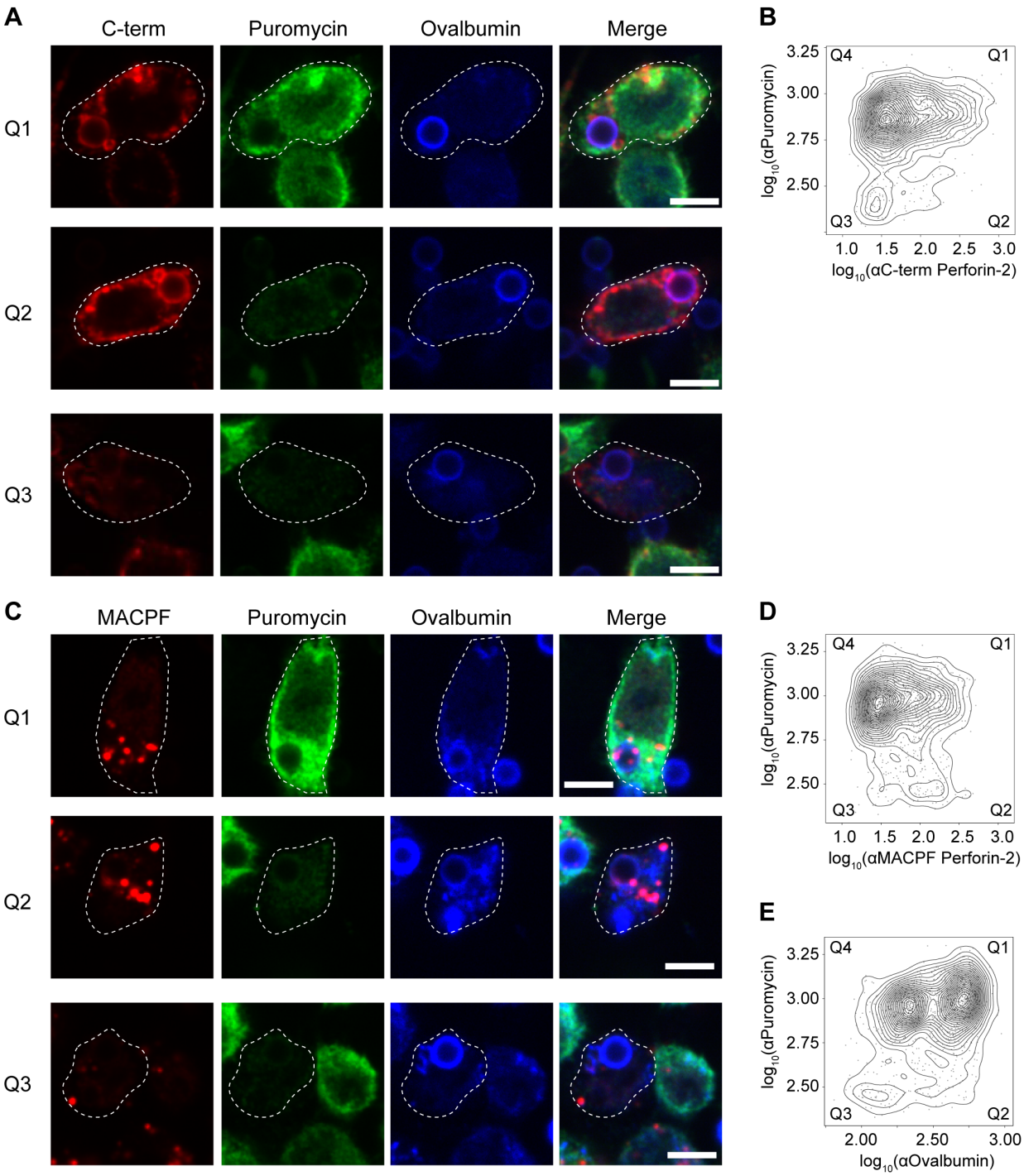

Fig. 5. 13. Correlating perforin-2 processing and saporin escape by microscopy. (**A, C**) Representative images for the samples plotted in (B) and (D). (**B, D, E**) The plots show the αPuromycin intensity of a cell and the αC-term (B), αMACPF (D) or Ova (E) signal on the internalised bead. The data are from the experiment described in Fig. 5.11.

5.3 Discussion

In this chapter, I investigated the role of proteolysis in the regulation of perforin-2. I found that perforin-2 is cleaved in the EGF domain, the P2 domain, the CTT domain and the TM domain. The cleavage in the CTT domain, which leads to ectodomain shedding, is mediated by pH-sensitive cysteine protease(s), potentially cathepsins and the remaining membrane

stub is cleaved by γ-secretase in the TMD. The cleavage in the P2 domain is mediated by AEP while the EGF cleavage is mediated by AEP and other pH-sensitive proteases. Strikingly, none of these cleavages appear to be required for perforin-2-mediated escape *in vivo*. The observation that the EGF and P2 cleavages were not required for perforin-2-mediated escape in AEP^{KO} MutuDCs is in line with *in vitro* data showing pore formation in the absence of these cleavages (*246, 247*). The data here now indicate that shedding may also not be required for perforin-2-mediated escape arguing against the hypothesis that the TMD anchor serves to prevent premature pore formation (*247, 314, 320, 362*).

Instead, the data are consistent with the interpretation that perforin-2-mediated escape can occur from early phagosomes in the absence of ectodomain shedding. The key observations for this conclusion from this chapter are that 1) inhibition of shedding by z-FA-FMK did not affect perforin-2-mediated escape and that 2) perforin-2-mediated escape was detected before ovalbumin degradation or turnover of the perforin-2 C-terminal tail on phagosomes. In addition, the results in Chapter 3 showed that even when phagosomal acidification and proteolysis were inhibited by BafA1, perforin-2-mediated escape was not prevented (Fig. 3.13). Thus, perforin-2 pore formation *in vivo* may require less acidification than previously thought, both from the perspective of pH-dependent proteolysis and pH-dependent conformational changes. This model is attractive as it would help to explain how perforin-2 may mediate endocytic escape in cDC1 in the absence of phagosomal acidification. However, further investigation is warranted to substantiate the idea of pore formation by TMD-anchored perforin-2 in early compartments. In particular, it will be necessary to more accurately define at which point of phagosome maturation the active pore forms, for example by developing conformation-specific labelling tools.

If proteolysis is not necessary to activate pore formation, it prompts a consideration of its other potential roles. While cleavages may serve different, or even opposing functions, one general possibility could be that proteolysis plays a crucial role in inactivating the pore. However, this seems unlikely as the inhibition of proteolysis did not result in hyperactivity. Another potential role could be that proteolysis serves to enhance the efficiency of escape. While this was not evident when saporin was used as the substrate, it may be relevant for physiological substrates. Finally, for some γ-secretase targets it has been reported that the released cytosolic tail translocates to the nucleus to mediate signalling pathways making this an interesting avenue to explore in the future (*367, 368*).

While the function of each cleavage remains unclear, it will be important to consider the order in which they occur when addressing this question. The data here suggest that the first cleavage could be in the CTT since in AEP^{KO} MutuDCs, with partly impaired EGF cleavage

and fully impaired P2 cleavage, only the p60 ectodomain accumulates but not a fragment containing the C-terminal tail. This is also supported by the phagoFACS data showing that the C-terminal tail begins to be lost soon after recruitment of the TMD-anchored perforin-2. In addition to the p60 fragment, AEP^{KO} MutuDCs also accumulate a p28 fragment (produced by EGF and CTT cleavages) which suggests that the P2 cleavage may happen after the EGF cleavage. However, to formally determine the order of cleavage events pulse-chase experiments, for example similar to those in Chapter 3 (Fig. 3.3) will be necessary.

An interesting observation is that inhibition of shedding by z-FA-FMK accumulated higher amounts of αC-term signal on phagosomes than inhibition of the TMD cleavage by DAPT (Fig. 5.8). This could have many explanations. For example, DAPT may not be 100% efficient so that a fraction of C-terminal membrane stubs is still being turned over. It is also possible that C-terminal signal is normally not only lost due to degradation but also due to recycling of the full-length protein and z-FA-FMK may inhibit this process. Yet another possibility is that phagosomes of untreated cells may fuse with compartments that contain already cleaved, soluble perfoirn-2, while in z-FA-FMK-treated cells, these compartments instead contain full-length perforin-2. Finally, z-FA-FMK may inhibit cytosolic proteases(s), for example caspases (*375*), that could cleave the cytosolic tail of perforin-2.

Chapter 6 – Disruption of trafficking leads to inhibition of perforin-2-mediated escape

6.1 Introduction

Perforin-2 is a type I transmembrane protein with a short C-terminal cytosolic tail that comprises 39 amino acids. As for many transmembrane proteins, the cytosolic tail contains several interesting regions that may be implicated in sorting of perforin-2 (**Fig. 6.1A**). Sorting signals are typically short, linear stretches of amino acids which are recognised by specific adaptor proteins that are peripherally associated with the cytosolic side of membranes (*379*). Several of these adaptor proteins can link the cargo to the coat protein clathrin and thus mediate the sorting of transmembrane cargo into clathrin-coated vesicles for endocytosis and transport within the endosome/lysosome system (*328, 380*). Among the best characterised sorting signals are the tyrosine-based YxxΦ motif (x, any residue; Φ, hydrophobic residue) and the two dileucine-based [D/E]xxxL[L/I] and DxxLL motifs (*379*). In addition to these peptide motifs, ubiquitination of cytosolic lysine residues may also serve as a sorting signal (*381*).

The cytosolic tail of perforin-2 features a patch of lysines (residues 678 and 680-682) which may act as ubiquitin acceptor sites as well as a canonical YxxΦ motif (684-**Y**QE**I**-687). In addition, it comprises two non-canonical dileucine-like motifs (689-**E**QES**LV**-694 and 700-**D**AT**VL**-704). The classical [D/E]xxxL[L/I] dileucine motif consists of an invariant leucine in the first position and a leucine or isoleucine in the second position (*382*). However, mutagenesis studies of a CD36/LIMP-II chimera have shown that valine (and alanine) can also be tolerated at the second position (*383*). Similarly, in the DxxLL motif, any of the two leucines may be substituted by a bulky hydrophobic residue including valine (*384*). Thus, it is possible that the 689-**E**QES**LV**-694 and 700-**D**AT**VL**-704 motifs in the perforin-2 tail function as sorting signals for selection into coated vesicles.

The YxxΦ and [D/E]xxxL[L/I] motifs frequently function as lysosomal targeting signals (*385*) The sorting of lysosomal transmembrane proteins with these motifs is mediated by adaptor protein (AP) complexes. Early studies have shown that the YxxΦ motif is bound by AP-1 and AP-2 (*386, 387*). AP-1 and AP-2 are both abundant components of clathrin-coated vesicles (CCVs) and facilitate their formation by linking the clathrin coat to the membrane (*388-391*). BLAST analysis conducted in later studies revealed the existence of a third and fourth AP complex (*392-394*). Unlike the other two AP complexes, AP-3 can bind clathrin but this interaction is not always necessary for its function (*395*) whereas AP-4 does not appear to associate with clathrin at all but nonetheless mediates the concentration of cargo into

vesicles (*393, 396*). All four AP complexes are heterotetramers composed of two large subunits (α/γ/δ/ε and β1–4), a medium subunit (μ1–4) and a small subunit (σ1-4) (*391*). The μ subunit of each AP complex can bind cargo proteins with a YxxΦ motif (*397, 398*). The respective σ subunits of AP-1, AP-2 and AP-3 are responsible for recognition of the [D/E]xxxL[L/I] motif (*399-401*).

Structural studies of AP-2 suggest that AP complexes exist in a closed conformation when in the cytosol and in an open conformation, capable of cargo binding, upon recruitment to the membrane (*402-404*). Membrane binding of AP-1, AP-3 and AP-4 is facilitated by the small GTPase Arf1 whereas AP-2 is primarily recruited by binding to phosphatidylinositol 4,5-bisphosphate (PIP2) (*380, 391*). AP-1 mediates transport between the trans-Golgi network (TGN) and early and/or recycling endosomes. In contrast, AP-2 localises to the plasma membrane and is primarily involved in endocytosis (*379, 380*). AP-3 is thought to facilitate sorting of transmembrane proteins from tubular sorting endosomes to lysosomes (*405*) and AP-4 appears to be required for sorting from the TGN to peripheral sites (*396*). Lysosomal transmembrane proteins can take different routes to reach the lysosome and have diverse AP complex requirements. They can take a direct route involving transport from the TGN to early/late endosomes and then to lysosomes (*406*). In addition, they can take an indirect route with the protein being transported from the TGN to the plasma membrane followed by endocytosis into early endosomes and eventual delivery to lysosomes (*406*). Notably, the direct and indirect pathways are not mutually exclusive, and many lysosomal transmembrane proteins use both routes to reach the lysosome (*385, 406*).

In contrast to the YxxΦ and [D/E]xxxL[L/I] motifs, the DxxLL motif is recognised by a different family of clathrin adaptors known as GGA (Golgi-localizing, γ-adaptin ear homology domain, ARF-interacting) proteins (*380, 407, 408*). GGA proteins are monomeric, associate with the membrane in a Arf1-dependent manner and mediate transport of transmembrane proteins from the TGN to endosomes/lysosomes (*380*).

Finally, ubiquitination on lysine residues within the cytosolic tail of transmembrane proteins can be recognised by an array of sorting adaptors containing a ubiquitin-binding domain (*409*). Two prominent examples are Epsin and Eps15 which link mono- or polyubiquitinated cargo at the plasma membrane to the clathrin machinery for endocytosis (*381, 410*). From early endosomes, ubiquitinated cargo may be recycled back to the plasma membrane or TGN (*340*). Alternatively, ubiquitinated transmembrane proteins can be sorted into intraluminal vesicles (ILVs) by the ESCRT apparatus to form multivesicular bodies (MVBs) (*381, 411*). MVBs may serve as temporary storage compartments (e.g. for MHC-II) or fuse with lysosomes for degradation of their contents (*411*). The initial selection of a

transmembrane protein for ubiquitination is regulated by a large family of E3 ligases (*381, 412*).

The functional roles of sorting signals in the cytosolic tail of perforin-2 are poorly characterised. One study implicated ubiquitination of the lysine patch in perforin-2 sorting following infection. It was shown that in MEF cells, the lysine patch of transfected human perforin-2 is ubiquitinated by a cullin-RING E3 ubiquitin ligase (CRL) complex upon infection with enteropathogenic E. *coli* or treatment with LPS (*268*). Mutagenesis of the lysines at position 678, 680 and 681 prevented ubiquitination and perforin-2 recruitment to the phagosome (*268*). Whether the ubiquitination of the lysine patch also plays a role in perforin-2 trafficking in the absence of PAMPs is unknown. Similarly, whether any of the other putative sorting signals are involved in the sorting of perforin-2 within endocytic compartments is completely unexplored.

To study the role of the sorting signals in the perforin-2 tail, I generated different mutants and expressed them by lentiviral transduction in Mpeg1^{KO} MutuDCs. I assessed the distribution and processing of these mutants by immunofluorescence and Western blot. I then characterised their processing at the phagosome by phagoFACS and tested their ability to mediate endocytic escape in the bead saporin-puromycin assay.

6.2 Results

6.2.1 Sorting motifs in the cytosolic tail are important for perforin-2 processing and activity

In order to investigate the contribution of the cytoplasmic tail in the function of perforin-2, I generated two mutant perforin-2 variants. In one mutant, the YxxΦ variant, only the YxxΦ motif was disrupted by a Y684A/I687A mutation (**Fig. 6.1A**). In a second mutant, the Tailless variant. all regions putatively implicated in sorting were disrupted. Accordingly, lysines at 680-682 were mutated to arginine (K678 was retained because mutations at this position led to ER retention), the YxxΦ and [D/E]xxxL[L/I]-like motif were replaced by eight alanines and the DxxLL-like motif was disrupted by a truncation and a K704A mutation (**Fig. 6.1A**). cDNAs encoding these variants, or wild-type perforin-2, were cloned into a plasmid with an IRES-mScarlet reporter cassette. Mpeg1^{KO} MutuDCs were then stably reconstituted by lentiviral transduction and sorted for equal levels of mScarlet expression. The sorted MutuDC lines were analysed by flow cytometry which showed that the mScarlet reporter was expressed at similar levels (**Fig. 6.1B**).

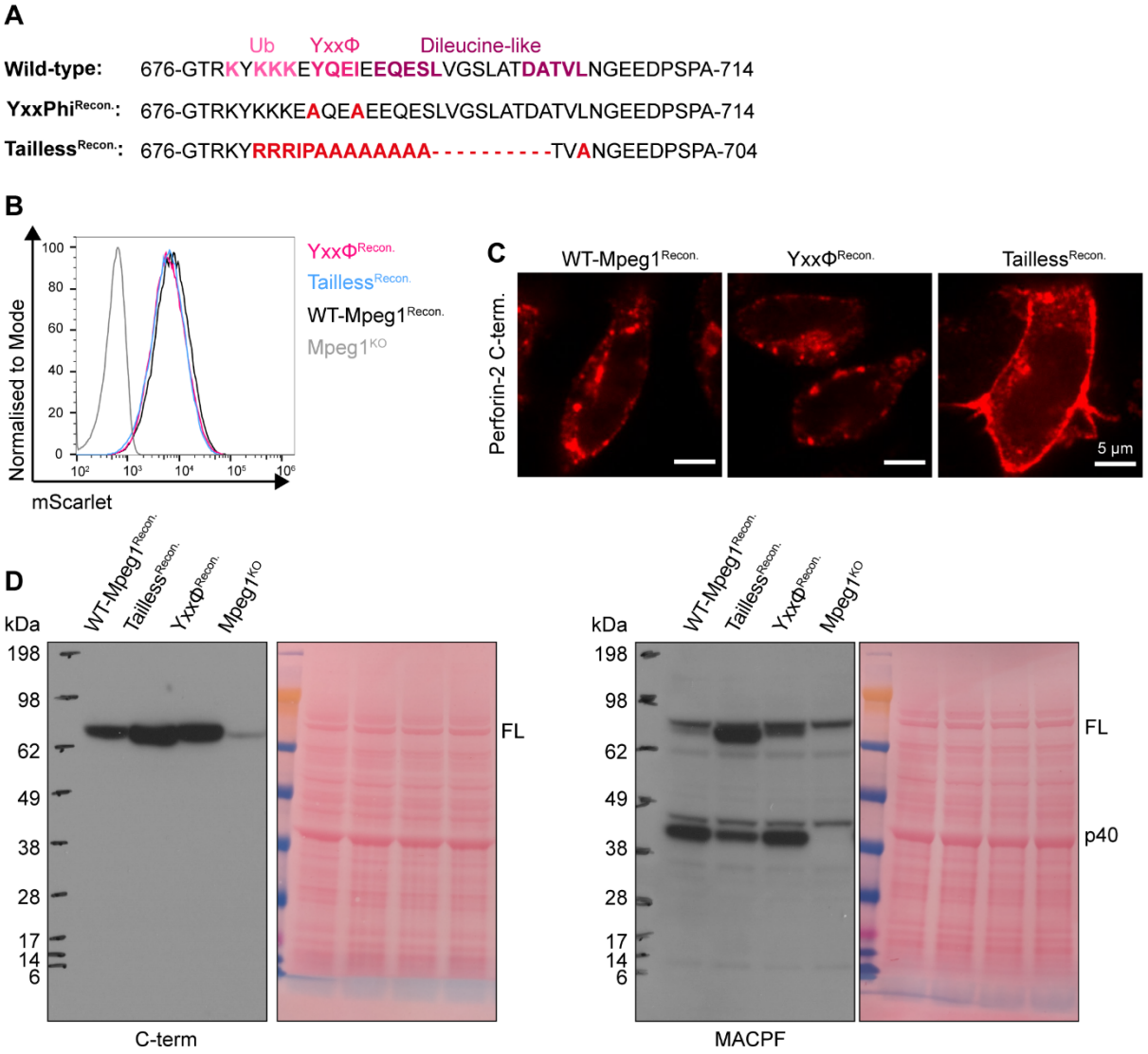

Fig. 6. 1. Generation of perforin-2 variants with mutated trafficking motifs. (**A**) Sequences of the perforin-2 cytosolic tail. Mutations in the YxxΦ and Tailless variants are indicated in red. (**B**) Flow cytometry analyses of IRES-mScarlet expression in the indicated MutuDC lines. (**C**) Confocal microscopy analysis of perforin-2 in the indicated MutuDC lines using the αC-term antibody. (**D**) Western blot analysis of whole cell lysate from the indicated MutuDC lines probed with the αC-term or αMACPF antibodies under reducing conditions. Data are representative for two independent experiments.

To test whether disruption of the sorting motifs had any effect on the steady-state distribution of perforin-2, WT-Mpeg1$^{Recon.}$, YxxΦ$^{Recon.}$, and Tailless$^{Recon.}$ MutuDCs were analysed by immunofluorescence using the αC-term antibody (**Fig. 6.1C**). The reconstituted wild-type perforin-2 displayed the typical vesicular distribution observed previously in NT MutuDCs (Fig. 3.1C). Similarly, the distribution of perforin-2 in YxxΦ$^{Recon.}$ MutuDCs was comparable to those of WT-Mpeg1^{Recon} cells. In contrast, the Tailless variant displayed a dramatic accumulation at the plasma membrane (PM). These observations suggest that the lysine patch and/or the dileucine-like motifs are necessary for targeting perforin-2 to endocytic compartments. Although the observed perforin-2 distribution in YxxΦ$^{Recon.}$ MutuDCs was unaltered, a potential PM accumulation of YxxΦ variant might have been missed as fixation

and permeabilisation can cause artefactual loss of cell surface proteins (*413, 414*). Moreover, the YxxΦ and Tailless variants may have additional intracellular sorting defects that were not detectable in the present analysis. To better characterise the mislocalisation phenotype, co-staining for endo- and lysosomal markers as well as quantification could be performed.

To assess whether the sorting motifs in the cytosolic tail are important for perforin-2 processing, WT-Mpeg1$^{Recon.}$, YxxΦ$^{Recon.}$, Tailless$^{Recon.}$ and Mpeg1^{KO} MutuDCs were analysed by Western blot using the αC-term and αMACPF antibodies. The αC-term Western blot showed that, despite similar expression levels (**Fig. 6.1B**), the full-length Tailless and YxxΦ variants accumulated at higher levels than wild-type perforin-2 (**Fig. 6.1D**). Notably, the Tailless variant exhibited higher accumulation compared to the YxxΦ variant. In addition, the αMACPF Western blot revealed decreased levels of the p40 fragment in cells expressing the Tailless variant while p40 levels in cells expressing the YxxΦ variant were similar to wild-type. These results are consistent with the PM phenotype in Tailless$^{Recon.}$ MutuDCs and suggest that the cytosolic tail is important for sorting perforin-2 into proteolytic compartments where it would normally undergo shedding as well as cleavages in the EGF and P2 domains. In addition, the increased accumulation of full-length YxxΦ variant suggests that a fraction of it may also fail to reach proteolytic compartments.

Nascent phagosomes derive most of their membranes from the PM (*210*). Since the Tailless variant (and potentially also the YxxΦ variant) is mislocalised to the PM, I wondered whether this variant is properly processed and functional when incorporated into phagosomes. I therefore analysed the reconstituted MutuDC lines in phagoFACS. Isolated phagosomes from cells pulse-chased with Ova beads were stained with antibodies against the perforin-2 C-terminus and Lamp1. Flow cytometry analysis showed that the proportion of C-term+ phagosome at 0 h was 2-fold higher in YxxΦ$^{Recon.}$ (~20%) and 4-fold higher in Tailless$^{Recon.}$ (~38%) compared to WT-Mpeg1$^{Recon.}$ (~10%) MutuDCs (**Fig**. **6.2, A and D**). The αC-term levels remained elevated throughout the chase, particularly in phagosomes of Tailless$^{Recon.}$ MutuDCs, likely due to the increased perforin-2 incorporation during phagosome formation. Wild-type perforin-2 was mostly detected in Lamp1^{Int} phagosomes whereas the YxxΦ and Tailless variants were also present on early Lamp1^{Low} phagosomes. The increased αC-term levels are consistent with a PM origin for the excess perforin-2 on phagosomes of YxxΦ$^{Recon.}$ and Tailless$^{Recon.}$ MutuDCs.

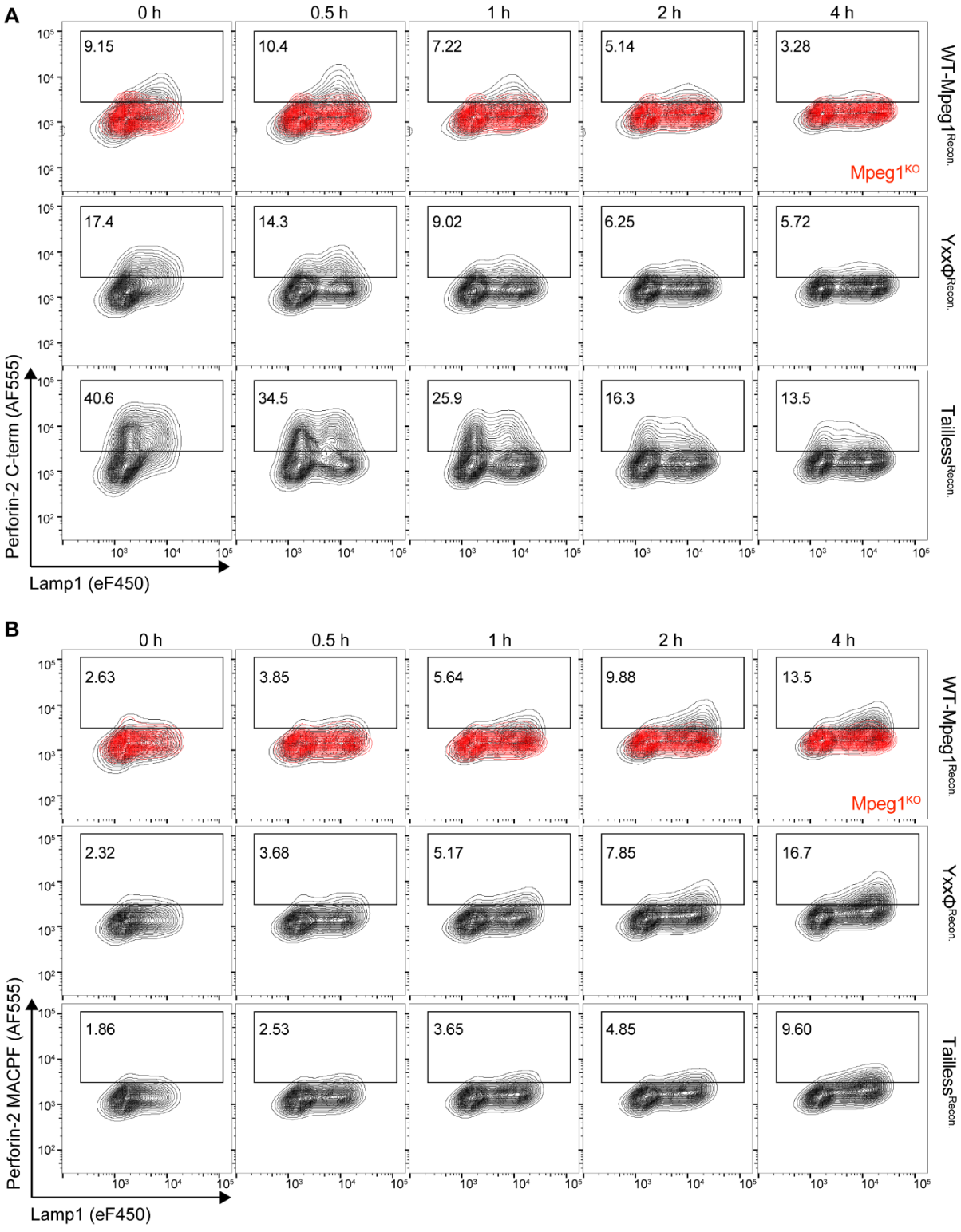

Fig. 6.2 (continues overleaf)

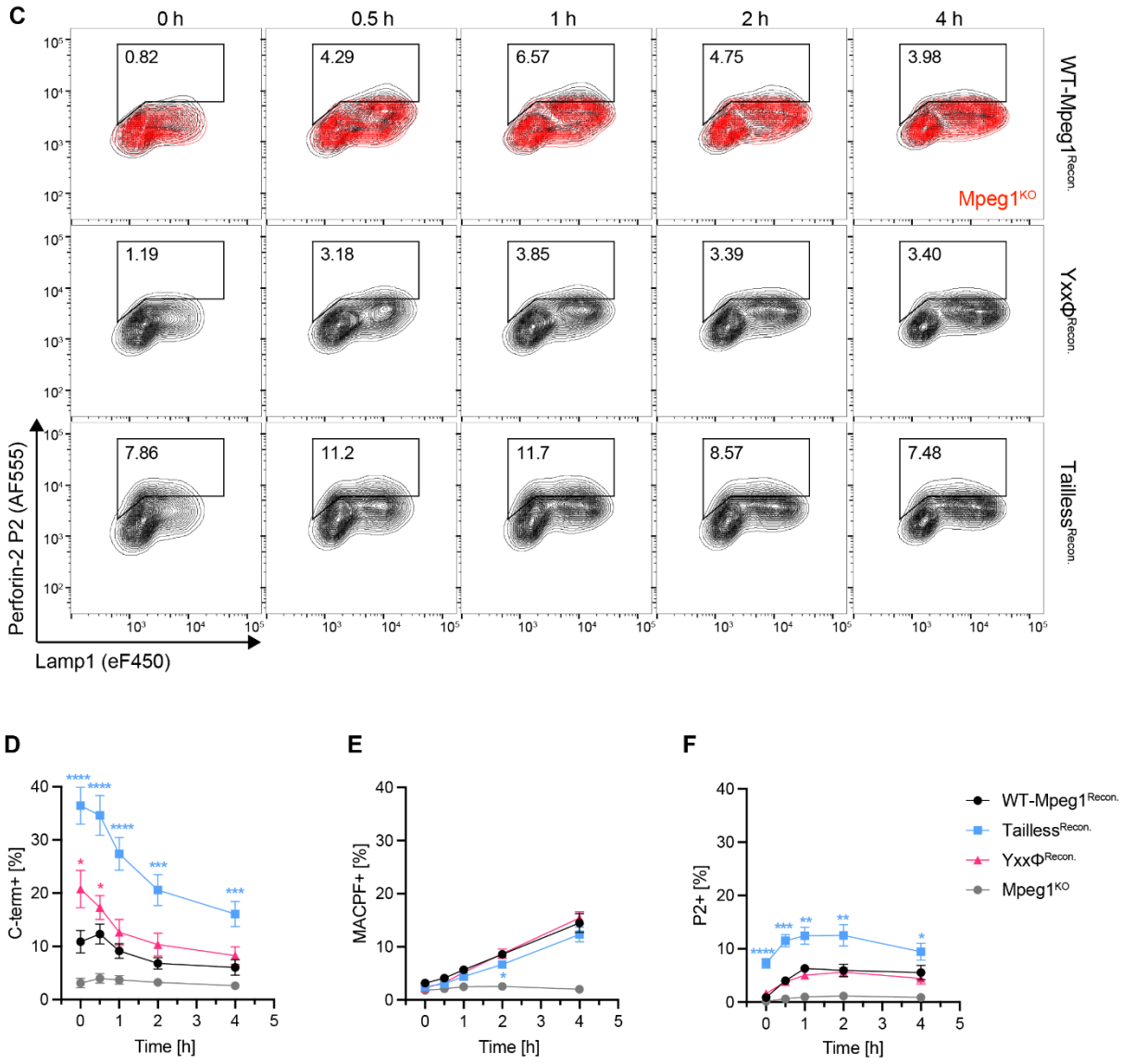

Fig. 6. 2. Processing of the YxxΦ and Tailless variants at the phagosome. (**A-C**) The indicated MutuDC lines were pulsed with OVA beads for 25 min at 16°C followed by 5 min at 37°C, washed and either immediately placed on ice (0 h) or chased for the indicated time. Isolated phagosomes were stained with αLamp1 and with αC-term (A) αMACPF (B) or αP2 (C) antibodies. (**D-F**) Quantification of perforin-2^{+} phagosomes based on the gating shown in A-C. Data represent mean and SEM of six independent experiments. **P<0.01; ***P<0.001; ****P<0.0001 using a multiple paired t-test (two-stage step-up, Benjamini, Krieger and Yekutieli) versus WT-Mpeg1.

Next, isolated phagosomes were stained with antibodies against the perforin-2 MACPF domain and Lamp1. Strikingly, despite the increased levels of recruitment detected by the αC-term antibody, the αMACPF antibody detected no appreciable difference in perforin-2 levels between wild-type and mutant variants (**Fig. 6.2, B and E**). These results are consistent with the hypothesis that the αMACPF epitope is only exposed following a conformational change or cleavage event. The observation that increased perforin-2 recruitment in YxxΦ$^{Recon.}$ or Tailless$^{Recon.}$ MutuDCs did not translate into an increased αMACPF signal could suggest that these variants are inherently impaired in undergoing the required processing step(s). A contributing factor may also be that a fraction of the recruited

YxxΦ and Tailless variants remain on Lamp1^{Low} phagosomes which may not be competent to mediate the required processing step(s) to reveal the αMACPF epitope.

Finally, isolated phagosomes were stained with antibodies against the perforin-2 P2 domain and Lamp1. Interestingly, despite the 2-fold increase in the number of αC-term+ phagosomes in YxxΦ$^{Recon.}$ MutuDCs (**Fig. 6.2, A and D**), the αP2 epitope was undetectable at time 0 h and became exposed with similar kinetics to those observed in WT-Mpeg1$^{Recon.}$ MutuDCs (**Fig. 6.2, C and F**). In contrast, in Tailless$^{Recon.}$ MutuDCs, ~8% of phagosome at time 0 h were αP2+ and remained elevated ~2-fold above wild-type levels throughout the remainder of the chase. The elevated levels of αP2 levels on Tailless$^{Recon.}$ phagosomes could simply be due to the increased perforin-2 recruitment observed with the αC-term antibody. However, in this case, one would also expect a proportional increase in αP2 levels on YxxΦ$^{Recon.}$ phagosomes. Thus, the increased accessibility of the αP2 epitope on Tailless$^{Recon.}$ phagosomes, particularly at 0 h, could instead be due to a conformational difference. Accordingly, the Tailless variant might preferentially adopt monomeric, pre-pore arc, or pore conformations which are predicted to have an exposed αP2 epitope (Fig. 5.1). In theory, the increased levels of αP2 staining could also be due to decreased AEP processing of the mistargeted Tailless variant which would preserve the epitope (whereas wild-type perforin-2 could be recruited with a cleaved αP2 epitope). However, phagoFACS experiments in AEP^{KO} MutuDCs have suggested that wild-type perforin-2 is recruited prior to AEP cleavage with an intact αP2 epitope (Fig. 5.9).

In summary, the data so far suggest that the sorting signals in the cytosolic tail are required for efficient sorting of perforin-2 into the endosome/lysosome system. Perforin-2 variants with disrupted sorting signals accumulate at the PM and display proteolytic processing defects at steady-state. The variants are recruited at increased levels to the phagosome, likely due to mistargeting to, or impaired internalisation from, the PM. The processing of recruited perforin-2 variants appears to be impaired although the phagoFACS data do not allow any conclusions regarding the underlying defect(s).

To test whether the increase in perforin-2 recruitment to phagosomes has any effect on perforin-2-mediated escape, I compared WT-Mpeg1$^{Recon.}$, YxxΦ$^{Recon.}$, Tailless$^{Recon.}$ and Mpeg1^{KO} MutuDCs in the bead saporin-puromycin assay. Thus, cells were incubated with saporin beads for 5 h at 37°C, pulsed with puromycin and then stained for analysis by flow cytometry. In YxxΦ$^{Recon.}$ MutuDCs, perforin-2-mediated escape of saporin was comparable to that in WT-Mpeg1$^{Recon.}$ MutuDCs (**Fig. 6.3**). In contrast, in Tailless$^{Recon.}$ MutuDCs, saporin escape was ~30% less efficient than in WT-Mpeg1$^{Recon.}$ MutuDCs. Importantly, gating on different levels of perforin-2 expression based on the IRES-mScarlet reporter revealed an

expression-dependent increase in saporin escape in all three cell lines confirming that the assay is sensitive to varying perforin-2 levels (**Fig. 6.4**). Since the increased levels of perforin-2 at the phagosomes of YxxΦ$^{Recon.}$ and Tailless$^{Recon.}$ MutuDCs did not translate into enhanced endocytic escape, it appears that the YxxΦ and Tailless variants are functionally impaired.

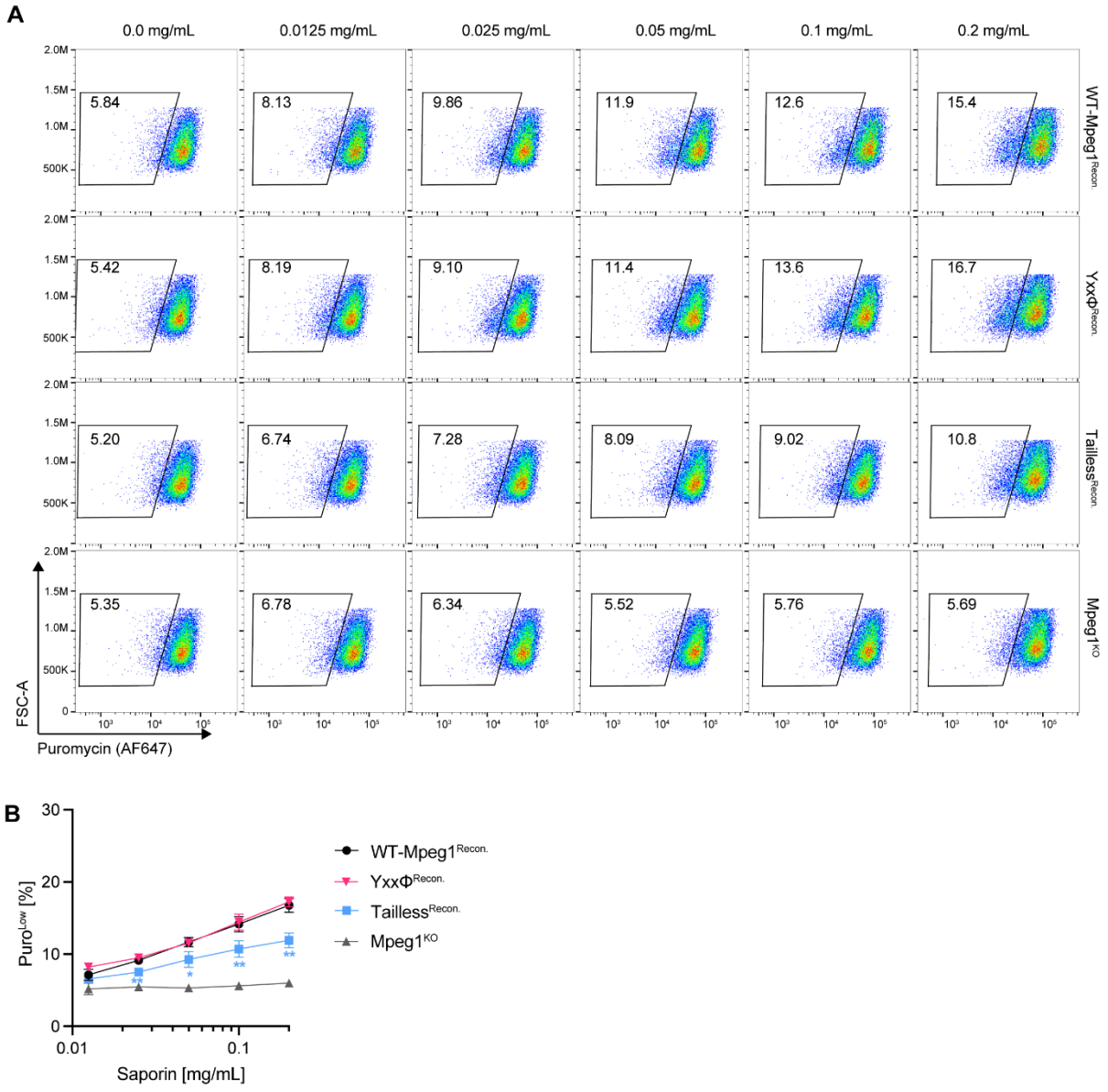

Fig. 6. 3. Activity of the YxxΦ and Tailless variants in the bead saporin-puromycin assay. (**A**) The indicated MutuDC lines were incubated with saporin beads for 5 h followed by an incubation with puromycin for 30 min. Cells were then placed on ice and outside beads labelled with an αOvalbumin antibody. After fixation and permeabilisation, levels of puromycin incorporation were detected with an αPuromycin antibody. The gating strategy is the same as in Fig. 3.10C. (**B**) Quantification of Puro^{Low} cells based on the gating shown in A. Data represent mean and SEM of three independent experiments. *P<0.1, **P<0.01 using a multiple paired t-test (two-stage step-up, Benjamini, Krieger and Yekutieli) versus WT-Mpeg1.

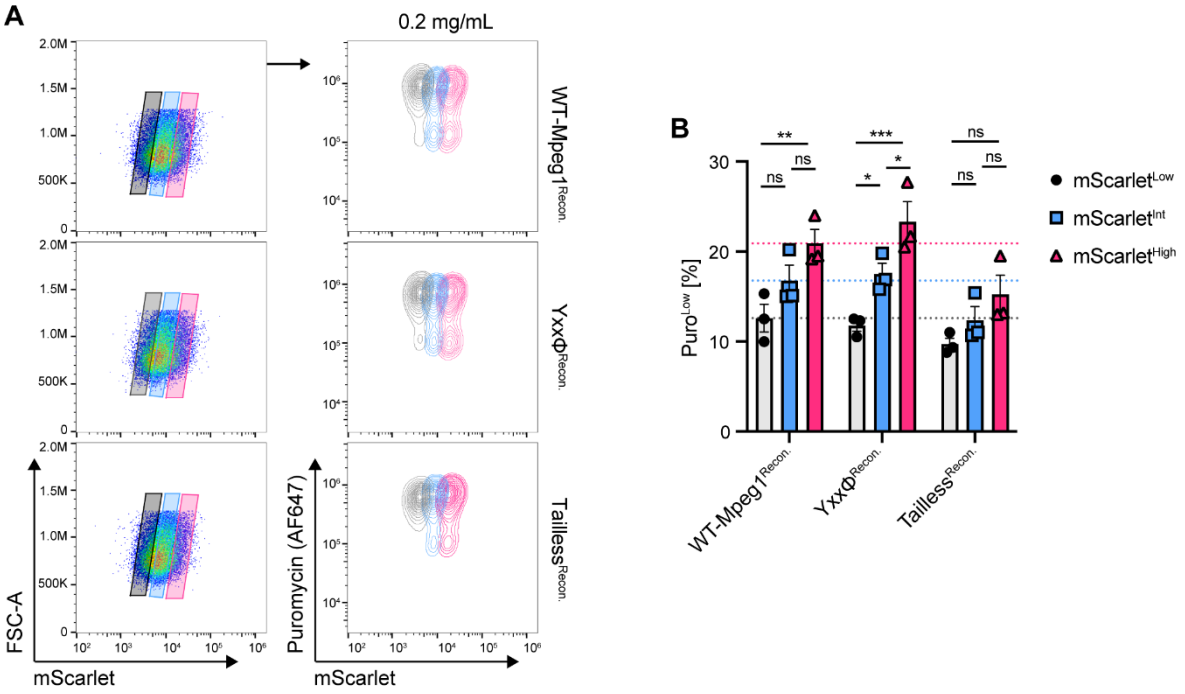

Fig. 6. 4. Saporin escape in cells with different levels of perforin-2 expression. (**A**) Cells from the experiment described in Fig. 6.3 were gated on different perforin-2 expression levels based on the IRES-mScarlet reporter and the proportion of Puro^{Low} cells was determined in each sub-population. (**B**) Quantification of Puro^{Low} cells based on the gating shown in A. Data represent mean and SEM of three independent experiments. ns, not significant; *P<0.1, **P<0.01, ***P<0.001 using a two-way ANOVA, Tukey's multiple comparison test. Dashed lines indicate the average value for WT-Mpeg1.

6.2.2 The effects of brefeldin A on the phagosomal recruitment of mistrafficked perforin-2

Based on the data presented so far, I hypothesised that PM-derived perforin-2 in YxxΦ$^{Recon.}$ and Tailless$^{Recon.}$ MutuDCs may be non-functional. Accordingly, a small fraction of the YxxΦ variant is mislocalised to the PM leading to increased recruitment to the phagosome. However, this PM-derived pool of perforin-2 is not active resulting in an escape efficiency that is comparable to wild-type. Analogously, a large fraction of the Tailless variant mislocalises to the PM which may deplete functional, intracellular pools of perforin-2 to the extent that it leads to the observed reduction in escape efficiency.

A prediction would therefore be that inhibiting the phagosomal recruitment of the remaining intracellular perforin-2 in Tailless$^{Recon.}$ MutuDCs with BFA would completely block saporin escape despite recruitment of large amounts of PM-derived perforin-2. However, given the non-specific effects of BFA in the saporin-puromycin assay (Fig. 3.12), this hypothesis could not be tested directly. Instead, I set out to establish whether a fraction of the Tailless variant is indeed recruited to phagosomes from BFA-sensitive intracellular compartments or only from the PM. I therefore analysed WT-Mpeg1$^{Recon.}$, Tailless$^{Recon.}$ and Mpeg1^{KO} MutuDCs in phagoFACS in the presence or absence of BFA during the chase period. Staining the

isolated phagosome with antibodies against the perforin-2 C-terminus and Lamp1 revealed that the increased recruitment of perforin-2 to Lamp1^{Low} phagosomes of Tailless$^{Recon.}$ MutuDCs was insensitive to BFA treatment consistent with a PM origin (**Fig. 6.5**).

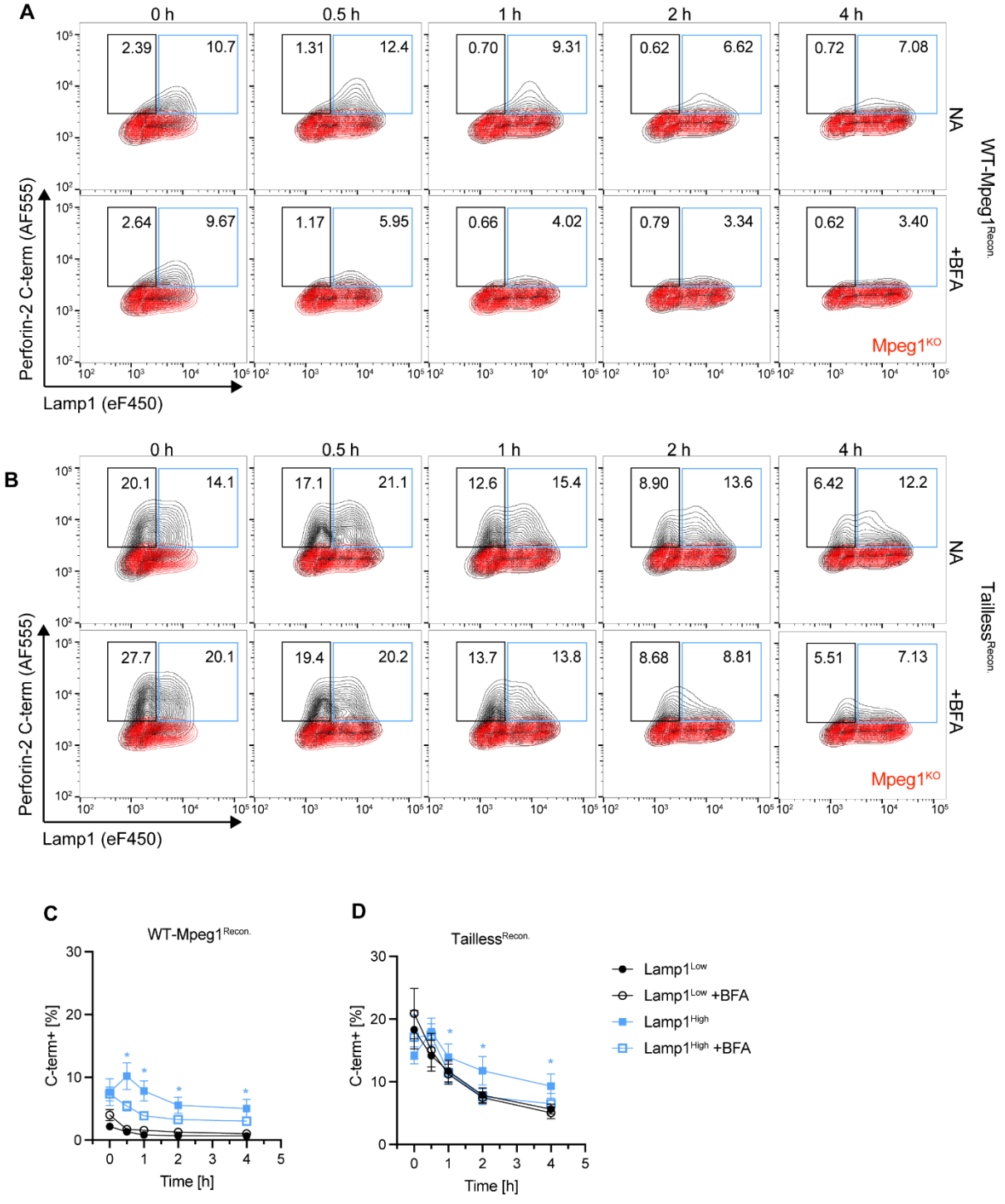

Fig. 6. 5. Effects of brefeldin A on the processing of Tailless perforin-2. (**A, B**) The indicated MutuDC lines were pulsed with OVA beads for 25 min at 16°C followed by 5 min at 37°C, washed and resuspended in fresh media with or without 5 uM brefeldin A. Samples were then either immediately placed on ice (0 h) or chased for the indicated time. Isolated phagosomes were stained with αC-term and αLamp1 antibodies. (**C, D**) Quantification of perforin-2^{+} phagosomes based on the gating shown in A and B. Data represent mean and SEM of six independent experiments. *P<0.1 using a multiple paired t-test (two-stage step-up, Benjamini, Krieger and Yekutieli) and comparing Lamp1^{High} +BFA versus Lamp1^{High}.

On the other hand, recruitment of perforin-2 to Lamp1^{High} phagosomes was impaired in the presence of BFA. In WT-Mpeg1$^{Recon.}$ MutuDCs, the effect of BFA was apparent within 0.5 h causing a ~50% decrease in αC-term+ phagosomes whereas in Tailless$^{Recon.}$ MutuDCs it was observed only after 2 h leading to a ~40% decrease. These data suggest that the Tailless variant is partly recruited from a BFA-sensitive intracellular compartment in addition to the PM-derived pool. However, due to the dynamic nature of perforin-2 recruitment and processing, it is challenging to confirm whether both cell lines recruit the same or different levels of intracellular perforin-2.

6.2.3 A potential role of a N-terminal cleavage in regulating perforin-2-mediated escape

To further investigate the defect underlying the reduced escape efficiency in Tailless$^{Recon.}$ MutuDCs, I generated another antibody against perforin-2. The custom-made antibody was raised against a peptide derived from the N-terminus of the MACPF domain (residues 20-34, **Fig. 6.6A**) as so far, detection of this domain was accompanied with ambiguity due to the unknown epitope of the commercial αMACPF antibody.

To validate the αN-term antibody, I performed a Western blot with whole cell lysates of WT-Mpeg1$^{Recon.}$, YxxΦ$^{Recon.}$, Tailless$^{Recon.}$ and Mpeg1^{KO} MutuDCs. The antibody detected full-length perforin-2 and revealed the expected difference (**Fig. 6.1D**) in perforin-2 abundance between wild-type and mutant variants (**Fig. 6.6B**). Surprisingly, the αN-term antibody did not detect the p40 fragment raising the possibility of an N-terminal cleavage that removes the antibody epitope. Additional evidence for this cleavage emerged from our collaboration with the Borner lab. Comparative proteomics analysis of tryptic and semi-tryptic peptides showed enrichment of the p22-35 peptide in BafA1-treated wild-type MutuDCs compared to mock-treated cells suggesting a pH-dependent cleavage that removes an N-terminal region spanning the αN-term epitope (**Fig. 6.6C**).

To study the N-terminal cleavage in the context of the phagosome, I pulse-chased WT-Mpeg1$^{Recon.}$, YxxΦ$^{Recon.}$, Tailless$^{Recon.}$ and Mpeg1^{KO} MutuDCs with Ova beads and stained the isolated phagosomes with αN-term and αLamp1 antibodies. In WT-Mpeg1$^{Recon.}$ MutuDCs, only ~2% of phagosomes were αN-term+ and the signal barely increased above levels observed in Mpeg1^{KO} MutuDCs (**Fig. 6.7**). Similar results were obtained for phagosomes of YxxΦ$^{Recon.}$ MutuDCs. However, in Tailless$^{Recon.}$ cells, ~14% of phagosomes were αN-term+ at time 0 h decreasing to ~6% after 4 h of chase. To investigate the origin of perforin-2 detected by the αN-term antibody, I pulse-chased WT-Mpeg1$^{Recon.}$ and Tailless$^{Recon.}$ MutuDCs with Ova beads in the presence of BFA. Interestingly, in contrast to the αC-term antibody (**Fig. 6.5**), the signal of the αN-term antibody was completely insensitive to BFA treatment (**Fig. 6.8**).

Thus, perforin-2 containing the αN-term epitope appears to be mostly PM-derived. These findings are consistent with the interpretation that mistrafficked perforin-2 in Tailless$^{Recon.}$ MutuDCs fails to undergo a N-terminal cleavage before recruitment to the phagosome. However, additional experiments will be necessary to validate this hypothesis.

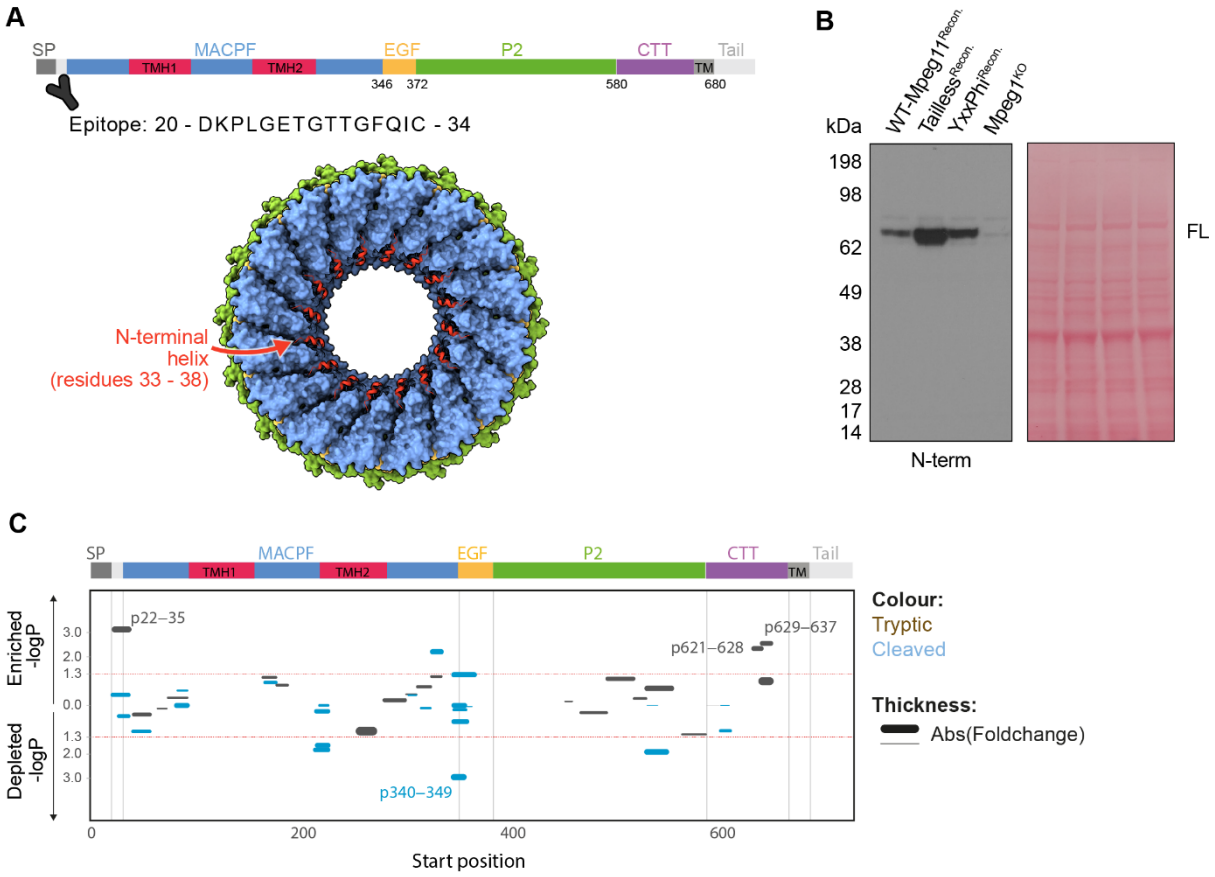

Fig. 6. 6. Validation of a custom-made antibody against the perforin-2 N-terminus. (**A**) Schematic illustrating the sequence and location of the epitope used to generate the αN-term antibody. The perforin-2 pore structure is displayed with the helix that is immediately C-terminal to the antibody epitope shown in red. (**B**) Western blot analysis of whole cell lysate from the indicated MutuDC lines probed with the αN-term antibody under reducing conditions. Data are representative for two independent experiments. (**C**) Data generated by the Borner lab showing BafA1-induced changes in the abundance of tryptic and semi-tryptic perforin-2 peptides. Control cells and cells treated with 1 μM BafA1 were analyzed by mass spectrometry, and peptide intensities were normalized to the corresponding protein intensities. Statistical analysis was performed with a two-sided student's *t* test. *P* values (*y* axis) and fold change in abundance (line thickness) in treated versus control cells are shown. The amino acid position indicates the location of the peptides along the different perforin-2 domains.

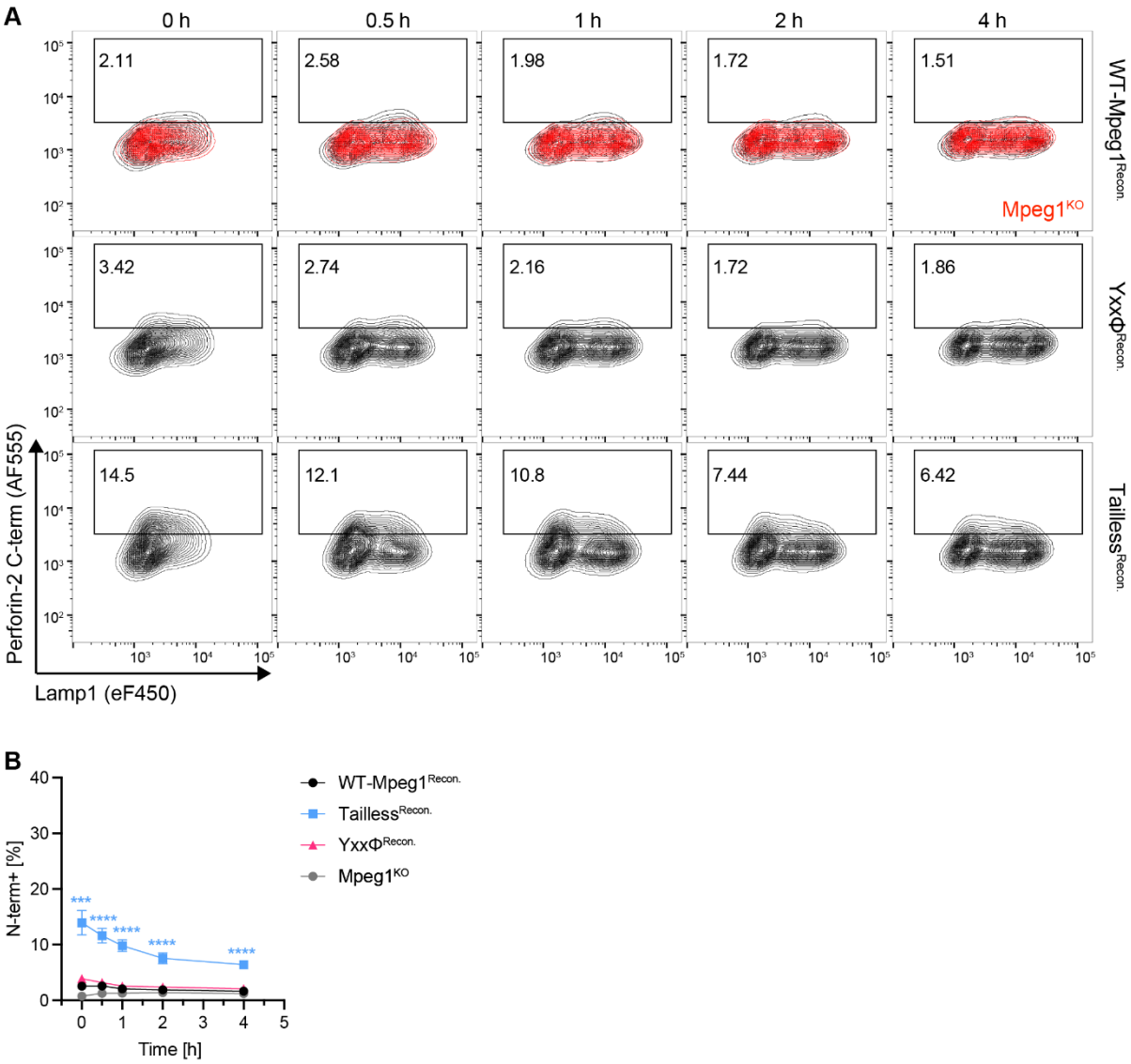

Fig. 6. 7. Analysis of N-terminal processing in wild-type, YxxΦ and Tailless perforin-2. (**A**) The indicated MutuDC lines were processed as in Fig. 6.2 and stained with αN-term and αLamp1 antibodies. (**B**) Quantification of perforin-2^{+} phagosomes based on the gating shown in A. Data represent mean and SEM of three independent experiments. ***P<0.001; ****P<0.0001 using a multiple unpaired t-test (two-stage step-up, Benjamini, Krieger and Yekutieli) versus WT-Mpeg1.

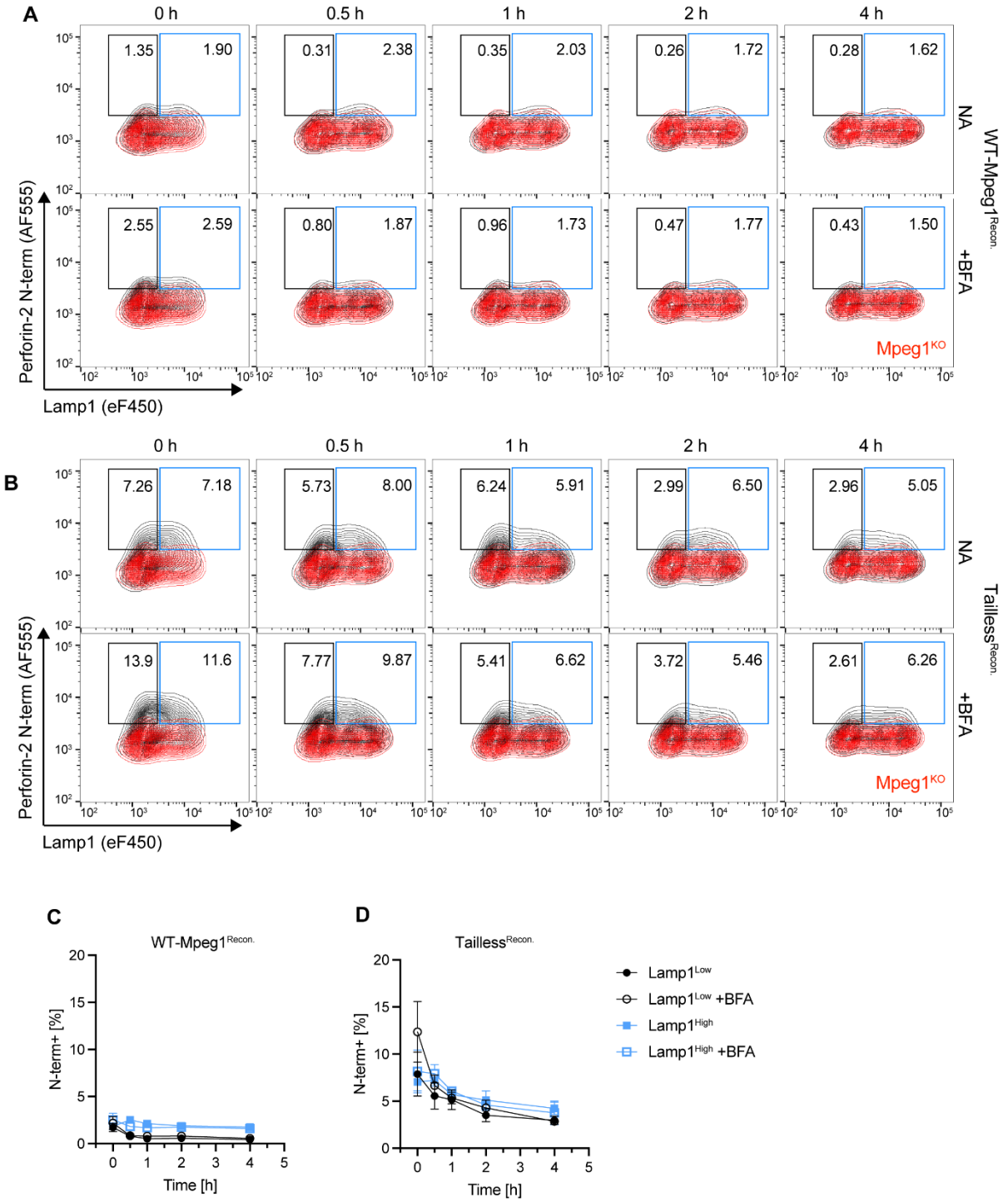

Fig. 6. 8. Effects of brefeldin A on the processing of Tailless perforin-2. (**A, B**) The indicated MutuDC lines were processed as in Fig. 6.5 and stained with αN-term and αLamp1 antibodies. (**C, D**) Quantification of perforin-2^{+} phagosomes based on the gating shown in A and B. Data represent mean and SEM of three independent experiments. Data were not significant using a multiple paired t-test (two-stage step-up, Benjamini, Krieger and Yekutieli) and comparing Lamp1^{High} +BFA versus Lamp1^{High}.

6.3 Discussion

The results in this chapter show that the sorting signals in the cytosolic tail are important for the sorting of perforin-2 within the endosome/lysosome system as well as its function in endocytic escape.

Mutagenesis of the YxxΦ motif alone led to the mislocalisation of a small fraction of perforin-2. Although the intracellular distribution was overtly normal as observed by microscopy, the increased recruitment of the YxxΦ variant during the pulse of the phagoFACS assay suggests mislocalisation to the PM. This inference is supported by numerous reports showing that mutagenesis of the YxxΦ motif results in the accumulation of endocytic receptors (e.g. transferrin receptor) and lysosomal membrane proteins (e.g. Lamp1) at the cell surface (*379*). Disruption of all putative sorting motifs in the Tailless variant led to a more severe PM accumulation which was evident in both microscopy and phagoFACS experiments. Thus, ubiquitinated lysines and/or the dileucine-like motifs also play an important role in perforin-2 sorting. To untangle the relative contributions of each sorting signal, it will be necessary to mutate the motifs individually and in combination.

As mentioned in Section 6.1, YxxΦ and dileucine motifs can mediate lysosomal targeting through a direct and an indirect route, the latter involving internalisation form the PM. Disruption of sorting signals in proteins trafficking via the indirect route may lead to their accumulation at the PM as they fail to engage with AP-2-mediated internalisation (*415*). In contrast, mutating motifs in proteins that traffic via the direct route may lead to PM mistargeting because they can no longer bind AP-1, AP-3 or GGA which mediate transport between the TGN and endosomes (AP-1 and GGA) and direct transport from endosomes to lysosomes (AP-3) (*405, 416, 417*). In such cases, the mistargeted proteins can be diverted to the PM through the constitutive secretory pathway where they accumulate if they cannot be internalised (*417, 418*). Whether the surface accumulation of the YxxΦ and Tailless variants reflects a defect in internalisation or whether wild-type perforin-2 normally follows a direct route to late endosomes/lysosomes warrants further investigation.

Mistargeted perforin-2 was less able to mediate endocytic escape despite increased levels of recruitment to the phagosome. One possible explanation for this could be that a fraction of YxxΦ and Tailless variants are delivered to phagosomes that are not competent to activate perforin-2-mediated escape (due to e.g. lack of co-factors or unfavourable ionic environment). Another possibility could be that PM-derived perforin-2 is inherently unable to mediate escape either because it lacks a modification or because it has been rendered inactive. In phagoFACS experiments, the αP2 and αMACPF signals did not change proportionally in response to the drastic increase in perforin-2 levels seen with the αC-term

antibody. However, deriving biological insights from these profiles is challenging. This is not only due to potential differences in antibody sensitivity, but also because the signal from each antibody could be influenced by multiple variables including recruitment, recycling, conformational changes, and proteolytic processing. The relative contribution of each of these variables to the overall signal is unknown. In addition, the ambiguity surrounding the accessibility of the αMACPF and αP2 epitopes does not allow definitive inferences about the nature of the occurring conformational changes. Likewise, it is unclear whether perforin-2 is recruited in a single event as a full-length protein early during phagosome maturation and then exclusively processed on the phagosome, or whether processed forms are also contributed by additional recruitment events at later stages.

One interesting insight came from staining phagosome with the αN-term antibody which suggested that PM-derived Tailless variant potentially failed to undergo a N-terminal cleavage whereas intracellular-derived pools were cleaved prior to recruitment. Intriguingly, N-terminal cleavage has been shown to regulate oligomerization of the plant MACPF family member Mpf2Ba1 (*419*). Although oligomerization of perforin-2 can still occur without an N-terminal cleavage *in vitro*, it is possible that the cleavage is required for oligomerization *in vivo* (*246, 247*). Our comparative proteomics analysis suggested that the N-terminal cleavage would remove parts, or all, of the helix that lines the pore lumen (Fig. 6.6). Thus, another possibility is that N-terminal cleavage primes perforin-2 for activation by removing the helix to allow efficient escape through the pore. However, it is equally plausible that the difference in αN-term signal merely mirrors the differences in phagosomal perforin-2 levels among the different cell lines. In this case, the αN-term antibody might be less sensitive than, for example, the αC-term antibody, hence it only detects perforin-2 on phagosomes with sufficiently high protein levels.

Chapter 7 – Discussion

The mechanisms of cross-presentation have been under investigation for decades, but a coherent understanding of how exogenous antigens are processed and presented on MHC-I molecules for priming CD8+ T cells has yet to emerge. In the phagosome-to-cytosol pathway of cross-presentation, a key unresolved question is how antigens can escape from endocytic compartments for proteasomal degradation in the cytosol. It was therefore exciting when a screen by the Kozik lab yielded perforin-2 as pore-forming effector of endocytic escape. Here, I have described the first molecular characterisation of this perforin-2-mediated endocytic escape pathway in cross-presenting cDC1s (**Fig. 7.1**).

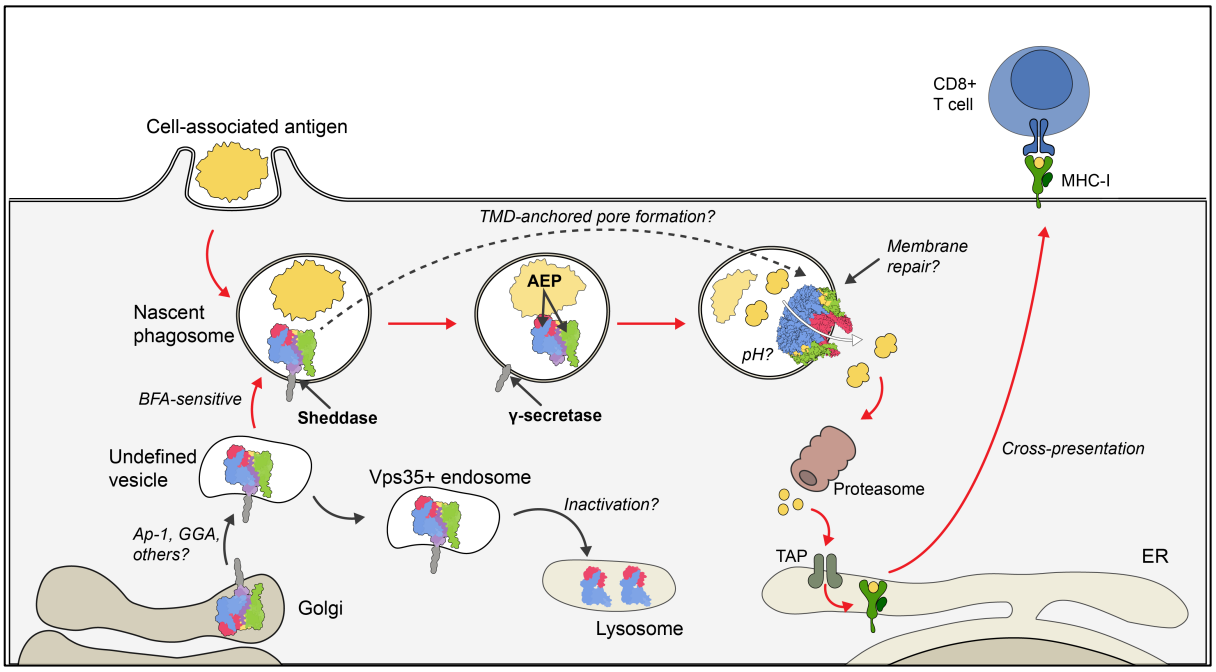

Fig. 7. 1. Model of perforin-2-mediated endocytic escape. At steady-state (black arrows), full-length perforin-2 is sorted into Vps35+ vesicles. Sorting within the endosome/lysosome system is regulated by motifs in the cytosolic tail which may be recognised by AP-1, GGA and other adaptors. Proteolytic processing (by a sheddase, AEP, other lysosomal proteases and γ-secretase; not shown) leads to the generation of the p40 fragment (among others) which accumulates in the lysosome lumen. Whether pore formation precedes the generation of the p40 fragment at steady-state is unknown. During perforin-2-mediated endocytic escape (red arrows), full-length perforin-2 is recruited from an undefined location to the phagosome via a BFA-sensitive pathway. During phagosome maturation, perforin-2 is shed, the remaining membrane stub removed by γ-secretase and the ectodomain further processed by AEP and other lysosomal proteases by cleavage in the EGF and P2 domains. Whether some, or all, of these cleavages normally precede pore formation is unknown. However, my results suggest that they are not a prerequisite and TMD-anchored perforin-2 may also be able to form pores. Although the exact pH supporting pore formation *in vivo* is unknown, my results suggest that V-ATPase activity is not required. Following pore formation, the resulting membrane lesions are likely to be quickly repaired by damage response pathways. The colour codes of the domains are the same as in Fig. 1.5.

My results show that: (1) perforin-2 is proteolytically processed with full-length and cleaved forms present in early and late endocytic compartments, respectively; (2) full-length perforin-2 is recruited to early phagosomes by a BFA-sensitive pathway; (3) phagosomal perforin-2 undergoes pH-dependent proteolytic processing; (4) shedding of the ectodomain is mediated by a cysteine proteases, the remaining membrane stub is removed by γ-secretase and the

ectodomain further processed by AEP and other lysosomal proteases; (5) neither acidification nor proteolytic processing appear to be essential for endocytic escape suggesting TMD-anchored perforin-2 can release antigens from early phagosomes; (6) perforin-2-mediated endocytic escape has no detectable effect on phagosomal pH; (7) trafficking of perforin-2 within the endocytic compartment is regulated by sorting motifs in its cytosolic tail; (8) the efficiency of perforin-2-mediated endocytic escape depends on the correct sorting of perforin-2 prior to its delivery to the phagosome. In the following paragraphs, I discuss some of these points and speculate on the broader context of perforin-2-mediated endocytic escape.

7.1 Perforin-2-mediated escape from early endocytic compartments

An interesting insight that has emerged from my results is that the perforin-2-mediated endocytic escape pathway may operate in early endocytic compartments. This is consistent with multiple studies showing that efficient cross-presentation in cDC1s relies on the preservation of exogenous antigen in low degradative endocytic compartments with mildly acidic/alkaline pH (*170, 182, 214-219, 245, 321, 348*). However, additional experiments are required to fully delineate the pH and proteolytic processing requirements for perforin-2 pore formation *in vivo* (discussed in Chapters 3.3, 4.3 and 5.3). It would be helpful to develop conformation-specific labelling tools, e.g. based on *in silico* designed protein-binding proteins (*420*), to specifically label active perforin-2 pores. Currently, pore formation can only be inferred after the fact by measuring saporin-mediated translation inhibition. Conformation-specific tools would allow to detect pore formation in real-time and could be employed in flow cytometry and microscopy experiments to ascertain whether proteolytic processing occurs before or after pore insertion and help to characterise the luminal pH and membrane composition of the pore-forming compartment.

Another question that remains to be addressed is whether perforin-2-mediated endocytic escape is selective for certain types of cargo or whether transit through the pore is non-specific. Endocytic escape in DCs has been shown to be size-dependent (*198, 421*) and it would be interesting to determine whether this is due to the size requirements of perforin-2-mediated endocytic escape. Curiously, saporin and lysosomal proteases such as cathepsin are of similar size (~30 kDa) yet there is no evidence for escape of the latter which would lead to cell death (*422*). It is possible that cathepsins are rapidly inactivated in the cytosol, potentially by cystatins (*423*) or serpins (*424*), or that accidental release of cathepsin is minimal due to pore formation taking place in early endocytic compartments. Alternatively, mechanisms beyond size selection may exist that control passage through the pore. While some MACPF family members like bacterial streptolysin O can deliver a wide range of

molecules (*425*), mammalian perforin-1 as well as the unrelated gasdermin D display some degree of cargo selectivity mediated by the charged lining of the pore lumen (*426-428*). The lumen of perforin-2 pores is predominantly negatively charged (*315*). It would be interesting to determine the electrostatic requirements for perforin-2-mediated escape using dextrans carrying different charges.

It will also be important to understand whether perforin-2-mediated endocytic escape is constitutive or induced, potentially by antigen uptake or co-stimulation. In many cases, sorting of cross-presented antigens into low degradative compartments is coupled to the mechanism of uptake and/or engagement of surface receptors (*170, 177, 209, 218, 219*). It is tempting to speculate that the regulation of perforin-2 is in some way integrated as part of this response as opposed to being a constitutive process. Accordingly, perforin-2 activity would be targeted towards antigen-containing compartments while avoiding unnecessary pore formation that could otherwise lead to cellular damage. To investigate this further, experiments could be designed to test whether perforin-2-mediated endocytic escape can be regulated by other known players in cross-presentation. These may include receptors such as TLR3 (*429*) or Clec9a (*177*) as well as regulators of protein trafficking such as Rab43 (*65*) or WDFY4 (*67*) both of which have recently been shown to be important for cross-presentation of cell-associated antigens by unknown mechanisms.

Finally, my results pose the question from which intracellular site perforin-2 is mobilised for its recruitment to the phagosome. One possibility is that perforin-2 is stored in a dedicated compartment, as has been reported for perforin-1 (*430*). However, the finding that BFA inhibits the delivery of perforin-2 to phagosomes argues against the existence of a static storage compartment as a source for phagosomal perforin-2. Instead, my results indicate that intracellular storage of perforin-2 may be a dynamic process. One interesting observation is that, under steady-state conditions, MutuDCs accumulate large amounts of the p40 fragment which is produced by the cleavage in the EGF domain. The fact that the p40 fragment lacks a membrane-targeting domain (P2 and TMD) and the finding that the majority of it is luminal rather than membrane-associated, suggests that the EGF cleavage renders subunits unable to form pores. This could imply that perforin-2 is synthesised only to be inactivated if it is not needed. One intriguing hypothesis is therefore that antigen uptake or co-stimulation may trigger trafficking events that divert perforin-2 away from inactivation and enable pore formation in antigen-containing compartments. Given the observed co-localisation of full-length perforin-2 with Vps35, this could conceivably involve retromer-mediated retrograde transport (*431*). Although keeping perforin-2 on stand-by through continuous synthesis and inactivation might seem wasteful, it could be important for the rapid deployment of subunits to mediate escape before the internalised antigens are

degraded. Future experiments that address the specific functions of the sorting motifs in the tail and the adaptor proteins involved will help to better understand how, and from where, perforin-2 is recruited.

7.2 Other potential regulators of perforin-2-mediated endocytic escape

It is possible that perforin-2-mediated escape is regulated by mechanisms beyond those explored in this thesis. The experiments reported here mostly focused on the regulation by pH and proteolysis as well as the trafficking of perforin-2 which underpins its regulation by dictating the intracellular environment. However, other post-translational modifications (PTMs), lipid composition, calcium binding, and membrane repair pathways may also be important regulators of the perforin-2-mediated endocytic escape pathway.

One PTM of interest is glycosylation. Structural studies have shown that perforin-2 is glycosylated at N185 and N269 and both sites are highly conserved across distantly related species (*246, 247, 315*). Glycosylation plays an important role in regulating perforin-1 by inhibiting premature oligomerisation through steric hinderance (*432*). It will be interesting to address whether glycosylation also plays a direct role in pore formation by perforin-2 or whether the conserved N-glycans are merely required for its stability. It should be possible to distinguish between these two possibilities by mutating the glycosylation sites or by inhibiting glycosyltransferases and assessing the effect on the expression and processing of perforin-2. Another PTM that warrants further investigation is the ubiquitination of the cytosolic tail which has been implicated in regulating the trafficking of perforin-2 by the results shown here (Chapter 6) as well as by others (*268*).

Membrane lipid composition is an established regulatory mechanism of many pore-forming proteins including the mammalian perforin-1 (*307, 433-435*), MAC (*287*) and gasdermins (*436-438*). The physical properties of the lipid bilayer (such as charge, lipid packing and surface tension) have been shown to determine membrane association of pore-forming proteins (*287, 307, 433-438*) as well as susceptibility to pore insertion (*439*). *In vitro* studies of the perforin-2 ectodomain have shown that its membrane-binding P2 domain preferentially binds to negatively charged lipids such as phosphatidylserine (PS), the phosphoinositides PI, PI(4)P, and PI(4,5)P_2 as well as the bacterial cardiolipin (*246, 247*). In mammalian cells, negatively charged PS and PIPs are mainly found on the inner leaflet of the plasma membrane while the outer leaflet is enriched in neutrally charged lipids including phosphatidylcholine and sphingomyelin. Crucially, inward budding of the phagosome means that the plasma membrane outer leaflet forms the luminal leaflet of the phagosome. However, the ectodomain of perforin-2 cannot bind to PC or SM *in vitro* raising the question of how membrane-binding is regulated (*246, 247*). The lipid composition of the cytosolic

leaflet of the phagosome is highly dynamic and extensively modified during phagosome maturation (*440, 441*). Surprisingly, changes to the lipid composition of the luminal leaflet are essentially unexplored (*442*). Thus, it is currently unknown whether the luminal leaflet of the phagosome acquires negatively charged lipids that would support perforin-2 membrane binding via its P2 domain. An interesting possibility, supported by my results in Chapter 5, is that the association of perforin-2 with the phagosomal membrane through its TMD is sufficient for pore formation and circumvents the dependence on negatively charged lipids. The regulation of perforin-2-mediated endocytic escape by lipid composition could be explored further by analysing the lipidome of perforin-2+ phagosomes by mass spectrometry (*443*) and by employing lipid-specific probes in microscopy experiments (*444*).

Calcium is an important regulator of perforin-1 with high Ca^{2+} concentrations being required efficient for membrane binding (*306, 445*). Mechanistically, it has been shown that Ca^{2+}-binding to the C2 domain of perforin-1 rearranges several hydrophobic residues to permit an interaction with the lipid bilayer (*445*). Notably, perforin-2 (as well as perforin-1 and C9) comprises an EGF-like domain and certain subtypes of this domain are known to bind Ca^{2+} (*446*). However, the EGF domain in perforin-2 does not conform to any canonical EGF domain subtype and it remains to be investigated whether it can bind Ca^{2+}. Preparations of perforin-2 for *in vitro* structural studies did not include Ca^{2} in any of the buffers suggesting that Ca^{2+}-binding is not essential for membrane association and pore formation (*246, 247, 315*). However, Ca^{2+}-binding to EGF domains is known to regulated protein-protein interactions (*447*) and it therefore remains possible that Ca^{2+}-binding play a role in the regulation of perforin-2 activity *in vivo.* This could be tested by loading phagosomes with the membrane impermeable calcium chelator BAPTA and measuring the effects on endocytic escape.

Finally, a relevant avenue to explore is how perforin-2 membrane lesions are repaired. My results have shown that perforin-2-mediated endocytic escape does not compromise the overall integrity of the phagosome suggesting that the ensuing membrane damage is efficiently contained. Multiple pathways have been described that can mediate membrane repair on endocytic compartments (*448-454*). A well characterised damage response is mediated by ESCRT proteins which are thought to repair lesions of up to 100 nm in diameter (*455*). Disruption of endocytic membranes causes localised calcium fluxes which are sensed by calcium effectors, including LKKR2, ALIX and ALG-2, leading to the recruitment of the ESCRT-III complex (*448, 449, 456*). Similar to its role in the formation of multivesicular bodies, the recruited ESCRT machinery is thought to remove membrane lesions by promoting the inward budding of the damaged membrane patch (*448, 449*). Recruitment of the ESCRT machinery to the plasma membrane has been shown to remove gasdermin D

pores supporting the idea that a similar mechanism may exist to remove perforin-2 pores from endocytic membranes (*457*). Indeed, ESCRT-dependent membrane repair has recently been described as a negative regulator of endocytic escape during cross-presentation (*243*). There are also several ESCRT-independent mechanisms, such as those mediated by PI4K2a (*451, 453*), annexins (*452*), lysosomal lipid scramblases (*450*) or stress granules (*454*), which could conceivably play a role in repairing perforin-2 lesions. As a first step, the role of membrane repair pathways in controlling perforin-2-mediated damage could be investigated by testing the recruitment of pathway markers such as Chmp4b, annexin A1/A2 or PI4K2A-ORF9 to perforin-2+ phagosome by microscopy or flow cytometry.

7.3 Perspectives

The data presented here on the mechanisms of perforin-2-mediated endocytic escape in cDC1s serves as a foundation for a more detailed characterisation of this pathway in the future. My results, while only preliminary, lead to several interesting hypotheses concerning the site of endocytic escape as well as the complex cellular mechanisms that regulate this fascinating pore-forming immune effector. The two main questions that may guide future research are (1) At which point of phagosome maturation are perforin-2 pores assembled to facilitate escape of antigen? and (2) How does the regulation of perforin-2-mediated endocytic escape interface with other known players of cross-presentation in cDC1s? The cell lines and assays developed in this thesis will be useful tools to address these questions. A better understanding of the perforin-2-mediated endocytic escape pathway will help to resolve the long-standing problem of how exogenous antigens can be cross-presented to initiate anti-viral and anti-cancer immune responses. Gaining insights into the regulation of endocytic escape has significant implications for medicine as it not only informs the enhancement of CD8+ T cell responses for improved vaccination and immunotherapy outcomes, but also paves the way for the effective delivery of a variety of therapeutics to intracellular targets.

References

1. J. Neefjes, M. L. M. Jongsma, P. Paul, O. Bakke, Towards a systems understanding of MHC class I and MHC class II antigen presentation. *Nat. Rev. Immunol.* **11**, 823-836 (2011).
2. N. Pishesha, T. J. Harmand, H. L. Ploegh, A guide to antigen processing and presentation. *Nat. Rev. Immunol.* **22**, 751-764 (2022).
3. A. H. Courtney, W.-L. Lo, A. Weiss, TCR Signaling: Mechanisms of Initiation and Propagation. *Trends in Biochemical Sciences* **43**, 108-123 (2018).
4. P. A. Roche, K. Furuta, The ins and outs of MHC class II-mediated antigen processing and presentation. *Nat. Rev. Immunol.* **15**, 203-216 (2015).
5. D. Jaraquemada, M. Marti, E. O. Long, An endogenous processing pathway in vaccinia virus-infected cells for presentation of cytoplasmic antigens to class II-restricted T cells. *Journal of Experimental Medicine* **172**, 947-954 (1990).
6. J. G. Nuchtern, W. E. Biddison, R. D. Klausner, Class II MHC molecules can use the endogenous pathway of antigen presentation. *Nature* **343**, 74-76 (1990).
7. M. J. Bevan, Cross-priming for a secondary cytotoxic response to minor H antigens with H-2 congenic cells which do not cross-react in the cytotoxic assay. *Journal of Experimental Medicine* **143**, 1283-1288 (1976).
8. R. N. Germain, Immunology: The ins and outs of antigen processing and presentations. *Nature* **322**, 687-688 (1986).
9. R. Wu, K. M. Murphy, DCs at the center of help: Origins and evolution of the three-cell-type hypothesis. *Journal of Experimental Medicine* **219**, (2022).
10. J. M. M. den Haan, S. M. Lehar, M. J. Bevan, Cd8+ but Not Cd8− Dendritic Cells Cross-Prime Cytotoxic T Cells in Vivo. *Journal of Experimental Medicine* **192**, 1685-1696 (2000).
11. M. L. Albert, B. Sauter, N. Bhardwaj, Dendritic cells acquire antigen from apoptotic cells and induce class I-restricted CTLs. *Nature* **392**, 86-89 (1998).
12. S. Jung *et al.*, In Vivo Depletion of CD11c+ Dendritic Cells Abrogates Priming of CD8+ T Cells by Exogenous Cell-Associated Antigens. *Immunity* **17**, 211-220 (2002).
13. C. Kurts, B. W. S. Robinson, P. A. Knolle, Cross-priming in health and disease. *Nat. Rev. Immunol.* **10**, 403-414 (2010).
14. H. Hasegawa, T. Matsumoto, Mechanisms of Tolerance Induction by Dendritic Cells In Vivo. *Front. Immunol.* **9**, 350 (2018).
15. C. Kurts, H. Kosaka, F. R. Carbone, J. F. A. P. Miller, W. R. Heath, Class I–restricted Cross-Presentation of Exogenous Self-Antigens Leads to Deletion of Autoreactive CD8+ T Cells. *Journal of Experimental Medicine* **186**, 239-245 (1997).
16. N. Luckashenak *et al.*, Constitutive Crosspresentation of Tissue Antigens by Dendritic Cells Controls CD8+ T Cell Tolerance In Vivo. *Immunity* **28**, 521-532 (2008).
17. C. A. Janeway, Approaching the Asymptote? Evolution and Revolution in Immunology. *Cold Spring Harbor Symposia on Quantitative Biology* **54**, 1-13 (1989).
18. J. Banchereau, R. M. Steinman, Dendritic cells and the control of immunity. *Nature* **392**, 245-252 (1998).
19. R. M. Steinman, H. Hemmi, in *From Innate Immunity to Immunological Memory,* B. Pulendran, R. Ahmed, Eds. (Springer Berlin Heidelberg, Berlin, Heidelberg, 2006), pp. 17-58.
20. M. Cabeza-Cabrerizo, A. Cardoso, C. M. Minutti, M. P. d. Costa, C. R. e. Sousa, Dendritic Cells Revisited. *Annual Review of Immunology* **39**, 131-166 (2021).
21. C. Reis e Sousa, Toll-like receptors and dendritic cells: for whom the bug tolls. *Seminars in Immunology* **16**, 27-34 (2004).
22. K. A. Fitzgerald, J. C. Kagan, Toll-like Receptors and the Control of Immunity. *Cell* **180**, 1044-1066 (2020).
23. J. K. Krishnaswamy, T. Chu, S. C. Eisenbarth, Beyond pattern recognition: NOD-like receptors in dendritic cells. *Trends in Immunology* **34**, 224-233 (2013).

24. J. Rehwinkel, M. U. Gack, RIG-I-like receptors: their regulation and roles in RNA sensing. *Nat. Rev. Immunol.* **20**, 537-551 (2020).
25. C. Reis e Sousa, Activation of dendritic cells: translating innate into adaptive immunity. *Current Opinion in Immunology* **16**, 21-25 (2004).
26. S. Zelenay, C. Reis e Sousa, Adaptive immunity after cell death. *Trends in Immunology* **34**, 329-335 (2013).
27. P. Matzinger, Tolerance, Danger, and the Extended Family. *Annual Review of Immunology* **12**, 991-1045 (1994).
28. P. Matzinger, The Danger Model: A Renewed Sense of Self. *Science* **296**, 301-305 (2002).
29. R. Saenz *et al.*, TLR4-dependent activation of dendritic cells by an HMGB1-derived peptide adjuvant. *Journal of Translational Medicine* **12**, 211 (2014).
30. M. Yu *et al.*, HMGB1 SIGNALS THROUGH TOLL-LIKE RECEPTOR (TLR) 4 AND TLR2. *Shock* **26**, 174-179 (2006).
31. H. Jonuleit *et al.*, Pro-inflammatory cytokines and prostaglandins induce maturation of potent immunostimulatory dendritic cells under fetal calf serum-free conditions. *European Journal of Immunology* **27**, 3135-3142 (1997).
32. B. Janela *et al.*, A Subset of Type I Conventional Dendritic Cells Controls Cutaneous Bacterial Infections through VEGFα-Mediated Recruitment of Neutrophils. *Immunity* **50**, 1069-1083.e1068 (2019).
33. F. Granucci *et al.*, A Contribution of Mouse Dendritic Cell–Derived IL-2 for NK Cell Activation. *Journal of Experimental Medicine* **200**, 287-295 (2004).
34. C. del Fresno *et al.*, DNGR-1 in dendritic cells limits tissue damage by dampening neutrophil recruitment. *Science* **362**, 351-356 (2018).
35. M. Mashayekhi *et al.*, CD8alpha+ Dendritic Cells Are the Critical Source of Interleukin-12 that Controls Acute Infection by Toxoplasma gondii Tachyzoites. *Immunity* **35**, 249-259 (2011).
36. S. Oh *et al.*, IL-15 as a mediator of CD4+ help for CD8+ T cell longevity and avoidance of TRAIL-mediated apoptosis. *Proc. Natl. Acad. Sci. U.S.A* **105**, 5201-5206 (2008).
37. E. S. Trombetta, M. Ebersold, W. Garrett, M. Pypaert, I. Mellman, Activation of Lysosomal Function During Dendritic Cell Maturation. *Science* **299**, 1400-1403 (2003).
38. I. Mellman, R. M. Steinman, Dendritic Cells: Specialized and Regulated Antigen Processing Machines. *Cell* **106**, 255-258 (2001).
39. A. Alloatti, F. Kotsias, J. G. Magalhaes, S. Amigorena, Dendritic cell maturation and cross-presentation: timing matters! *Immunological Reviews* **272**, 97-108 (2016).
40. B. C. Gil-Torregrosa *et al.*, Control of cross-presentation during dendritic cell maturation. *European Journal of Immunology* **34**, 398-407 (2004).
41. M. Cella, A. Engering, V. Pinet, J. Pieters, A. Lanzavecchia, Inflammatory stimuli induce accumulation of MHC class II complexes on dendritic cells. *Nature* **388**, 782-787 (1997).
42. T. Worbs, S. I. Hammerschmidt, R. Förster, Dendritic cell migration in health and disease. *Nat. Rev. Immunol.* **17**, 30-48 (2017).
43. R. S. Allan *et al.*, Migratory Dendritic Cells Transfer Antigen to a Lymph Node-Resident Dendritic Cell Population for Efficient CTL Priming. *Immunity* **25**, 153-162 (2006).
44. C. Reis e Sousa, Dendritic cells in a mature age. *Nat. Rev. Immunol.* **6**, 476-483 (2006).
45. R. M. Steinman , Z. A. Cohn IDENTIFICATION OF A NOVEL CELL TYPE IN PERIPHERAL LYMPHOID ORGANS OF MICE : I. MORPHOLOGY, QUANTITATION, TISSUE DISTRIBUTION. *Journal of Experimental Medicine* **137**, 1142-1162 (1973).
46. R. M. Steinman, G. Kaplan, M. D. Witmer, Z. A. Cohn, Identification of a novel cell type in peripheral lymphoid organs of mice. V. Purification of spleen dendritic cells,

new surface markers, and maintenance in vitro. *Journal of Experimental Medicine* **149**, 1-16 (1979).
47. R. M. Steinman, M. D. Witmer, Lymphoid dendritic cells are potent stimulators of the primary mixed leukocyte reaction in mice. *Proc. Natl. Acad. Sci. U.S.A* **75**, 5132-5136 (1978).
48. L. Perié, S. H. Naik, Toward defining a 'lineage' – The case for dendritic cells. *Seminars in Cell & Developmental Biology* **41**, 3-8 (2015).
49. K. Shortman, P. Sathe, D. Vremec, S. Naik, M. O'Keeffe, in *Advances in Immunology,* K. M. Murphy, M. Merad, Eds. (Academic Press, 2013), vol. 120, pp. 105-126.
50. R. J. Dress *et al.*, Plasmacytoid dendritic cells develop from Ly6D+ lymphoid progenitors distinct from the myeloid lineage. *Nat. Immunol.* **20**, 852-864 (2019).
51. P. F. Rodrigues *et al.*, Distinct progenitor lineages contribute to the heterogeneity of plasmacytoid dendritic cells. *Nat. Immunol.* **19**, 711-722 (2018).
52. K. Liu *et al.*, In Vivo Analysis of Dendritic Cell Development and Homeostasis. *Science* **324**, 392-397 (2009).
53. S. H. Naik *et al.*, Development of plasmacytoid and conventional dendritic cell subtypes from single precursor cells derived in vitro and in vivo. *Nat. Immunol.* **8**, 1217-1226 (2007).
54. A. Schlitzer *et al.*, Identification of cDC1- and cDC2-committed DC progenitors reveals early lineage priming at the common DC progenitor stage in the bone marrow. *Nat. Immunol.* **16**, 718-728 (2015).
55. D. A. Anderson, C.-A. Dutertre, F. Ginhoux, K. M. Murphy, Genetic models of human and mouse dendritic cell development and function. *Nat. Rev. Immunol.* **21**, 101-115 (2021).
56. J. A. Villadangos, L. Young, Antigen-Presentation Properties of Plasmacytoid Dendritic Cells. *Immunity* **29**, 352-361 (2008).
57. M. Colonna, G. Trinchieri, Y.-J. Liu, Plasmacytoid dendritic cells in immunity. *Nat. Immunol.* **5**, 1219-1226 (2004).
58. M. Merad, P. Sathe, J. Helft, J. Miller, A. Mortha, The Dendritic Cell Lineage: Ontogeny and Function of Dendritic Cells and Their Subsets in the Steady State and the Inflamed Setting. *Annual Review of Immunology* **31**, 563-604 (2013).
59. L. Ziegler-Heitbrock, T. Ohteki, F. Ginhoux, K. Shortman, H. Spits, Reclassifying plasmacytoid dendritic cells as innate lymphocytes. *Nat. Rev. Immunol.* **23**, 1-2 (2023).
60. C. M. Minutti *et al.*, Distinct ontogenetic lineages dictate cDC2 heterogeneity. *Nat. Immunol.* **25**, 448-461 (2024).
61. C. C. Brown *et al.*, Transcriptional Basis of Mouse and Human Dendritic Cell Heterogeneity. *Cell* **179**, 846-863.e824 (2019).
62. C. A. Luber *et al.*, Quantitative Proteomics Reveals Subset-Specific Viral Recognition in Dendritic Cells. *Immunity* **32**, 279-289 (2010).
63. H. Hochrein *et al.*, Differential Production of IL-12, IFN-α, and IFN-γ by Mouse Dendritic Cell Subsets1. *The Journal of Immunology* **166**, 5448-5455 (2001).
64. K. Hildner *et al.*, Batf3 Deficiency Reveals a Critical Role for CD8alpha+ Dendritic Cells in Cytotoxic T Cell Immunity. *Science* **322**, 1097-1100 (2008).
65. N. M. Kretzer *et al.*, RAB43 facilitates cross-presentation of cell-associated antigens by CD8α+ dendritic cells. *Journal of Experimental Medicine* **213**, 2871-2883 (2016).
66. R. A. Ohara, K. M. Murphy, The evolving biology of cross-presentation. *Seminars in Immunology* **66**, 101711 (2023).
67. D. J. Theisen *et al.*, WDFY4 is required for cross-presentation in response to viral and tumor antigens. *Science* **362**, 694-699 (2018).
68. E. Giampazolias *et al.*, Secreted gelsolin inhibits DNGR-1-dependent cross-presentation and cancer immunity. *Cell* **184**, 4016-4031.e4022 (2021).
69. A. Alloatti *et al.*, Critical role for Sec22b-dependent antigen cross-presentation in antitumor immunity. *Journal of Experimental Medicine* **214**, 2231-2241 (2017).

70. S. L. Ng, Y. J. Teo, Y. A. Setiagani, K. Karjalainen, C. Ruedl, Type 1 conventional CD103+ dendritic cells control effector CD8+ T cell migration, survival, and memory responses during influenza infection. *Frontiers in Immunology* **9**, 3043 (2018).
71. K. Asano *et al.*, CD169-Positive Macrophages Dominate Antitumor Immunity by Crosspresenting Dead Cell-Associated Antigens. *Immunity* **34**, 85-95 (2011).
72. P. Leirião, C. del Fresno, C. Ardavín, Monocytes as effector cells: Activated Ly-6Chigh mouse monocytes migrate to the lymph nodes through the lymph and cross-present antigens to CD8+ T cells. *European Journal of Immunology* **42**, 2042-2051 (2012).
73. C. Schliehe *et al.*, CD8− Dendritic Cells and Macrophages Cross-Present Poly(D,L-lactate-co-glycolate) Acid Microsphere-Encapsulated Antigen In Vivo. *The Journal of Immunology* **187**, 2112-2121 (2011).
74. P. Kaliński, C. M. U. Hilkens, E. A. Wierenga, M. L. Kapsenberg, T-cell priming by type-1and type-2 polarized dendritic cells: the concept of a third signal. *Immunology Today* **20**, 561-567 (1999).
75. P. Bretscher, M. Cohn, A Theory of Self-Nonself Discrimination. *Science* **169**, 1042-1049 (1970).
76. D. L. Mueller, M. K. Jenkins, Molecular mechanisms underlying functional T-cell unresponsiveness. *Current Opinion in Immunology* **7**, 375-381 (1995).
77. J. M. Curtsinger , D. C. Lins , M. F. Mescher Signal 3 Determines Tolerance versus Full Activation of Naive CD8 T Cells : Dissociating Proliferation and Development of Effector Function. *Journal of Experimental Medicine* **197**, 1141-1151 (2003).
78. J. P. Allison, CD28-B7 interactions in T-cell activation. *Current Opinion in Immunology* **6**, 414-419 (1994).
79. J. Hendriks , Y. Xiao , J. Borst CD27 Promotes Survival of Activated T Cells and Complements CD28 in Generation and Establishment of the Effector T Cell Pool. *Journal of Experimental Medicine* **198**, 1369-1380 (2003).
80. C. E. Rudd, A. Taylor, H. Schneider, CD28 and CTLA-4 coreceptor expression and signal transduction. *Immunological Reviews* **229**, 12-26 (2009).
81. T. H. Watts, TNF/TNFR FAMILY MEMBERS IN COSTIMULATION OF T CELL RESPONSES. *Annual Review of Immunology* **23**, 23-68 (2005).
82. S. Iborra *et al.*, Optimal Generation of Tissue-Resident but Not Circulating Memory T Cells during Viral Infection Requires Crosspriming by DNGR-1+ Dendritic Cells. *Immunity* **45**, 847-860 (2016).
83. O. Schulz *et al.*, CD40 Triggering of Heterodimeric IL-12 p70 Production by Dendritic Cells In Vivo Requires a Microbial Priming Signal. *Immunity* **13**, 453-462 (2000).
84. M. Wiesel, W. Kratky, A. Oxenius, Type I IFN Substitutes for T Cell Help during Viral Infections. *The Journal of Immunology* **186**, 754-763 (2011).
85. J.-A. Keene , J. Forman Helper activity is required for the in vivo generation of cytotoxic T lymphocytes. *Journal of Experimental Medicine* **155**, 768-782 (1982).
86. N. A. Mitchison, C. O'Malley, Three-cell-type clusters of T cells with antigen-presenting cells best explain the epitope linkage and noncognate requirements of the in vivo cytolytic response. *European Journal of Immunology* **17**, 1579-1583 (1987).
87. S. R. M. Bennett *et al.*, Help for cytotoxic-T-cell responses is mediated by CD40 signalling. *Nature* **393**, 478-480 (1998).
88. S. P. Schoenberger, R. E. M. Toes, E. I. H. van der Voort, R. Offringa, C. J. M. Melief, T-cell help for cytotoxic T lymphocytes is mediated by CD40–CD40L interactions. *Nature* **393**, 480-483 (1998).
89. J. Borst, T. Ahrends, N. Bąbała, C. J. M. Melief, W. Kastenmüller, CD4+ T cell help in cancer immunology and immunotherapy. *Nat. Rev. Immunol.* **18**, 635-647 (2018).
90. J. P. Ridge, F. Di Rosa, P. Matzinger, A conditioned dendritic cell can be a temporal bridge between a CD4+ T-helper and a T-killer cell. *Nature* **393**, 474-478 (1998).
91. A. Lanzavecchia, Licence to kill. *Nature* **393**, 413-414 (1998).

92. M. Cella *et al.*, Ligation of CD40 on dendritic cells triggers production of high levels of interleukin-12 and enhances T cell stimulatory capacity: T-T help via APC activation. *Journal of Experimental Medicine* **184**, 747-752 (1996).
93. R. Wu *et al.*, Mechanisms of CD40-dependent cDC1 licensing beyond costimulation. *Nat. Immunol.* **23**, 1536-1550 (2022).
94. M. J. Bevan, Helping the CD8+ T-cell response. *Nat. Rev. Immunol.* **4**, 595-602 (2004).
95. C. Bourgeois, B. Rocha, C. Tanchot, A Role for CD40 Expression on CD8+ T Cells in the Generation of CD8+ T Cell Memory. *Science* **297**, 2060-2063 (2002).
96. E. M. Janssen *et al.*, CD4+ T cells are required for secondary expansion and memory in CD8+ T lymphocytes. *Nature* **421**, 852-856 (2003).
97. T. Ahrends *et al.*, CD4+ T Cell Help Confers a Cytotoxic T Cell Effector Program Including Coinhibitory Receptor Downregulation and Increased Tissue Invasiveness. *Immunity* **47**, 848-861.e845 (2017).
98. M. Binnewies *et al.*, Unleashing Type-2 Dendritic Cells to Drive Protective Antitumor CD4+ T Cell Immunity. *Cell* **177**, 556-571.e516 (2019).
99. Jyh L. Hor *et al.*, Spatiotemporally Distinct Interactions with Dendritic Cell Subsets Facilitates CD4+ and CD8+ T Cell Activation to Localized Viral Infection. *Immunity* **43**, 554-565 (2015).
100. S. Eickhoff *et al.*, Robust Anti-viral Immunity Requires Multiple Distinct T Cell-Dendritic Cell Interactions. *Cell* **162**, 1322-1337 (2015).
101. S. T. Ferris *et al.*, cDC1 prime and are licensed by CD4+ T cells to induce anti-tumour immunity. *Nature* **584**, 624-629 (2020).
102. M. J. Bevan, Minor H Antigens Introduced on H-2 Different Stimulating Cells Cross-React at the Cytotoxic T Cell Level during in Vivo Priming1. *The Journal of Immunology* **117**, 2233-2238 (1976).
103. P. Matzinger, M. J. Bevan, Induction of H-2-restricted cytotoxic T cells: in vivo induction has the appearance of being unrestricted. *Cellular Immunology* **33**, 92-100 (1977).
104. L. R. Gooding, C. B. Edwards, H-2 antigen requirements in the in vitro induction of SV40-specific cytotoxic T lymphocytes. *The Journal of Immunology* **124**, 1258-1262 (1980).
105. R. M. Zinkernagel, P. C. Doherty, Restriction of in vitro T cell-mediated cytotoxicity in lymphocytic choriomeningitis within a syngeneic or semiallogeneic system. *Nature* **248**, 701-702 (1974).
106. R. M. Zinkernagel, P. C. Doherty, Immunological surveillance against altered self components by sensitised T lymphocytes in lymphocytes choriomeningitis. *Nature* **251**, 547-548 (1974).
107. M. J. Bevan, Interaction antigens detected by cytotoxic T cells with the major histocompatibility complex as modifier. *Nature* **256**, 419-421 (1975).
108. R. Korngold, J. Sprent, Selection of cytotoxic T-cell precursors specific for minor histocompatibility determinants. I. Negative selection across H-2 barriers induced with disrupted cells but not with glutaraldehyde-treated cells: evidence for antigen processing. *Journal of Experimental Medicine* **151**, 314-327 (1980).
109. R. Shimonkevitz, J. Kappler, P. Marrack, H. Grey, Antigen recognition by H-2-restricted T cells. I. Cell-free antigen processing. *Journal of Experimental Medicine* **158**, 303-316 (1983).
110. S. Shimonkevitz R Fau - Colon, J. W. Colon S Fau - Kappler, P. Kappler Jw Fau - Marrack, H. M. Marrack P Fau - Grey, H. M. Grey, Antigen recognition by H-2-restricted T cells. II. A tryptic ovalbumin peptide that substitutes for processed antigen.
111. B. P. Babbitt, P. M. Allen, G. Matsueda, E. Haber, E. R. Unanue, Binding of immunogenic peptides to Ia histocompatibility molecules. *Nature* **317**, 359-361 (1985).

112. A. R. M. Townsend, F. M. Gotch, J. Davey, Cytotoxic T cells recognize fragments of the influenza nucleoprotein. *Cell* **42**, 457-467 (1985).
113. A. R. M. Townsend *et al.*, The epitopes of influenza nucleoprotein recognized by cytotoxic T lymphocytes can be defined with short synthetic peptides. *Cell* **44**, 959-968 (1986).
114. P. J. Bjorkman *et al.*, Structure of the human class I histocompatibility antigen, HLA-A2. *Nature* **329**, 506-512 (1987).
115. P. J. Bjorkman *et al.*, The foreign antigen binding site and T cell recognition regions of class I histocompatibility antigens. *Nature* **329**, 512-518 (1987).
116. Y. Yanagi *et al.*, A human T cell-specific cDNA clone encodes a protein having extensive homology to immunoglobulin chains. *Nature* **308**, 145-149 (1984).
117. S. M. Hedrick, D. I. Cohen, E. A. Nielsen, M. M. Davis, Isolation of cDNA clones encoding T cell-specific membrane-associated proteins. *Nature* **308**, 149-153 (1984).
118. K. L. Rock, E. Reits, J. Neefjes, Present Yourself! By MHC Class I and MHC Class II Molecules. *Trends in Immunology* **37**, 724-737 (2016).
119. T. Shiina, A. Blancher, H. Inoko, J. K. Kulski, Comparative genomics of the human, macaque and mouse major histocompatibility complex. *Immunology* **150**, 127-138 (2017).
120. E. T. Abualrous, J. Sticht, C. Freund, Major histocompatibility complex (MHC) class I and class II proteins: impact of polymorphism on antigen presentation. *Current Opinion in Immunology* **70**, 95-104 (2021).
121. K. Falk, O. Rötzschke, S. Stevanović, G. Jung, H.-G. Rammensee, Allele-specific motifs revealed by sequencing of self-peptides eluted from MHC molecules. *Nature* **351**, 290-296 (1991).
122. K. M. Ashby, K. A. Hogquist, A guide to thymic selection of T cells. *Nat. Rev. Immunol.* **24**, 103-117 (2024).
123. P. Golstein, G. M. Griffiths, An early history of T cell-mediated cytotoxicity. *Nat. Rev. Immunol.* **18**, 527-535 (2018).
124. U. Schubert *et al.*, Rapid degradation of a large fraction of newly synthesized proteins by proteasomes. *Nature* **404**, 770-774 (2000).
125. E. A. J. Reits, J. C. Vos, M. Grommé, J. Neefjes, The major substrates for TAP in vivo are derived from newly synthesized proteins. *Nature* **404**, 774-778 (2000).
126. S. Khan *et al.*, Cutting Edge: Neosynthesis Is Required for the Presentation of a T Cell Epitope from a Long-Lived Viral Protein1. *The Journal of Immunology* **167**, 4801-4804 (2001).
127. E. A. Hughes, C. Hammond, P. Cresswell, Misfolded major histocompatibility complex class I heavy chains are translocated into the cytoplasm and degraded by the proteasome. *Proc. Natl. Acad. Sci. U.S.A* **94**, 1896-1901 (1997).
128. A. Ciechanover, Proteolysis: from the lysosome to ubiquitin and the proteasome. *Nature Reviews Molecular Cell Biology* **6**, 79-87 (2005).
129. T. Saric, C. I. Graef, A. L. Goldberg, Pathway for Degradation of Peptides Generated by Proteasomes: A KEY ROLE FOR THIMET OLIGOPEPTIDASE AND OTHER METALLOPEPTIDASES *J. Biol. Chem.* **279**, 46723-46732 (2004).
130. R. T. Sauer, T. A. Baker, AAA+ Proteases: ATP-Fueled Machines of Protein Destruction. *Annual Review of Biochemistry* **80**, 587-612 (2011).
131. M. Gaczynska, K. L. Rock, A. L. Goldberg, γ-Interferon and expression of MHC genes regulate peptide hydrolysis by proteasomes. *Nature* **365**, 264-267 (1993).
132. S. Murata, Y. Takahama, M. Kasahara, K. Tanaka, The immunoproteasome and thymoproteasome: functions, evolution and human disease. *Nat. Immunol.* **19**, 923-931 (2018).
133. R. E. M. Toes *et al.*, Discrete Cleavage Motifs of Constitutive and Immunoproteasomes Revealed by Quantitative Analysis of Cleavage Products. *Journal of Experimental Medicine* **194**, 1-12 (2001).
134. D. A. Ferrington, D. S. Gregerson, in *Progress in Molecular Biology and Translational Science,* T. Grune, Ed. (Academic Press, 2012), vol. 109, pp. 75-112.

135. U. Seifert *et al.*, Immunoproteasomes Preserve Protein Homeostasis upon Interferon-Induced Oxidative Stress. *Cell* **142**, 613-624 (2010).
136. E. Reits *et al.*, Peptide Diffusion, Protection, and Degradation in Nuclear and Cytoplasmic Compartments before Antigen Presentation by MHC Class I. *Immunity* **18**, 97-108 (2003).
137. S. Eggensperger, R. Tampé, The transporter associated with antigen processing: a key player in adaptive immunity. *Biological Chemistry* **396**, 1059-1072 (2015).
138. P. Cresswell, N. Bangia, T. Dick, G. Diedrich, The nature of the MHC class I peptide loading complex. *Immunological Reviews* **172**, 21-28 (1999).
139. P. Tan *et al.*, Recruitment of MHC Class I Molecules by Tapasin into the Transporter Associated with Antigen Processing-Associated Complex Is Essential for Optimal Peptide Loading. *The Journal of Immunology* **168**, 1950-1960 (2002).
140. B. Ortmann *et al.*, A Critical Role for Tapasin in the Assembly and Function of Multimeric MHC Class I-TAP Complexes. *Science* **277**, 1306-1309 (1997).
141. A. G. Grandea, III *et al.*, Impaired Assembly yet Normal Trafficking of MHC Class I Molecules in Tapasin Mutant Mice. *Immunity* **13**, 213-222 (2000).
142. A. P. Williams, C. A. Peh, A. W. Purcell, J. McCluskey, T. Elliott, Optimization of the MHC Class I Peptide Cargo Is Dependent on Tapasin. *Immunity* **16**, 509-520 (2002).
143. M. Howarth, A. Williams, A. B. Tolstrup, T. Elliott, Tapasin enhances MHC class I peptide presentation according to peptide half-life. *Proc. Natl. Acad. Sci. U.S.A* **101**, 11737-11742 (2004).
144. I. K. Müller *et al.*, Structure of an MHC I–tapasin–ERp57 editing complex defines chaperone promiscuity. *Nat. Commun.* **13**, 5383 (2022).
145. P. A. Wearsch, P. Cresswell, Selective loading of high-affinity peptides onto major histocompatibility complex class I molecules by the tapasin-ERp57 heterodimer. *Nat. Immunol.* **8**, 873-881 (2007).
146. D. C. Chapman, D. B. Williams, ER quality control in the biogenesis of MHC class I molecules. *Seminars in Cell & Developmental Biology* **21**, 512-519 (2010).
147. T. Serwold, F. Gonzalez, J. Kim, R. Jacob, N. Shastri, ERAAP customizes peptides for MHC class I molecules in the endoplasmic reticulum. *Nature* **419**, 480-483 (2002).
148. E. T. Spiliotis, M. Osorio, M. C. Zúñiga, M. Edidin, Selective Export of MHC Class I Molecules from the ER after Their Dissociation from TAP. *Immunity* **13**, 841-851 (2000).
149. W.-K. Suh *et al.*, Interaction of MHC Class I Molecules with the Transporter Associated with Antigen Processing. *Science* **264**, 1322-1326 (1994).
150. J.-O. Koopmann *et al.*, Export of Antigenic Peptides from the Endoplasmic Reticulum Intersects with Retrograde Protein Translocation through the Sec61p Channel. *Immunity* **13**, 117-127 (2000).
151. J. G. Donaldson, D. B. Williams, Intracellular Assembly and Trafficking of MHC Class I Molecules. *Traffic* **10**, 1745-1752 (2009).
152. K. M. Paulsson *et al.*, Association of Tapasin and COPI Provides a Mechanism for the Retrograde Transport of Major Histocompatibility Complex (MHC) Class I Molecules from the Golgi Complex to the Endoplasmic Reticulum *. *J. Biol. Chem.* **277**, 18266-18271 (2002).
153. C. Howe *et al.*, Calreticulin-dependent recycling in the early secretory pathway mediates optimal peptide loading of MHC class I molecules. *The EMBO Journal* **28**, 3730-3744 (2009).
154. E. Ghanem *et al.*, The transporter associated with antigen processing (TAP) is active in a post-ER compartment. *J Cell Sci* **123**, 4271-4279 (2010).
155. J. D. Smith, W. R. Lie, J. Gorka, N. B. Myers, T. H. Hansen, Extensive peptide ligand exchange by surface class I major histocompatibility complex molecules independent of exogenous beta 2-microglobulin. *Proc. Natl. Acad. Sci. U.S.A* **89**, 7767-7771 (1992).
156. G. B. Zagorac *et al.*, Early endosomal rerouting of major histocompatibility class I conformers. *Journal of Cellular Physiology* **227**, 2953-2964 (2012).

157. J. M. Blander, The comings and goings of MHC class I molecules herald a new dawn in cross-presentation. *Immunological Reviews* **272**, 65-79 (2016).
158. H. Mahmutefendić, G. Blagojević, M. I. Tomaš, N. Kučić, P. Lučin, Segregation of open Major Histocompatibility Class I conformers at the plasma membrane and during endosomal trafficking reveals conformation-based sorting in the endosomal system. *The International Journal of Biochemistry & Cell Biology* **43**, 504-515 (2011).
159. J. M. Blander, Regulation of the Cell Biology of Antigen Cross-Presentation. *Annual Review of Immunology* **36**, 717-753 (2018).
160. J. Gruenberg, F. R. Maxfield, Membrane transport in the endocytic pathway. *Current Opinion in Cell Biology* **7**, 552-563 (1995).
161. S. Caplan *et al.*, A tubular EHD1-containing compartment involved in the recycling of major histocompatibility complex class I molecules to the plasma membrane. *The EMBO Journal* **21**, 2557-2567 (2002).
162. P. Nair-Gupta *et al.*, TLR Signals Induce Phagosomal MHC-I Delivery from the Endosomal Recycling Compartment to Allow Cross-Presentation. *Cell* **158**, 506-521 (2014).
163. K. L. Rock, S. Gamble, L. Rothstein, Presentation of Exogenous Antigen with Class I Major Histocompatibility Complex Molecules. *Science* **249**, 918-921 (1990).
164. K. Inaba, J. P. Metlay, M. T. Crowley, R. M. Steinman, Dendritic cells pulsed with protein antigens in vitro can prime antigen-specific, MHC-restricted T cells in situ. *Journal of Experimental Medicine* **172**, 631-640 (1990).
165. L. D. Falo, M. Kovacsovics-Bankowski, K. Thompson, K. L. Rock, Targeting antigen into the phagocytic pathway in vivo induces protective tumour immunity. *Nature Medicine* **1**, 649-653 (1995).
166. M. Kovacsovics-Bankowski, K. Clark, B. Benacerraf, K. L. Rock, Efficient major histocompatibility complex class I presentation of exogenous antigen upon phagocytosis by macrophages. *Proc. Natl. Acad. Sci. U.S.A* **90**, 4942-4946 (1993).
167. C. Reis e Sousa, R. N. Germain, Major histocompatibility complex class I presentation of peptides derived from soluble exogenous antigen by a subset of cells engaged in phagocytosis. *Journal of Experimental Medicine* **182**, 841-851 (1995).
168. S. Bertholet *et al.*, Leishmania Antigens Are Presented to CD8+ T Cells by a Transporter Associated with Antigen Processing-Independent Pathway In Vitro and In Vivo. *The Journal of Immunology* **177**, 3525-3533 (2006).
169. S. Burgdorf, A. Kautz, V. Böhnert, P. A. Knolle, C. Kurts, Distinct Pathways of Antigen Uptake and Intracellular Routing in CD4 and CD8 T Cell Activation. *Science* **316**, 612-616 (2007).
170. B. Chatterjee *et al.*, Internalization and endosomal degradation of receptor-bound antigens regulate the efficiency of cross presentation by human dendritic cells. *Blood* **120**, 2011-2020 (2012).
171. D. H. Schuurhuis *et al.*, Antigen-Antibody Immune Complexes Empower Dendritic Cells to Efficiently Prime Specific CD8+ CTL Responses In Vivo1. *The Journal of Immunology* **168**, 2240-2246 (2002).
172. P. Schnorrer *et al.*, The dominant role of CD8+ dendritic cells in cross-presentation is not dictated by antigen capture. *Proc. Natl. Acad. Sci. U.S.A* **103**, 10729-10734 (2006).
173. A. O. Kamphorst, P. Guermonprez, D. Dudziak, M. C. Nussenzweig, Route of Antigen Uptake Differentially Impacts Presentation by Dendritic Cells and Activated Monocytes. *The Journal of Immunology* **185**, 3426-3435 (2010).
174. O. Schulz, C. Reis e Sousa, Cross-presentation of cell-associated antigens by CD8α+ dendritic cells is attributable to their ability to internalize dead cells. *Immunology* **107**, 183-189 (2002).
175. D. Sancho *et al.*, Identification of a dendritic cell receptor that couples sensing of necrosis to immunity. *Nature* **458**, 899-903 (2009).

176. S. Iborra *et al.*, The DC receptor DNGR-1 mediates cross-priming of CTLs during vaccinia virus infection in mice. *The Journal of Clinical Investigation* **122**, 1628-1643 (2012).
177. J. Canton *et al.*, The receptor DNGR-1 signals for phagosomal rupture to promote cross-presentation of dead-cell-associated antigens. *Nat. Immunol.* **22**, 140-153 (2021).
178. R. E. Shrimpton *et al.*, CD205 (DEC-205): A recognition receptor for apoptotic and necrotic self. *Molecular Immunology* **46**, 1229-1239 (2009).
179. M. Subramanian *et al.*, An AXL/LRP-1/RANBP9 complex mediates DC efferocytosis and antigen cross-presentation in vivo. *The Journal of Clinical Investigation* **124**, 1296-1308 (2014).
180. J. D. Pfeifer *et al.*, Phagocytic processing of bacterial antigens for class I MHC presentation to T cells. *Nature* **361**, 359-362 (1993).
181. M. Kovacsovics-Bankowski, K. L. Rock, A phagosome-to-cytosol pathway for exogenous antigens presented on MHC class I molecules. *Science* **267**, 243-246 (1995).
182. I. Cebrian *et al.*, Sec22b Regulates Phagosomal Maturation and Antigen Crosspresentation by Dendritic Cells. *Cell* **147**, 1355-1368 (2011).
183. N. Merzougui, R. Kratzer, L. Saveanu, P. van Endert, A proteasome-dependent, TAP-independent pathway for cross-presentation of phagocytosed antigen. *EMBO reports* **12**, 1257-1264 (2011).
184. L. Shen, L. J. Sigal, M. Boes, K. L. Rock, Important Role of Cathepsin S in Generating Peptides for TAP-Independent MHC Class I Crosspresentation In Vivo. *Immunity* **21**, 155-165 (2004).
185. J. Helft *et al.*, GM-CSF Mouse Bone Marrow Cultures Comprise a Heterogeneous Population of CD11c+MHCII+ Macrophages and Dendritic Cells. *Immunity* **42**, 1197-1211 (2015).
186. R. Song, C. V. Harding, Roles of proteasomes, transporter for antigen presentation (TAP), and beta 2-microglobulin in the processing of bacterial or particulate antigens via an alternate class I MHC processing pathway. *The Journal of Immunology* **156**, 4182-4190 (1996).
187. M. F. Bachmann *et al.*, TAP1-independent loading of class I molecules by exogenous viral proteins. *European Journal of Immunology* **25**, 1739-1743 (1995).
188. M. Grommé *et al.*, Recycling MHC class I molecules and endosomal peptide loading. *Proc. Natl. Acad. Sci. U.S.A* **96**, 10326-10331 (1999).
189. L. V. Kaer, P. G. Ashton-Rickardt, H. L. Ploegh, S. Tonegawa, TAP1 mutant mice are deficient in antigen presentation, surface class I molecules, and CD4-8+ T cells. *Cell* **71**, 1205-1214 (1992).
190. G. Barbet *et al.*, TAP dysfunction in dendritic cells enables noncanonical cross-presentation for T cell priming. *Nat. Immunol.* **22**, 497-509 (2021).
191. R. A. Ohara, K. M. Murphy, Recent progress in type 1 classical dendritic cell cross-presentation - cytosolic, vacuolar, or both? *Current Opinion in Immunology* **83**, 102350 (2023).
192. F. M. Cruz, A. Chan, K. L. Rock, Pathways of MHC I cross-presentation of exogenous antigens. *Seminars in Immunology* **66**, 101729 (2023).
193. J. E. Grotzke, D. Sengupta, Q. Lu, P. Cresswell, The ongoing saga of the mechanism(s) of MHC class I-restricted cross-presentation. *Current Opinion in Immunology* **46**, 89-96 (2017).
194. D. Sengupta *et al.*, Cutting Edge: Phagosome-associated Autophagosomes Containing Antigens and Proteasomes Drive TAP-Independent Cross-Presentation. *The Journal of Immunology* **212**, 1063-1068 (2024).
195. D. Sengupta, M. Graham, X. Liu, P. Cresswell, Proteasomal degradation within endocytic organelles mediates antigen cross-presentation. *The EMBO Journal* **38**, e99266 (2019).

196. R. Zhang *et al.*, Lipid-anchored proteasomes control membrane protein homeostasis. *Science Advances* **9**, eadj4605 (2023).
197. C. C. Norbury, L. J. Hewlett, A. R. Prescott, N. Shastri, C. Watts, Class I MHC presentation of exogenous soluble antigen via macropinocytosis in bone marrow macrophages. *Immunity* **3**, 783-791 (1995).
198. A. Rodriguez, A. Regnault, M. Kleijmeer, P. Ricciardi-Castagnoli, S. Amigorena, Selective transport of internalized antigens to the cytosol for MHC class I presentation in dendritic cells. *Nat. Cell Biol.* **1**, 362-368 (1999).
199. C. C. Norbury, B. J. Chambers, A. R. Prescott, H.-G. Ljunggren, C. Watts, Constitutive macropinocytosis allows TAP-dependent major histocompatibility compex class I presentation of exogenous soluble antigen by bone marrow-derived dendritic cells. *European Journal of Immunology* **27**, 280-288 (1997).
200. M. L. Lin *et al.*, Selective suicide of cross-presenting CD8+ dendritic cells by cytochrome c injection shows functional heterogeneity within this subset. *Proc. Natl. Acad. Sci. U.S.A* **105**, 3029-3034 (2008).
201. P. Guermonprez *et al.*, ER–phagosome fusion defines an MHC class I cross-presentation compartment in dendritic cells. *Nature* **425**, 397-402 (2003).
202. A. Y. C. Huang, A. T. Bruce, D. M. Pardoll, H. I. Levitsky, In Vivo Cross-Priming of MHC Class I-Restricted Antigens Requires the TAP Transporter. *Immunity* **4**, 349-355 (1996).
203. P. J. Chefalo, A. G. Grandea, III, L. Van Kaer, C. V. Harding, Tapasin−/− and TAP1−/− Macrophages Are Deficient in Vacuolar Alternate Class I MHC (MHC-I) Processing due to Decreased MHC-I Stability at Phagolysosomal pH1. *The Journal of Immunology* **170**, 5825-5833 (2003).
204. E. Firat *et al.*, The Role of Endoplasmic Reticulum-Associated Aminopeptidase 1 in Immunity to Infection and in Cross-Presentation1. *The Journal of Immunology* **178**, 2241-2248 (2007).
205. L. Saveanu *et al.*, IRAP Identifies an Endosomal Compartment Required for MHC Class I Cross-Presentation. *Science* **325**, 213-217 (2009).
206. A. L. Ackerman, C. Kyritsis, R. Tampé, P. Cresswell, Early phagosomes in dendritic cells form a cellular compartment sufficient for cross presentation of exogenous antigens. *Proc. Natl. Acad. Sci. U.S.A* **100**, 12889-12894 (2003).
207. M. Houde *et al.*, Phagosomes are competent organelles for antigen cross-presentation. *Nature* **425**, 402-406 (2003).
208. F.-X. Campbell-Valois *et al.*, Quantitative Proteomics Reveals That Only a Subset of the Endoplasmic Reticulum Contributes to the Phagosome*. *Molecular & Cellular Proteomics* **11**, M111.016378-016371-M016111.016378-016313 (2012).
209. S. Burgdorf, C. Schölz, A. Kautz, R. Tampé, C. Kurts, Spatial and mechanistic separation of cross-presentation and endogenous antigen presentation. *Nat. Immunol.* **9**, 558-566 (2008).
210. N. Touret *et al.*, Quantitative and Dynamic Assessment of the Contribution of the ER to Phagosome Formation. *Cell* **123**, 157-170 (2005).
211. F. M. Cruz, J. D. Colbert, K. L. Rock, The GTP ase Rab39a promotes phagosome maturation into MHC-I antigen-presenting compartments. *The EMBO journal* **39**, e102020 (2020).
212. D. Accapezzato *et al.*, Chloroquine enhances human CD8+ T cell responses against soluble antigens in vivo. *Journal of Experimental Medicine* **202**, 817-828 (2005).
213. M. Samie, P. Cresswell, The transcription factor TFEB acts as a molecular switch that regulates exogenous antigen-presentation pathways. *Nat. Immunol.* **16**, 729-736 (2015).
214. A. Alloatti *et al.*, Toll-like Receptor 4 Engagement on Dendritic Cells Restrains Phago-Lysosome Fusion and Promotes Cross-Presentation of Antigens. *Immunity* **43**, 1087-1100 (2015).

215. L. Delamarre, M. Pack, H. Chang, I. Mellman, E. S. Trombetta, Differential Lysosomal Proteolysis in Antigen-Presenting Cells Determines Antigen Fate. *Science* **307**, 1630-1634 (2005).
216. A. Savina *et al.*, NOX2 Controls Phagosomal pH to Regulate Antigen Processing during Crosspresentation by Dendritic Cells. *Cell* **126**, 205-218 (2006).
217. C. Jancic *et al.*, Rab27a regulates phagosomal pH and NADPH oxidase recruitment to dendritic cell phagosomes. *Nat. Cell Biol.* **9**, 367-378 (2007).
218. S. Burgdorf, V. Lukacs-Kornek, C. Kurts, The Mannose Receptor Mediates Uptake of Soluble but Not of Cell-Associated Antigen for Cross-Presentation1. *The Journal of Immunology* **176**, 6770-6776 (2006).
219. P. J. Tacken *et al.*, Targeting DC-SIGN via its neck region leads to prolonged antigen residence in early endosomes, delayed lysosomal degradation, and cross-presentation. *Blood* **118**, 4111-4119 (2011).
220. P. Kozik *et al.*, Small Molecule Enhancers of Endosome-to-Cytosol Import Augment Anti-tumor Immunity. *Cell Rep.* **32**, 107905-107905 (2020).
221. J.-P. Bikorimana *et al.*, Promoting antigen escape from dendritic cell endosomes potentiates anti-tumoral immunity. *Cell Reports Medicine* **3**, (2022).
222. S. Beaudoin *et al.*, ChAcNLS, a Novel Modification to Antibody-Conjugates Permitting Target Cell-Specific Endosomal Escape, Localization to the Nucleus, and Enhanced Total Intracellular Accumulation. *Molecular Pharmaceutics* **13**, 1915-1926 (2016).
223. M. Gros, S. Amigorena, Regulation of Antigen Export to the Cytosol During Cross-Presentation. *Front. Immunol.* **10**, 41 (2019).
224. E. J. H. J. Wiertz *et al.*, Sec6l-mediated transfer of a membrane protein from the endoplasmic reticulum to the proteasome for destruction. *Nature* **384**, 432-438 (1996).
225. A. L. Ackerman, A. Giodini, P. Cresswell, A Role for the Endoplasmic Reticulum Protein Retrotranslocation Machinery during Crosspresentation by Dendritic Cells. *Immunity* **25**, 607-617 (2006).
226. M. Zehner *et al.*, The Translocon Protein Sec61 Mediates Antigen Transport from Endosomes in the Cytosol for Cross-Presentation to CD8+ T Cells. *Immunity* **42**, 850-863 (2015).
227. J. Imai, H. Hasegawa, M. Maruya, S. Koyasu, I. Yahara, Exogenous antigens are processed through the endoplasmic reticulum-associated degradation (ERAD) in cross-presentation by dendritic cells. *International Immunology* **17**, 45-53 (2004).
228. K. Römisch, A Case for Sec61 Channel Involvement in ERAD. *Trends in Biochemical Sciences* **42**, 171-179 (2017).
229. J. E. Grotzke *et al.*, Sec61 blockade by mycolactone inhibits antigen cross-presentation independently of endosome-to-cytosol export. *Proceedings of the National Academy of Sciences* **114**, E5910-E5919 (2017).
230. P. Carvalho, A. M. Stanley, T. A. Rapoport, Retrotranslocation of a Misfolded Luminal ER Protein by the Ubiquitin-Ligase Hrd1p. *Cell* **143**, 579-591 (2010).
231. Y. Ye, Y. Shibata, C. Yun, D. Ron, T. A. Rapoport, A membrane protein complex mediates retro-translocation from the ER lumen into the cytosol. *Nature* **429**, 841-847 (2004).
232. J. E. Grotzke, P. Cresswell, Are ERAD components involved in cross-presentation? *Molecular Immunology* **68**, 112-115 (2015).
233. Y. Ye, H. H. Meyer, T. A. Rapoport, The AAA ATPase Cdc48/p97 and its partners transport proteins from the ER into the cytosol. *Nature* **414**, 652-656 (2001).
234. J. Ménager *et al.*, Cross-Presentation of Synthetic Long Peptides by Human Dendritic Cells: A Process Dependent on ERAD Component p97/VCP but Not sec61 and/or Derlin-1. *PLOS ONE* **9**, e89897 (2014).
235. A. Ruggiano, O. Foresti, P. Carvalho, ER-associated degradation: Protein quality control and beyond. *Journal of Cell Biology* **204**, 869-879 (2014).

236. A. Giodini, P. Cresswell, Hsp90-mediated cytosolic refolding of exogenous proteins internalized by dendritic cells. *The EMBO Journal* **27**, 201-211 (2008).
237. T. Imai *et al.*, Heat shock protein 90 (HSP90) contributes to cytosolic translocation of extracellular antigen for cross-presentation by dendritic cells. *Proc. Natl. Acad. Sci. U.S.A* **108**, 16363-16368 (2011).
238. I. Dingjan *et al.*, Lipid peroxidation causes endosomal antigen release for cross-presentation. *Scientific Reports* **6**, 22064 (2016).
239. I. Dingjan *et al.*, VAMP8-mediated NOX2 recruitment to endosomes is necessary for antigen release. *European Journal of Cell Biology* **96**, 705-714 (2017).
240. A. W. Girotti, Lipid hydroperoxide generation, turnover, and effector action in biological systems. *Journal of Lipid Research* **39**, 1529-1542 (1998).
241. S. C. Nalle *et al.*, Aquaporin-3 regulates endosome-to-cytosol transfer via lipid peroxidation for cross presentation. *PLOS ONE* **15**, e0238484 (2020).
242. S. A. Fuertes Marraco *et al.*, Novel Murine Dendritic Cell Lines: A Powerful Auxiliary Tool for Dendritic Cell Research. *Frontiers in Immunology* **3**, (2012).
243. M. Gros *et al.*, Endocytic membrane repair by ESCRT-III controls antigen export to the cytosol during antigen cross-presentation. *Cell Rep.* **40**, (2022).
244. D. Sancho *et al.*, Tumor therapy in mice via antigen targeting to a novel, DC-restricted C-type lectin. *The Journal of Clinical Investigation* **118**, 2098-2110 (2008).
245. A. Savina *et al.*, The Small GTPase Rac2 Controls Phagosomal Alkalinization and Antigen Crosspresentation Selectively in CD8+ Dendritic Cells. *Immunity* **30**, 544-555 (2009).
246. S. S. Pang *et al.*, The cryo-EM structure of the acid activatable pore-forming immune effector Macrophage-expressed gene 1. *Nat. Commun.* **10**, 4288 (2019).
247. T. Ni *et al.*, Structure and mechanism of bactericidal mammalian perforin-2, an ancient agent of innate immunity. *Sci. Adv.* **6**, eaax8286 (2020).
248. L. Barbieri, M. G. Battelli, F. Stirpe, Ribosome-inactivating proteins from plants. *Biochimica et Biophysica Acta (BBA) - Reviews on Biomembranes* **1154**, 237-282 (1993).
249. P. Rodríguez-Silvestre *et al.*, Perforin-2 is a pore-forming effector of endocytic escape in cross-presenting dendritic cells. *Science* **380**, 1258-1265 (2023).
250. K. Spilsbury *et al.*, Isolation of a Novel Macrophage-Specific Gene by Differential cDNA Analysis. *Blood* **85**, 1620-1629 (1995).
251. E. R. Podack, V. Deyev, M. Shiratsuchi, in *Current Topics in Innate Immunity,* J. D. Lambris, Ed. (Springer New York, New York, NY, 2007), pp. 325-341.
252. J. Tschopp, D. Masson, K. K. Stanley, Structural/functional similarity between proteins involved in complement- and cytotoxic T-lymphocyte-mediated cytolysis. *Nature* **322**, 831-834 (1986).
253. Y. Shinkai, K. Takio, K. Okumura, Homology of perforin to the ninth component of complement (C9). *Nature* **334**, 525-527 (1988).
254. M. G. Lichtenheld *et al.*, Structure and function of human perforin. *Nature* **335**, 448-451 (1988).
255. J. A. Trapani, M. J. Smyth, Functional significance of the perforin/granzyme cell death pathway. *Nat. Rev. Immunol.* **2**, 735-747 (2002).
256. M. J. Walport, Complement. *New England Journal of Medicine* **344**, 1058-1066 (2001).
257. S. F. Altschul *et al.*, Gapped BLAST and PSI-BLAST: a new generation of protein database search programs. *Nucleic Acids Research* **25**, 3389-3402 (1997).
258. C. J. Rosado *et al.*, The MACPF/CDC family of pore-forming toxins. *Cellular Microbiology* **10**, 1765-1774 (2008).
259. S. A. Mah, G. W. Moy, W. J. Swanson, V. D. Vacquier, A perforin-like protein from a marine mollusk. *Biochemical and Biophysical Research Communications* **316**, 468-475 (2004).

260. G.-D. Wang *et al.*, Molecular cloning and responsive expression of macrophage expressed gene from small abalone Haliotis diversicolor supertexta. *Fish & Shellfish Immunology* **24**, 346-359 (2008).
261. K.-J. Wang, H.-L. Ren, D.-D. Xu, L. Cai, M. Yang, Identification of the up-regulated expression genes in hemocytes of variously colored abalone (Haliotis diversicolor Reeve, 1846) challenged with bacteria. *Developmental & Comparative Immunology* **32**, 1326-1347 (2008).
262. X. He, Y. Zhang, Z. Yu, An Mpeg (macrophage expressed gene) from the Pacific oyster Crassostrea gigas: Molecular characterization and gene expression. *Fish & Shellfish Immunology* **30**, 870-876 (2011).
263. M. Wiens *et al.*, Innate Immune Defense of the Sponge Suberites domuncula against Bacteria Involves a MyD88-dependent Signaling Pathway: INDUCTION OF A PERFORIN-LIKE MOLECULE. *J. Biol. Chem.* **280**, 27949-27959 (2005).
264. M. E. D'Angelo, M. A. Dunstone, J. C. Whisstock, J. A. Trapani, P. I. Bird, Perforin evolved from a gene duplication of MPEG1, followed by a complex pattern of gene gain and loss within Euteleostomi. *BMC Evol Biol* **12**, 59 (2012).
265. R. McCormack, L. R. de Armas, M. Shiratsuchi, J. E. Ramos, E. R. Podack, Inhibition of intracellular bacterial replication in fibroblasts is dependent on the perforin-like protein (perforin-2) encoded by macrophage-expressed gene 1. *J. Innate Immun.* **5**, 185-194 (2013).
266. K. A. Fields, R. McCormack, L. R. de Armas, E. R. Podack, Perforin-2 restricts growth of Chlamydia trachomatis in macrophages. *Infect. Immun.* **81**, 3045-3054 (2013).
267. R. M. McCormack *et al.*, Perforin-2 is essential for intracellular defense of parenchymal cells and phagocytes against pathogenic bacteria. *Elife* **4**, e06508 (2015).
268. R. M. McCormack, K. Lyapichev, M. L. Olsson, E. R. Podack, G. P. Munson, Enteric pathogens deploy cell cycle inhibiting factors to block the bactericidal activity of Perforin-2. *Elife* **4**, (2015).
269. R. McCormack *et al.*, Perforin-2 Protects Host Cells and Mice by Restricting the Vacuole to Cytosol Transitioning of a Bacterial Pathogen. *Infect. Immun.* **84**, 1083-1091 (2016).
270. R. M. McCormack *et al.*, MPEG1/perforin-2 mutations in human pulmonary nontuberculous mycobacterial infections. *JCI Insight* **2**, (2017).
271. R. McCormack, E. R. Podack, Perforin-2/Mpeg1 and other pore-forming proteins throughout evolution. *J. Leukoc. Biol.* **98**, 761-768 (2015).
272. E. R. Podack, G. P. Munson, Killing of Microbes and Cancer by the Immune System with Three Mammalian Pore-Forming Killer Proteins. *Front. Immunol.* **7**, 464 (2016).
273. F. Bai *et al.*, Perforin-2 Breaches the Envelope of Phagocytosed Bacteria Allowing Antimicrobial Effectors Access to Intracellular Targets. *J. Immunol.* **201**, 2710-2720 (2018).
274. S. Ebrahimnezhaddarzi *et al.*, Mpeg1 is not essential for antibacterial or antiviral immunity, but is implicated in antigen presentation. *Immunology & Cell Biology* **100**, 529-546 (2022).
275. S. C. Kondos *et al.*, The structure and function of mammalian membrane-attack complex/perforin-like proteins. *Tissue Antigens* **76**, 341-351 (2010).
276. E. R. Podack, G. Dennert, Assembly of two types of tubules with putative cytolytic function by cloned natural killer cells. *Nature* **302**, 442-445 (1983).
277. J. Tschopp, H. J. Müller-Eberhard, E. R. Podack, Formation of transmembrane tubules by spontaneous polymerization of the hydrophilic complement protein C9. *Nature* **298**, 534-538 (1982).
278. M. A. Hadders, D. X. Beringer, P. Gros, Structure of C8 -MACPF Reveals Mechanism of Membrane Attack in Complement Immune Defense. *Science* **317**, 1552-1554 (2007).

279. C. J. Rosado *et al.*, A Common Fold Mediates Vertebrate Defense and Bacterial Attack. *Science* **317**, 1548 (2007).
280. G. Anderluh, M. Kisovec, N. Kraševec, R. J. C. Gilbert, in *MACPF/CDC Proteins - Agents of Defence, Attack and Invasion,* G. Anderluh, R. Gilbert, Eds. (Springer Netherlands, Dordrecht, 2014), pp. 7-30.
281. A. P. Heuck, R. K. Tweten, A. E. Johnson, Assembly and topography of the prepore complex in cholesterol-dependent cytolysins. *J Biol Chem* **278**, 31218-31225 (2003).
282. R. Ramachandran, A. P. Heuck, R. K. Tweten, A. E. Johnson, Structural insights into the membrane-anchoring mechanism of a cholesterol-dependent cytolysin. *Nat. Struct. Biol.* **9**, 823-827 (2002).
283. R. Ramachandran, R. K. Tweten, A. E. Johnson, Membrane-dependent conformational changes initiate cholesterol-dependent cytolysin oligomerization and intersubunit β-strand alignment. *Nature Structural & Molecular Biology* **11**, 697-705 (2004).
284. J. Rossjohn, S. C. Feil, W. J. McKinstry, R. K. Tweten, M. W. Parker, Structure of a Cholesterol-Binding, Thiol-Activated Cytolysin and a Model of Its Membrane Form. *Cell* **89**, 685-692 (1997).
285. O. Shatursky *et al.*, The Mechanism of Membrane Insertion for a Cholesterol-Dependent Cytolysin: A Novel Paradigm for Pore-Forming Toxins. *Cell* **99**, 293-299 (1999).
286. S. J. Tilley, E. V. Orlova, R. J. C. Gilbert, P. W. Andrew, H. R. Saibil, Structural Basis of Pore Formation by the Bacterial Toxin Pneumolysin. *Cell* **121**, 247-256 (2005).
287. E. S. Parsons *et al.*, Single-molecule kinetics of pore assembly by the membrane attack complex. *Nat. Commun.* **10**, 2066 (2019).
288. B. A. Spicer *et al.*, The first transmembrane region of complement component-9 acts as a brake on its self-assembly. *Nat. Commun.* **9**, 3266 (2018).
289. C. Leung *et al.*, Real-time visualization of perforin nanopore assembly. *Nat. Nanotechnol.* **12**, 467-473 (2017).
290. S. Tomlinson, P. W. Taylor, B. P. Morgan, J. P. Luzio, Killing of gram-negative bacteria by complement. Fractionation of cell membranes after complement C5b-9 deposition on to the surface of Salmonella minnesota Re595. *Biochemical Journal* **263**, 505-511 (1989).
291. M. Nakamura *et al.*, Quantification of the CD55 and CD59, Membrane Inhibitors of Complement on HIV-1 Particles as a Function of Complement-Mediated Virolysis. *Microbiology and Immunology* **40**, 561-567 (1996).
292. D. L. Hoover, M. Berger, C. A. Nacy, W. T. Hockmeyer, M. Meltzer, Killing of Leishmania tropica amastigotes by factors in normal human serum. *Journal of immunology (Baltimore, Md.: 1950)* **132**, 893-897 (1984).
293. D. Ricklin, G. Hajishengallis, K. Yang, J. D. Lambris, Complement: a key system for immune surveillance and homeostasis. *Nat. Immunol.* **11**, 785-797 (2010).
294. A. E. Aleshin, R. G. DiScipio, B. Stec, R. C. Liddington, Crystal Structure of C5b-6 Suggests Structural Basis for Priming Assembly of the Membrane Attack Complex. *J. Biol. Chem.* **287**, 19642-19652 (2012).
295. A. E. Aleshin *et al.*, Structure of Complement C6 Suggests a Mechanism for Initiation and Unidirectional, Sequential Assembly of Membrane Attack Complex (MAC). *J. Biol. Chem.* **287**, 10210-10222 (2012).
296. R. G. DiScipio, D. N. Chakravarti, H. J. Muller-Eberhard, G. H. Fey, The structure of human complement component C7 and the C5b-7 complex. *J Biol Chem* **263**, 549-560 (1988).
297. R. G. DiScipio, C. A. Smith, H. J. Muller-Eberhard, T. E. Hugli, The activation of human complement component C5 by a fluid phase C5 convertase. *J. Biol. Chem.* **258**, 10629-10636 (1983).
298. K. T. Preissner, E. R. Podack, H. J. Müller-Eberhard, The membrane attack complex of complement: relation of C7 to the metastable membrane binding site of the

intermediate complex C5b-7. *Journal of immunology (Baltimore, Md.: 1950)* **135**, 445-451 (1985).
299. A. Menny *et al.*, CryoEM reveals how the complement membrane attack complex ruptures lipid bilayers. *Nat. Commun.* **9**, 5316 (2018).
300. S. Meri *et al.*, Human protectin (CD59), an 18,000-20,000 MW complement lysis restricting factor, inhibits C5b-8 catalysed insertion of C9 into lipid bilayers. *Immunology* **71**, 1 (1990).
301. H. Ninomiya, P. Sims, The human complement regulatory protein CD59 binds to the alpha-chain of C8 and to the “b” domain of C9. *J. Biol. Chem.* **267**, 13675-13680 (1992).
302. R. A. Brodsky, Complement in hemolytic anemia. *Blood* **126**, 2459-2465 (2015).
303. J. Tschopp, A. Chonn, S. Hertig, L. French, Clusterin, the human apolipoprotein and complement inhibitor, binds to complement C7, C8 beta, and the b domain of C9. *Journal of immunology (Baltimore, Md.: 1950)* **151**, 2159-2165 (1993).
304. E. Podack, K. Preissner, H. Müller-Eberhard, Inhibition of C9 polymerization within the SC5b-9 complex of complement by S-protein. *Acta pathologica, microbiologica, et immunologica Scandinavica. Supplement* **284**, 89-96 (1984).
305. I. Voskoboinik, J. C. Whisstock, J. A. Trapani, Perforin and granzymes: function, dysfunction and human pathology. *Nat Rev Immunol* **15**, 388-400 (2015).
306. I. Voskoboinik *et al.*, Calcium-dependent Plasma Membrane Binding and Cell Lysis by Perforin Are Mediated through Its C2 Domain A CRITICAL ROLE FOR ASPARTATE RESIDUES 429, 435, 483, AND 485 BUT NOT 491. *J. Biol. Chem.* **280**, 8426-8434 (2005).
307. J. Tschopp, S. Schäfer, D. Masson, M. C. Peitsch, C. Heusser, Phosphorylcholine acts as a Ca2+-dependent receptor molecule for lymphocyte perforin. *Nature* **337**, 272-274 (1989).
308. I. G. House *et al.*, Regulation of perforin activation and pre-synaptic toxicity through C-terminal glycosylation. *EMBO reports* **18**, 1775-1785 (2017).
309. A. J. Brennan *et al.*, Protection from endogenous perforin: glycans and the C terminus regulate exocytic trafficking in cytotoxic lymphocytes. *Immunity* **34**, 879-892 (2011).
310. R. Uellner *et al.*, Perforin is activated by a proteolytic cleavage during biosynthesis which reveals a phospholipid-binding C2 domain. *EMBO J.* **16**, 7287-7296 (1997).
311. K. Baran *et al.*, The Molecular Basis for Perforin Oligomerization and Transmembrane Pore Assembly. *Immunity* **30**, 684-695 (2009).
312. F. Jiao *et al.*, Perforin-2 clockwise hand-over-hand pre-pore to pore transition mechanism. *Nat. Commun.* **13**, 5039 (2022).
313. E. Boura, J. H. Hurley, Structural basis for membrane targeting by the MVB12-associated β-prism domain of the human ESCRT-I MVB12 subunit. *Proc. Natl. Acad. Sci. U.S.A* **109**, 1901-1906 (2012).
314. C. Bayly-Jones, S. S. Pang, B. A. Spicer, J. C. Whisstock, M. A. Dunstone, Ancient but Not Forgotten: New Insights Into MPEG1, a Macrophage Perforin-Like Immune Effector. *Frontiers in Immunology* **11**, 2690 (2020).
315. X. Yu, T. Ni, G. Munson, P. Zhang, R. J. C. Gilbert, Cryo-EM structures of perforin-2 in isolation and assembled on a membrane suggest a mechanism for pore formation. *The EMBO Journal* **41**, e111857 (2022).
316. J. Garin *et al.*, The Phagosome Proteome: Insight into Phagosome Functions. *Journal of Cell Biology* **152**, 165-180 (2001).
317. C. A. Luber *et al.*, Quantitative proteomics reveals subset-specific viral recognition in dendritic cells. *Immunity* **32**, 279-289 (2010).
318. S. A. Fuertes Marraco *et al.*, Novel murine dendritic cell lines: a powerful auxiliary tool for dendritic cell research. *Front. Immunol.* **3**, 331 (2012).
319. Q.-G. Steiner *et al.*, In vivo transformation of mouse conventional CD8α+ dendritic cells leads to progressive multisystem histiocytosis. *Blood* **111**, 2073-2082 (2008).

320. P. A. Krawczyk, M. Laub, P. Kozik, To Kill But Not Be Killed: Controlling the Activity of Mammalian Pore-Forming Proteins. *Frontiers in immunology* **11**, 601405-601405 (2020).
321. A. R. Mantegazza *et al.*, NADPH oxidase controls phagosomal pH and antigen cross-presentation in human dendritic cells. *Blood* **112**, 4712-4722 (2008).
322. E. Hoffmann *et al.*, Autonomous phagosomal degradation and antigen presentation in dendritic cells. *Proc. Natl. Acad. Sci. U.S.A* **109**, 14556-14561 (2012).
323. E. Hoffmann, A.-M. Pauwels, A. Alloatti, F. Kotsias, S. Amigorena, Analysis of Phagosomal Antigen Degradation by Flow Organellocytometry. *Bio Protoc* **6**, e2014 (2016).
324. P. Chardin, F. McCormick, Brefeldin A: The Advantage of Being Uncompetitive. *Cell* **97**, 153-155 (1999).
325. R. D. Klausner, J. G. Donaldson, J. Lippincott-Schwartz, Brefeldin A: insights into the control of membrane traffic and organelle structure. *Journal of Cell Biology* **116**, 1071-1080 (1992).
326. J. Lippincott-Schwartz *et al.*, Brefeldin A's effects on endosomes, lysosomes, and the TGN suggest a general mechanism for regulating organelle structure and membrane traffic. *Cell* **67**, 601-616 (1991).
327. S. J. Scales, M. Gomez, T. E. Kreis, in *International Review of Cytology,* K. W. Jeon, Ed. (Academic Press, 1999), vol. 195, pp. 67-144.
328. J. S. Bonifacino, J. Lippincott-Schwartz, Coat proteins: shaping membrane transport. *Nature Reviews Molecular Cell Biology* **4**, 409-414 (2003).
329. M. S. Robinson, T. E. Kreis, Recruitment of coat proteins onto Golgi membranes in intact and permeabilized cells: effects of brefeldin A and G protein activators. *Cell* **69**, 129-138 (1992).
330. A. Wähe *et al.*, Golgi-to-phagosome transport of acid sphingomyelinase and prosaposin is mediated by sortilin. *J Cell Sci* **123**, 2502-2511 (2010).
331. M. J. Clague, F. Urbé S Fau - Aniento, J. Aniento F Fau - Gruenberg, J. Gruenberg, Vacuolar ATPase activity is required for endosomal carrier vesicle formation. *J. Biol. Chem.* **269**, 21-24 (1994).
332. V. Marshansky, M. Futai, The V-type H+-ATPase in vesicular trafficking: targeting, regulation and function. *Current Opinion in Cell Biology* **20**, 415-426 (2008).
333. C. C. Scott, J. Gruenberg, Ion flux and the function of endosomes and lysosomes: pH is just the start. *BioEssays* **33**, 103-110 (2011).
334. S. Kissing *et al.*, Vacuolar ATPase in Phagosome-Lysosome Fusion. *J. Biol. Chem.* **290**, 14166-14180 (2015).
335. S. Bagga, D. Seth, J. K. Batra, The Cytotoxic Activity of Ribosome-inactivating Protein Saporin-6 Is Attributed to Its rRNA N-Glycosidase and Internucleosomal DNA Fragmentation Activities. *J. Biol. Chem.* **278**, 4813-4820 (2003).
336. S. L. Gessner, J. D. Irvin, Inhibition of elongation factor 2-dependent translocation by the pokeweed antiviral protein and ricin. *J. Biol. Chem.* **255**, 3251-3253 (1980).
337. E. K. Schmidt, G. Clavarino, M. Ceppi, P. Pierre, SUnSET, a nonradioactive method to monitor protein synthesis. *Nature Methods* **6**, 275-277 (2009).
338. R. Singh, P. Cresswell, Defective Cross-Presentation of Viral Antigens in GILT-Free Mice. *Science* **328**, 1394-1398 (2010).
339. N. Lukoyanova *et al.*, Conformational Changes during Pore Formation by the Perforin-Related Protein Pleurotolysin. *PLOS Biology* **13**, e1002049 (2015).
340. J. Huotari, A. Helenius, Endosome maturation. *The EMBO Journal* **30**, 3481-3500 (2011).
341. H.-J. Ullrich, W. L. Beatty, D. G. Russell, Direct delivery of procathepsin D to phagosomes: implications for phagosome biogenesis and parasitism by Mycobacterium. *European journal of cell biology* **78**, 739-748 (1999).
342. R. A. Fratti, J. Chua, I. Vergne, V. Deretic, Mycobacterium tuberculosis glycosylated phosphatidylinositol causes phagosome maturation arrest. *Proc. Natl. Acad. Sci. U.S.A* **100**, 5437-5442 (2003).

343. F. Giansanti *et al.*, Dissecting the Entry Route of Saporin-based a-CD7 Immunotoxins in Human T-Cell Acute Lymphoblastic Leukaemia Cells. *Antibodies* **2**, 50-65 (2013).
344. T. H. Hudson, F. G. Grillo, Brefeldin-A enhancement of ricin A-chain immunotoxins and blockade of intact ricin, modeccin, and abrin. *J. Biol. Chem.* **266**, 18586-18592 (1991).
345. J. Westman, S. Grinstein, Determinants of Phagosomal pH During Host-Pathogen Interactions. *Front Cell Dev Biol* **8**, 624958 (2020).
346. K. K. Huynh, S. Grinstein, Regulation of Vacuolar pH and Its Modulation by Some Microbial Species. *Microbiology and Molecular Biology Reviews* **71**, 452-462 (2007).
347. A. Savina, S. Amigorena, Phagocytosis and antigen presentation in dendritic cells. *Immunological Reviews* **219**, 143-156 (2007).
348. M. Embgenbroich, S. Burgdorf, Current Concepts of Antigen Cross-Presentation. *Front. Immunol.* **9**, 1643 (2018).
349. J. M. Rybicka, D. R. Balce, S. Chaudhuri, E. R. O. Allan, R. M. Yates, Phagosomal proteolysis in dendritic cells is modulated by NADPH oxidase in a pH-independent manner. *The EMBO Journal* **31**, 932-944 (2012).
350. A.-M. Pauwels *et al.*, Spatiotemporal Changes of the Phagosomal Proteome in Dendritic Cells in Response to LPS Stimulation*. *Molecular & Cellular Proteomics* **18**, 909-922 (2019).
351. Y. Ding *et al.*, The lectin Siglec-G inhibits dendritic cell cross-presentation by impairing MHC class I–peptide complex formation. *Nat. Immunol.* **17**, 1167-1175 (2016).
352. K. Salao *et al.*, CLIC1 regulates dendritic cell antigen processing and presentation by modulating phagosome acidification and proteolysis. *Biology Open* **5**, 620-630 (2016).
353. P. Nunes-Hasler *et al.*, STIM1 promotes migration, phagosomal maturation and antigen cross-presentation in dendritic cells. *Nat. Commun.* **8**, 1852 (2017).
354. M. Oberkampf *et al.*, Mitochondrial reactive oxygen species regulate the induction of CD8+ T cells by plasmacytoid dendritic cells. *Nat. Commun.* **9**, 2241 (2018).
355. A. C. Olatunde, L. P. Abell, A. E. Landuyt, E. Hiltbold Schwartz, Development of endocytosis, degradative activity, and antigen processing capacity during GM-CSF driven differentiation of murine bone marrow. *PLOS ONE* **13**, e0196591 (2018).
356. J. R. Foote, A. A. Patel, S. Yona, A. W. Segal, Variations in the Phagosomal Environment of Human Neutrophils and Mononuclear Phagocyte Subsets. *Front. Immunol.* **10**, 188 (2019).
357. S. C. Khouili *et al.*, SHP-1 Regulates Antigen Cross-Presentation and Is Exploited by Leishmania to Evade Immunity. *Cell Rep.* **33**, (2020).
358. S. H. Naik *et al.*, Cutting Edge: Generation of Splenic CD8+ and CD8− Dendritic Cell Equivalents in Fms-Like Tyrosine Kinase 3 Ligand Bone Marrow Cultures1. *The Journal of Immunology* **174**, 6592-6597 (2005).
359. C. T. Mayer *et al.*, Selective and efficient generation of functional Batf3-dependent CD103+ dendritic cells from mouse bone marrow. *Blood* **124**, 3081-3091 (2014).
360. J. K. Hurst, J. M. Albrich, T. R. Green, H. Rosen, S. Klebanoff, Myeloperoxidase-dependent fluorescein chlorination by stimulated neutrophils. *J. Biol. Chem.* **259**, 4812-4821 (1984).
361. R. J. Gilbert, Protein–lipid interactions and non-lamellar lipidic structures in membrane pore formation and membrane fusion. *Biochimica et Biophysica Acta (BBA)-Biomembranes* **1858**, 487-499 (2016).
362. L. C. Merselis, Z. P. Rivas, G. P. Munson, Breaching the Bacterial Envelope: The Pivotal Role of Perforin-2 (MPEG1) Within Phagocytes. *Front. Immunol.* **12**, 597951 (2021).
363. J. R. Dunkelberger, W.-C. Song, Complement and its role in innate and adaptive immune responses. *Cell Research* **20**, 34-50 (2010).
364. P. Devant, J. C. Kagan, Molecular mechanisms of gasdermin D pore-forming activity. *Nat. Immunol.* **24**, 1064-1075 (2023).

365. J.-S. Kim, M. E. Monroe, D. G. Camp, II, R. D. Smith, W.-J. Qian, In-Source Fragmentation and the Sources of Partially Tryptic Peptides in Shotgun Proteomics. *Journal of Proteome Research* **12**, 910-916 (2013).
366. S. E. Ewald *et al.*, Nucleic acid recognition by Toll-like receptors is coupled to stepwise processing by cathepsins and asparagine endopeptidase. *Journal of Experimental Medicine* **208**, 643-651 (2011).
367. G. Güner, S. F. Lichtenthaler, The substrate repertoire of γ-secretase/presenilin. *Seminars in Cell & Developmental Biology* **105**, 27-42 (2020).
368. R. Kopan, M. X. G. Ilagan, γ-Secretase: proteasome of the membrane? *Nature Reviews Molecular Cell Biology* **5**, 499-504 (2004).
369. G. Struhl, A. Adachi, Requirements for Presenilin-Dependent Cleavage of Notch and Other Transmembrane Proteins. *Molecular Cell* **6**, 625-636 (2000).
370. S. F. Lichtenthaler, M. K. Lemberg, R. Fluhrer, Proteolytic ectodomain shedding of membrane proteins in mammals—hardware, concepts, and recent developments. *The EMBO Journal* **37**, e99456 (2018).
371. P. Schotte, W. Declercq, S. Van Huffel, P. Vandenabeele, R. Beyaert, Non-specific effects of methyl ketone peptide inhibitors of caspases. *FEBS Letters* **442**, 117-121 (1999).
372. N. K. Ahmed *et al.*, Peptidyl fluoromethyl ketones as inhibitors of cathepsin B: implication for treatment of rheumatoid arthritis. *Biochemical pharmacology* **44**, 1201-1207 (1992).
373. B. Park *et al.*, Granulin Is a Soluble Cofactor for Toll-like Receptor 9 Signaling. *Immunity* **34**, 505-513 (2011).
374. A. Citarella, N. Micale, Peptidyl fluoromethyl ketones and their applications in medicinal chemistry. *Molecules* **25**, 4031 (2020).
375. F. J. Lopez-Hernandez, M. A. Ortiz, Y. Bayon, F. J. Piedrafita, Z-FA-fmk inhibits effector caspases but not initiator caspases 8 and 10, and demonstrates that novel anticancer retinoid-related molecules induce apoptosis via the intrinsic pathway. *Molecular cancer therapeutics* **2**, 255-263 (2003).
376. H. Hara *et al.*, Inhibition of interleukin 1β converting enzyme family proteases reduces ischemic and excitotoxic neuronal damage. *Proc. Natl. Acad. Sci. U.S.A* **94**, 2007-2012 (1997).
377. B. Arunachalam, U. T. Phan, H. J. Geuze, P. Cresswell, Enzymatic reduction of disulfide bonds in lysosomes: Characterization of a Gamma-interferon-inducible lysosomal thiol reductase (GILT). *Proc. Natl. Acad. Sci. U.S.A* **97**, 745-750 (2000).
378. U. T. Phan, B. Arunachalam, P. Cresswell, Gamma-Interferon-Inducible Lysosomal Thiol Reductase (GILT): MATURATION, ACTIVITY, AND MECHANISM OF ACTION. *J. Biol. Chem.* **275**, 25907-25914 (2000).
379. J. S. Bonifacino, L. M. Traub, Signals for Sorting of Transmembrane Proteins to Endosomes and Lysosomes. *Annual Review of Biochemistry* **72**, 395-447 (2003).
380. M. S. Robinson, Adaptable adaptors for coated vesicles. *Trends in Cell Biology* **14**, 167-174 (2004).
381. R. C. Piper, I. Dikic, G. L. Lukacs, Ubiquitin-Dependent Sorting in Endocytosis. *Cold Spring Harbor Perspectives in Biology* **6**, (2014).
382. F. Letourneur, R. D. Klausner, A novel di-leucine motif and a tyrosine-based motif independently mediate lysosomal targeting and endocytosis of CD3 chains. *Cell* **69**, 1143-1157 (1992).
383. I. V. Sandoval *et al.*, The residues Leu(Ile)475-Ile(Leu, Val, Ala)476, contained in the extended carboxyl cytoplasmic tail, are critical for targeting of the resident lysosomal membrane protein LIMP II to lysosomes. *J. Biol. Chem.* **269**, 6622-6631 (1994).
384. L. Jacobsen *et al.*, The sorLA cytoplasmic domain interacts with GGA1 and -2 and defines minimum requirements for GGA binding. *FEBS Letters* **511**, 155-158 (2002).
385. T. Braulke, J. S. Bonifacino, Sorting of lysosomal proteins. *Biochimica et Biophysica Acta (BBA) - Molecular Cell Research* **1793**, 605-614 (2009).

386. W. Boll *et al.*, Sequence requirements for the recognition of tyrosine-based endocytic signals by clathrin AP-2 complexes. *The EMBO journal* **15**, 5789-5795 (1996).
387. H. Ohno *et al.*, Interaction of tyrosine-based sorting signals with clathrin-associated proteins. *Science* **269**, 1872-1875 (1995).
388. J. H. Keen, Clathrin assembly proteins: affinity purification and a model for coat assembly. *The Journal of cell biology* **105**, 1989-1998 (1987).
389. S. Zaremba, J. H. Keen, Assembly polypeptides from coated vesicles mediate reassembly of unique clathrin coats. *The Journal of cell biology* **97**, 1339-1347 (1983).
390. B. Pearse, M. Robinson, Purification and properties of 100-kd proteins from coated vesicles and their reconstitution with clathrin. *The EMBO journal* **3**, 1951-1957 (1984).
391. A. Sanger, J. Hirst, A. K. Davies, M. S. Robinson, Adaptor protein complexes and disease at a glance. *J Cell Sci* **132**, (2019).
392. F. Simpson *et al.*, A novel adaptor-related protein complex. *The Journal of cell biology* **133**, 749-760 (1996).
393. E. C. Dell'Angelica, C. Mullins, J. S. Bonifacino, AP-4, a novel protein complex related to clathrin adaptors. *J. Biol. Chem.* **274**, 7278-7285 (1999).
394. E. C. Dell'Angelica *et al.*, AP-3: an adaptor-like protein complex with ubiquitous expression. *The EMBO journal* **16**, 917-928 (1997).
395. A. A. Peden, R. E. Rudge, W. W. Lui, M. S. Robinson, Assembly and function of AP-3 complexes in cells expressing mutant subunits. *The Journal of cell biology* **156**, 327-336 (2002).
396. R. Mattera, S. Y. Park, R. De Pace, C. M. Guardia, J. S. Bonifacino, AP-4 mediates export of ATG9A from the trans-Golgi network to promote autophagosome formation. *Proc. Natl. Acad. Sci. U.S.A* **114**, E10697-E10706 (2017).
397. H. Ohno *et al.*, The Medium Subunits of Adaptor Complexes Recognize Distinct but Overlapping Sets of Tyrosine-based Sorting Signals *. *J. Biol. Chem.* **273**, 25915-25921 (1998).
398. R. C. Aguilar *et al.*, Signal-binding Specificity of the mu4 Subunit of the Adaptor Protein Complex AP-4 *. *J. Biol. Chem.* **276**, 13145-13152 (2001).
399. B. Doray, I. Lee, J. Knisely, G. Bu, S. Kornfeld, The γ/σ1 and α/σ2 hemicomplexes of clathrin adaptors AP-1 and AP-2 harbor the dileucine recognition site. *Molecular biology of the cell* **18**, 1887-1896 (2007).
400. K. Janvier *et al.*, Recognition of dileucine-based sorting signals from HIV-1 Nef and LIMP-II by the AP-1 γ–σ1 and AP-3 δ–σ3 hemicomplexes. *The Journal of cell biology* **163**, 1281-1290 (2003).
401. B. T. Kelly *et al.*, A structural explanation for the binding of endocytic dileucine motifs by the AP2 complex. *Nature* **456**, 976-979 (2008).
402. B. M. Collins, A. J. McCoy, H. M. Kent, P. R. Evans, D. J. Owen, Molecular Architecture and Functional Model of the Endocytic AP2 Complex. *Cell* **109**, 523-535 (2002).
403. L. P. Jackson *et al.*, A large-scale conformational change couples membrane recruitment to cargo binding in the AP2 clathrin adaptor complex. *Cell* **141**, 1220-1229 (2010).
404. B. T. Kelly *et al.*, AP2 controls clathrin polymerization with a membrane-activated switch. *Science* **345**, 459-463 (2014).
405. A. A. Peden *et al.*, Localization of the AP-3 adaptor complex defines a novel endosomal exit site for lysosomal membrane proteins. *Journal of Cell Biology* **164**, 1065-1076 (2004).
406. W. Hunziker, H. J. Geuze, Intracellular trafficking of lysosomal membrane proteins. *BioEssays* **18**, 379-389 (1996).
407. S. Misra, R. Puertollano, Y. Kato, J. S. Bonifacino, J. H. Hurley, Structural basis for acidic-cluster-dileucine sorting-signal recognition by VHS domains. *Nature* **415**, 933-937 (2002).

408. T. Shiba *et al.*, Structural basis for recognition of acidic-cluster dileucine sequence by GGA1. *Nature* **415**, 937-941 (2002).
409. K. Husnjak, I. Dikic, Ubiquitin-binding proteins: decoders of ubiquitin-mediated cellular functions. *Annual review of biochemistry* **81**, 291-322 (2012).
410. A. Sen, K. Madhivanan, D. Mukherjee, R. C. Aguilar, The epsin protein family: coordinators of endocytosis and signaling. *Biomolecular concepts* **3**, 117-126 (2012).
411. R. C. Piper, D. J. Katzmann, Biogenesis and function of multivesicular bodies. *Annu. Rev. Cell Dev. Biol.* **23**, 519-547 (2007).
412. L. Hicke, R. Dunn, Regulation of membrane protein transport by ubiquitin and ubiquitin-binding proteins. *Annual review of cell and developmental biology* **19**, 141-172 (2003).
413. K. L. Goldenthal, K. Hedman, J. W. Chen, J. T. August, M. C. Willingham, Postfixation detergent treatment for immunofluorescence suppresses localization of some integral membrane proteins. *Journal of Histochemistry & Cytochemistry* **33**, 813-820 (1985).
414. A. Vernay, P. Cosson, Immunofluorescence labeling of cell surface antigens in Dictyostelium. *BMC research notes* **6**, 1-4 (2013).
415. K. Janvier, J. S. Bonifacino, Role of the Endocytic Machinery in the Sorting of Lysosome-associated Membrane Proteins. *Molecular Biology of the Cell* **16**, 4231-4242 (2005).
416. R. Puertollano, R. C. Aguilar, I. Gorshkova, R. J. Crouch, J. S. Bonifacino, Sorting of mannose 6-phosphate receptors mediated by the GGAs. *Science* **292**, 1712-1716 (2001).
417. K. F. Johnson, S. Kornfeld, The cytoplasmic tail of the mannose 6-phosphate/insulin-like growth factor-II receptor has two signals for lysosomal enzyme sorting in the Golgi. *The Journal of cell biology* **119**, 249-257 (1992).
418. D. Stalder, D. C. Gershlick, in *Seminars in cell & developmental biology*. (Elsevier, 2020), vol. 107, pp. 112-125.
419. G. Marini *et al.*, Structural journey of an insecticidal protein against western corn rootworm. *Nat. Commun.* **14**, 4171 (2023).
420. L. Cao *et al.*, Design of protein-binding proteins from the target structure alone. *Nature* **605**, 551-560 (2022).
421. A. Mant, F. Chinnery, T. Elliott, A. P. Williams, The pathway of cross-presentation is influenced by the particle size of phagocytosed antigen. *Immunology* **136**, 163-175 (2012).
422. P. Boya, G. Kroemer, Lysosomal membrane permeabilization in cell death. *Oncogene* **27**, 6434-6451 (2008).
423. S. M. Soond, M. V. Kozhevnikova, P. A. Townsend, A. A. Zamyatnin Jr, Cysteine cathepsin protease inhibition: an update on its diagnostic, prognostic and therapeutic potential in cancer. *Pharmaceuticals* **12**, 87 (2019).
424. S. S. Burgener *et al.*, Cathepsin G inhibition by Serpinb1 and Serpinb6 prevents programmed necrosis in neutrophils and monocytes and reduces GSDMD-driven inflammation. *Cell Rep.* **27**, 3646-3656. e3645 (2019).
425. I. Walev *et al.*, Delivery of proteins into living cells by reversible membrane permeabilization with streptolysin-O. *Proc. Natl. Acad. Sci. U.S.A* **98**, 3185-3190 (2001).
426. M. E. Ivanova *et al.*, The pore conformation of lymphocyte perforin. *Science advances* **8**, eabk3147 (2022).
427. S. E. Stewart *et al.*, The perforin pore facilitates the delivery of cationic cargos. *J. Biol. Chem.* **289**, 9172-9181 (2014).
428. S. Xia *et al.*, Gasdermin D pore structure reveals preferential release of mature interleukin-1. *Nature* **593**, 607-611 (2021).
429. O. Schulz *et al.*, Toll-like receptor 3 promotes cross-priming to virus-infected cells. *Nature* **433**, 887-892 (2005).

430. E. R. Podack, J. Young, Z. A. Cohn, Isolation and biochemical and functional characterization of perforin 1 from cytolytic T-cell granules. *Proc. Natl. Acad. Sci. U.S.A* **82**, 8629-8633 (1985).
431. C. Burd, P. J. Cullen, Retromer: a master conductor of endosome sorting. *Cold Spring Harbor perspectives in biology* **6**, a016774 (2014).
432. I. G. House *et al.*, Regulation of perforin activation and pre-synaptic toxicity through C-terminal glycosylation. *EMBO Rep.* **18**, 1775-1785 (2017).
433. A. W. Hodel, J. A. Rudd-Schmidt, J. A. Trapani, I. Voskoboinik, B. W. Hoogenboom, Lipid specificity of the immune effector perforin. *Faraday Discussions* **232**, 236-255 (2021).
434. R. Antia, R. A. Schlegel, P. Williamson, Binding of perforin to membranes is sensitive to lipid spacing and not headgroup. *Immunology letters* **32**, 153-157 (1992).
435. J. A. Rudd-Schmidt *et al.*, Lipid order and charge protect killer T cells from accidental death. *Nat. Commun.* **10**, 5396 (2019).
436. Y. Wang *et al.*, Chemotherapy drugs induce pyroptosis through caspase-3 cleavage of a gasdermin. *Nature* **547**, 99-103 (2017).
437. X. Liu *et al.*, Inflammasome-activated gasdermin D causes pyroptosis by forming membrane pores. *Nature* **535**, 153-158 (2016).
438. J. Ding *et al.*, Pore-forming activity and structural autoinhibition of the gasdermin family. *Nature* **535**, 111-116 (2016).
439. R. Basu *et al.*, Cytotoxic T cells use mechanical force to potentiate target cell killing. *Cell* **165**, 100-110 (2016).
440. T. Yeung *et al.*, Receptor activation alters inner surface potential during phagocytosis. *Science* **313**, 347-351 (2006).
441. M. E. Maxson, S. Grinstein, The role of membrane surface charge in phagocytosis. *Molecular and Cellular Biology of Phagocytosis*, 43-54 (2020).
442. S. Grinstein, Imaging signal transduction during phagocytosis: phospholipids, surface charge, and electrostatic interactions. *American Journal of Physiology-Cell Physiology* **299**, C876-C881 (2010).
443. K. Yang, X. Han, Lipidomics: techniques, applications, and outcomes related to biomedical sciences. *Trends in biochemical sciences* **41**, 954-969 (2016).
444. M. Maekawa, G. D. Fairn, Molecular probes to visualize the location, organization and dynamics of lipids. *J Cell Sci* **127**, 4801-4812 (2014).
445. D. A. K. Traore *et al.*, Defining the interaction of perforin with calcium and the phospholipid membrane. *Biochem. J.* **456**, 323-335 (2013).
446. M. A. Wouters *et al.*, Evolution of distinct EGF domains with specific functions. *Protein Science* **14**, 1091-1103 (2005).
447. Z. Rao *et al.*, The structure of a Ca2+-binding epidermal growth factor-like domain: its role in protein-protein interactions. *Cell* **82**, 131-141 (1995).
448. M. L. Skowyra, P. H. Schlesinger, T. V. Naismith, P. I. Hanson, Triggered recruitment of ESCRT machinery promotes endolysosomal repair. *Science* **360**, (2018).
449. M. Radulovic *et al.*, ESCRT-mediated lysosome repair precedes lysophagy and promotes cell survival. *The EMBO journal* **37**, e99753 (2018).
450. P. Niekamp *et al.*, Ca2+-activated sphingomyelin scrambling and turnover mediate ESCRT-independent lysosomal repair. *Nat. Commun.* **13**, 1875 (2022).
451. M. Radulovic *et al.*, Cholesterol transfer via endoplasmic reticulum contacts mediates lysosome damage repair. *The EMBO journal* **41**, e112677 (2022).
452. W. W.-Y. Yim, H. Yamamoto, N. Mizushima, Annexins A1 and A2 are recruited to larger lysosomal injuries independently of ESCRTs to promote repair. *FEBS Letters* **596**, 991-1003 (2022).
453. J. X. Tan, T. Finkel, A phosphoinositide signalling pathway mediates rapid lysosomal repair. *Nature* **609**, 815-821 (2022).
454. C. Bussi *et al.*, Stress granules plug and stabilize damaged endolysosomal membranes. *Nature* **623**, 1062-1069 (2023).

455. A. J. Jimenez *et al.*, ESCRT Machinery Is Required for Plasma Membrane Repair. *Science* **343**, 1247136 (2014).
456. S. Herbst *et al.*, LRRK 2 activation controls the repair of damaged endomembranes in macrophages. *The EMBO journal* **39**, e104494 (2020).
457. S. Rühl *et al.*, ESCRT-dependent membrane repair negatively regulates pyroptosis downstream of GSDMD activation. *Science* **362**, 956 (2018).